

PHYSICALLY BASED POINT SNOWMELT MODELING AND
ITS DISTRIBUTION IN UPPER EUPHRATES BASIN

A THESIS SUBMITTED TO
THE GRADUATE SCHOOL OF NATURAL AND APPLIED SCIENCES
OF
MIDDLE EAST TECHNICAL UNIVERSITY

BY

AYNUR ŞENSOY

IN PARTIAL FULFILLMENT OF THE REQUIREMENTS
FOR
THE DEGREE OF DOCTOR OF PHILOSOPHY
IN
CIVIL ENGINEERING

MARCH 2005

Approval of the Graduate School of Natural and Applied Sciences

Prof. Dr. Canan Özgen
Director

I certify that this thesis satisfies all the requirements as a thesis for the degree of Doctor of Philosophy.

Prof. Dr. Erdal Çokca
Head of Department

This is to certify that we have read this thesis and that in our opinion it is fully adequate, in scope and quality, as a thesis for the degree of Doctor of Philosophy.

Prof. Dr. A. Ünal Şorman
Supervisor

Examining Committee Members

Prof. Dr. Mehmet Karaca	(ITU, JEO)	_____
Prof. Dr. A. Ünal Şorman	(METU, CE)	_____
Prof. Dr. Alparslan Arıkan	(HU, HYD)	_____
Asst. Prof. Dr. A. Burcu Altan Sakarya	(METU, CE)	_____
Asst. Prof. Dr. Zuhale Akyürek	(METU, GGIT)	_____

I hereby declare that all information in this document has been obtained and presented in accordance with academic rules and ethical conduct. I also declare that, as required by these rules and conduct, I have fully cited and referenced all material and results that are not original to this work.

Name, Last name : Aynur Şensoy

Signature :

ABSTRACT

PHYSICALLY BASED POINT SNOWMELT MODELING AND ITS DISTRIBUTION IN UPPER EUPHRATES BASIN

Şensoy, Aynur

Ph.D., Department of Civil Engineering

Supervisor : Prof. Dr. A. Ünal Şorman

March 2005, 225 Pages

Since snowmelt runoff is important in the mountainous parts of the world, substantial efforts have been made to develop snowmelt models with many different levels of complexity to simulate the processes at the ground, within the snow, and at the interface with the atmosphere. The land-atmosphere interactions and processing influencing heat transfer to and from a snowpack are largely variable and the conceptual representation of this temporal and spatial variability is difficult.

A physically based, two layer point model, is applied to calculate the energy and mass balance of snowmelt in the Upper Karasu Basin, eastern part of Turkey during 2002-2004 snow seasons. The climate data are provided from automated weather stations installed and upgraded to collect quantitative and qualitative data with automated transfer. Each form of energy transfer is evaluated to understand the key processes that have major impact on the snow simulation during accumulation and ablation in two-hourly timesteps. The model performance is evaluated as accurate according to the results, compared with observed snow water equivalents, snow depth and lysimeter runoff yield. In the second part, calculated snowmelt values based on energy and mass balance at the automated

stations are related to radiation index model through regression. Then, the spatial patterns of snow water equivalent, solar illumination, albedo and air temperature are used to predict the melt at each grid cell over the whole watershed. The results of distributed model application are evaluated in terms of snow covered area of satellite products, observed snow water equivalent at points through snow pillows and discharge values at the outlet runoff station.

Key words: Snow modeling, energy and mass balance, radiation index, Turkey

ÖZ

YUKARI FIRAT HAVZASINDA FİZİKSEL BAZLI NOKTASAL KAR ERİME MODELLEMESİ VE DAĞILIMI

Şensoy, Aynur

Doktora, İnşaat Mühendisliği Bölümü

Tez Yöneticisi : Prof. Dr. A. Ünal Şorman

Mart 2005, 225 Sayfa

Dünyanın dağlık bölgelerinde kar erimesinden meydana gelen akımın önemli olması nedeniyle, yer - kar -atmosfer arayüzündeki işlemlerin benzeşimini yapmak üzere farklı karmaşıklık seviyelerine sahip kar modellerinin geliştirilmesine büyük bir emek harcanmıştır. Kar kütlesinden ve kar kütlesine doğru ısı değişimini etkileyen işlemler ve yer-atmosfer etkileşimi çok değişkendir ve bu zamansal ve alansal çeşitliliği kavramsal olarak göstermek oldukça zordur.

Türkiye'nin doğusunda yer alan Yukarı Karasu Havzasında, kar kütlesinin 2002-2004 kar sezonları süresince enerji ve kütle dengesinin hesaplanabilmesi için iki katmanlı fiziksel bir nokta modeli kullanılmıştır. İklim verisi, çok miktarda ve kaliteli veriyi otomatik olarak transfer etmek üzere yeni kurulmuş ve güncellenmiş olan otomatik kar ve meteoroloji istasyonlarından alınmıştır. Kar erime ve birikme süreçlerinde kar benzeşimine en çok etkisi olan işlemleri anlamak için tüm enerji elemanları iki saatlik periyotlarda hesaplanmıştır. Model performansı, model sonuçları gözlenmiş kar su eşdeğeri, kar derinliği ve lizemetre akım değerleri ile karşılaştırılarak, doğru olarak değerlendirilmiştir. İkinci bölümde, havzadaki indeks noktalarda enerji ve kütle dengesine dayanılarak hesaplanan erime değerleri regrasyon yoluyla radyasyon index modeliyle ilişkilendirilmiştir. Daha

sonra, kar su eşdeđeri, güneşlenme, yansıma ve hava sıcaklığının alansal dağılımı kullanılarak, havzadaki herbir hücrede erime tahmin edilmiştir. Alansal dağılımlı model uygulama sonuçları, uydu ürünlerinin sağladığı karla kaplı alan görüntüleri, istasyonlarda kar yastıklarında gözlenen kar su eşdeđerleri ve havza çıkışındaki akım istasyonunda gözlenen debi deđerleriyle karşılaştırılarak deđerlendirilmiştir.

Anahtar kelimeler: Kar modellemesi, enerji ve kütle dengesi, radyasyon indeksi, Türkiye

To my lovely mother and best friend,
BAĖDAT

ACKNOWLEDGEMENTS

My gratitude goes to Prof. Dr. A.Ünal Şorman for providing me with the opportunity to undertake the projects and his guidance, advice, support, criticism, encouragement, insight and friendship throughout the research.

My deepest thanks go to Dr. David Garen for the valuable hours he has spend for advising and encouraging me. He is not only an excellent scientist, but a friend and the most peace- and help-loving American.

The valuable comments and work of Asst. Prof. Dr. Zuhul Akyürek on earlier drafts significantly improved the quality of my dissertation. Her successful standpoint in the academic platform besides her mother identity motivates me.

I would also like to thank Prof. Dr. Alparslan Arıkan for his expressive encouragements all throughout the study. Thank you very much to Prof. Dr. Mehmet Karaca and Asst. Prof. Dr. Burcu Altan Sakarya for their valuable review of my thesis and understanding that made life rather easy.

My deepest emotion and thanks go to my beloved, Arda, for his tireless accompany throughout my studies. Arda, you have been my inspiration since the day I met you! Thank you for walking shoulder to shoulder with me at the office, field site and every part of the life as my love, friend and colleague...

I am indebted to my colleague Ahmet Emre who is a part of snow hydrology group at METU although he hates from cold and wetness! Emre, thank you for providing every kind of technical support as well as a multitude of brain bashing and stress relieving office sessions, and for the time spent with you as a valuable friend.

I would like to express my gratitude to Musa Yılmaz as being my right arm and a search specialist (Moogler). Thank you very much for your being with me at each step of my study and endless discussions about technology and life in general!

My special thanks go to Nermin Şarlak and Emrah Erduran for their guiding me through the many difficulties encountered. Furthermore, I would like to remember the pleasant spare-time activities which contributed a lot to my stressful life during the thesis.

The cooperation of General and VIII. Regional Directorate of State Hydraulic Works is greatly appreciated. Thanks to Ziyaattin Durmaz for his valuable support both in Ankara and Erzurum. I would particularly like to thank Nurullah Sezen, who trudged up to the field site on many occasions with and without us, in snow, rain or sunshine. Assistance from A.Kadir Yazıcı with his pleasant work and talks, Faruk, Recep, Atilla and my colleague Orhan in the field work was invaluable!

The support of General Directorate of State Meteorological Organization also needs acknowledgement for providing us invaluable data.

I am sincerely grateful to Mustafa Tombul, who encouraged me to be a member of Anadolu University, for his incredible support during the last months. I would like to gratefully acknowledge the generosity of Ahmet Tuncan and Mustafa Tuncan having allowed me to spend a considerable amount of time working on the thesis.

Numerous other people have contributed to the successful completion of this thesis in different ways. I would like to express my gratitude to all of them, to name a few my thanks go to Bilgen, Özgün, Tülin and Tülay.

The last but not the least thanks go to each member of Şensoy and Şorman family for their endless patience and support that made us concentrate fully on our work, it was not possible to complete the thesis without their help.

This study was supported by the State Planning Organization (DPT) Grants: BAP-03-03-DPT-2001K120990 and BAP-03-03-DPT-2003K1290-01.

TABLE OF CONTENTS

PLAGIARISM.....	iii
ABSTRACT	iv
ÖZ.....	vi
DEDICATION	viii
ACKNOWLEDGEMENT	ix
TABLE OF CONTENTS	xi
LIST OF FIGURES.....	xv
LIST OF TABLES.....	xviii
1. INTRODUCTION	1
1.1. General	1
1.2. Objectives	2
1.3. Thesis Outline.....	4
2. LITERATURE REVIEW.....	6
2.1. Snow and Snowmelt.....	6
2.2. Overview of Physical Process	7
2.2.1. Snow Surface Energy Exchange and Snowmelt	8
2.2.1.1. Net Radiation (R_{net}).....	10
2.2.1.2. Turbulent Fluxes (H and L_vE)	17
2.2.1.3. Heat Flux Advected by Precipitation (M).....	19
2.2.1.4. Ground Heat Flux (G)	19
2.3. Literature Review on Modeling Snowpack Processes.....	20
2.3.1. Snow Process Models	21
2.3.1.1. Temperature Index Model.....	22
2.3.1.2. Energy Balance Models	23
2.3.1.3. Hybrid Models	26
2.3.2. Spatial Variation in Snow Process Models	27

2.3.2.1. Lumped Model Approach	28
2.3.2.2. Distributed (Semi-Fully) Model Approach	28
2.3.3. Comparison of Modeling Approaches.....	32
3. FIELD SITE and INSTRUMENTATION.....	34
3.1. Field Site	34
3.2. Instrumentation and Data Management	39
3.2.1. Snow Data	44
3.2.2. Radiation Data	48
3.2.3. Precipitation Data.....	49
3.2.4. Temperature Data	50
3.2.5. Wind Speed, Direction and Humidity	52
3.2.6. Lysimeter.....	54
3.2.7. Runoff Data.....	55
3.3. Spatial Data	56
3.3.1. Remotely Sensed Areal Snow Cover	57
3.3.2. Topographic Data.....	60
4. THE MODEL SNOBAL AND APPLICATIONS IN THE UPPER KARASU BASIN	62
4.1. The Model SNOBAL.....	62
4.2. Energy and Mass Balance Calculations	66
4.3. Model Inputs	67
4.3.1. Measurement Heights and Depths Record (Constants).....	67
4.3.2. Snow Properties Record (Initial Conditions)	67
4.3.3. Precipitation Record	68
4.3.4. Input Data Record (Forcing Data)	69
4.3.5. Model Time Steps (Data Timestep and Run Timestep).....	69
4.4. Model Outputs	70
4.5. Methodology.....	71
4.6. Model Application.....	71
4.7. Model Inputs	72
4.7.1. Measurement Records.....	72
4.7.2. Precipitation Record	73

4.7.3. Climate Input Data Preparation.....	75
4.7.3.1 Net Shortwave Radiation.....	77
4.7.3.2 Incoming Longwave	80
4.7.3.3 Air Temperature, Vapor pressure and Wind Speed	83
4.7.3.4 Soil Temperature	84
4.8. Model Outputs	85
4.8.1. Temporal Analysis of Model Applications	102
4.8.1.1 Snow Cover Energy Balance.....	102
4.8.1.2 Snow Cover Mass Balance	107
4.8.2. Spatial Analysis of Model Applications.....	113
4.8.2.1 Snow Cover Energy Balance.....	115
4.8.2.2 Snow Cover Mass Balance	118
4.8.3. Discussion on Snow Pillow Performance	119
4.8.4. Evaluation of Model Performance.....	122
5. DISTRIBUTED MODEL APPLICATION	126
5.1. Distributed Model Approach.....	126
5.2. The Methodology	129
5.2.1. GIS and Topographic Data	134
5.2.2. Initial Snow Cover, Temperature and Precipitation	134
5.2.3. Spatial Solar Radiation Model.....	138
5.2.4. Albedo.....	141
5.3. Distributed Model Application.....	141
5.3.1. Distributed Snow Cover, Temperature and Precipitation	142
5.3.2. Distributed Solar Radiation	144
5.3.3. Distributed Albedo	148
5.3.4. Calibration of Radiation Index Model Parameters.....	150
5.4. Model Results and Verification.....	153
5.4.1. Comparison of Snow Cover Area with Satellite Data.....	154
5.4.2. Comparison of Snow Water Equivalent	169
5.4.3. Comparison of Discharge with Daily Modeled Melt.....	170

6. CONCLUSIONS AND RECOMMENDATIONS.....	173
6.1. Introduction	173
6.2. Summary	174
6.2.1. Physically Based Snow Process Model	174
6.2.2. Distributed Radiation Index Model.....	177
6.3. Implications of Results	182
6.4. Limitations of the Work Presented.....	184
6.4.1. Data Acquisition.....	184
6.4.2. Model Limitations.....	185
6.5. Recommendations for Future Work.....	186
REFERENCES.....	190
APPENDICES.....	210
A. The Methodology of the Model and Model Inputs	210
CURRICULUM VITAE	225

LIST OF FIGURES

FIGURES

Figure 2.1	Schematic diagram of snow energy exchanges	9
Figure 3.1	Location of Karasu Basin (Upper Euphrates River) in Turkey and the locations of stream gauges in the basin	36
Figure 3.2	DEM of the Upper Karasu Basin with the locations of automatic weather and runoff gauging stations.....	37
Figure 3.3	Snow condition of Turkey for 1 and 20 April, 2003 (NOAA, 2003)	37
Figure 3.4	General view from the Guzelyayla AWS.....	44
Figure 3.5	Snow pillow installation (Cat).....	46
Figure 3.6	Long term averages of SWE values	46
Figure 3.7	Comparison of manual snow course data and continuous snow pillow data (SWE) at GY site.....	47
Figure 3.8	Comparison of manual and automatic snow depth observations at GY	47
Figure 3.9	Net pyronometer and net pyrgeometer at Ovacik AWS.....	49
Figure 3.10	Temperature data for GY, OVA and CAT during March 2004	51
Figure 3.11	Wind speed data for GY and CAT during March 2004	53
Figure 3.12	Wind directions at GY and CAT sites	53
Figure 3.13	Snowmelt lysimeter and rain-gauge in Guzelyayla station.....	54
Figure 3.14	Snow lysimeter and its comparison with discharge from two stream gauging stations	55
Figure 4.1	Schematic diagram of the snowmelt model structure and components	65
Figure 4.2	Snow depth and SWE comparison at SK and GY sites.....	76
Figure 4.3	Maximum and minimum temperatures at SK and GY sites.....	76
Figure 4.4	Observed and modeled albedo values for march-april 2003, GY.....	79
Figure 4.5	Snow surface and air temperature relations, OVA, 2004	82
Figure 4.6	Incoming longwave modeling at two hourly timesteps, OVA.....	83

Figure 4.7	Model outputs for energy and mass balance at GY, 2001-2002.....	86
Figure 4.8	Model outputs for energy and mass balance at GY, 2002-2003.....	87
Figure 4.9	Model outputs for energy and mass balance at GY, 2003-2004.....	88
Figure 4.10	Model outputs for energy and mass balance at OVA, 2003- 2004.....	89
Figure 4.11	Model outputs for energy and mass balance at CAT, 2003- 2004.....	90
Figure 4.12	Energy flux outputs at GY, 2001-2002.....	91
Figure 4.13	Energy flux outputs at GY, 2002-2003.....	92
Figure 4.14	Energy flux outputs at GY, 2003-2004.....	93
Figure 4.15	Energy flux outputs at OVA, 2003-2004.....	94
Figure 4.16	Energy flux outputs at CAT, 2003-2004.....	95
Figure 4.17	Daily average sensible and latent heat flux values.....	96
Figure 4.18	Energy percentages within the total energy, GY.....	97
Figure 4.19	Energy percentages within the total energy (GY, OVA, CAT).....	98
Figure 4.20	Total energy comparisons for three years, GY.....	99
Figure 4.21	Total energy comparisons for three sites, 2003-2004.....	99
Figure 4.22	Modeled and observed snow depths, GY.....	100
Figure 4.23	SWE, cumulative modeled runoff and lysimeter yield, 2003, GY.....	109
Figure 4.24	Two hourly rates of modeled runoff and lysimeter yield, 2003, GY.....	109
Figure 4.25	SWE, cumulative modeled runoff and lysimeter yield, 2004, GY.....	110
Figure 4.26	Two hourly rates of modeled runoff and lysimeter yield, 2004, GY.....	110
Figure 4.27	Modeled liquid water content at GY for 2002-2003 snow season.....	112
Figure 4.28	Model input categorization for 2003-2004 season evaluation.....	114
Figure 4.29	Model output categorization for 2003-2004 season evaluation.....	116
Figure 5.1	Flow chart of the distributed model application.....	133
Figure 5.2	Initial snow cover including SWE values on 23 March 2004.....	143
Figure 5.3	Modeled and observed total global radiation at four stations and cloud cover percentages at ERZ station.....	145

Figure 5.4	Observed to modeled global ratio in relation to cloud cover at each site	146
Figure 5.5	Cloud corrected radiation model results and comparison with observations at three sites.....	147
Figure 5.6	Albedo depletion curve at observation sites	148
Figure 5.7	Albedo modeling for three different melting periods	149
Figure 5.8	Snowmelt comparison at AWS using index and energy balance models	152
Figure 5.9	Visual comparison of snow cover area of the model and MODIS (Yellow: snow cover, blue: cloud or unclassified pixels, white: land cover)	155
Figure 5.10	The comparison of model result and MODIS with respect to different thematic maps	159
Figure 5.11	Initial snow cover a) used in the application b) including ERZ_CITY	160
Figure 5.12	SWE map (1 April) a) model result b) alternative result with ERZ_CITY	160
Figure 5.13	Linear regression between modeled and observed SCA.....	164
Figure 5.14	Modeled snow cover depletion curve and its consistency with MODIS.....	164
Figure 5.15	Comparison of modeled and observed snow water equivalents	169
Figure 5.16a	Comparison of average daily snowmelt and observed discharge	171
Figure 5.16b	Comparison of average daily snowmelt and change in observed discharge	171
Figure 5.17	Comparison of lagged daily average snowmelt and observed discharge	172
Figure A.1	Climate input parameters for 2001-2002 snow season, GY.....	215
Figure A.2	Climate input parameters for 2002-2003 snow season, GY.....	217
Figure A.3	Climate input parameters for 2003-2004 snow season, GY.....	219
Figure A.4	Climate input parameters for 2003-2004 snow season, OVA	221
Figure A.5	Climate input parameters for 2003-2004 snow season, CAT	223

LIST OF TABLES

TABLES

Table 2.1	Albedo values for different surfaces.....	13
Table 2.2	Summary of the extrapolation methods for meteorological variables (Fox, 2003).....	31
Table 3.1	Topographic characteristics of the Upper Karasu Basin by elevation zones.....	38
Table 3.2	Data requirements for snow analysis (ASCE, 1996)	40
Table 3.3	Snow instrumentation at the sites.....	43
Table 3.4	Radiation instrumentation at the sites.....	43
Table 3.5	Meteorological instrumentation at the sites	43
Table 3.6	Monthly averages of climatic data for Erzurum central station.....	51
Table 4.1	Comparison of different snowmelt models (Essery and Yang, 2001).....	64
Table 4.2	State variables predicted and forcing variables required by the model.....	64
Table 4.3	Look-up table for precipitation input.....	69
Table 4.4	The model outputs in five daily averages at GY, 2001-2002.	103
Table 4.5	The model outputs in five daily averages at GY, 2002-2003.	103
Table 4.6	The model outputs in five daily averages at GY, 2003-2004.	104
Table 4.7	Statistical model evaluation.....	123
Table 5.1a	Calibrated model coefficients (Equation 5.1) for Period_1.....	151
Table 5.1b	Calibrated model coefficients for Period_2.....	151
Table 5.1c	Calibrated model coefficients for Period_3.....	151
Table 5.2	Comparison of model results with MODIS for DEM and aspect classes on March 25, 2004	162

Table 5.3	Comparison of model results with MODIS for land use on March 25, 2004	162
Table 5.4	Comparison of model results with MODIS for DEM and aspect classes on April 9, 2004	163
Table 5.5	Comparison of model results with MODIS for land use on April 9, 2004.....	163
Table 5.6	Error matrix for the intercomparison between the model results and MODIS product integrating cloud pixels	165
Table 5.7	Grid by grid comparison of model percent omission and commission errors in different elevation bands.....	167
Table 5.8	Grid by grid comparison of model percent omission and commission errors in different aspect classes.....	168

CHAPTER 1

INTRODUCTION

1.1. General

Snowmelt runoff is a major source for river discharge and groundwater recharge over large areas of the mid-latitudes and is vital for agriculture, hydropower generation, industry and domestic use in these areas (Ferguson, 1999). Snowmelt runoff can also be a significant flood risk (Marks et al., 1998). However, the task of accurately simulating the timing and magnitude of snowmelt runoff is complicated by the great spatial variability in snow processes in mountainous areas (Kirnbauer et al., 1994; Blöschl, 1999). This issue has been approached in a variety of ways, ranging from lumped conceptual models to fully distributed physically based snow process models; the approaches are reviewed, two methods are applied and discussed in the following chapters.

Euphrates and Tigris Rivers and their tributaries served as the cradle for many civilizations that developed in Mesopotamia, 'the land between two rivers'. The Euphrates River, the longest in southwest Asia, is formed by the union of two major tributaries: the Karasu, which rises in the highlands of eastern Turkey, and the Murat, which originates north of Lake Van (Cullen and deMenocal, 2000). The Euphrates-Tigris basin is largely fed from snow precipitation over the uplands of northern and eastern Turkey. A sustained period of high flows during the spring months resulting from melting of the snowpack causes not only extensive flooding, inundating large areas, but also the loss of much needed water required for irrigation and power generation purposes during the summer season (Altınbilek, 2004). Managing several large dams on the Euphrates River and water resources

effectively requires the behavior of the streamflow, particularly during the snowmelt period, be understood and predicted. Thus, snowmelt models can be very helpful in the Upper Karasu Basin of Turkey in this regard.

The work contained in this thesis has evolved directly from previous snow hydrology research; applications of snowmelt models in Turkey have been limited largely to temperature index model applications concentrating on meso and macro-scale. This lumped model application relies solely on basin-wide, optimized parameters for hydrological simulation and oversimplifies the physical processes by neglecting some of the major physical processes controlling melt production. However, the data requirements of physically realistic models are too numerous to make these types of models practical to apply at the meso or macro-scales.

In order to address the need for improved management of the melting snow as a critical resource, an energy and mass balance snowmelt runoff model is applied at automated weather stations designed and upgraded by snow hydrology working group at Middle East Technical University and State Hydraulic Works. In addition, radiation index (modified degree-day) method is applied over a grid based topographic structure of the basin, represented by Digital Elevation Model.

1.2. Objectives

In mountainous catchments where snow is a significant part of the hydrologic cycle, snowmelt is a primary water input to the soil and stream system. Since predicting and understanding the spatio-temporal variability of snow related quantities plays a key role in catchment hydrology, it is essential to simulate snow accumulation and melt accurately. In common with many areas of hydrology (Anderson and Burt, 1990), an alternative and complementary approach to field-based snow hydrology research is the adoption of physically based and operational modeling strategies at different scales with the aim of explaining and ultimately predicting how mountainous snowy hydrological systems function.

Information on timing, magnitude and contributing area of snowmelt under changing climate conditions are required for successful water and resource management. This is achieved through a combined monitoring and modeling approach using some advanced techniques of Remote Sensing (RS) and Geographic Information Systems (GIS). The snow cover is a key link in the climate system via its effect on the surface energy and water balance. Therefore, the first objective of the study is to a better understanding of the key processes that have major impact on the snow simulation and climate effects on the hydrologic cycle with an accurate representation of energy and mass balance of snowpack at a point scale with small time intervals. The second objective of research presented in this study is to develop the distributed version of the process-based snow model with the help of GIS tools and test the model in the meso-scale size headwater mountain catchment of the Euphrates Basin in Turkey with the help of snow covered area products of RS.

Specific aims that are addressed can be summarized as theoretical understanding of snow processes, testing a process based snow model suitable and capable of simulating accumulation and ablation at a point scale, the implementation of the model in a spatially distributed framework across a catchment, the calculation of spatial and temporal variations in snowmelt and validation of model results.

A two layer point model is applied to calculate the energy and mass balance of snowmelt in the Upper Karasu Basin, a tributary to the Euphrates in eastern Turkey, during 2002-2004 snow seasons. The data on snow and climate are provided from automated snow and meteorological stations installed and upgraded to collect high quality data with automated data transfer. Each form of energy transfer is evaluated during snow accumulation and ablation periods using a two-hourly computational time step. The model results are appraised with respect to both temporal distribution -- the model application for three consecutive snow seasons at one site -- and spatial distribution -- the model application to three different sites for one season. The model performance is evaluated comparing the results with observed snow water equivalent, snow depth and lysimeter yield.

In the second part of the study, calculated snowmelt amounts at automatic weather stations are related to radiation index method. A combination of radiation and temperature index approach is used to estimate snowmelt during the melting period of 2003-2004. From the climate and hydrologic viewpoints, the most crucial time for snow modeling is during the spring snowmelt period. A better description of this period could contribute substantially to understanding the relationships between snow cover, atmospheric processes, surface energy and water budgets for different snow cover regimes. Detailed daily time-series climate surfaces necessary to drive distributed model are successfully developed using limited data and relatively simple methods with corrections according to topography. The spatial patterns of solar illumination, albedo and air temperature are used to predict the spatial distribution of melt over the whole watershed. The generated output surfaces are evaluated to determine if they are reasonable approximations of actual conditions in terms of snow water equivalents at stations, snow covered area from satellite products and streamflow records measured at the outlet station of the pilot basin.

1.3. Thesis Outline

The structure of this thesis closely follows the order in which the work was undertaken in response to the aims as they were initially conceived. It consists of six further chapters.

Chapter 2 places the work in the context of previous and contemporary related research. It briefly reviews, snow processes which occur in mountainous environments and approaches to modeling these processes.

Chapter 3 introduces the field site, summaries the techniques used and data collected during the study. Energy and mass balance models require time-series climate surfaces of air temperature, humidity, wind speed, precipitation, solar and thermal radiation to accurately simulate both the development and melting of a

seasonal snow cover in the mountainous basins. Unfortunately, climate monitoring in these basins is very limited; the full range of elevations and exposures that affect climate conditions is seldom sampled. The data on snow and climate are provided from automated snow and meteorological stations installed and upgraded to collect high quality data with automated data transfer. These comprehensive data sets form the basis of modeling work undertaken in subsequent chapters.

Chapter 4 describes the application and results of a physically based snow process model. A coupled energy and mass-balance model SNOBAL is used to simulate the development and melting of the seasonal snow cover in the mountainous basin of eastern Turkey. All energy terms (radiation, turbulent and ground fluxes) are evaluated to understand the key processes that have a major impact on the snow simulation. Model performance is assessed and the implications of the results are discussed.

Chapter 5 takes this work further by incorporating the snow processes model into a distributed framework across the basin. In order to achieve this, a methodology based on calculated melts from point energy and mass balance model application and topography is described. A combination of radiation and temperature index, for the estimation of spatially distributed snowmelt, is applied; model results are tested and discussed. RS products of satellite images from MODIS are used to validate the model performance in terms of snow covered area.

Finally, Chapter 6 summarizes the main results of the previous two chapters, discusses the implications of the work within the context of existing snow and snow hydrology literature, and makes recommendations for further work.

CHAPTER 2

LITERATURE REVIEW

2.1. Snow and Snowmelt

The occurrence of precipitation in the solid form (snow) as opposed to the liquid form (rain) causes a change in drainage basin response to the input of water, because snow is stored in a basin for an extended period of time before it returns into the runoff. At the end of the accumulation period the seasonal snow cover melts in several weeks to months depending on the amount of snow and location.

Engineering applications considering snow as a factor in the hydrologic cycle include hydrologic studies for defining the effect of snow on runoff, design flood determinations, day to day and seasonal runoff forecasting of river flows and water levels. This runoff serves many beneficial uses: as a domestic and livestock supply, irrigation, hydropower generation, wildlife habitat, for recharging soil water reserves and other purposes; conversely, it may cause flooding, soil erosion and drainage problems. Thus, various researchers concerned with water management have a keen interest in the development of methods for predicting the time of melt, the snowmelt rate and the volume of runoff. The derivation of a detailed design flood or forecasting of flood runoff in a snow dominated basin, research and development applications would require more detailed simulation of snow and snowmelt through the use of theoretical and empirical equations as described later.

Although forming only a small subsection of hydrological sciences, snow hydrology is still a mature discipline with a large and varied literature. It would be

difficult to attempt to review all areas; therefore, an emphasis is placed on areas most pertinent to this study, specifically the energy balance of the snowpack and how these processes can be incorporated into distributed models. The important snowpack processes of heat transfer and metamorphism within the snowpack have also a relation with much of the work in this study and are reviewed briefly.

2.2. Overview of Physical Process

The formation of snow and rain in the atmosphere is a dynamic process. Meteorological (air temperature, wind, atmospheric circulation patterns, lapse rate and stability of air mass) and topographic factors (elevation, slope, aspect and vegetation cover) are influencing the amount and distribution of precipitation in the form of snow and the snow water equivalent. Metamorphism has an important impact on a range of snowpack properties, including temperature, density, mechanical stability, porosity and permeability. Freshly fallen dry snow exists in the clearly defined crystalline state with sharply defined edges. Metamorphism of the snow occurs over time, which leads to the characteristic change of freshly fallen snow crystals into larger and more rounded grains. This entire process commonly called “ripening” and is brought about by heat exchanges at the snow surface and ground, the percolation of rain and melts through the snowpack, snowpack settlement and wind packing. The density of the newly fallen snow is typically on the order of 10%, with variations 6-30% depending upon the meteorological conditions involved. As metamorphism occurs, density increases, reaching values of 45-50% at the end of the season. A snowpack ripe for melt also contains a small amount of free liquid water on the order of 3-5%. Melt-freeze metamorphism describes changes in the snowpack that result from the presence of liquid water in the snowpack that then refreezes. This will increase its density and mechanical strength, but obviously reduce its porosity and permeability. As a result of early melt or rain-on-snow events when liquid water percolates into sub-freezing snow, ice layers are generally formed. A ripe snowpack is said to be “primed” to produce runoff when it contains all the water it can hold against gravity. As the snow

reaches its primed condition, the snowpack becomes completely isothermal at near 0°C. Generally, the snowpack is a result of more than one snow deposition event and so it has a layered profile. The layers may have different densities, grain sizes and types, however, once the melt season begins and the snowpack becomes isothermal, equilibrium temperature processes dominate and snowpack structure rapidly becomes much more homogeneous with an increase in density and the loss of distinctive layers (Colbeck, 1982; Elder et al., 1991).

2.2.1. Snow Surface Energy Exchange and Snowmelt

Metamorphism within the snowpack during the accumulation and melt periods is controlled by the energy of the snowpack (Figure 2.1). Energy exchange include shortwave solar radiation, terrestrial/atmospheric longwave radiation, turbulent flux (convective heat transfer from the air and latent heat of vaporization by condensation from the air), energy fluxes associated with exchange of mass (the energy comes with falling rain and is carried away by meltwater) and conduction between the snow and underlying ground. The process of melting snow involves the transformation of snow/ice from its solid to liquid water through the application of these heat energy fluxes from outside sources as in Equation 2.1

$$\Delta H_s + \Delta H_l = R_{net} + H + L_v E + M + G \quad (2.1)$$

where

ΔH_s = change in snowpack sensible heat content (W/m²)

ΔH_l = change in snowpack latent heat content (W/m²)

R_{net} = net all-wave radiation flux across the snowpack surface (W/m²)

H = sensible heat flux across the snowpack surface (W/m²)

$L_v E$ = latent heat flux across the snowpack surface (W/m²)

M = heat flux advected by precipitation across the snowpack surface (W/m²)

G = ground heat flux across the snowpack base (W/m²)

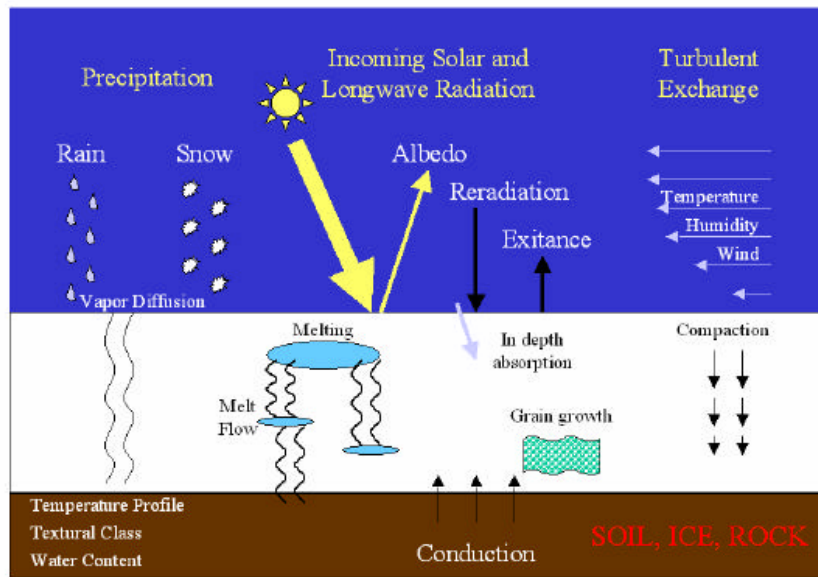


Figure 2.1 Schematic diagram of snow energy exchanges

As spring progresses, daily increases in the net radiation flux into the snowpack surface mean that the energy balance of the snowpack becomes positive as energy gains during daylight hours exceed losses during the night. The temperature of the snowpack increases to 0°C as meltwater percolates down further into the snowpack. Once the snowpack becomes isothermal through its entire depth, meltwater produced at the surface can start to flow out of the base of the snowpack through pores and fingers.

Of these fluxes the radiation exchange is the most important during the day whether one is considering a mountainous terrain, a plains area or a forest. The amount of heat transferred to the snowpack by this prime source of energy at the earth's surface varies with latitude, aspect, season, time of day, atmospheric conditions, forest cover and reflectivity of the snow surface (albedo). Longwave radiation is also an important process of energy exchange to the snowpack. Snow is very nearly a perfect blackbody with respect to longwave radiation. The longwave radiation exchange between the snow surface and the atmosphere is highly variable, depending upon cloud cover conditions, atmospheric water vapor, nighttime cooling and highly dense vegetation as forest cover.

In general, the turbulent exchange process is of secondary importance, although it can have a significant influence on melt rates largely because of its ability to assist or counteract the radiation flux. Turbulent heat exchange between the snow surface and the atmosphere is dependent upon the atmospheric air temperature and vapor pressure gradients together with the wind gradient in the atmosphere immediately above the snow surface. These processes are particularly important under storm conditions with warm air advection and low relative humidity. Therefore, snow hydrology involves two distinct types of runoff situations; snowmelt dominated runoff that is exemplified by spring/summer floods and rain-on-snow events (typical of winter floods). Rain-on-snow has an important influence on the water retention characteristics of snow and water movement in the pack but is of minor importance as an energy flux. Similarly the ground heat flux is small in amount, but it can have an influence over the winter season.

There is an extensive literature describing the different point energy balance processes controlling the rate and timing of changes in snowpack metamorphism and melt (US Army, 1956; de Quervain, 1973; Anderson, 1976; Male and Grey, 1981; Morris, 1983; 1985; 1989; 1991; Marks and Dozier, 1992; Cline, 1997 and Hock, 2003). Overview of the main processes will be given here, but the controls on spatial variations in these processes, which need to be included in a distributed model, will be examined later. There is no process of heat exchange with the snowpack that may be universally applied, but the relative importance of each processes is dependent on atmospheric, environmental and geographic conditions for a particular location and a particular time of season.

2.2.1.1. Net Radiation (R_{net})

For the majority of studies involving radiation at the earth's surface the incoming flux is considered as two separate streams; shortwave radiation originating from the sun, which is generally considered to fall within the wavelength range 0.3 μm to 2.2 μm and longwave radiation from the sky and the surrounding terrain, which

falls between 6.8 μm and 100 μm . The interval between these contain both types of radiation, although it amounts to less than 5 % of the total (Geiger, 1966). The net radiation at a snow surface is described by Equations 2.2 - 2.3

$$R_{net} = S_{net} + L_{net} \quad (2.2)$$

$$R_{net} = (1 - \alpha)S_i + L_i - L_o \quad (2.3)$$

where R_{net} , the net all-wave radiation at the surface, is the sum of net solar radiation, S_{net} , and net longwave radiation, L_{net} . S_i is the incoming or global shortwave radiation, α is the reflected shortwave radiation, L_i and L_o are the incoming and outgoing longwave radiation, respectively. Cloud and forest cover radically influence the relative magnitudes of the shortwave and longwave fluxes, but R_{net} still remains the dominant surface flux for most snow covered terrain. The net shortwave component, primarily governs both the timing of melt and the snowmelt rate; the net longwave flux affects the time of release of snow cover runoff because of its influence on nighttime refreezing and thus on the internal energy status of a snow cover (Granger and Gray, 1990).

Net Shortwave Radiation

Net shortwave radiation, S_{net} , is equal to the incoming shortwave flux (S_i) received by the surface less the amount reflected by the surface (α), that is;

$$S_{net} = (1 - \alpha)S_i \quad (2.4)$$

Incident Shortwave

At a mean earth-sun distance of 149.5×10^6 km, the shortwave flux perpendicular to the sun's rays is equal to the solar constant, 1.35 kW/m^2 . Extra terrestrial flux incident to a horizontal plane at the top of the earth's atmosphere (Q_A) varies with latitude, season and time of day; but at a fixed geographical position and time it is constant. The amount of solar radiation which is transmitted through the

atmosphere and reaches the surface varies with latitude, season, time of day, topography (slope, altitude and orientation) and atmospheric turbidity (Granger and Gray, 1990). While passing through the atmosphere, radiation is reflected by clouds, scattered diffusely by air molecules, aerosols, dust and other particles and absorbed by ozone, water vapor, carbon dioxide and nitrogen compounds. The portion absorbed increases the ambient air temperature which in turn increases the amount of longwave radiation emitted to the earth's surface and outer space.

The total shortwave flux incident at the snow surface (the global radiation, S_i , consists of two components, a direct beam passes and a diffuse component. As the direct beam passes through the atmosphere it is attenuated by both absorption and scattering processes. Both the direct beam radiation and the diffuse components are reflected at the snow surface.

R_{net} in equation (2.1) exhibits large temporal and spatial variability. However, most of this variation results from changes in the shortwave radiation terms. At micro- and meso-scales, spatial variation in S_i results largely from topographical effects. The intensity of direct shortwave radiation receipt is a function of atmospheric attenuation, slope angle, aspect and the amount of shading caused by surrounding terrain (Dozier, 1980; Munro and Young, 1982; Dozier and Frew, 1990; Varley et al., 1996). Temporally, there are predictable seasonal and daily variations in S_i due to changing solar altitude, but this is affected by atmospheric factors, particularly cloud cover which influences both the overall magnitude of S_i and also the partitioning between direct and diffuse components (Oke, 1990). Therefore, the common approach used to model S_i moderates the extraterrestrial shortwave flux by atmospheric transmittance and cloud cover. The transmissivity represents the fraction of the direct beam radiation which is allowed to penetrate a clear atmosphere and reach the earth's surface along the zenith path. Its magnitude is therefore affected by the mass of atmosphere lying between the sun and the earth's surface, the amount of water vapor, ozone, dirt and other impurities it contains. Transmissivity varies with location and is highest in winter and lowest in summer (Granger and Gray, 1990).

Albedo

Incoming solar radiation that strikes the earth's surface is partially reflected and partially absorbed, in proportion to surface reflectivity (Equation 2.4). The ratio of reflected and incoming radiation is termed albedo, which can vary considerably as a function of the condition and age of the snow surface. Darker surfaces have a lower albedo and absorb more solar energy than do lighter surfaces. The albedo values go from "0" (no reflection) to "1" (all reflection) or can be expressed in terms of percent. Table 2.1 shows albedo values for different surfaces.

Table 2.1 Albedo values for different surfaces

Future	Albedo (%)
Fresh Snow	80-90
Old Snow	50-60
Grass	20-25
Forest	5-10

The reflectivity of snow is high compared to other natural surfaces. The reflectance properties of snow vary widely depending on wetness, impurity content, particle size, density and composition, surface roughness, the spectral composition and direction of the illuminating beam. In view of the dominance of the global irradiance at a snow surface, albedo is one of the most important parameters in many hydrologic snowmelt models (Granger and Gray, 1990).

The albedo is highest for light which strikes the snow surface most obliquely. Thus, the proportion of diffuse to direct radiation incident on a surface influences albedo. In general albedo is not a property of snow alone; cloud cover, atmospheric parameters such as the amount of water vapor, the dust concentration and the amount of ozone which influence the spectral distribution of the incident radiation, can in turn influence the albedo. The explanation for an increase in albedo with cloud cover lies in the multiple reflection process between the snow surface and the clouds which involves primarily the diffuse component of the global radiation. Reflectance values for the near infrared part of the spectrum are lower than for the visible part (Granger and Gray, 1990).

The albedo of snow is generally at a maximum after a fresh snowfall and decreases with time due to growth in grain sizes, the accumulation of dust and debris on the snow surface (US Army, 1956). The rate of grain growth increases with snow temperature and in particular with the presence of liquid water (Wiscombe and Warren, 1980; Marshall and Warren, 1987; Brandt and Warren, 1993; Glendinning and Morris, 1999). The most important process controls on albedo are reflected in the parameterization suggested by various authors; Dickinson et al. (1993) and Brock et al. (2000a) proposed a parameterization of albedo as a function of accumulated positive air temperatures since the last snowfall, Brun et al. (1992) proposed a parameterization of albedo as a function of time after snowfall, grain size and grain type, Marks and Dozier (1992) and Marshall and Warren (1987) modeled grain size increase and parameterized albedo in visible and infrared bands as a function of grain size. These parameterizations play a major role in the model performance because albedo is a key factor for calculating the snowmelt. (Essery and Yang, 2001) In addition to temporal variation in the controlling factors of albedo, they can also exhibit large spatial variation (Brock, et al., 2000a).

The decrease in the albedo can be divided into three periods:

Pre-melt: During this period, except for increases produced by snowfall and decreases caused by periodic melt events, albedo decreases at a relatively low, but constant rate, 0.0062/day (Sand, 1990), due to metamorphic processes.

Melt: During melt the decay of albedo (0.071/day, Sand, 1990) is accelerated by changes in the optical properties of the snow cover and the reflection of shortwave radiation penetrating to the ground surface.

Post-melt: Following the disappearance of the snow cover the albedo of the ground surface takes a relatively constant value (0.18/day, Granger and Gray, 1990).

Net Longwave Radiation

A given volume of the atmosphere partially absorbs and partially transmits incident longwave radiation. In contrast to the solar flux, the atmosphere does not scatter longwave radiation and the total longwave flux at the surface is the sum of

the radiation transmitted through the atmosphere and the radiation emitted by the atmosphere. Both the atmosphere and the snow surface emit blackbody longwave radiation that is proportional to the fourth power of its temperature. Thus, the incoming longwave, L_i , outgoing longwave, L_o , and net longwave, L_{net} , radiations (all in W/m^2) can be expressed with the following equations:

$$L_i = (\varepsilon_a \sigma T_a^4) \quad (2.5)$$

$$L_o = (\varepsilon_s \sigma T_s^4) \quad (2.6)$$

$$L_{net} = L_i - L_o \quad (2.7)$$

Where, ε_a is the atmospheric and ε_s surface emissivities, σ is Stefan–Boltzmann constant ($5.67 \times 10^{-8} W m^{-2} K^{-4}$), T_a and T_s are air and surface temperatures (K) respectively.

Incoming longwave radiation is emitted mostly by water vapor in the atmosphere, carbon dioxide and ozone. Variation in L_i is thus largely a result of variation in cloud cover, the amount and temperature of the water vapor. Since the layers of the atmosphere nearest the earth surface ordinarily have the greatest moisture content and the highest air temperature, they have the greatest influence on the atmospheric longwave radiation. The temperature and moisture content of the upper atmosphere have comparatively little variation, so their contributions to the downward longwave radiation are fairly constant (Sand, 1990).

Incoming longwave radiation from the atmosphere is related to the vertical distribution of air mass properties (air temperature, vapor pressure) and the presence of clouds (Obled and Harder, 1979). While several parameterizations are available based on surface air temperature and vapor pressure to relate clear-sky emissivity (Brunt, 1932; Brutsaert, 1975; Satterland, 1979) or effective emissivity, in which cloud cover is incorporated directly (Ohmura, 1981; Konzelmann et al., 1994) there is considerable uncertainty in these estimates due to atmospheric

variability. The coefficients used in the parameterizations are very variable, which is to be expected as they vary with time of year and location. Radiative transfer models overcome some of this uncertainty at the cost of more substantial data requirements, providing profiles of air temperature, water vapor, knowledge of the distribution and concentration of carbon dioxide and ozone (Elligson et al., 1991). In alpine environments, significant spatial variation in L_i can be caused by the surrounding topography. Sky irradiance is reduced by the portion of the sky which is obscured by surrounding terrain, but conversely, additional radiation is received from surfaces on the surrounding terrain; Olyphant (1986) and Plüss and Ohmura (1997) point out both these effects can be significant.

Outgoing longwave radiation, the radiation emitted by and reflected from the snow surface is calculated directly by Equation 2.6. The emissivity of a smooth snow surface varies within a relatively narrow range (dirty snow-0.97; fresh snow-0.99). The accuracy of this estimate depends strongly on the measure of snow surface temperature and therefore it is usually more reliable under melting conditions than under non-melt situations. The data on snow surface temperatures are very scarce and manual measurements are subjected to errors. Since the snowpack reaches isothermal conditions with the surface temperature of 0°C during ablation, the corresponding L_o becomes 315.6 W/m^2 .

Overall, the temporal pattern in R_{net} has two distinct components; on a daily timescale, it tends to be positive during the day as a result of incoming direct solar radiation and negative at night when direct solar radiation receipt is zero and L_o tends to exceed L_i . This daily pattern is superimposed over a seasonal trend whereby R_{net} is negative during mid-winter, dominated by longwave components and then becomes positive during the melt season, dominated by the net shortwave term (Marks and Dozier, 1992; Cline, 1997). This is due to S_i being low during mid-winter when day length is short and solar altitude low and L_o generally exceeding L_i . However, as the melt season begins there is a rapid increase in S_i as day length and solar altitude increase and a decline in albedo over the same period.

2.2.1.2. Turbulent Fluxes (H and L_vE)

The two turbulent fluxes of sensible heat (H) and latent heat (L_vE) can be important sources of energy exchange between the snowpack surface and lower boundary layer of the atmosphere (Morris, 1985; 1989). Not only does significant energy transfer occur by turbulent exchange, but significant mass loss can occur from sublimation. Sensible heat flux is a result of direct contact between the surface and overlying air, the temperature differences determine the direction and the size of the flux. Latent heat energy is gained through condensation of water vapor in the air onto the snow or lost if snow sublimates or liquid water held in the snow evaporates.

A review of the turbulent energy transfer over a specific surface, such as snow, requires a hybrid approach since the turbulent transfer of momentum, heat and water vapor at the snow surface are the most complicated forms of energy exchange and are not easily measured in a natural environment. The data required to calculate them are difficult to measure at a point and they have a highly variable distribution over a topographic surface (Marks and Dozier, 1992). Turbulent fluxes over snow can be measured directly using eddy correlation techniques, but the relative complexity of the instrumentation required to do this leads to rare and limited studies to short time periods (Munro, 1989; Forrer and Rotach, 1997).

Still, the most common way to express turbulent processes is based on relatively simple measurements of temperature, vapor and wind speed gradients (Bruland, 2002). Sensible heat fluxes depend on the temperature gradient and turbulent diffusion due to wind. Latent heat fluxes depend on the vapor pressure gradient and turbulent diffusion due to wind. The rate of energy exchanges between the air and surface depends on surface roughness, wind speed and air stability. High wind speeds transport saturated "old" air away while bringing "fresh" air down to the snow surface. A rough surface creates turbulence that leads to more efficient exchanges of boundary air masses. However, on a very rough surface with, for instance shrubs or tall vegetation, "old" air can be trapped even at high wind

speeds. The air mass stability mainly influences the exchange rate when the air is calm with low wind speeds (Bruland, 2002). As detailed profile measurements are not usually available, the majority of investigators obtain estimates of the turbulent transfer of sensible and latent heat over snow with the use of aerodynamic formula (Brock et al., 2000b; Oerlemans, 2000) where turbulent fluxes can be expressed as:

$$H = \rho_{air} c_{air} C_H u (T_a - T_s) \quad (2.8)$$

$$L_v E = \rho_{air} L_v C_E u (e_a - e_s) \quad (2.9)$$

Where T_a and T_s are air temperature at a reference height and surface temperature (K) respectively, e_a and e_s are water vapor pressure (mb) at a reference height above the surface and at the surface respectively and u is the wind speed at the reference height (m/s). C_H is the bulk transfer coefficient for sensible heat and C_E the bulk transfer coefficient for latent heat. These parameters specify the effectiveness of the transfer process and depend upon aerodynamic roughness lengths and atmospheric stability.

The snow surface temperature is important, first, in determination of the temperature gradient between the air and the snow cover and second, because humidity at the snow surface is calculated as the saturation humidity at T_s . H tends to be small and fluctuate in direction between the snowpack and the atmosphere during the winter as the snow surface temperature follows changes in air temperature when it is below freezing (Marks and Dozier, 1992). However, during the melt season, when air temperatures are normally above freezing, at least during the day, H normally becomes increasingly positive as snow surface temperatures are constrained to 0°C (Cline, 1997). The magnitude of the turbulent fluxes taken together may be less than expected as the two components may be of similar magnitude but opposite direction (Marks and Dozier, 1992). Thus, warm air, which would favor larger sensible heat transfer into the snowpack, also tends to have higher vapor pressure deficits, which encourages sublimation and the loss of latent heat from the snowpack surface.

Beside the net radiation terms, the turbulent fluxes exhibit marked temporal and spatial variations. Spatial variations in the turbulent fluxes results from variations in the driving variables that are wind speed, air temperature, vapor pressure and aerodynamic roughness length. In alpine environments, wind speed (and direction) is strongly influenced by topographical controls causing areas of convergence and acceleration, divergence and deceleration. Air temperatures and consequently vapor pressures, vary with altitude, conforming to elevation lapse rates. Aerodynamic roughness length varies with the magnitude, density of surface roughness features (Lettau, 1969; Munro, 1989; Brock et al., 2000b) and in response to changing snow surface conditions that depend up near-surface metamorphism and wind packing processes (Fox, 2003).

2.2.1.3. Heat Flux Advected by Precipitation (M)

The heat transferred to the snow by rain is the difference between its energy content before falling on the snow and its energy content on reaching equilibrium within the pack. The amount of advected heat into snowpacks by rainfall is generally thought to be small as there is normally only a small difference between the temperature of the falling rain and the snowpack (Neale and Fitzharris, 1997). However, if the snowpack is cold, then considerable heat can be liberated to warm the snowpack if percolating rainfall refreezes (Male and Grey, 1981; Conway and Benedict, 1994). When rain falls on a snowpack which has a temperature below 0°C, some of the rain will freeze in the pack, thereby releasing heat by fusion.

2.2.1.4. Ground Heat Flux (G)

The low thermal conductivity of snow greatly reduces heat exchange between the ground and the atmosphere so that snow serves as an insulating blanket for the underlying surface. The ground heat flux may be positive or negative depending upon the temperature gradient at the snow-ground interface.

In comparison to the net radiation and turbulent fluxes, heat flux conducted into the base of the snowpack from the underlying substrate can normally be taken to be negligible in alpine environments. However, it is generally constant throughout the whole period that the seasonal snow cover is on the ground and so is most important during mid-winter when radiation fluxes are at a minimum (Marks and Dozier, 1992).

2.3. Literature Review on Modeling Snowpack Processes

The topic of snow accumulation, distribution and melting is a large area in the standpoint of general hydrology, which involves the considerations such as the physics of snow formation, effect of terrain cover, determination of areal distribution of snow from point measurements, snowmelt runoff determination. The techniques of analyzing snow in the hydrologic cycle and for quantifying snowmelt rates are described generally in terms of computer modeling of some sort, whether it is a continuous simulation throughout the accumulation and ablation of the snow or a single-event analysis of flood (ASCE, 1996)

There are a number of comprehensive reviews on snow processes modeling, including those concerned with snow model applications (Morris, 1985; Dozier, 1987; Leavesley, 1989; Ferguson, 1999), the use of models in conjunction with remote sensing (Dozier, 1992, Rango, 1993) and the range of spatial modeling approaches (Bales and Harrington, 1995; Kirnbauer et al., 1994). Numerous alternatives present themselves as the best approach for computing snowmelt in hydrological engineering analysis. Melloh (1999) provides an inter-comparison of several snow model algorithms and Slater (2000) compares the performance of several models used in land surface schemes of climate models. Bergstrom (1991) addresses questions of complexity and validation in snow models and Blöschl (1999) offers an overview of scaling issues (Fox, 2003).

2.3.1. Snow Process Models

Snow process models take many forms and are used for a variety of purposes. These include predicting catchment's runoff in operational hydrological models (Melloh et al., 1997), providing lower boundary conditions and hydrology in atmospheric circulation models (Essery, 1997) and predicting impacts of snow processes in ecological studies (Groffman et al., 1999). Many of the snow models are now used for various applications such as hydrology, global circulation model, monitoring, snow physics research and avalanche forecasting (Essery and Yang, 2001).

The degree of complexity of these models is highly variable from simple index methods to multi-layer models simulating the snow cover stratigraphy and texture. There have been many advances made in the understanding of snow processes using models (Marsh, 1999) from all parts of the spectrum of model complexity, but the two most commonly applied approaches are temperature index models and physically based models using full solutions of the energy and mass flow equations. In addition to these two approaches the hybrid models, methods in between index and energy balance models, become applicable recently.

Each of the heat fluxes listed in Equation 2.1 is, in itself, a function of several components, some of which can be difficult to quantify for practical applications. In actual practice then, the theoretical relationships involved are reduced to empirically derived equations that have been found to work satisfactorily in simulation models. The energy budget solution employs equations that represent key energy fluxes and temperature index solution uses air temperature as a primary independent variable through the use of fixed or variable melt rate factor instead of full solution of Equation 2.1. The choice of methodology to employ depends upon data availability, the amount of effort to be expended and the type and scale of application involved.

2.3.1.1. Temperature Index Model

The degree-day method, for snowmelt runoff calculations, has been used in different ways for almost 70 years. Several operational models used to forecast runoff from mountainous areas use temperature index approach, including the Snowmelt Runoff Model (SRM) (Martinec, 1975; Martinec et al., 1994) and HBV (Bergstrom, 1975; SMHI, 1996). The main advantage of this approach, the importance of which can not be underestimated when working on mountainous environments, is that data requirements may be limited to average daily air temperatures, the most easily measured and widely available meteorological variable. The method has been shown many times to produce accurate runoff predictions for alpine drainage basins (WMO, 1986). Since temperature is one of the key climate variables to be affected by climate change, the approach is easily adaptable to evaluation of various climate change scenarios associated with a temperature change (Rango and van Katwijk, 1990; Martinec, 1989). However, this is also potentially their biggest drawback to use air temperature only as other factors control melt rates. In particular, radiation is often the most important factor controlling melt rates in mid-latitude mountainous areas and though air temperature and net radiation may be correlated (Ferguson, 1999) simple temperature index models can not incorporate variation in radiation receipt directly. These models physically lump all the components of the surface energy balance into a degree day factor, which is a proportionality coefficient that calculates melt rates on the basis of air temperature (normally in excess of some threshold value) alone. While temperature is reasonable good index of energy flux in heavily forested areas, it is less so in open areas where shortwave radiation or wind velocity play a more important role in the melt process. Even though air temperature is an important control over turbulent fluxes, wind speed and surface roughness also play a role and are not included in a degree day factor, along with other controlling factors which change during the course of the melt season such as albedo, thermal properties of the snowpack and snow cover continuity. Most temperature index models operate on a daily time step, so that no information can be available on the diurnal variations in meltwater flux and surface refreezing.

In Turkey, early model studies using HEC-1, which is an interface model in a watershed modeling system, is carried out to simulate precipitation/runoff process based on degree day model in a pilot study area. The model calculates discharge hydrographs from storm events (Şensoy, 2000; Şensoy and Şorman, 2001; Şensoy et al., 2003). The Snowmelt Runoff Model, SRM is applied in the Upper Euphrates River Basin using depletion curves methodology with the use of NOAA images for the years 1997 and 1998 (Kaya, 1999; Tekeli 2000). SRM and HBV are also being under study using MODIS images by Tekeli (2005) and Şorman (2005), respectively. Another study is also applied using SLURP (Lacroix and Martz, 1997) model at a smaller scale (Uzunoglu, 1999). The predicted hydrographs are compared and model threshold parameters are determined using models. Conclusions are drawn out about which kind of models are more suitable for different basin characteristics and sizes (Şorman et al., 2001, Şorman et al., 2002).

2.3.1.2. Energy Balance Models

The snowmelt process is dependent on the net heat exchange between the snowpack and its environment. The use of temperature index to predict rates of snowmelt is accepted to be a considerable simplification of the energy balance. Thus for computing the amount of melt the only strictly correct way is using the energy and mass balance approach since it is the physical framework of the snowmelt models. The primary advantage of using physically based snow process models, like all physically based hydrological models, is that in theory they have applicability in a wide range of conditions, environments and provides valuable research data. Their big disadvantage is the extensive amount of input data required for forcing, testing and the measurement of these variables is complicated. These data may be available for experimental simulations, but present major difficulties when these models are utilized in spatially distributed frameworks. The different sources and processes influencing heat transfer to and from a snowpack are largely variable both in space and time.

Several groups continued to develop energy balance snowmelt models as research tools. All of these involved some level of parameterization of the forcing inputs, the physics of the energy balance or the spatial distribution across the topographic structure of the sites. Those models that retain accurate representation of the energy balance and snow cover structure are generally point applications or simulations over small experimental sites. The SNTHERM model (Jordan, 1991) accurately simulates snow cover energy and mass balance, but requires extensive forcing and snow cover structure data. Flerchinger and Saxton (1989) developed the SHAW model to simulate the energy and mass balance of the soil and snow cover as a system. This model accurately represents the processes involved, but is too complicated to explicitly distribute over a grid. Flerchinger et al. (1994) used SHAW model in point mode showing that a physically based model could provide detailed information on how spatially and temporally varying snowpack impacts basin hydrology and soil moisture. Tarbaton et al. (1995) showed that UTAH energy balance model (UEB) is too complicated for a distributed application over areas larger than a few hectares. In general, only the more parameterized models have been widely applied over mountain drainages. The USGS PRMS model (Leavesley et al., 1983) is one such model that has extensively parameterized the critical energy exchange processes and is only quasi-distributed, relying on a limited number of topographic zones. Though it can be applied over larger basins, its limited representation of complex hydrologic processes leaves much to be desired (Risley et al., 1997).

The snow cover energy and mass balance model (SNOBAL) presented in this thesis represents the physics of the snow cover energy balance and snowmelt and has been shown to accurately represent both the development and ablation of the snow cover during a wide range of climate, snow cover conditions and geographic locations (Marks et al., 1998). The grid based, spatially distributed version of this model, ISNOBAL, is explicitly distributed over a topographic grid.

Different models simulate the surface energy balance in similar ways with more or less complex treatments of albedo and often ignoring the less important energy

terms. However, there is considerable variation between models in the ways in which the internal distribution of heat and mass are represented within the snow profile. The most complex 'layered models' utilize vertically distributed implementations of coupled partial differential equations to represent heat and mass transfer (Anderson, 1976; Brun et al., 1989; Jordan, 1991; Morris et al., 1993). These models simulate details of snowpack stratigraphy, temperature gradients and meltwater movement. They are perhaps most suitable for examining processes occurring on short, hourly times scales, such as nocturnal refreezing of the surface and meltwater outflow from the base of the snow. However, many models that incorporate energy balance schemes at the snowpack surface treat the snowpack as a single, lumped layer as in the SHE model (Morris, 1982; Abbot et al., 1986) and the DHVSM (Wigmosta et al., 1994). In these models, internal state variables such as temperature or density are treated as average values for the whole snowpack. There have been a number of comparative studies between single and multilayered snow models (Morris, 1982; Blöschl and Kirnbauer, 1991) and these have concluded that single layer models do not accurately predict timing and magnitude of melt when there is nocturnal refreezing of the snowpack surface. (Fierz et al., 2003) These studies established that processes internal to the snow cover are important for improved performance and understanding in most of the cited applications (Essery and Yang, 2001). Not only do we need to account for surface properties for modeling, but internal processes such as heat conduction through and phase changes within the snow cover have to be included. One approach to address this need is used in the SNOBAL and ISNOBAL models (Marks et al., 1999a; Link and Marks, 1999) in which there is a thin surface layer of fixed thickness, which accommodates nocturnal freezing and a lower layer that varies in thickness dependent on mass and density. Alternative approaches are used in the SNAP model (Albert and Krakeski, 1998), which simulates the penetration of the nocturnal freezing front using the heat transfer function and in the model of Kondo and Yamazaki (1990), which relies on simplifying the representation of internal heat transfer to an ordinary differential equation. A major limitation with both these models is that they can not successfully simulate premelt season conditions when the snow profile is below 0°C at depth (Fox, 2003).

2.3.1.3. Hybrid Models

Given the advantages and disadvantages of both temperature index and physically based models discussed above, attempts have been made to generate hybrid approaches, which efforts to keep the simplicity of the degree day approach, but also explicitly represent other important components of the surface energy balance, principally radiation. Although physically realistic models can be implemented at the micro-scale, the data requirements are often too numerous to make these types of models practical to apply at the meso- or macro-scales. On the other hand, the standard lumped model approach often oversimplifies the physical processes (Hamlin et al., 1998). There is a gradual transition from temperature index type models to energy balance type models by increasing the number of input variables into model formulations. The most common addition though to temperature index type models is the simple incorporation of measured shortwave radiation (Martinec, 1989) or net radiation (e.g. Martinec and de Quervain, 1975; Ambach et al., 1981; Kustas and Rango, 1994; Brubaker et al., 1996).

Just as these hybrid models occupy the grey area between temperature index and physically based models in terms of their complexity, recent developments are moving them into the area where they can be considered as distributed models (Fox, 2003). Only a few studies have attempted to apply extended formulation of temperature index models in a distributed manner (Cazorzi and Fontana, 1996; Hamlin et al., 1998; Dunn and Colohan, 1999; Hock, 1999; Daly et al., 2000). These generally calculate melt rates as a function of some radiation index derived from topographic information, although the model developed by Daly et al. (2000) uses distribution a melt factor on the basis of an antecedent temperature index. Dunn and Colohan (1999) divided the model domain in slope and aspect classes and vary the melt factor as a function of snow albedo, rainfall rate and the partitioning of incoming shortwave radiation. Cazorzi and Fontana (1996) used monthly raster maps of clear-sky all-wave radiation, with melt rates calculated for each topographic grid. Hock (1999) proposed a further development of this idea, varying the melt factor on an hourly basis for each grid according to the temporal

and spatial variation of clear sky direct radiation, calculated using standard solar algorithms. The model developed by Hock (1999) was found to considerably improve simulations of spatial and temporal variations in melt rates compared with a model using a single degree-day melt factor and only little additional improvement in model performance was achieved using a fully distributed energy balance model. Adding a radiation extension to HBV led to an improvement in model performance in small upland catchments (Braun and Lang, 1986; Braun et al., 1994). Hamlin et al. (1998) was found that the radiation index model, while more data intensive, produced better results than that of simple temperature index model during the calibration process. Williams and Tarbaton (1999) described the ABC model, which is both simple enough to use in practical applications for melt estimations over large areas and rigorous enough to capture the fundamental physics of melt and to provide spatially explicit estimations, as an efficient way to predict the spatial distribution of snowmelt in a watershed.

2.3.2. Spatial Variation in Snow Process Models

With both technical and theoretical advances in our understanding of snow hydrology, there has been growing awareness of the importance of the heterogeneous nature of the snow cover over a wide range of scales. In snowmelt models, adequate representation of the most important aspects of the spatial variability occurring at a number of scales in both snow accumulation and ablation is essential if the timing and magnitude of snowmelt runoff are to be accurately simulated (Bales and Harrington, 1995; Blöschl, 1999; Kirnbauer et al., 1994).

Incorporating spatial variations into snow models can be achieved through either:

- a 'lumped' approach using effective parameters or distribution functions (implicit parameterization)
- a 'distributed' approach through subdivision of the model domain (explicit representation) (Blöschl and Sivapalan, 1995).

2.3.2.1. Lumped Model Approach

The general approaches for implicit parameterization of variation in snow process modeling fall into two categories: using effective parameters and using distribution functions of fluxes or state variables. Effective parameterization assigns a parameter value that represents the 'average' value for parameter variation at scales smaller than the model element. This approach is often used for distributed models with fine grid scales for which it is implicitly assumed that point parameter values can be used for the whole model cell (Arnold et al., 1998; Cline et al., 1998; Hartman et al., 1999). However, defining effective parameter values can be problematic. The heterogeneity of the process represented by an effective parameter may not be known, which makes defining an average value difficult (Fox, 2003). Distribution functions are most commonly used to define internal distributions of state variables for catchment-scale model elements (Ferguson, 1986; Turpin et al., 1999) although recent work has begun to consider their use for grid-scale model elements in distributed models (Liston, 1999; Liston et al., 1999; Luce et al., 1999).

2.3.2.2. Distributed (Semi-Fully) Model Approach

In explicit approaches to modeling, the spatial variations in snow processes are represented through subdivision of the modeled domain into grid-scale model elements that have their own parameters and state variables. One of the first issues to consider in spatially distributed models is the extent of spatial disaggregating (Fox, 2003). The development of distributed hydrological models over the last decade has led to a variety of rationales for basin discretization (Kite and Pietroniro, 1996). For example, a technique proposed by Wood et al. (1998) requires discretization of the basin into representative elemental areas (REA). The REA is defined as an areal element within a basin where the hydrological properties are definable and would not be significantly different if a smaller scale of discretization were used. Basin discretization can be based on the grouped

response unit (GRU) approach (Kouwen et al., 1993) which is derived from REAs. A GRU is defined as a spatial unit of a watershed that can be characterized by spatially constant rainfall/snowmelt and in which runoff generation dominates the response (Hamlin et al., 1998)

A wide number of model studies have employed elevation zones as a means to explicitly represent spatial variation in snow processes (Martinec, 1975; Blöschl et al., 1990; Bell and Moore, 1999; Turpin et al., 1999). Models which only use elevation for spatial subdivision are often referred to as 'semi-distributed' models. Elevation banding may be fixed (Bell and Moore, 1999; Swamy and Brivio, 1997; Turpin et al., 1999), or dynamic, varying according to the position of the snow line and zero degree isotherms (Blöschl et al., 1990). The general tendency for a deeper snowpack at higher elevations is captured by the use of elevation zones, but the model elements are often large, internally disparate and do not allow for other controls of topographic features on snow accumulation or melt rates. This subject will be discussed in Chapter 5 with the use of remote sensing satellites as well as the topographic features generated from digital elevation model (DEM).

An alternative form of spatial disaggregation is a fully distributed approach, in which a model domain is often divided into the grid cells of an underlying DEM. Such spatially distributed approaches have been common in rainfall-runoff modeling for many years (Abbot et al., 1986; Wigmosta et al., 1994) and have also now gained popularity in snow hydrology (Blöschl et al., 1991a; Blöschl et al., 1991b; Davis et al., 1995; Melloh et al., 1997; Arnold et al., 1998; Cline et al., 1998; Hartman et al., 1999; Luce et al., 1999; Marks et al., 1999a; Anderton et al., 2002). The increase in popularity of fully spatially distributed snow process models has been due, at least in part, to increasing availability of remote sensing imagery, digital elevation models and larger computing power (Fox, 2003).

Spatially distributed snow process models have recently shown their potential to improve operational hydrology and they have become an area of intensive research development (Davis et al., 2001). However, their use in snow hydrology is

facing the same challenges that have been encountered previously in other areas of hydrological sciences (Beven, 1993; Blöschl and Sivapalan, 1995; Beven, 2001). Within each grid-scale model element, most models have to assume laterally isotropic conditions in boundary conditions and state variables. Analysis of the heterogeneity of the topography and land cover can be used as a guide to select suitable model element scales (Blöschl, 1999). Practical scales of application for distributed snow models are determined by the resolution of the data available for model parameterization and by computational requirements, especially for larger catchments or where the snowmelt model is being run as part of a wider hydrological model. Typically minimum grid scales are of the order of tens of meters for small catchment applications (Blöschl et al., 1991a,b), ranging to hundreds of meters for larger catchments (Marks et al., 1999a). Most authors have assumed that spatial heterogeneity at sub-grid scales can be neglected, although some recent work has addressed this issue (Liston, 1999; Luce et al., 1999). Inevitably, the model scale affects model outcome (Brun et al., 1994; Kite, 1995; Cline et al., 1998). Once a catchment has been divided into individual grid-scale model elements at a suitable resolution, model inputs including local parameter values, initial conditions and driving variables must be defined for each model run (Susong et al., 1999). The difficulty of doing this should not be underestimated particularly in environments where data acquisition is difficult and meteorological stations are few and located at low elevations.

The spatially distributed snow process models rely on extrapolating meteorological driving variables on the basis of physical relationships with topography. The variables that can be extrapolated with the highest level of certainty are air temperature and net radiation, which is fortunate as these variables are normally used to determine whether precipitation falls as rain or snow, and are the dominant control on melt rates. However, even lapse rates used to extrapolate measured air temperature to individual cells can vary greatly over space and in time. The models have been developed to compute spatial variation in incoming shortwave radiation for use in fully distributed models (Dozier, 1980; Munro and Young, 1982; Varley et al., 1996). A simpler approach is to extrapolate

measured incoming shortwave radiation across the model domain to each grid cell. The spatial distribution of some other meteorological inputs is often much more difficult to quantify. This is particularly true for meso- and microscale distributions of precipitation, wind speed and direction. With regard to precipitation, the record at the meteorological station may be in error due to systematic undercatch by rain gauges, especially in windy conditions. Although there had been considerable work on blowing snow prior to the late 1970s (Dyunin, 1959; Budd et al., 1966; Schmidt, 1972) attempts to represent the redistribution of snow by wind in a physically based manner are still at a preliminary stage (Essery et al., 1999; Liston and Sturm, 1998). Table 2.2 presents a summary of the extrapolation methods used to spatially distribute a number of meteorological driving variables in some of the models referred to in this section (Fox, 2003).

Table 2.2 Summary of the extrapolation methods for meteorological variables (Fox, 2003).

Variable	Method	Reference
Air temperature	Fixed elevation lapse rate	Blöschl et al., 1991a; Arnold et al., 1998; Cline et al., 1998; Hartman et al., 1999; Marks et al., 1999a; Anderton et al., 2002
	Variable elevation lapse rate	Martinec et al., 1994
	Kriging of detrended data	Susong et al., 1999
Shortwave radiation	Topographically-based clear sky model	Hartman et al., 1999
	Topographically-based clear sky model with cloud cover correction	Blöschl et al., 1991a; Arnold et al., 1998; Cline et al., 1998; Susong et al., 1999; Anderton et al., 2002
Longwave radiation	Relationships with air temperature and vapor pressure	Blöschl et al., 1991a; Arnold et al., 1998; Cline et al., 1998; Susong et al., 1999
Vapor pressure	Elevation lapse rate	Susong et al., 1999
	Relationship with air temperature	Cline et al., 1998; Hartman et al., 1999
Wind speed	Physically-based wind model	Hartman et al., 1999
	Elevation lapse rate	Cline et al., 1998; Susong et al., 1999
Precipitation	Elevation lapse rates	Hartman et al., 1999; Susong et al., 1999
	Relationship with variety of terrain variables	Blöschl et al., 1991a
Drift factors	Based on field SWE measurements	Luce et al., 1999

Elder et al. (1998) used binary decision trees to interpolate from a detailed snow survey, in order to estimate the spatial variability in snow depth and SWE for basins with great extremes of topography, energy balance and elevation. Such a technique was able to explain 60-70% of the observed variance of SWE. Using a very different approach, Cline et al. (1998) used a combination of a distributed energy balance model and satellite images over the melt period to evaluate the spatial variations in SWE over a complex mountainous basin. Although this approach cannot forecast SWE, it may be useful if year to year similarities in SWE variability can be used along with meteorological parameters (Marsh, 1999).

2.3.3. Comparison of Modeling Approaches

Several studies have compared some of the different ways of incorporating spatial variation into snow process models (Fox, 2003). The most important of input and output of any snowmelt model is the snow water equivalent (SWE) which determines the volume of water available for runoff generation. Snow covered area (SCA) is often defined as the percentage that influences basin wide SWE. Snow depletion curve to areal mean SWE and snow depth are fundamental tools to represent snow cover distribution and have been included in most of the operational models such as SRM. Blöschl et al. (1991a) compare the performance of a fully spatially distributed model, a semi-distributed model based on elevation zones and a lumped snow process model with a SWE-SCA relationship similar to that proposed by Ferguson (1986). They found the fully distributed model gave the best estimate of SCA variation over time, but that the lumped model gave almost as good predictions of melt runoff as the fully distributed model. They suggested the better performance of the fully distributed model in predicting SCA was due to its ability to accurately simulate both SWE and spatial variation in the energy balance (Fox, 2003). Hock (1999) compared the results of a conventional temperature index model, a distributed temperature index model and a fully distributed energy balance model. She found that the distributed temperature index model simulated stream discharge much better than the conventional

degree-day model and performed almost as well as the fully distributed energy balance model. Hartman et al. (1999) found that incorporating snow redistribution by wind significantly improved predictions of both SWE distribution and melt runoff in a catchment. Similarly, Luce et al. (1998) found that winter redistribution of snow by wind was more important than spatial variation in energy balance in the spring in controlling the evolution of basin averaged SWE during the melt season. In further work, Luce et al. (1999) found a lumped distribution function model with a parameterization of spatial variation in SWE distribution performed as well as a fully distributed energy balance model in terms of basin average SWE. Anderton et al. (2002) also found that initial SWE distribution at the start of the melt season was nearly as important as spatial variation in energy balance in controlling SWE evolution for a very small catchment in the Pyrenees. However, in such a small catchment micro-scale variation in meteorological driving variables was limited and melt rates were similar across the catchment (Fox, 2003).

CHAPTER 3

FIELD SITE AND INSTRUMENTATION

3.1. Field Site

The Euphrates and Tigris rivers and their tributaries served as the cradle for many civilizations that involved in Mesopotamia, 'the land between two rivers'. The Euphrates River, the longest in southwest Asia (2700 km), is formed by the union of two major tributaries: the Karasu which rises in the highlands of eastern Turkey north of Erzurum and the Murat which issues from the north of Lake Van (Cullen and deMenocal, 2000) (Figure 3.1). The Euphrates-Tigris basin is largely fed from snow precipitation over the uplands of northern and eastern Turkey. The characteristic feature that distinguishes the hydrological regime of the Euphrates-Tigris river system is the irregularity of flow both between and within years with large floods originating from the snowmelt in spring. About two thirds of the precipitation occur in winter and may remain on the form of snow for half of the year. The concentration of discharge over the months of April and May causes not only extensive spring flooding, inundating large areas, but also the loss of much needed water required for irrigation and power generation purposes during the summer season (Altınbilek, 2004).

The Karasu Basin, a sub-basin of the Euphrates River, is chosen as a pilot basin for the application of the snowmelt models. The basin, located in Karasu Basin in the eastern part of Turkey, is controlled by the stream gauging station EIE 2119 under the supervision of General Directorate of Electrical Power Resources Survey and Development Administration (EIE). The total catchment area is 10,144 km² and the elevation ranges between 1125 m and 3487 m a.s.l. The location of the pilot basin,

Karasu Basin; the stream gauging stations together with the stream network are shown in Figure 3.1. The region is rather mountainous, in which most of the water originate from snowmelt at the higher elevations and contribute sequentially to dams Keban, Karakaya and Atatürk on the Euphrates River. When the long-term analysis of the hydrographs of runoff station EIE 2119 is examined, it can be seen that about 65-70% of total annual volume contribute to the flow during the snowmelt period (Kaya, 1999).

The snowmelt model applications in this study focus on three measurement sites details of which are given in the forthcoming pages. Therefore, the study area is basically the headwaters of Karasu Basin, the Upper Karasu Basin, represented by the drainage area of stream gauging station 2154 (40° 45' E - 39° 56' N). The basin has an area of 2818 km² and the elevation within the basin ranges from 1640 to 3112 m, as observed from the digital elevation model (DEM) of the basin derived from 1/25,000 scale maps. The basin is surrounded by high rock peaks to the north, north-east and south-east (Figure 3.2) with the following characteristics; mean slope of the whole basin is 10.3% and in terms of aspect, the basin has 42% south-southwest-southeast facing, 39% north-northwest-northeast facing, 10% west facing, 7% east facing and 2% of it is flat. Hypsometric mean elevation of the basin is about 2112 m and topographic characteristics of the basin under five zones are shown in Table 3.1 in terms of elevation-area relation. Pasture and poor pasture as a land cover constitutes 59% of the whole basin: bareland and fallow are 14% and 10%, respectively and forest cover is only 1.5% of the total basin area (Akyürek and Şorman, 2002).

The seasonal snow cover begins to accumulate in late November or early December. During winter nearly all precipitation falls as snow and partial areal precipitation event are common in the catchment. During spring and early summer, mixed rain/snow events occur. The climatic characteristics give rise to a typical hydrological regime: low flows generally prevail over the winter which is followed by a sustained period of high flows during the spring resulting from melting of the winter snowpack. Flow generally declines after snow disappears

from the catchment in early summer. Snow covered area of Turkey within the global framework in Northern Hemisphere can be seen in Figure 3.3.

The area is predominantly steppe (a plain without trees other than those near rivers). It is similar to a prairie, although a prairie is generally reckoned as being dominated by tall grasses, while short grasses are said to be the norm in the steppe. It may be semi-desert, or covered with grass or shrubs, or both depending on the season. The term is also used to denote the climate encountered in such regions, too dry to support a forest but not so dry as to make it a desert.

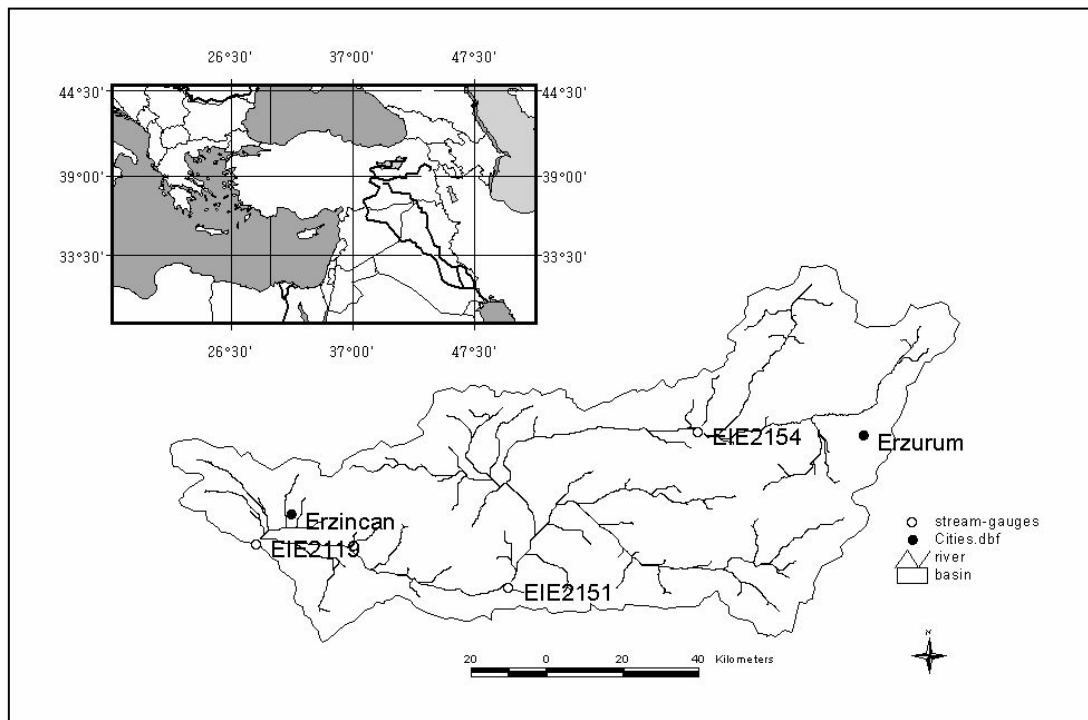


Figure 3.1 Location of Karasu Basin (Upper Euphrates River) in Turkey and the locations of stream gauges in the basin.

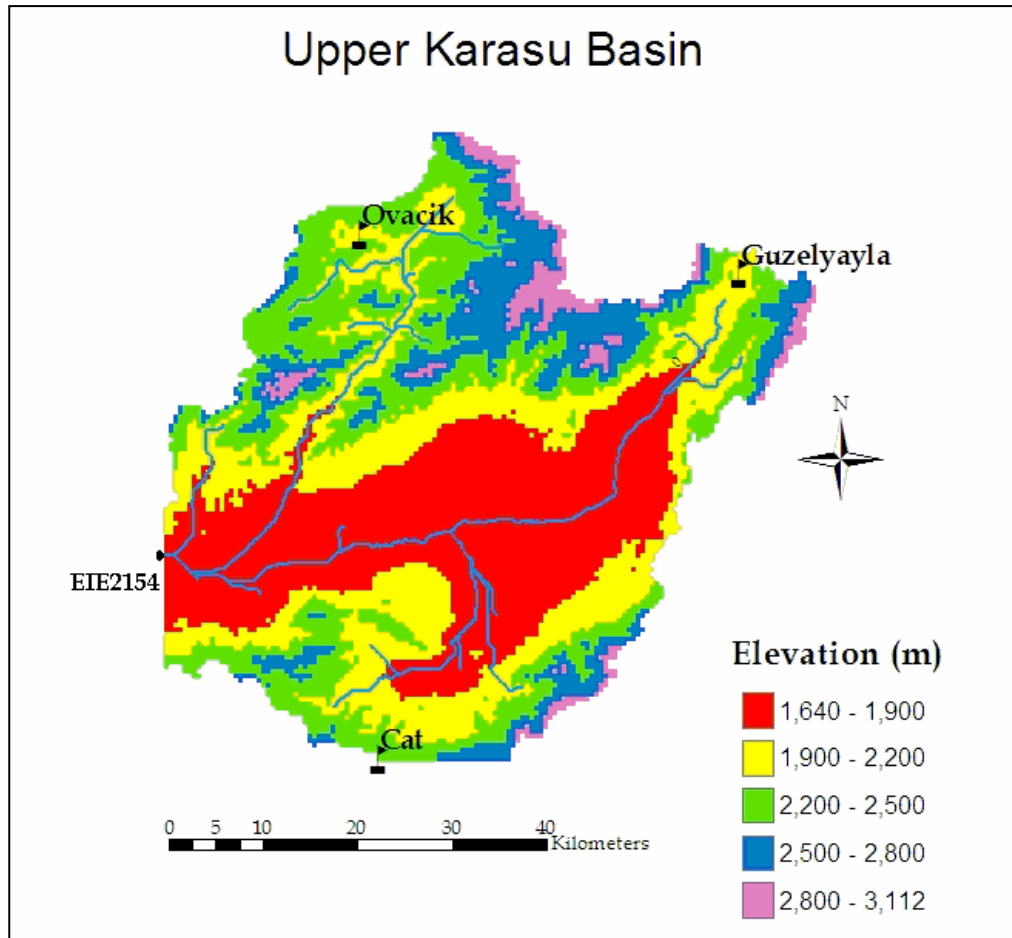


Figure 3.2 DEM of the Upper Karasu Basin with the locations of automatic weather (flag in notation) and runoff gauging stations.

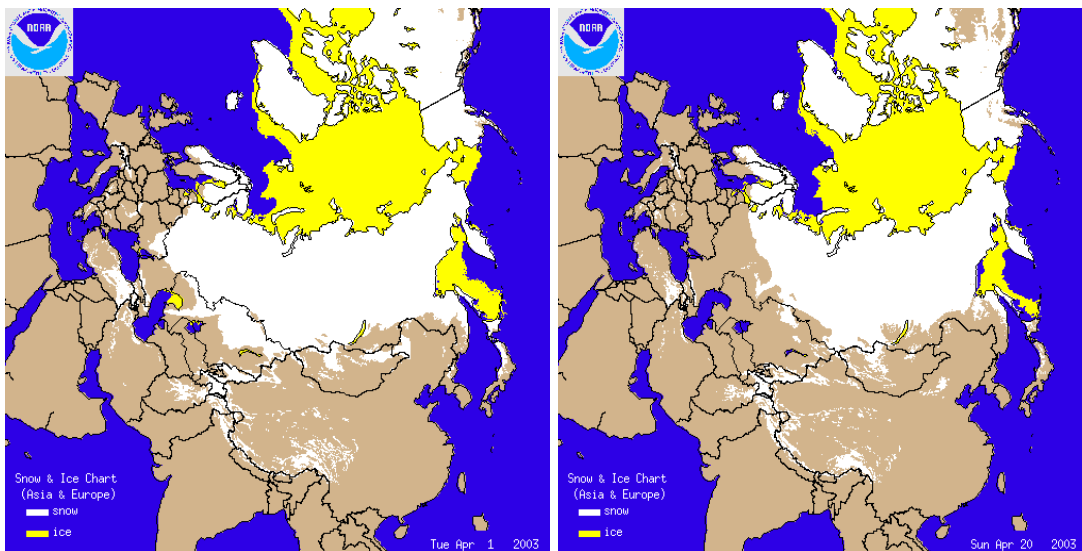


Figure 3.3 Snow condition of Turkey for 1 and 20 April, 2003 (NOAA, 2003)

Table 3.1 Topographic characteristics of the Upper Karasu Basin by elevation zones

Elevation Range (m)	Area (km ²)	Area (%)	Slope (%)
1640-1900	900.2	31.95	3.0
1900-2200	746.9	26.51	11.3
2200-2500	698.2	24.78	15.1
2500-2800	369.4	13.11	16.0
2800-3112	102.8	3.65	13.7
1640-3112	2817.5	100	10.3

The snow process model application of energy and mass balance focus, especially, on three automated weather stations (AWS), namely Güzelyayla, Ovacık and Çat (Figure 3.3). Güzelyayla Station (GY) is at 2065 m elevation and located on the northeastern edge of the Upper Karasu Basin. The study site can be described as flat from the point of view of topography. The general climatological conditions indicate that it is a cold, dry and windy location. It has an unobstructed fetch in the prevailing wind direction of north-east to south-west. Ovacık Station (OVA) is at 2130 m elevation and located on the north- northwest edge of the Upper Karasu Basin. The general climatologic conditions indicate that it is very cold and dry location. In contrast to the other stations, where average wind speeds are around 3.5 and 4 m/s during the snow season, wind speeds are rather lower at OVA, taking an average value of 1.5 m/s. Çat Station (CAT) is located at 2340 m elevation, which is the highest snow-meteorological station in Turkey, and it is at the south boundary of the Upper Karasu Basin. The wind effect is more pronounced at this site than the others though being the highest station, mean air temperatures are very similar to those at GY. It has also an unobstructed fetch in the prevailing wind direction of northeastern to southwestern. OVA and CAT has a mild slope from the point of view of topography and south facing aspect. All of the sites can be described as open in terms of vegetation.

There are two more AWS in and around Karasu Basin that are not utilized directly in this study but rather used for data interpretation; Hacımahmut (HM) is located at 1950 m where the climate conditions are mild and Sakaltutan (ST) is located at

2150 m and provides scarce data. There are also two non-automated stations operated by Turkish State Meteorological Service (DMI); ERZ is at airport (1758 m) and ERZ_CITY is at the city center (1869 m) and mostly affected from micro-climatological conditions.

3.2. Instrumentation and Data Management

It is hard, dangerous and expensive to get snow data from higher altitudes and snow study is also hard especially for extreme climatic conditions. However, it is essential to characterize climate conditions over the snow surface in mountainous watersheds of eastern Turkey to evaluate the effect of these parameters have on snow accumulation, distribution and snowmelt, which then will produce water resources potential for the large dams on Euphrates River.

The science and practice of hydrology includes managing, assessing and forecasting the quantity and quality of water. Both historical and real-time hydrological data are collected, stored and analyzed. An important prerequisite is the availability of accurate and reliable data. In developed countries, virtually all data collection made by agencies with official program responsibilities and is available in computer databases. In addition to storing data, the databases allow for data retrieval, report generation, statistical analysis, model calibration and input data preparation for hydrologists and model users. Unfortunately, Turkey does not have such an archiving agency and data source in terms of snow studies. Therefore, one of the main aspects of the present research is the formation of the snow database. The ultimate goals of graphical, tabular output, statistical analysis, geographic information system integration capability and report availability should be satisfied with the help of governmental organizations.

The data requirements for a fully energy budget approach are available only for hypothetical design conditions and specifically well instrumented watersheds. Investigations of the snow cover energy balance and snowmelt in remote alpine

watersheds require detailed monitoring of the surface climate. Snow metamorphism, melting and runoff are controlled by the magnitude of energy available to drive these processes and these energy fluxes are determined by the combination of local meteorological inputs of precipitation and energy. Table 3.2 summarizes the possible data types that are needed in snow hydrological analysis along with comments on the purpose and application of the data from a specifically instrumented watershed. (ASCE, 1996)

Table 3.2 Data requirements for snow analysis (ASCE, 1996)

Data type	Physical process measured or indexed	Analysis application
Snow water equivalent	Estimate of precipitation Index to basin water supply Snowpack quantity during ablation	Hydrograph analysis Water supply forecasting Modeling snowmelt
Snow depth	Estimate of SWE, precipitation Estimate of weight	SWE applications Snow load on structures
Snow density	Estimate of SWE, precipitation Condition of snow	SWE, precipitation application Avalanche conditions, loads
Areal snow cover	Extent of basin snow cover Snow line elevation	Model calibration Parameter in forecasting models
Precipitation	Estimate of SWE Rain on snow Basin moisture input	Hydrograph analysis Water supply forecasting
Air temperature	Rain/snow interface Index to all energy exchanges Factor in energy budget estimates	Modeling snow accumulation Modeling snowmelt
Snow albedo	Solar energy absorption	Modeling
Solar radiation	Solar energy flux	Modeling
Longwave radiation	Longwave energy flux	Modeling
Wind velocity	Factor in estimate of convection/ condensation energy flux and sublimation	Modeling
Humidity	Factor in estimate of condensation energy flux and sublimation	Modeling
Streamflow	Continuous discharge Runoff volumes	Water supply analysis, forecasting Model calibration

In this study, the data are required for: a) application and testing of energy and mass balance model concentrating on surface energy balance, melt rates and runoff at representative points, b) application and testing of distributed version of the simplified process model. Therefore, driving variables including a time series of meteorological variables are used to calculate snowpack surface energy balance. Computing hydro-meteorological elements on the basis of discretely defined grid cells for distributed modeling requires physical data related to the characteristics of the watersheds.

The project sponsored by NATO-SfS TU-REMOSSEN (1996-2000) provided the installation of new snow and meteorological gauging stations at higher elevations (1800-2400 m) of the mountainous study area. At that moment, most work has been done using index methods which do not require detailed snow and climate monitoring. A number of master thesis, Kaya (1999), Uzunoğlu (1999), Şensoy (2000), Tekeli (2000) in which temperature index model was applied within different hydrological models (SRM, Slurp, HEC-1) were completed during this period.

The existing infrastructure and experience on the projects meant it was necessary to conduct more fieldwork on the area in addition to collect more refined and specific data for model development and testing. Data were collected as part of NATO-Sfs and DPT (BAP-2001K120990 and 2003K120920-01) projects. The decision was made to instrument a new and well equipped station (GY, 2065 m) and this work was supplemented by further measurements by means of upgrading of other stations (HM, 1965 m; OVA, 2130 m; CAT, 2340 m) with new meteorological sensors, replacement of old metal pillows with the new hypolon type snow pillows and constructing snow lysimeters. The most importantly, data become transferable through satellite system (Inmarsat Mini M), Global System for Mobile Communication (GSM) and cable connection with telephone (station to DSI and METU) in real time with this project.

Tables 3.3 to 3.5 give the snow station names, measured hydro-meteorological and snow data (current version) along with their respective site elevations. During the period of the study, the meso-scale size basin was extensively instrumented for monitoring climate and discharge throughout the year. Through these sites are all within the mid portion of the snow zone in the basin, they do represent a range elevations (1700 - 2400 m), topographic structures and site conditions. A general view from the GY site can be seen in the Figure 3.4 below.

Data collected during the 2001-2004 snow seasons were used in this study. The data collection program consisted of continuous automated measurements of a number of hydro-meteorological variables at automatic weather stations (AWS) as well as manual snow surveys, which provided validation data set on snow depth and density data over the course of snow seasons nearby AWS. Dataloggers are taken measurements at every 30 seconds and logging the mean values (total for rainfall and yield from lysimeters) every two hours. In addition, the daily mean, maximum, minimum values and their time of occurrences are also stored in the dataloggers. The logged values are further transmitted to the Water Resources Laboratory of Civil Engineering Department of METU where all the data are stored and analyzed.

The data had become transferable in real time with this project via Inmarsat and GSM however due to its high cost, satellite communications were transferred to cable transfer system in the two stations. Although this transmission is preferable due to expenses, there are serious problems because of the noise in data connection. The noise makes the connection very difficult besides the severe weather conditions since it causes an incompatibility between modem and datalogger.

Even the most common meteorological parameters are difficult to measure continuously at a remote site because both the instrumentation and recording equipment exhibit varying degrees of instability depending on environmental conditions. Extreme weather conditions lead to instability for sensors that give

physically meaningless values and these should be eliminated. All of the collected data are carefully evaluated to determine their reliability under a variety of conditions. At a remote alpine site it is not possible to attend instrumentation at more than weekly intervals during most of the year. Careful attention has been paid to both the precision and accuracy of this climatology, but the absolute uncertainty is not well known.

Table 3.3 Snow instrumentation at the sites

Stations Elevation	Latitude Longitude	Snow Pillow	Snow Depth	Lysi- meter	Data Transfer	Time Interval
HM (1965 m)	39° 48' 21"N 40° 43' 45"E	Steel	UDS		GSM	Daily
GY (2065 m)	40° 12' 01"N 41° 28' 22"E	Hypolon	UDS	Yes	Cable	Two hourly
OVA (2130 m)	40° 14' 48"N 41° 00' 03"E	Hypolon	UDS	Yes	Cable	Two hourly
ST (2150 m)	39° 52' 24"N 39° 07' 54"E	Steel	UDS		Inmarsat	Daily
CAT (2340 m)	39° 44' 37"N 41° 00' 34"E	Hypolon	UDS		Inmarsat	Two hourly

Table 3.4 Radiation instrumentation at the sites

	Net Radiation	Global Radiation	Albedo	Net Longwave
HM (1965 m)		Yes		
GY (2065 m)	Yes	Yes	Yes	
OVA (2130 m)		Yes	Yes	Yes
CAT (2340 m)	Yes	Yes		

Table 3.5 Meteorological instrumentation at the sites

	Prec.	Temp.	Wind Speed	Wind Direction	Air Pressure	Humidity
HM (1965 m)		Yes	Yes	Yes	Yes	Yes
GY (2065 m)	Yes	Yes	Yes	Yes	Yes	Yes
OVA (2130 m)	Yes	Yes	Yes			Yes
CAT (2340 m)		Yes	Yes	Yes	Yes	Yes



Figure 3.4 General view from the Güzelyayla AWS

3.2.1. Snow Data

Snow data are collected in the form of SWE on a hourly basis in the case of automated stations using snow pillows or monthly (or bimonthly) in the case of manually measured snow courses. SWE data as applied to flood runoff analysis are needed as an independent variable for simplified analyses, seasonal runoff forecasting and as data to assist in calibrating and verifying simulation models. SWE data are used to forecast water flow during the snowmelt season to predict flood events and to manage the water supply. Since snow stations may be the only source of high elevation precipitation data, they also can be used to help in estimating basin wide precipitation input to simulation or statistical models. The oldest technique for monitoring snowpack is to take manual measurements of snow depth and water equivalent using a snow sampling tube. Depths of each of several samples are noted and all samples are carefully weighed. Density and SWE are then calculated from the average depth and mass of the samples. This method shows a large variance between pairs of samples, especially when snow densities

are low or when ice lenses or frozen layers are present. SWE is measured at automated sites by a pressure pillow. The pillow made of stainless steel or rubber-like material (hypolon) and filled with an antifreeze fluid. It ranges from 2-11 square meters and connected by a tube to a pressure transducer, which converts the fluid pressure caused by the weight of the snow top the pillow to an electric signal. The fluid level in the precipitation gage is also sensed by a pressure transducer. Figure 3.5 shows the appearance of snow pillow after installation which was the third experience of the group members after GY (2001) and OVA (2002) site studies. There were old steel snow pillows at OVA and CAT, those were changed with the new and more sensitive hypolon ones with the efforts of group members of METU and State Hydraulic Works (DSI).

Long term snow water equivalent data analysis had been done in order to see the general pattern of SWE values through whole snow season both for development and melting period of snow cover. The analysis is very valuable due to its reach data content, it includes manual snow course measurements for SWE between 1976-2003 for GY, OVA, CAT and ST sites. The values for SWE are grouped into ten day composites since the observations are unevenly distributed within the month. The chart provided below, Figure 3.6, represents the long term averages for SWE values for the period including December to mid April. Unfortunately, the snow course data are generally taken only during the accumulation periods. The long term analysis of SWE data supposed to be very helpful for determining the dry and wet years.

An accurate and continuous record of snow depth is required as an independent test of modeled melt rates and to calculate transit times of meltwater down through the snowpack. Surface lowering was measured constantly at the AWS using an ultrasonic depth gauge (UDG). Snow depth is continuously measured at all sites. Figure 3.7 and Figure 3.8 shows the consistency of snow pillow data and ultra sonic depth data with the snow course data. Small discrepancies can be attributed in part to manual measuring site, close to the continuous recording site, and wind drift observed at stations.



Figure 3.5 Snow pillow installation (Cat)

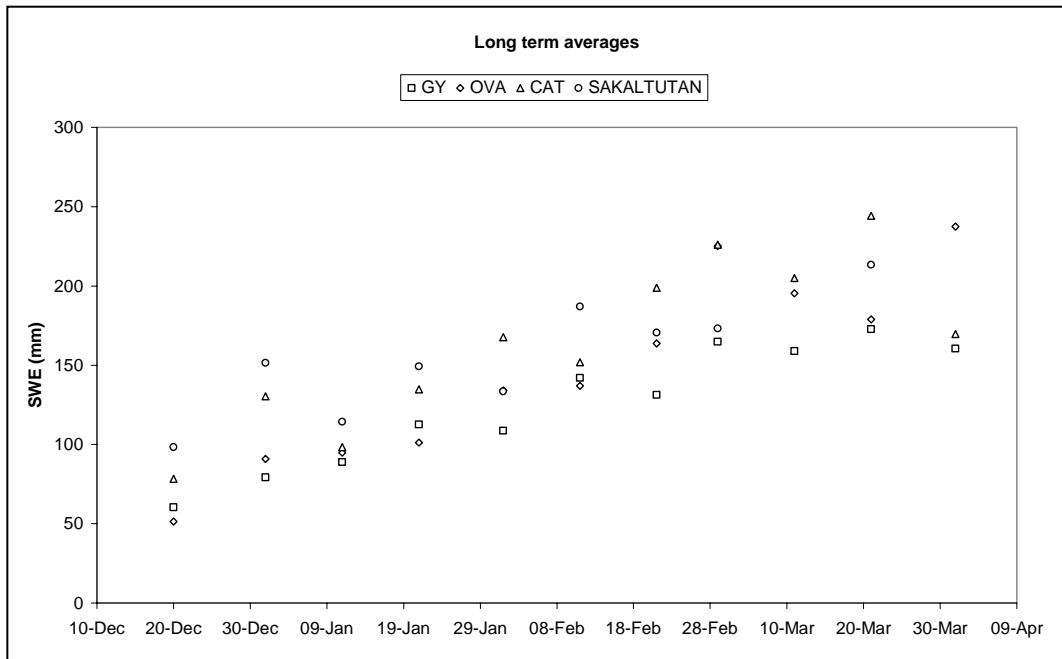


Figure 3.6 Long term averages of SWE values

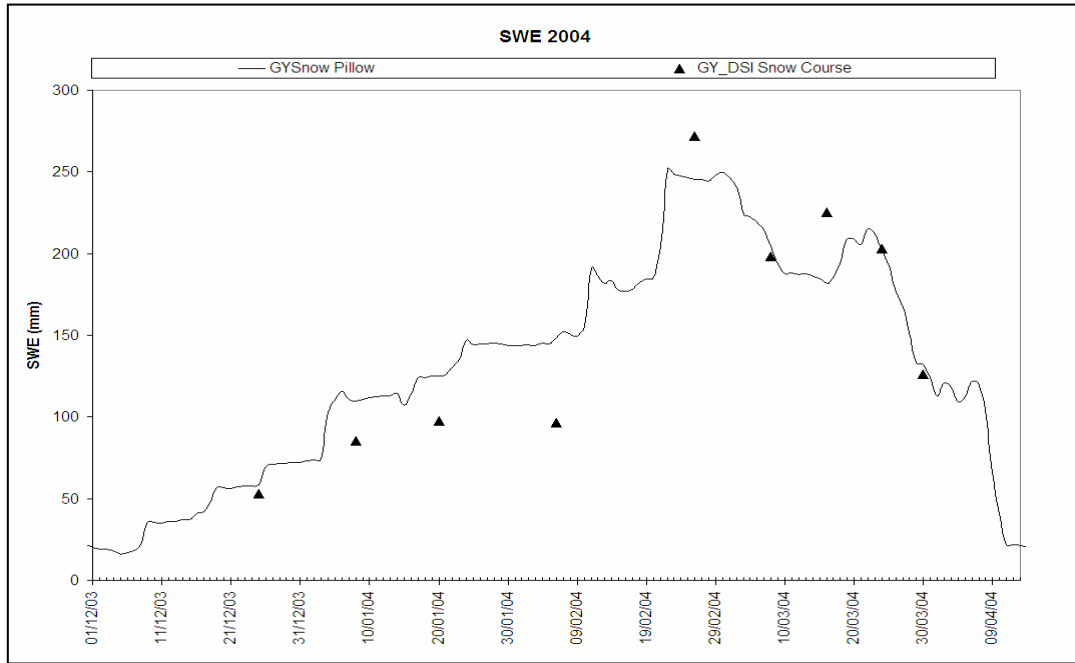


Figure 3.7 Comparison of manual snow course data and continuous snow pillow data (SWE) at GY site

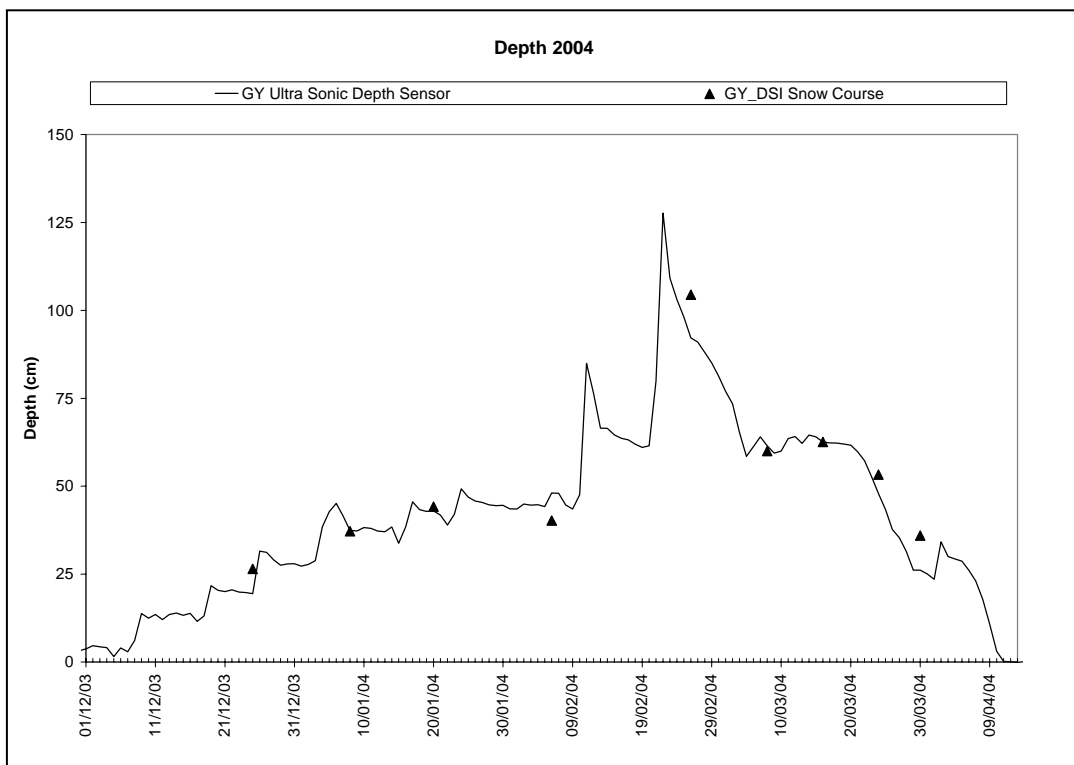


Figure 3.8 Comparison of manual and automatic snow depth observations at GY

3.2.2. Radiation Data

Radiometers in hydrology are widely used in studies of evaporation and snowmelt (see Chapter 2). For most studies of evaporation, incident all wave radiation data are adequate, since the reflectivity of water is nearly constant. The reflectivity of the snow, however, is highly dependent upon wavelength and its albedo may range from 40 to 95 percent. Hence, both incident shortwave and longwave radiation data are required.

A pyronometer having a plane receiver surface mounted horizontally weights the incoming and reflected radiation from different angles according to the cosine of the incidence angle (Male and Granger, 1981). Radiation is monitored at each of the sites: net radiations are measured in the spectral bands of 0.3-100 μm at GY and CAT; pyronometers are used to measure solar radiation and reflection in the range of 0.305-2.8 μm at sites GY, OVA and CAT; net pyrgeometers are used to measure both the incident and outgoing longwave radiation within the range of 5-25 μm at site OVA.

The combination of a net pyrgeometer and a net pyronometer is used at OVA station to measure net total radiation (Table 3.4). This kind of measurement has many advantages over conventional net radiation sensors with plastic domes; robustness and maintainability are better, separate data on solar and longwave radiation is offered. Figure 3.9 shows combination of pyronometers and pyrgeometers at OVA site.

Topographic differences in elevation, shading and exposure between the stations cause distinct differences in measured solar radiation. The contribution of solar and thermal radiation to the energy balance of the snow cover has been theoretically discussed later.

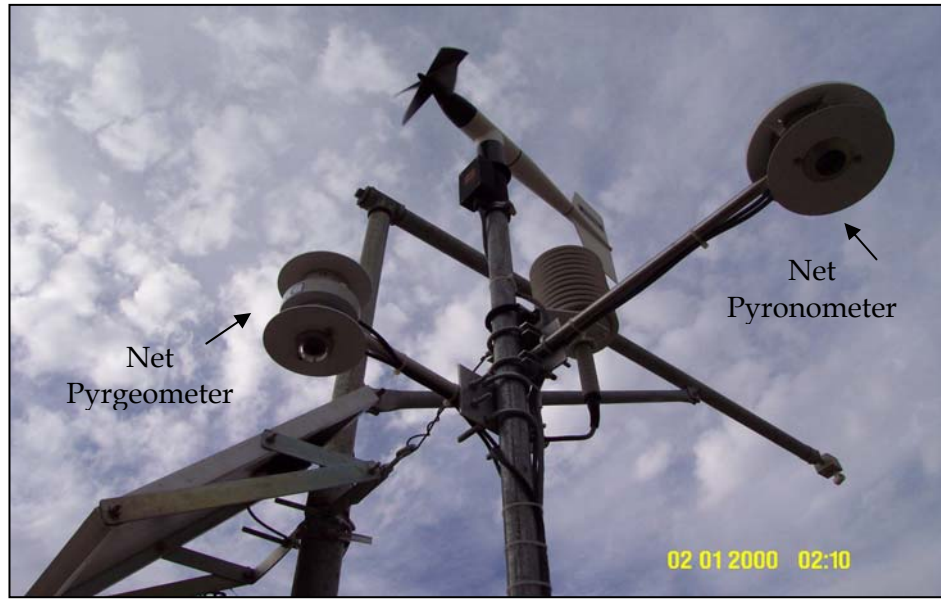


Figure 3.9 Net pyronometer and net pyrgeometer at Ovacık AWS

3.2.3. Precipitation Data

Precipitation in the Upper Karasu Basin is principally snowfall. Rates and volumes of falling snow are very difficult to evaluate from precipitation gage records because they are affected not only by wind, site characteristics and precipitation intensity but also by variations in the density and structure of the snow crystals as they fall. The collection of precipitation data in areas subject to snow accumulation presents additional problems in gauging due to gage freezing, “capping” of gage by snow and high winds. There is uncertainty in all precipitation data, but because rainfall is of higher and constant density, rainfall data are not as difficult to analyze as snow. Peck (1972) summarizes the problem of monitoring snowfall, stating that most measurements of snowfall rates and volumes are the least accurate of the meteorological measurements used in hydrologic modeling. There are rain gages at GY and OVA stations, they are generally used to measure rainfall amount and rate; snowfall data are computed according to snow pillow and depth sensors at which rain gages and snowfall measurements from other stations used as supplementary data. Details of these computations will be given in Chapter 4.

The simulation of the turbulent exchange process is not as advanced as that of radiation exchange. The measurement of the latent and sensible heat exchanges is difficult, even at well instrumented sites and methods of extrapolating such measurement to larger areas based on changes in elevation, latitude, state of the air mass or topographic characteristics are non existent (Male and Granger, 1981). Therefore, temperature, humidity and wind speed values are measured separately to be used in turbulent energy equations.

3.2.4. Temperature Data

The most common meteorological data collected anywhere are of air temperature. Ideally, these measurements should be made at a specified height above the snow surface, shielded from the effects of radiation or conduction from sources other than the atmosphere. In practice, this is seldom the case. Some radiant heating or cooling of the instrument shelter is inevitable, but in most locations this produces only a minor effect (Marks and Dozier, 1992). The high reflectivity of the snow and surrounding terrain causes the air temperature sensor to receive solar energy from all sides. This problem is maximized when wind speeds are low and mixing of the air is small. Fortunately, for energy exchange calculations this problem does not cause significant errors, because at low wind speeds, turbulent energy exchanges are also minimized. A sample data for the three stations is given in Figure 3.10 in order to compare the relative temperatures for the month March of the year 2004.

Monthly average minimum and maximum temperatures (1927-2000) and total rainfall amounts (1929-2000) observed at ERZ_CITY (1869 m) are presented in Table 3.6 to give a better insight through the province. Yearly average precipitation is 453 mm for Erzurum, snow falls for 50 days and stays for about 114 days.

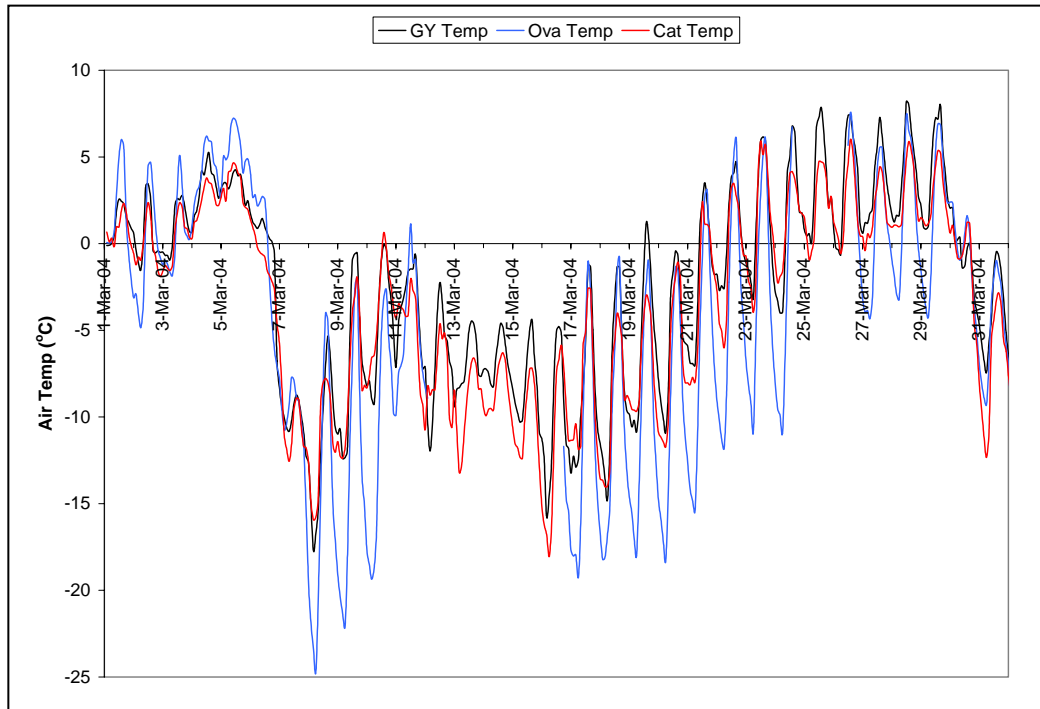


Figure 3.10 Temperature data for GY, OVA and CAT during March 2004

Table 3.6 Monthly averages of climatic data for Erzurum central station

	Jan	Feb	Mar	Apr	May	Jun	Jul	Aug	Sep	Oct	Nov	Dec
Min temp (°C)	-13.4	-12.3	-7.4	0.2	4.6	7.6	11.4	11.4	6.9	2.1	-3.3	-9.7
Max temp (°C)	-3.9	-2.5	1.9	10.6	16.6	21.4	26.1	26.8	22.3	14.8	6.6	-1.0
Prec. (mm)	23.1	27.5	35.8	52.2	72.5	49.9	28.2	17.9	25.4	45.8	35.1	23.0

Snow Surface Temperature

Snow surface temperature is difficult to measure by physical thermometry. Davis et al. (1984) showed that the near-surface temperature of the snow tends to follow the air temperature. This occurs because the insulating characteristics of the snow cover allow the surface layer to come into temperature equilibrium with the atmosphere even though this may create large temperature differences between

the surface and lower layers. Manual measurements of snow surface temperature were taken at GY and a linear relationship is found between air temperature and snow surface temperature details of which will be presented in Chapter 4. Snow surface temperature is constrained to be $\leq 0^{\circ}\text{C}$ and once air temperature remain above this temperature for any length of time, the snow surface temperature becomes constant. The estimates of snow surface temperature are reasonable for the top few centimeters of the snow cover as a radiant thermometer indicated at OVA station.

3.2.5. Wind Speed, Direction and Humidity

The air motion is an important part of the weather process; wind exerts considerable influence in evaporative and snowmelt processes. Wind is highly variable in both time and space and is difficult to characterize by sampling in either of these dimensions. Wind speed is measured by anemometers, of which there are several types. It is monitored at all the sites, however, its direction is deemed to site-specific. Figure 3.11 shows that OVA station is more protected from the wind than the GY and CAT sites. Wind direction is greatly influenced by orientation of orographic barriers. Diurnal variation of wind direction may occur in mountain regions, the winds blowing upslope in the daytime and downslope at night. Although there is a prevailing wind direction at GY and CAT stations (Figure 3.12), this is not the case at OVA station.

The air contains a certain amount of water vapor and this vapor is called as humidity. The standard instrument used to measure relative humidity of the air is the hygrometer or psychrometer; relative humidity is monitored at all stations.

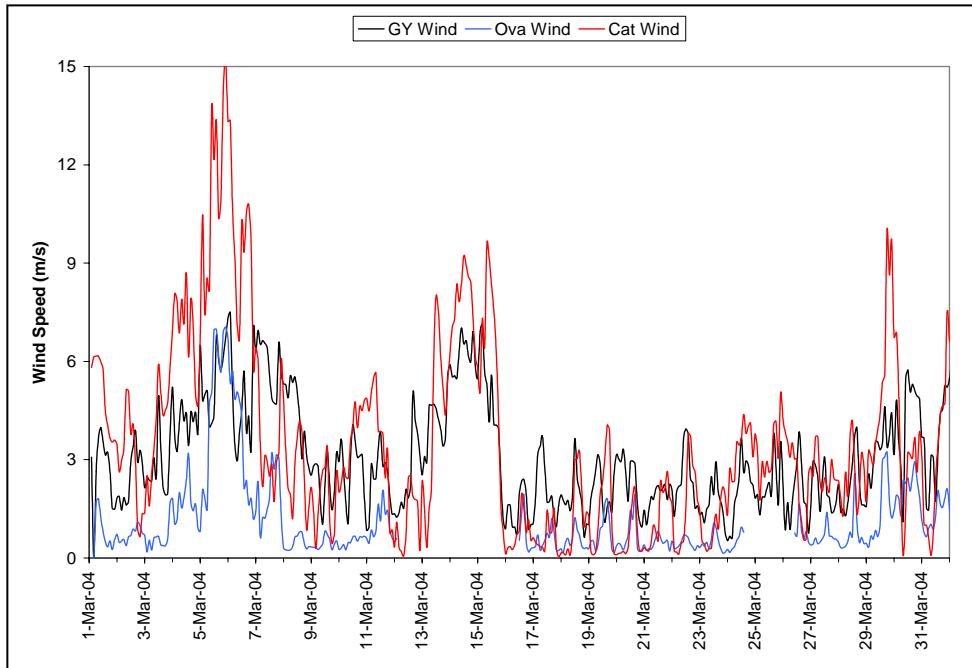


Figure 3.11 Wind speed data for GY and CAT during March 2004

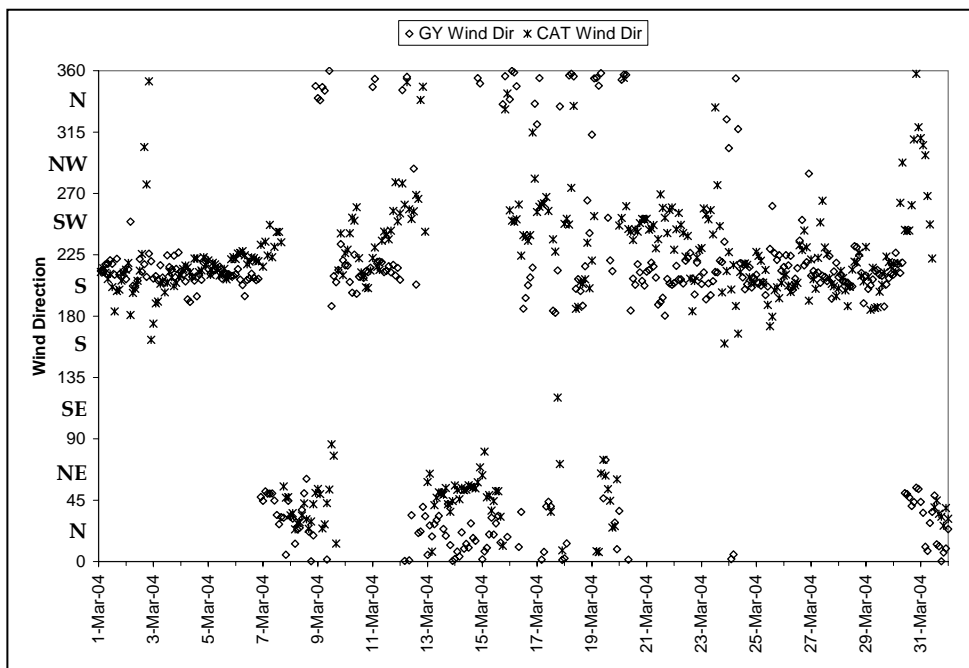


Figure 3.12 Wind directions at GY and CAT sites

3.2.6. Lysimeter

Determinations of the amounts and the temporal distributions of snowmelt runoff require additional analysis of the storage of the snowmelt in the snowpack and transmission of the snowmelt through the snowpack as well as along the surface of the ground as it courses its way to the stream channel. Water release from the base of the snow pack is an attractive observation to use for model evaluation since it serves as the output of the snow routine and the input of the runoff production routine. Snow lysimeters are used to provide a physical measurement for testing models of snow pack energy balance and/or melt water production (Kattelman, 2000). Based on this, a snow lysimeter was constructed and built in place of GY (Figure 3.13). The results are very compatible with rainfall data and SWE values. It was surprising to see the agreement between the lysimeter data and the discharges measured at the basin outlets in micro and macro scales (Tekeli et al., 2005a). The lysimeter yields are compared with the runoff values of stream gauging stations Kirkgöze (243 km²) and Keban (67 500 km²) in Figure 3.14.



Figure 3.13 Snowmelt lysimeter and rain-gauge in Güzelyayla station

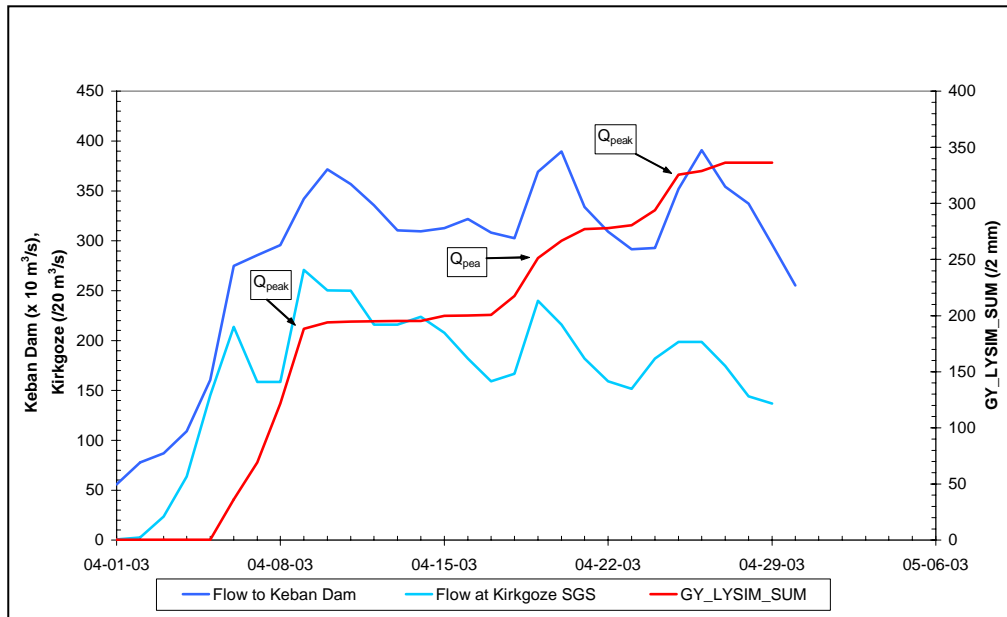


Figure 3.14 Snow lysimeter and its comparison with discharge from two stream gauging stations

3.2.7. Runoff Data

In order to compare results of the model applications in terms of runoffs and since the collection of river flow data from different organizations causes real delay to analyze those data, one of the runoff stations operated by DSI, 2101, has been converted to a new shaft encoder system that can transmit data via GSM. New shaft encoder systems that can transmit data via GSM was already installed on the runoff stations EIE2119 and DSI2154 by September 2004. The early flooding during 29 Feb – 6 Mar 2004 has shown the importance of accessing near real time data in rivers for forecasting and model calibration.

These measurement techniques for albedo, long-wave radiation and lysimeter are pioneer applications in Turkey. The new measurements enable the development of new and detailed modeling approaches for the parameters that can not be measured in the past. This effort is required to develop a high quality time series

of integrated climate data and the evaluation of the energy balance components of the snow cover during both deposition and ablation conditions.

Snow data from the site are being used to support numerous runoff forecasting and hydrologic studies, in determining the relative importance of meteorological variables during snowmelt, development and evaluation of snow models. The hydro-meteorological data will be analyzed in more detail (Chapter 4) since they constitute the input part of the point energy and mass balance model application at representative stations which are already described.

3.3. Spatial Data

Areal modeling relates to the fields of meteorology and hydrology. Generally in the hydrological field, models are classified into lumped, semi and fully distributed models that needs spatial data from the consideration of the treatment of the area considered. The typical example of areal models is the distributed model. In this thesis, the distributed model is analyzed on the relation of remote sensing (RS) and Geographic Information Systems (GIS).

Up until a decade ago, hydrologists relied mostly on conventional data network systems based on ground measurements. However, characterized by insufficient spatial and temporal coverage of the Earth's surface, the conventional networks are being supplemented by remotely sensed data network systems because of several unique aspects. First, remote sensing techniques have the ability to measure spatial information as opposed to point data. Second, remote sensing techniques have the ability to measure the state of the Earth's surface over large and especially remote areas. Finally, they, especially those which utilize satellite sensors, have the ability to assemble long term data for multi purposes (Engman and Gurney, 1991).

3.3.1. Remotely Sensed Areal Snow Cover

Knowledge of snow accumulation on the ground (snow cover) and their spatial distribution throughout the area of interest is required for the effective use of snowmelt runoff models. Thus, operational snowmelt forecasting programs must include activities to measure or acquire snowfall characteristics and snow cover data at least on a daily basis enabling continuous spatially distributed information in meso-scale catchments. Remote sensing of snow covered areas from satellites using optical and microwave images has become feasible, while sensing of other snow attributes is still in the research phase. Land surface parameters of high temporal variability like soil moisture and snow properties are hardly available and rarely used in operational forecasts.

According to Rango (1994), only satellites enable seasonal snow cover to be monitored periodically, efficiently and on a sufficiently large scale. A high temporal resolution is important; particularly for monitoring changes in snow extend due to melt or accumulation. Although snow cover can be detected and monitored with a variety of remote sensing devices, the greatest application has been found in the visible (VIS) and the near infrared (NIR) region of the electro magnetic spectrum (Hall et al., 2002).

In the past, several methods were developed and published for the classification of snow cover and to distinguish snow from clouds by their respective spectral signatures. They are based on the fact that in contrast to the clouds, snow covered surfaces show a low reflectivity in the shortwave-infrared section of the electromagnetic spectrum, while both surfaces have high reflectance in the visible. Specific spectral reflectance of snow (higher reflectance in the visible compared to the mid-infrared electromagnetic spectrum) allows snow covered areas (SCA) to be accurately discriminated from snow-free areas in the absence of clouds or vegetation canopies using optical remote sensing methods (Zhou, 2002). Compared with other remote sensing techniques such as microwave which can be used to

map SWE (Goodison and Walker, 1995; Shi and Dozier, 2000), optical remote sensing which is used to map snow areal extent has much higher resolution. SCA has long been recognized as an important hydrologic and climatological variable for surface water runoff prediction (Zhou et al., 2005). Problems during operational application arise due to the low temporal frequency of high resolution optical information and the frequent appearance of cloud cover.

Measurement of SCA is fairly easy, once the cloudy area can be masked from the image obtained by remote sensing during processing. However, a heavily clouded area in the image occurs at a critical moment in early spring and the SCA cannot always be observed in every repeat period of the satellite. The cloud cover makes many of the satellite images unusable on a regular basis. This limits the availability to cloud-free conditions and data on SCA. This meant that comparisons could only be made on a few days during the snowmelt season (Garen and Marks, 2005). Consequently they are not utilized as model input in the same sense as precipitation and temperature. SWE may be observed by microwave sensors like SSM/I and SAR (Bernier et al., 1999, Pulliainen and Hallikainen, 2001).

Operationally, satellite information on snow is mainly provided by optical sensors like NOAA-AVHRR (Hastings and Emery, 1992) and TERRA-MODIS (Masuoka et al., 1998). Snow cover maps of the Northern Hemisphere have been available since 1966 from the National Oceanic and Atmospheric Administration (NOAA, <http://www.noaa.org>). These maps have continually been improved as new satellite data have become available. On December 18, 1999, the Earth Observing System (EOS) Terra spacecraft was launched with a complement of five instruments, one of which is the Moderate Resolution Imaging Spectroradiometer (MODIS). Snow mapping algorithms for MODIS on EOS Terra and Aqua platforms generate a suite of snow cover products of various levels (Hall et al., 2002; Rigs et al., 2003). The MODIS snow cover maps were obtained from NASA Distributed Active Archive Center (DAAC) located at the National Snow and Ice Data Center (NSIDC, <http://www.nsidc.org>). MODIS data are now being used to produce snow cover products from automated algorithms. The MODIS snow cover maps

represent a potential improvement relative to hemispherical scale snow maps that are available today mainly because of the improved spatial resolution and snow/cloud discrimination capabilities of MODIS and the frequent global coverage. Their accuracy, however, has not yet been established, nor has the accuracy of existing operational maps. The improved spatial resolution of the MODIS snow maps (500 m), relative to snow maps derived from other available sensors, NOAA's Advanced Resolution Radiometer (AVHRR) at 1.1 km resolution, should benefit hydrologists for snow-cover mapping (Hall et al., 2002).

MODIS daily products have 500 m spatial resolution, higher than nominal 1 km resolution products. Several spectral bands are employed to provide multiple indices so that multiple criteria are available to be used to discriminate snow surface from other types of terrestrial surface (Klein et al., 1998), which will enhance the snow mapping capability, especially in topographically complex regions (Maurer et al., 2003). MODIS product algorithms are automated so that the consistency in mapping of snow in different areas and at different times is improved (Hall et al., 2002; Riggs et al., 2003, Zhou et al., 2005)

MODIS is an imaging spectroradiometer that employs a cross-track scan mirror, collecting optics and a set of individual detector elements to provide imagery of the Earth's surface and clouds in 36 discrete, narrow spectral bands from approximately 0.4 to 14.0 μm (Barnes et al., 1998). Key land surface objectives are to study global vegetation and land cover, global land surface change, vegetation properties, surface albedo, surface temperature and snow and ice cover on a daily or near daily basis (Justice et al., 1998). The spatial resolution of the MODIS instrument varies with spectral band and ranges from 250 m to 1 km at nadir (Hall et al., 2002). To evaluate the performance of the model during clear days, we assume the cloud mask employed in the algorithm is accurate so that the cloudy days as identified in the MOD10A1 product are the true cloudy days. Currently, there is no single means of assessing the performance of the MODIS snow cover products (Zhou et al., 2005).

As in the case of conventional hydrological modeling practices, the structure of the hydrological model using remote sensing data is usually a function of the scale of the system under consideration. About the relationship between areal scales and hydrological models, in the WMO (1999) report, it is stated as follows: the structure of the model should subdivide the hydrological systems into area elements of pixel size, if the available spatial resolution of remote sensing data is to be fully utilized. In the case of meso-scale hydrological models, the number of area elements has to be reduced considerably as compared to the micro-scale models.

3.3.2. Topographic Data

For engineering purposes such as flood control and water resources management, it is necessary to accurately understand the time and space distribution of various hydrological parameters in river basins and to assess suitably of the status of their distributions. The preparedness of various spatial data and the development of GIS are making it possible to incorporate areal information in analyzing hydrological environments in the river basin with relative ease. A hydrologically oriented GIS has the functions to store, manipulate and display geomorphological data related to the basin landscape domain resulting in an appropriate set of operational tools oriented to solve hydrological problems; databases are the fundamental skeleton over which information analysis can be performed (WMO, 1999).

A model which describes the spatial information on terrain in the river basin is referred to, in general, as the "Digital Terrain Model or DTM." In particular, a model related to elevation data is called the "Digital Elevation Model or DEM". In recent years, the analysis of terrain and runoff in river basins using DTM are often made in hydrology. In these analyses, DTM is used in analyzing river channels and slopes of river basins, and the resulting terrain model is used to obtain the parameters of characteristic quantities for physically-based distributed runoff models (WMO, 1999). The square grid type DEM is advantageous in that it is easily

obtainable and can be connected easily with the remote sensing data and is suitable for processing the combination with GIS in the computer.

Remote sensing data are the image data of spatial information with a wide coverage and are generally processed by the GIS. It can be said, therefore, that the studies in remote sensing generally use the GIS in a broad sense. The cell based GIS analysis is most appropriate for image processing of remote sensing data.

DEM, area-elevation data, type and density of forest cover, aspect and slope of watershed elements, exposure to prevailing winds are of prime importance in mountainous regions. Lapse rate (vertical temperature and precipitation profile) must either be assumed to be a fixed value or estimated from ground measurements from stations at different elevations. The data is also required in validation of the model, so that model results can be comparable with the observed ones.

CHAPTER 4

THE MODEL SNOBAL AND APPLICATIONS IN THE UPPER KARASU BASIN

4.1. The Model SNOBAL

To address the need for improved management of the melting snow as a critical resource, an energy balance snowmelt runoff model was applied at representative points within the study area. The model used to simulate the accumulation and melt of snow is called SNOBAL (Marks, 1988). A basic overview of the structure and the model input requirements of SNOBAL to compute snow cover mass and energy fluxes are provided in this chapter.

The modeling approach for SNOBAL is an adaptation of the model developed by Marks (1988) and Marks and Dozier (1992). It is a detailed energy budget model that has been successfully applied to several areas of the western USA. The model follows from the work of Anderson (1976) who showed that it is possible to accurately simulate the energy balance of snow cover to predict snowmelt. The modeling approach similar to that used by Jordan (1991) and Tarboton et al. (1995), but the requirements are simpler and more generalizable. Application of the point version of the model SNOBAL was presented by Marks et al. (1998), Link (1998) and Link and Marks (1999). SNOBAL, part of a software package called Image Processing Workbench, IPW, (<http://cirque.ars.pn.usbr.gov/~ipw>) is originally developed by Frew (1990), modified by Longley and Marks (1991) and Longley et al., (1992) and then extensively expanded by Marks et al. (1999b).

Comprehensive simulation of the internal heat and mass dynamics of the snowpack requires a vertically distributed model. However, computational expense of running vertically distributed as part of a fine resolution laterally distributed model is likely to be prohibitive. Conversely, simple vertically lumped energy balance models are prone to considerable error (Blöschl and Kirnbauer, 1991; Morris, 1982). As a compromise between simplicity and accurate process representation, an approach used by Marks et al. (1999) was adopted, whereby the snowpack's energy balance and associated melt, refreezing and water percolation are represented by a two-layer system, with a thin surface layer of fixed thickness and a lower layer of variable thickness. This approach allowed adequate representation of rapid changes in the thermal status of the snowpack surface layer without the computational expense of a fully vertically distributed model (Anderton et al., 2002). Percolation of melt water from each layer was represented by a simple gravity drainage model, whereby the hydraulic conductivity of wet snow is a function of its water content (Colbeck and Davidson, 1973).

The two-layer model, SNOBAL, simulates each component of the snow cover energy balance and accumulates mass and thermal conditions for the next time-step. The snowmelt model is initialized by measurement heights and snow cover state variables if the snow cover exists at the start of the model run. If there is no snow at the start of the simulation, initial conditions are set to zero and the snow depth, density and other properties are generated by the model from meteorological conditions during the simulation period. It is then driven by independent inputs of meteorological parameters, including precipitation mass, temperature and estimated density to calculate the energy and mass balance and runoff from the snow cover. It predicts melt in two snow cover layers, runoff from the base of the snow cover and adjusts the snow cover mass, thickness, thermal properties and measurement heights at each time-step. Different snow models are compared and the variables required by the SNOBAL are presented in Table 4.1 and Table 4.2, respectively. State variables are input as initial conditions and then predicted by the model during the run. Forcing variables are used by the model to predict the state variables and are input at each time-step of the model run.

Table 4.1 Comparison of different snowmelt models (Essery and Yang, 2001)

Model	Multi-layer	Soil model	Variable CH	Variable density	Albedo f (Age)	Albedo f (Snow type)	Liquid storage	References
CLASS		Yes	Yes	Yes	Yes			Verseghy (1991)
CROCUS	Yes		Yes	Yes	Yes	Yes	Yes	Brun et al. (1989)
ISBA		Yes	Yes	Yes	Yes			Douville et al. (1995)
SNOBAL	Yes		Yes	Yes	Yes		Yes	Marks (1988)
SNOW-17				Yes			Yes	Anderson (1973)
SNOWPACK	Yes	Yes	Yes	Yes		Yes	Yes	Bartelt and Lehning (2002)
SNTHERM	Yes	Yes	Yes	Yes		Yes	Yes	Jordan (1991)
SWAP		Yes	Yes	Yes			Yes	Gusev and Nasonova (1998)

Table 4.2 State variables predicted and forcing variables required by the model.

State Variables	Forcing Variables
Snow depth (m)	Net solar radiation (Wm^{-2})
Snow density ($kg\ m^{-3}$)	Incoming thermal radiation (Wm^{-2})
Snow surface layer temperature ($^{\circ}C$)	Air temperature ($^{\circ}C$)
Average snow cover temperature ($^{\circ}C$)	Vapor pressure (Pa)
Average snow liquid water content (%)	Wind speed ($m\ s^{-1}$)
	Soil temperature ($^{\circ}C$)

A basic overview of the structure and equations solved by SNOBAL, its input requirements and output parameters to compute snow cover mass and energy fluxes are discussed below and in Appendix A. The energy and water fluxes simulated by the model are depicted in Figure 4.1. The surface snow layer is where all of the energy exchanges with the atmosphere occur; these processes do not penetrate very far, so the thickness of this layer is set at a physically reasonable value of 0.25 m in the model. The lower layer is simply the remainder of the snow cover. Both layers are assumed to be homogeneous and are characterized by their average temperature, density, and liquid water content.

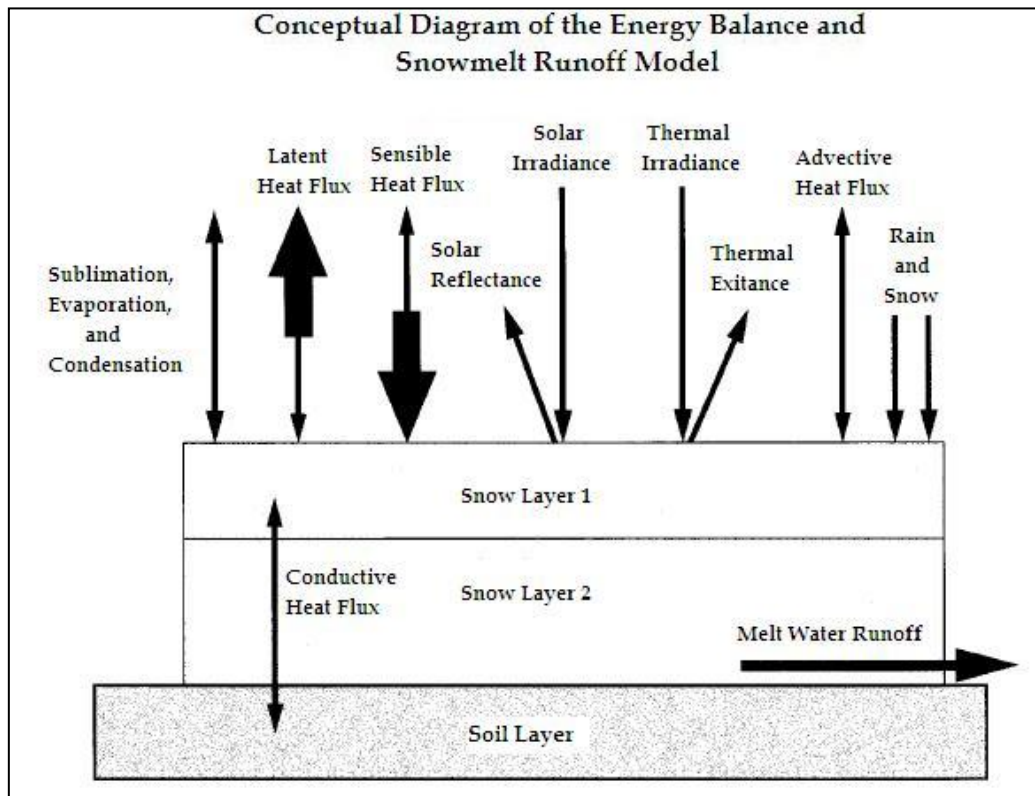


Figure 4.1 Schematic diagram of the snowmelt model structure and components (Marks et al., 1999a)

The model assumes that energy is transferred between the surface layer and the lower layer and between the lower layer and the soil by conduction and diffusion. At each time step, the model computes the energy balance and the snow surface temperature and then adjusts the temperature and specific mass of each layer. If the computed energy balance is negative, the cold content, or the energy required to bring the temperature of the snow cover to 0°C, increases, and the layer temperature decreases. If the energy balance is positive, the layer cold content decreases until it is zero. Additional input of energy causes the model to predict melt. If melt occurs, it is assumed to displace air in the snow cover, causing densification and increasing the average liquid water content of both layers. Liquid water in excess of a specified threshold becomes snowmelt outflow. Though it is usually generated in the surface layer, outflow is removed from the lower layer. The thickness of the surface layer remains constant until the lower layer is completely melted. At that time, the model treats the snow cover as a single layer.

4.2. Energy and Mass Balance Calculations

In a seasonal snow cover, snow is thermodynamically unstable, undergoing continuous metamorphism until it melts and becomes runoff during spring months. These metamorphic changes and final melting are driven by temperature and vapor density gradients within the snow cover, which are caused by heat exchange at the snow surface and at the snow-soil interface. In general, the energy balance of a snow cover is expressed as:

$$\Delta Q = R_n + H + L_v E + G + M \quad (4.1)$$

where ΔQ is change in snow cover energy, and R_n , H , $L_v E$, G and M are net radiative, sensible, latent (L_v is the latent heat of vaporization and E is the mass of water evaporated or condensed), ground (conductive) and advective energy fluxes, respectively (all in W/m^2).

In thermal equilibrium, $\Delta Q=0$: a negative energy balance will cool the snow cover, increasing its cold content, while a positive energy balance will warm the snow cover. The snow cover cannot be warmer than $0^\circ C$ and melt cannot occur in significant amounts until the entire snow cover has reached this temperature. Once the entire snow cover is isothermal at $0^\circ C$, positive values of ΔQ result in melt.

The model approximates the snow cover as being composed of two layers, a surface fixed thickness active layer and lower layer, solving for the temperature ($^\circ C$) and the specific mass (kg/m^2) or depth of water equivalent per unit area (mm) for each (Marks et al., 1999a). The thickness of the lower snow layer is set as the differences between the total snow cover thickness and the thickness of the surface active snow layer. Once the initial snow cover and measurement height parameters are set, the thermal, mass and wetness conditions of the snow cover are calculated. The specific mass (mass per unit area) of each layer and the whole snow cover is calculated from layer thickness and average snow cover density.

4.3. Model Inputs

Input data are specified for the initial conditions, precipitation and meteorological data for the model run. The initial parameter ranges are based on a number of sources, including field measurements, values cited in the literature and physical reasoning. Basically there are four groups of data sets:

4.3.1. Measurement Heights and Depths Record (Constants)

The following set are the starting data and are then assumed constant over the solution region of the site for the duration of the run.

time_z = time since start (hr) (first entry must match times in first entry of snow properties)

z_u = height above the ground of wind speed measurement (m)

z_T = height above the ground of air temperature and vapor pressure measurement (m) (z_u can equal z_T)

z_0 = roughness length (m) (for snow: 0.01 to 0.0001)

z_g = depth of soil-temperature measurement (m) (0 to 1.0)

4.3.2. Snow Properties Record (Initial Conditions)

Initial conditions are specified by the following data;

time_s = time since start (hr) (first entry is model run's start time)

z_s = total snow cover depth (m)

rho = average snow cover density (kg/m³)

T_s_0 = active snow layer temperature (°C)

T_s = average snow cover temperature (°C)

h2o_sat = % of liquid H₂O saturation (relative water content, i.e., ratio of water in snow cover to water that snow cover could hold at saturation)

4.3.3. Precipitation Record

These data are used to calculate advected heat from the precipitation (snow and/or rain) that is added or lost during the event and to update the specific mass of the snow cover. Rain either becomes runoff (if there is little or no snow) or is added to the liquid water content.

time_pp = time since start (hr) (first entry must be \geq start time)
m_pp = total precipitation mass (kg/m²)
%_snow = % of precipitation mass that was snow (0 to 1.0)
rho_snow = density of snowfall (kg/m³)
T_pp = average precipitation temperature (°C) (from dew point temperature if available, or can be estimated from minimum daily temperature)

The user must estimate average density and percent snow if depth data are unavailable. While the user may define the temperature density percentage of snow relationship, the default relationship is shown in Table 4.3 (Marks et al., 1999a). The model makes the following assumptions about the snow temperature, rain temperature, and liquid water saturation of the snow:

when $0.0 < \%_{\text{snow}} < 1.0$, (a mixed rain/snow event)

snow temperature = 0.0
rain temperature = T_pp
liquid H₂O sat. = 100%

when $\%_{\text{snow}} = 1.0$ and $T_{\text{pp}} \Rightarrow 0.0$, (a warm snow-only event)

snow temperature = 0.0
liquid H₂O sat. = 100%

when $\%_{\text{snow}} = 1.0$ and $T_{\text{pp}} < 0.0$, (a cold snow event)

snow temperature = T_pp
liquid H₂O sat. = 0%

Table 4.3 Look-up table for precipitation input

Temperature (°C)	% of Snow	Density of snow (kg/m ³)
$T_p < -5$	100	75
$-5 < T_p < -3$	100	100
$-3 < T_p < -1.5$	100	150
$-1.5 < T_p < -0.5$	75	175
$-0.5 < T_p < 0$	25	200
$< T_p < 0.5$	0	250

4.3.4. Input Data Record (Forcing Data)

Input records of certain climate parameters are required to drive the model. These data may be measured, simulated or estimated and are independent of the model.

S_n = net solar radiation (W/m²)

I_{lw} = incoming thermal (longwave) radiation (W/m²)

T_a = air temperature (°C)

e_a = vapor pressure (Pa)

u = wind speed (m/sec)

T_g = soil temperature (°C)

[ro] = specific discharge/runoff (m/sec) (may be omitted)

4.3.5. Model Time Steps (Data Timestep and Run Timestep)

Model time steps are used to control the frequency of model inputs, calculations and outputs. The "data timestep" is the time interval between the input records of climate data and the model assumes that this interval is constant. Since the snow cover energy balance is very sensitive to diurnal variations in climate (radiation, temperature, etc.), the "data timestep" must be 6 hours or less. Best results are achieved with a data timestep of 3 hours or less. Data timesteps greater than an hour must be multiples of whole hours (e.g., 2 hours, or 3 hours) (<http://cirque.ars.pn.usbr.gov/~ipw>).

A "run timestep" is the internal timestep that the model actually runs at. Because input values are assumed to be averages over a run timestep, it is always an hour or less to insure a stable model solution. There are three lengths of run timesteps: "normal, medium and small". By default, the model uses the normal run timestep which is the longest of the three run timesteps. When either layer's mass drops below a specified threshold, the model divides a larger run timestep into shorter run timesteps. Solution instabilities occur when the run time step is too long to account for rapid changes in the energy balance or when a layer's mass is too small to accommodate the assumption of an average flux over the run time step.

4.4. Model Outputs

In the energy and mass flux output, the energy flux parameters are averaged over the number of run timesteps between outputs, the mass fluxes are summed over the number of run timesteps (Marks et al., 1999). Energy and mass flux outputs are:

Time_s	= elapsed time since start of model run (hours)
R_n	= net allwave radiation (W/m ²)
H	= sensible heat transfer (W/m ²)
L_v_E	= latent heat exchange (W/m ²)
G	= snow/soil heat exchange (W/m ²)
M	= advected heat from precipitation (W/m ²)
delta_Q	= sum of energy balance terms for snowcover (W/m ²)
G_0	= heat exchange between snow layers (W/m ²)
delta_Q_0	= sum of energy balance terms for surface layer (W/m ²)
cc_s_0	= surface layer cold content (J/m ²)
cc_s_1	= lower layer cold content (J/m ²)
cc_s	= snowcover cold content (J/m ²)
E_s	= evaporation (kg/m ²)
Melt	= melt (kg/m ²)
ro_predict	= predicted runoff (kg, or mm/m ²)

Snow conditions output are:

z_{s_0}	=	predicted depth of surface layer (m)
z_{s_1}	=	predicted depth of lower layer (m)
z_s	=	predicted depth of snowcover (m)
ρ	=	predicted average snow density (kg/m^3)
m_{s_0}	=	predicted specific mass of surface layer (kg/m^2)
m_{s_1}	=	predicted specific mass of lower layer (kg/m^2)
m_s	=	predicted specific mass of snowcover (kg/m^2)
h_{2o}	=	predicted liquid H ₂ O in snowcover (kg/m^2)
T_{s_0}	=	predicted temperature of surface layer ($^{\circ}\text{C}$)
T_{s_1}	=	predicted temperature of lower layer ($^{\circ}\text{C}$)
T_s	=	predicted average temp of snowcover ($^{\circ}\text{C}$)

4.5. Methodology

The snowpack is represented by two layers, a surface layer of 25 cm thickness in which all energy exchanges with the atmosphere occur and a lower layer, which is the remainder of the snowpack. At each computational time step, the energy balance, snow temperature, mass and density of both layers are computed. Meltwater outflow is generated when the cold content of the snowpack is zero and liquid water has filled the voids in the snow. Mass lost to outflow is removed from the lower layer. Details of the methodology are discussed in Appendix A.

4.6. Model Application

A point energy budget snow model used to simulate snowmelt in two hourly time intervals for three years (2002-2004) in the Upper Karasu Basin, Turkey. The snow water equivalent and snow depth simulated by the model were compared very favorably to measurements at AWS as well as the ground truth observations from

snow courses. There are a total of five point energy and mass balance model applications for snowmelt: GY applications for the snow seasons 2002-2004, OVA and CAT applications for 2003-2004 snow season. Therefore, there are three temporally distributed point model applications at one site (GY for 2002-2004) and three spatially distributed point applications for the same snow season (GY, OVA, CAT for 2003-2004 snow season).

The first model application is at GY during 5 February - 15 April 2002. The simulation was not started at the beginning of the snow accumulation due to a lack of data resulting from equipment failure, as this was the initial year for the installation and operation of AWS at GY. The second application includes the simulation of the seasonal cover during 7 December 2002 - 13 April 2003, while the third simulation covered the period of permanent snow cover during 9 December 2003 - 11 April 2004.

Finally, the model was applied to the OVA and CAT sites for the 2003-2004 snow season before which the stations were upgraded with new snow pillows and sensors providing precise data. To avoid instability problems due to accumulation and melt of very shallow snow depth early in the season, the application periods are taken as 18 December 2003 - 27 April 2004 and 1 December 2003 - 30 April 2004 at OVA and CAT, respectively.

4.7. Model Inputs

4.7.1. Measurement Records

Height above the ground surface for wind speed, air temperature and vapor pressure measurements are almost three meters at all the stations.

The effective snow surface roughness, required for the turbulent transfer calculations, has been shown to be a dynamic property that is dependent on wind

speeds and micro-topography of the snow surface (Andreas, 1987). It is difficult to measure and is, therefore, usually estimated based on values reported in the literature ranging from 0.0001 to 0.01 m (Anderson, 1976, Moore, 1983) depending on snow depths and conditions. Since it is difficult to estimate how snow surface feature change over time, most snow models use approximate snow surface roughness values that do not vary in time or between sites. For applications of SNOBAL model snow surface roughness was varied from 0.001 to 0.0025 as snow depth changes, for both open and sheltered sites (Marks et al., 1999a). It has been found that the aerodynamic roughness increases with increasing wind speed due to the influence of the drifting snow itself (Marsh, 1999). Roughness length is set to 0.001 m for GY and CAT, but it is 0.0001 for OVA. Therefore, the values used in the model applications are within the range of values cited in the literature.

The soil temperature sensor was installed (20 cm depth) at GY site on October, 2003. However, it could not work properly and the data it provided could not be used in the studies; instead the values for soil temperature were provided from another station Sarikamis (SK, 2150m), operated by DMI, which shows similar temperature, snow accumulation and ablation patterns with GY (see section 4.7.2).

The model requires the climatological data in addition to aforementioned initial conditions; precipitation, net solar radiation, incoming thermal radiation, air temperature, vapor pressure, wind speeds and soil temperatures. Data preparation and input file generation are explained in the forthcoming pages.

4.7.2. Precipitation Record

The determination of total precipitation mass due to snowfall is possible from the measurements done by rain gages with heater. Unfortunately, it is not possible to use heater at the site due to its power requirement. Since the sites are cold (and windy for GY and CAT), there is an undercatch and freezing problem for snowfall, the recorded values are unbelievably small in amount compared to snow depth,

SWE at the stations and snowfall values of other stations. This underestimation is improved by the information gathered from the snow data measured with snow pillow and also from the nearby microclimatologic stations.

The researchers working with the model SNOBAL indicate the use of change in SWE values with some restrictions for precipitation computation (Personal communications with Dr. Garen). Then, such an analysis was carried out with the data provided from the site. The data acquired from SK station in a daily manner provided verification for the precipitation analysis. It was surprising to see similar patterns between two stations in terms of snow depth, SWE (Figure 4.2), min, max and average air temperatures (Figure 4.3) especially for 2002-2003 snow season even the station is not within the pilot basin boundary but in the adjacent basin. There are reliable precipitation values of SK station including snowfall at 7:00, 14:00, 21:00 and daily totals. In the same manner, daily snow depth values and densities (densities are not daily but at least three times a week) are also available. Thus, the station is used to check the results of analysis at GY. First, daily computations for snowfall were carried out according to changes in SWE and then two hourly analysis were computed depending on the following criteria:

- a) If the summation of only the positive changes in SWE (positive means accumulation) within a day exceeds 1 mm, snowfall is assumed to be occurred:

$$\sum_{i=0}^n \Delta SWE_{(+)} > 1 \text{ mm} \quad n = 0, 2, 4, \dots, 22 \text{ (hours in a day)} \quad (4.2)$$

- b) The amount of snowfall (P) is computed from the summation of both positive and negative changes in SWE within a day

$$P = \sum_{i=0}^n \Delta SWE_{(+ \text{ and } -)} \quad n = 0, 2, 4, \dots, 22 \text{ (hours in a day)} \quad (4.3)$$

c) Then, a simple fractioning approach was used to disaggregate the daily fields into two hourly fields, where a set of twelve fractions was estimated for each day by an averaging and smoothing process based on each station's data. While computing two hourly values for snowfall, the percentages of $\Delta\text{SWE}_{(+)}$ in a day are computed and then daily precipitation is distributed according to these percentages through a day. However, the snowfall is eliminated when the air temperature is less than '-15°C'.

New precipitation values sound more reliable than the ones used before. The danger in looking only at the positive SWE value changes is if the sensor "bounces", that is, for one time period a '+' change can be seen, then the very next time period, a '-' change of exactly the same amount can be observed. This is watched out and zero change was assumed in these kinds of occurrences. Summing positive and negative changes over the course of a day is equivalent to taking the difference between midnight readings to give a daily change.

Dew point temperatures are calculated using air temperature and relative humidity data from the stations. Then, Table 4.3 is utilized to obtain percent and density of new falling snowfall.

4.7.3. Climate Input Data Preparation

The climate parameters discussed in this sub-section were either measured directly or derived from measured values. Data of air temperature, wind speed, relative humidity and incoming solar radiation are available in two hourly timesteps from AWS for all of the simulation years whereas albedo and incoming longwave values had to be modeled. Precipitation amounts in the form of snowfall are computed with the logic explained above; rainfall amounts are either measured directly at sites operated by the project team or carried from the other meteorological stations operated by DMI.

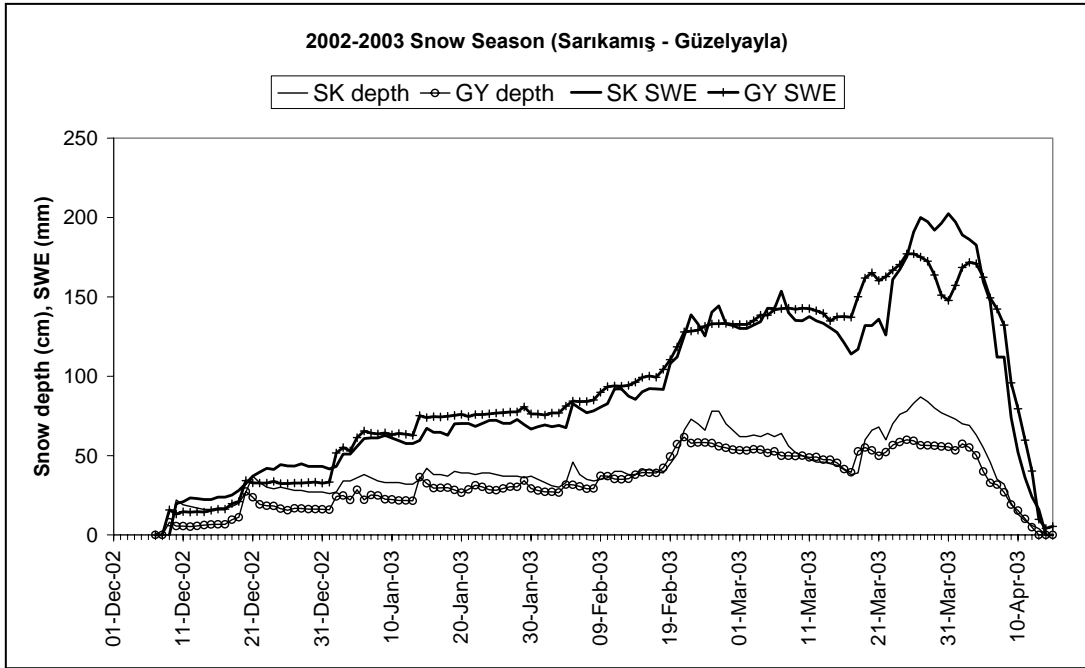


Figure 4.2 Snow depth and SWE comparison at SK and GY sites

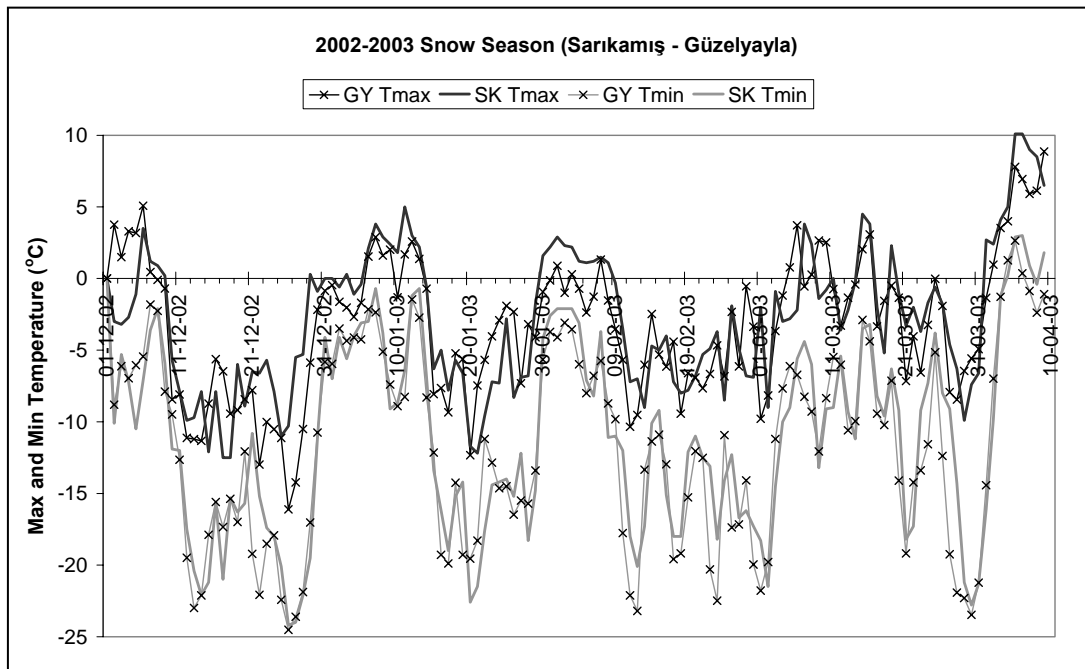


Figure 4.3 Maximum and minimum temperatures at SK and GY sites

4.7.3.1. Net Shortwave Radiation

The net shortwave component primarily governs both the timing of melt and the snowmelt rate. The amount of solar radiation penetrating the atmosphere to be received by the earth's surface depends on the turbidity of the atmosphere, cloud cover, topography (altitude, slope and orientation) and other factors. Incoming shortwave radiation (global radiation) is measured at all the sites. Therefore, there is no need to model these values at a point scale where the model is applied for.

Incoming solar radiation that strikes the earth's surface is partially reflected and partially absorbed, in proportion to surface reflectivity (albedo). It will be demonstrated that the surface energy balance during the melt period is often dominated by solar radiation receipt, which is, in turn, strongly controlled by snow albedo. This means that the treatment of albedo in snow models has an important effect on overall model success and needs careful consideration. The snow albedo shows seasonal and daily variations depending on a wide variety of sources of influence like aging, wetness, impurity content, particle size, snow density and composition, surface roughness, topographic features, cloud cover, the spectral composition and direction of illuminating beam.

Albedo is continuously observed at GY except for the first winter (2002). Therefore, it was decided to replace a physically based algorithm of albedo computation with a new parameterized scheme developed specifically for the site since there is a lack of data using the observed data for 2002-2003 snow season. This scheme is based on a scenario using both a linear parameterization (Equation 4.4) derived from step wise regression analysis and an albedo decay function determined from aging (Equation 4.5). Principal component analysis (PCA) was applied to the observed data at GY for the 2002-2003 snow season, which lead to the selection of snow depth, global radiation and temperature as predictor variables, then step wise regression equation was used to derive coefficients for standardized variables. Finally, the two equations have been adapted according to snowfall condition; since snowfall occurs continuously, linear equation (4.4) is employed during

February, whereas nonlinear aging equation (4.5) is used dominantly for the month April since there is no snowfall and in March both equations have been utilized to compute albedo. The model results are shown in Figure 4.4; observed and modeled albedo values are presented both in two hourly and daily timesteps, beside the linear relationship and best fit for the melting period of 2003 at GY. The same modeling approach is also used for CAT where there is no albedo measurement during the model application of 2003-2004 snow season.

$$\text{Albedo} = 0.75 + 0.185 * d - 0.1 * S_i - 0.0001 * T_{\text{air}} \quad (4.4)$$

$$\text{Albedo} = 0.77 - 0.15 \ln (t) \quad (4.5)$$

Where all the variables are standardized and d is snow depth, S_i is the global radiation, T_{air} is the air temperature and t is aging time in days from last snowfall.

The albedo values thus estimated were used to determine the reflected shortwave radiation, which was subtracted from the measured incoming radiation to obtain net shortwave radiation. Since global radiation and albedo are both measured at GY for the other two years and OVA for the last year, it is possible to compute net solar radiation in two hourly bases and put into the input file for model runs.

A major problem with the radiation and albedo measurements during snow accumulation phase is the formation of ice cap on top of the glass shield of the equipments. Since the temperatures are lower at OVA than that observed at the other stations, this phenomenon was generally occurred at OVA. In these cases, the values are replaced with the last or next physically reasonable value or modified with the values observed at the other station according to the climatic conditions.

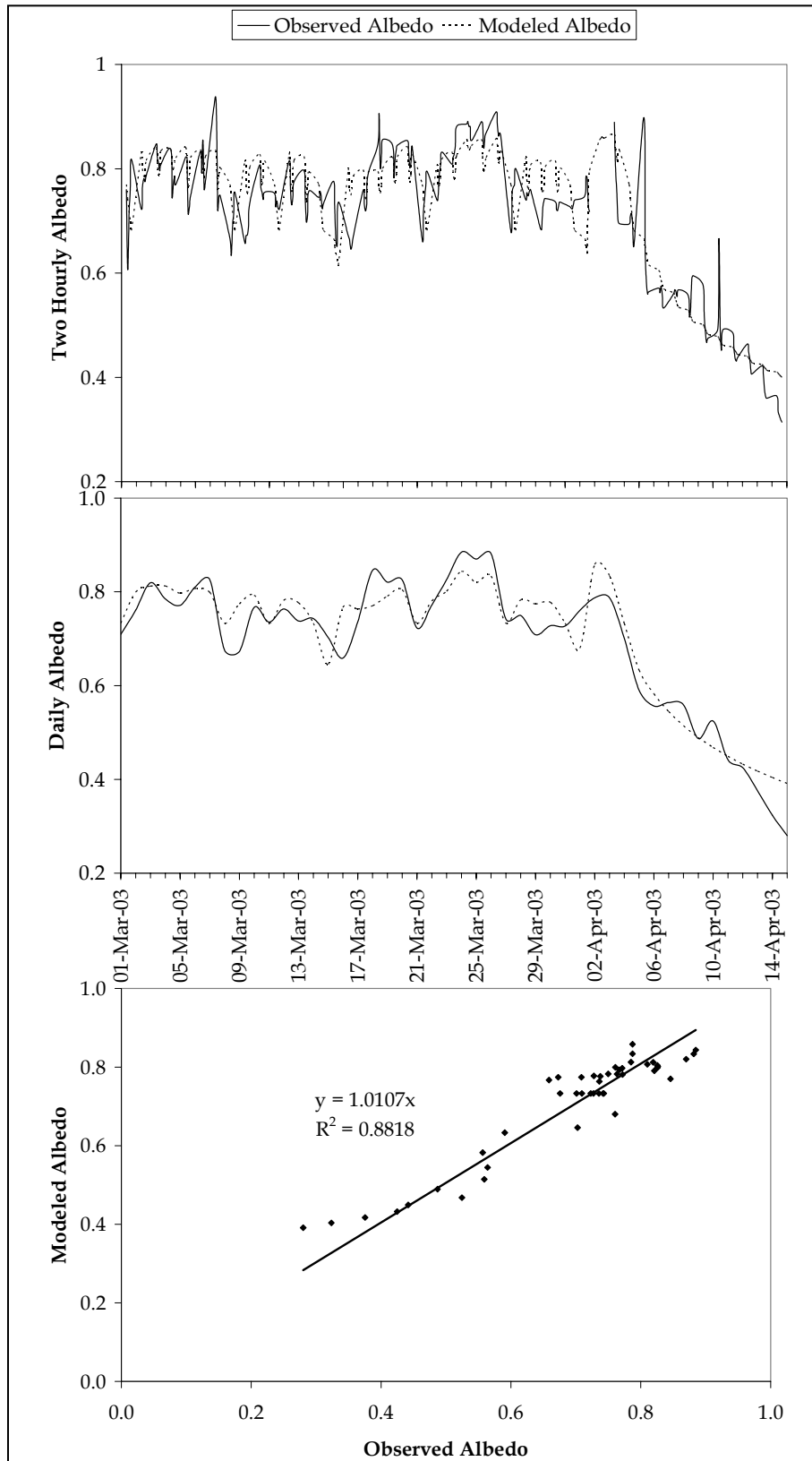


Figure 4.4 Observed and modeled albedo values for march-april 2003, GY

4.7.3.2. Incoming Longwave

Every physical body with a finite temperature radiates electromagnetic waves. A body capable of absorbing the entire radiation incident on it would have to be black. The emissivity of this ideal black body is given by the Stefan Boltzman law, which states that the energy flux radiated per unit surface area of a black body is proportional to the fourth power of its thermodynamic temperature.

In order to compute incoming longwave radiation the air and snow temperatures, global radiation, albedo and net radiation values are used at both GY and CAT according to equations stated below. A linear relation between air and snow surface temperatures was developed using manual data observed at GY:

$$T_{snow} = 1.02T_{air} - 3.17 \quad (4.6)$$

Where T_{snow} is the snow surface temperature ($^{\circ}\text{C}$) and T_{air} is the air temperature ($^{\circ}\text{C}$), with the constraint of maximum $T_{snow} = 0^{\circ}\text{C}$. Incoming longwave radiation is calculated using measured net radiation values as:

$$L_i = R_{net} - S_{net} + \varepsilon_{snow} \sigma T_{snow}^4 \quad (4.7)$$

Where L_i is the incoming longwave radiation (W/m^2), R_{net} is the net radiation (W/m^2), S_{net} is the net shortwave radiation (W/m^2), ε_{snow} is the emissivity of the snow surface (0.99), T_{snow} is the snow surface temperature (K) and σ is the Stefan Boltzman constant ($5.67 \times 10^{-8} \text{ W}/\text{m}^2/\text{K}^4$).

The outgoing longwave radiation observations at OVA were used to check the snow surface temperature computations. Snow surface temperature values were computed from measured terrestrial longwave radiation concerning the Equation 2.8 and then compared with the results of the empirical formula obtained from manual measurements (Equation 4.6). Figure 4.5 presents this relation between air

temperature and snow surface temperature in terms of both the observed values derived from the pyrgeometer and computed ones derived from the empirical formulation of manual measurements (Equation 4.6). All the graphics (Figure 4.5) are drawn using 2004 data in two hourly timesteps, while there is considerable scatter in the relation between the two data sets, a strong correlation is found between them. The first graphic gives a trend line parallel to the empirical one, however it yields somewhat lower snow surface temperature values; the second graph does not include the hours with high temperature values 1200, 1400, 1600 and finally the last graphic, more scattered than the other two presents the data belonging to only 1200, 1400, 1600. According to these graphics, the empirical equation adequately represents the snow surface temperature values overall; however, it may be more appropriate to separate the equation into two parts, one for the afternoon hours (1200-1600) at which the air temperatures will be relatively high and one for the rest of the time of the day for which the equation explains about 90% of the relation. The main discrepancies occur when the air temperature was above freezing, which is reasonable because the snow surface should be at freezing when the air temperature is higher (Shusun et al., 1999).

Although several longwave radiation models have been developed (e.g. Idso, 1981; Satterland, 1979) and these models can successfully represent daily average atmospheric longwave radiation with cloud cover correction, they are not adequate to represent diurnal variations for a two hourly computational timestep (Figure 4.6). Therefore, it was preferred to use snow surface temperature data together with observed radiation values (net, global and albedo) to compute atmospheric longwave radiation instead of other empirical models. To show the difference in the modeling results for two hourly timesteps clear-sky thermal radiation from the atmosphere was also simulated with a method developed by Marks and Dozier (1979) as a function of altitude, air and dew-point temperatures. No cloud-cover adjustments were used to enhance the results for either of the cases.

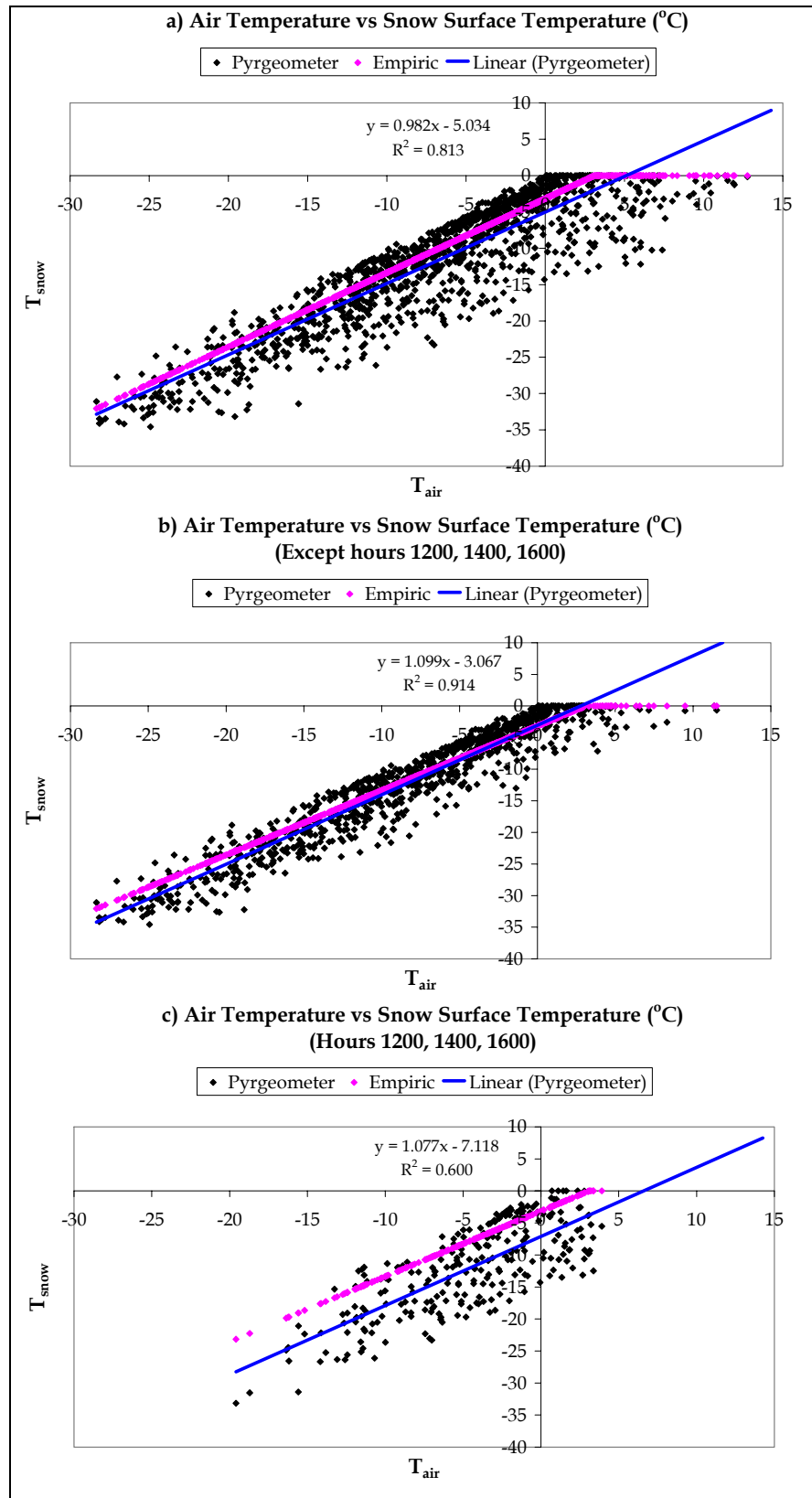


Figure 4.5 Snow surface and air temperature relations, OVA, 2004

One of the more interesting patterns is how inferred cloudiness varied with time of day; the data show pronounced favoritism for night and early morning fog. The observed to modeled (with Marks and Dozier, 1979) incoming longwave ratio changes through the day and is around 1.4 for night and morning; however it is around 1.1 for noon and afternoon hours. On the other hand, the observed to modeled (with air temperature) ratio is around 1.0 (1.03) through the day, being maximum of 1.05 in the night and minimum of 1.00 at the noon (Figure 4.6).

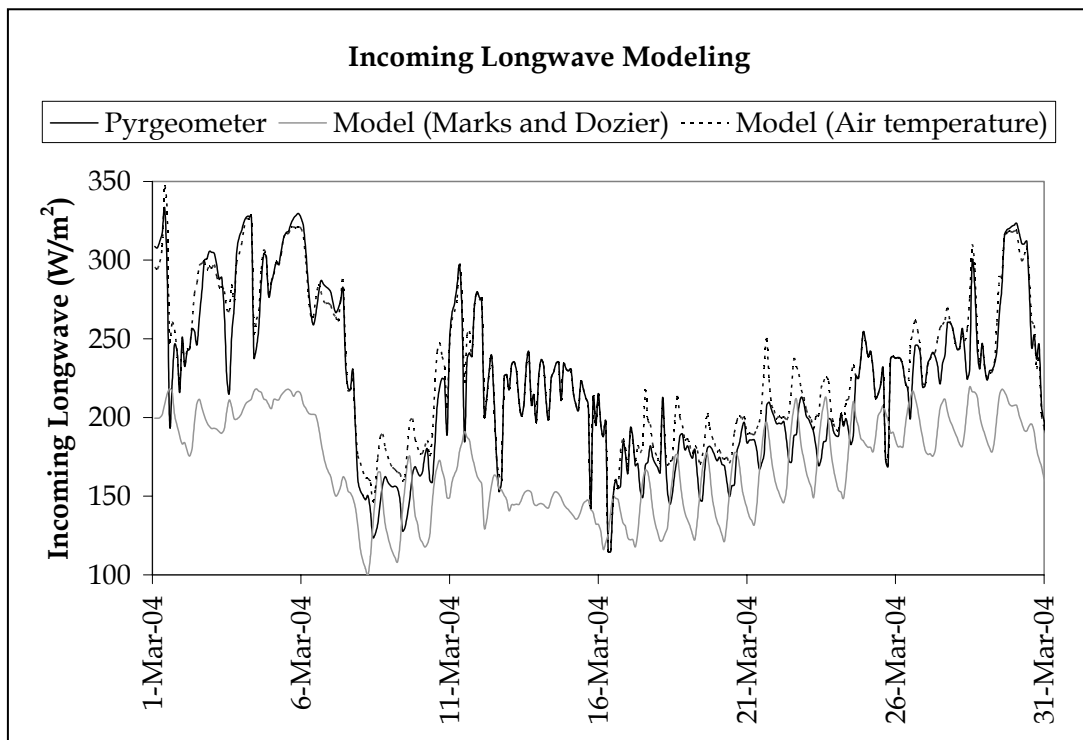


Figure 4.6 Incoming longwave modeling at two hourly time steps, OVA

4.7.3.3. Air Temperature, Vapor pressure and Wind Speed

In addition to the low wind speeds it has, generally there is an inverse temperature relation at OVA where the coldest air temperature values are observed. Thus, the site is a distinct in that its temperatures are cooler than one would expect based on its elevation and the temperature trends based on the other sites. Having the highest wind speed values CAT is more exposed than the others. Vapor pressure

for the individual sites was computed from site air temperatures and relative humidity values, using algorithms presented by Marks et al. (1999a). These three variables are important basically in the calculation of turbulent energy fluxes.

4.7.3.4. Soil Temperature

Since the sites appear to be cold and sometimes having a shallow snowpack (especially at GY), setting the soil temperature to a constant of 0°C is not a very feasible assumption. Using this assumption in model simulations led to an unrealistically high simulated heat transfer from the soil to the snow during the early model applications (Personal contact with Dr. Garen). Therefore, the soil temperature data from another station were used for soil temperatures at 20 cm depth. The thermal regimes of the soil and lower snow cover would be expected to be similar everywhere in the watershed. Most of the difference between sites would be in the initiation of the isothermal condition. During snowmelt, the ground temperature should be close to zero, because the melt water infiltrates into the soil. The maximum allowable soil temperature during melt should be zero.

Since snow accumulation and ablation patterns at GY are very similar to that at SK, the soil temperature values observed at SK are used in the model applications. As seen in Figure 4.2 snowpack developed and melted at the same temporal manner for GY and SK; therefore, exactly the same values are used in model application for 2002-2003 snow season. On the other hand, due to early disappearing of snowpack at SK for the other two seasons, to prevent unrealistically high ground heat fluxes during melt, soil temperature values of SK are used with minor modifications. Since the exact time of occurrence for 0°C soil temperature can not be known for application sites, it was preferred to use “-0.5°C” instead of zero during the melting period except for the year 2003.

The climatic input data for GY, OVA and CAT point applications are presented in Appendix A. Although the model is applied in two hourly time intervals, the input

parameters are (net shortwave radiation, incoming longwave radiation, temperature, wind speed, vapor pressure and soil temperature) presented in daily averages for clearer illustration.

4.8. Model Outputs

The model results obtained from simulation runs will be analyzed under two main topics with two more subtopics under each. The first topic is the temporal analysis of the point applications at one station (GY) for three consecutive snow seasons (2001-2004), and the second is the spatial analysis of the point applications at three stations (GY, OVA, CAT) for one snow season (2003-2004). Each analysis will be further evaluated both in terms of snow cover energy balance and snow cover mass balance. The results are encouraging, because not only did simulated melt track measured melt and runoff, but the model showed how sensitive the melt process is to changes in climate conditions. Convincing verification of the model would require a direct measure of snow cover development and depletion both of which are available in terms of SWE and snow depth (Marks et al., 1999a).

The results of model applications; the model outputs in terms of SWE and runoff, in accordance with energy fluxes, temperature and precipitation, for temporal (GY, 2001-2004) and spatial analysis (GY, OVA, CAT, 2003-2004) are presented in Figures 4.7-4.9 and Figures 4.9-4.11, respectively; daily average energy fluxes (net radiation, turbulent flux including both sensible and latent heat, ground heat and total energy except for advective energy that is small in amount) are presented in Figures 4.12-4.14 (temporal) and Figures 4.14-4.16 (spatial); Figure 4.17 depicts the sensible and latent heat fluxes for each application; energy percentages within the total energy are given in Figure 4.18 (temporal) and Figure 4.19 (spatial); total energy comparison are shown in Figure 4.20 (temporal) and Figure 4.21 (spatial); Figure 4.22 presents observed and modeled snow depth values.

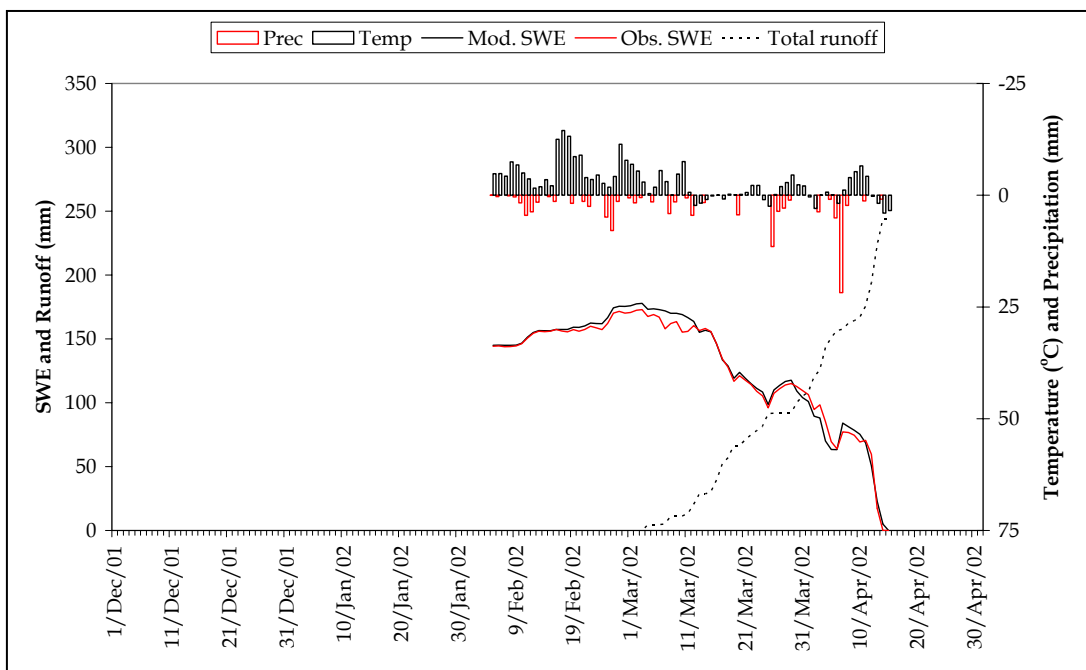
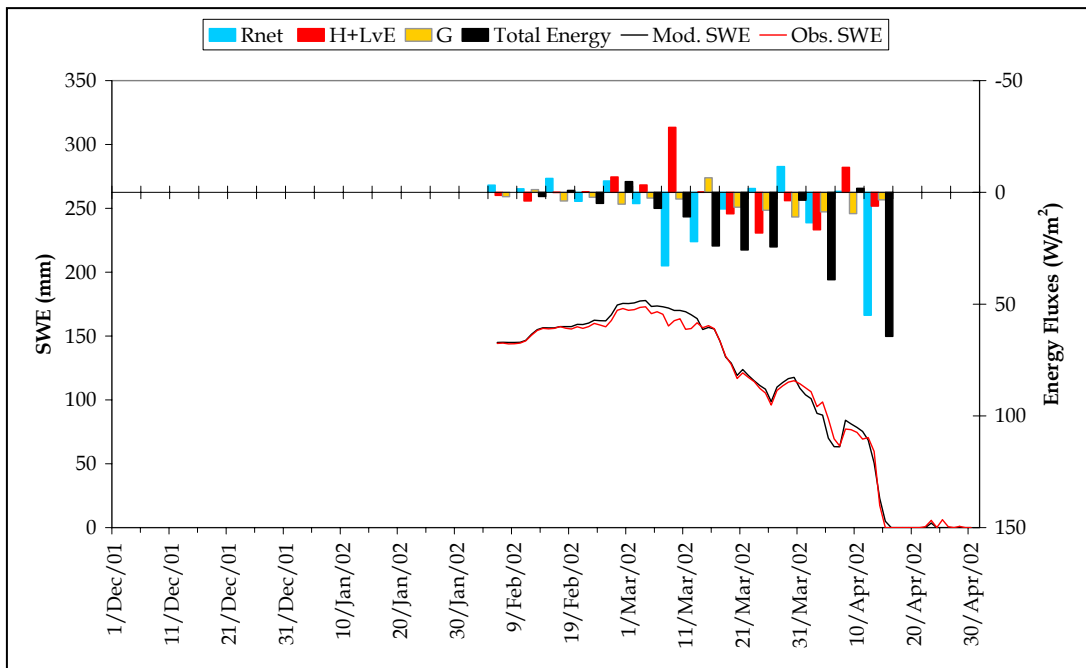


Figure 4.7 Model outputs for energy and mass balance at GY, 2001-2002

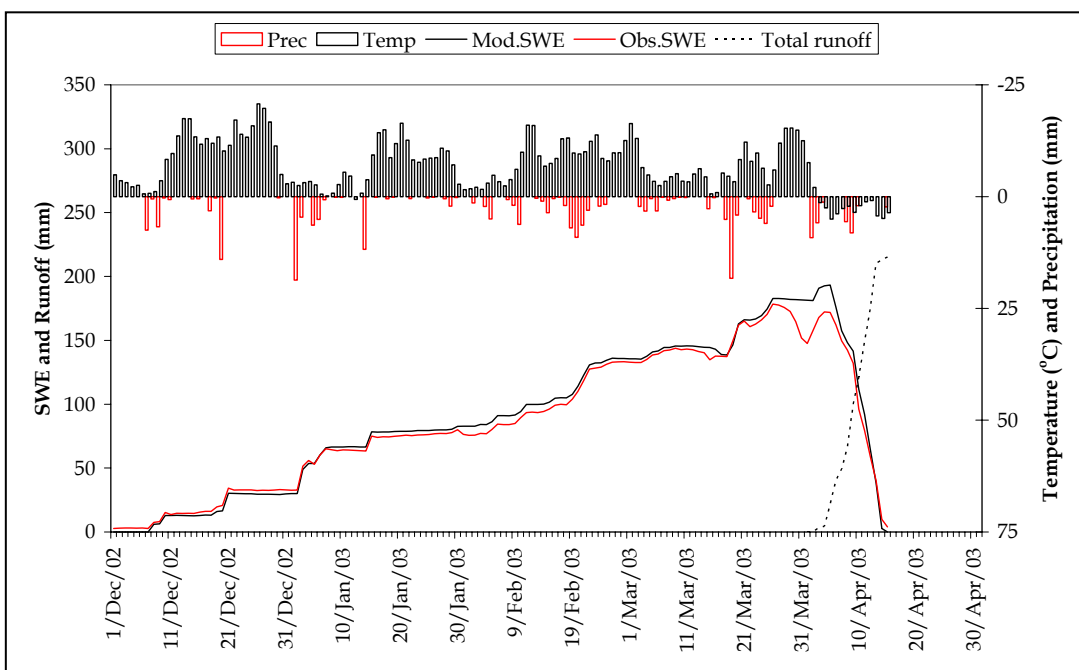
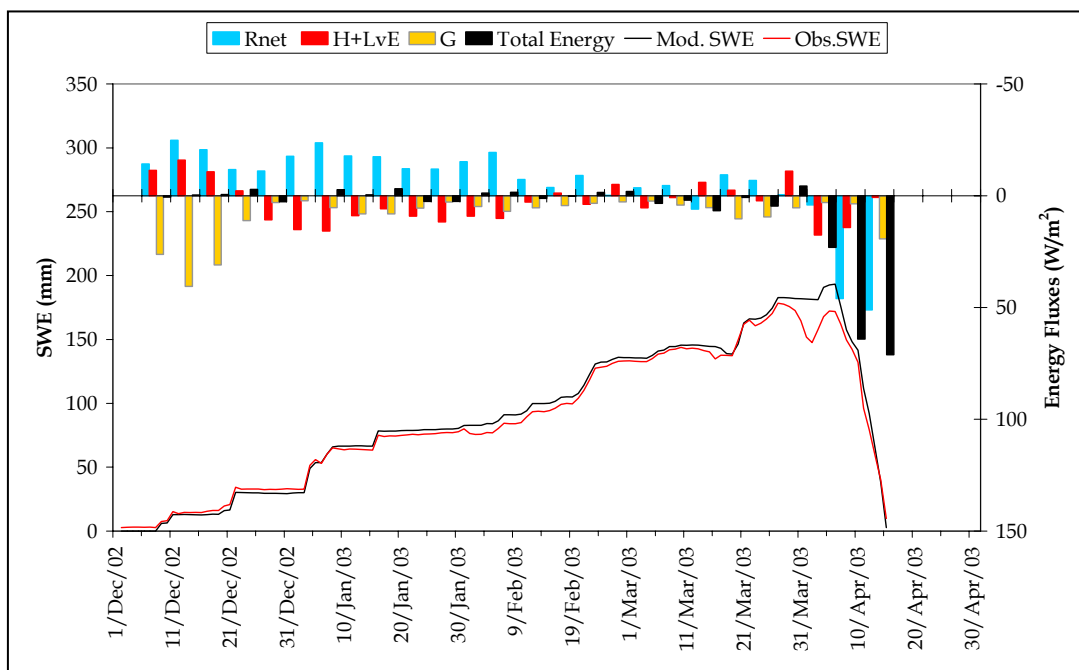


Figure 4.8 Model outputs for energy and mass balance at GY, 2002-2003

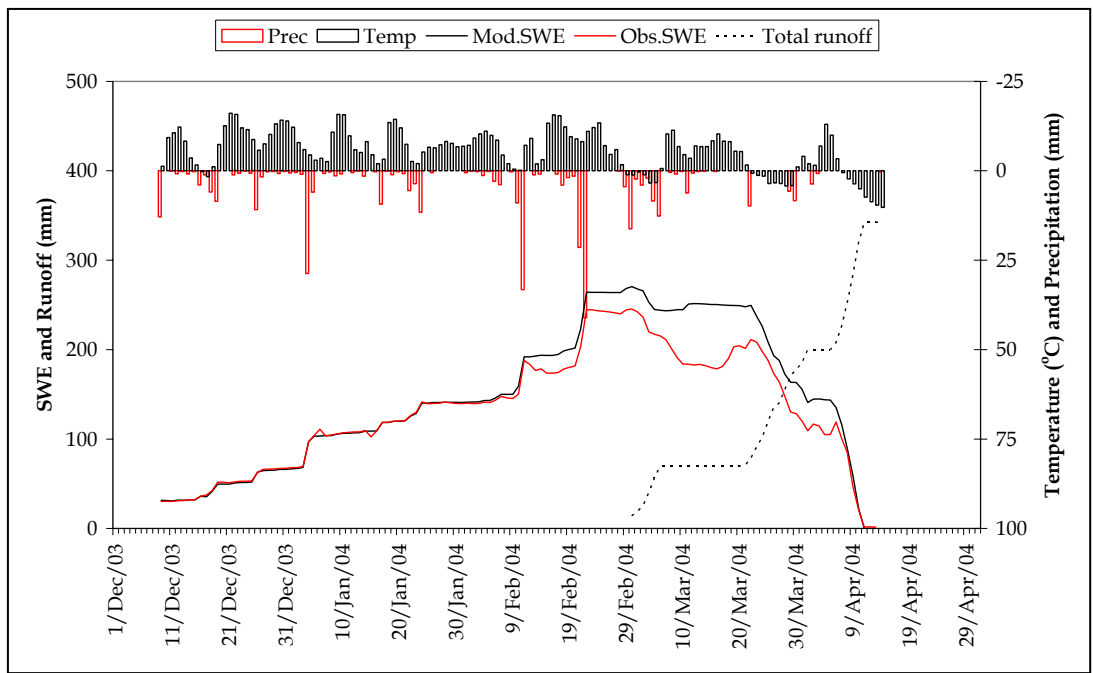
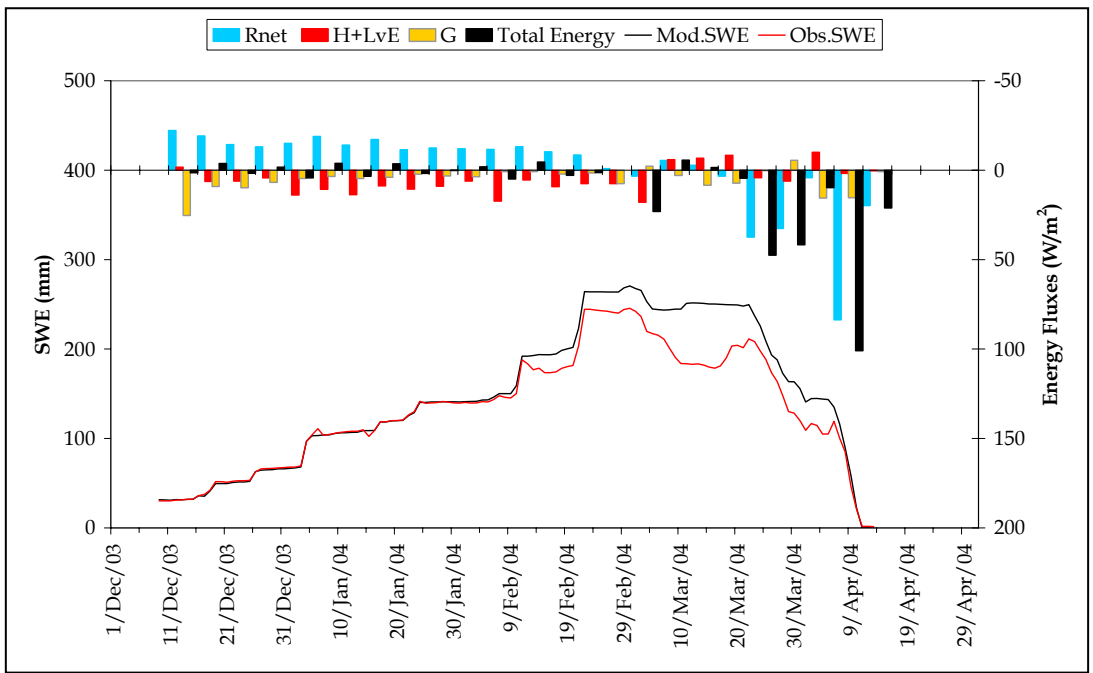


Figure 4.9 Model outputs for energy and mass balance at GY, 2003-2004

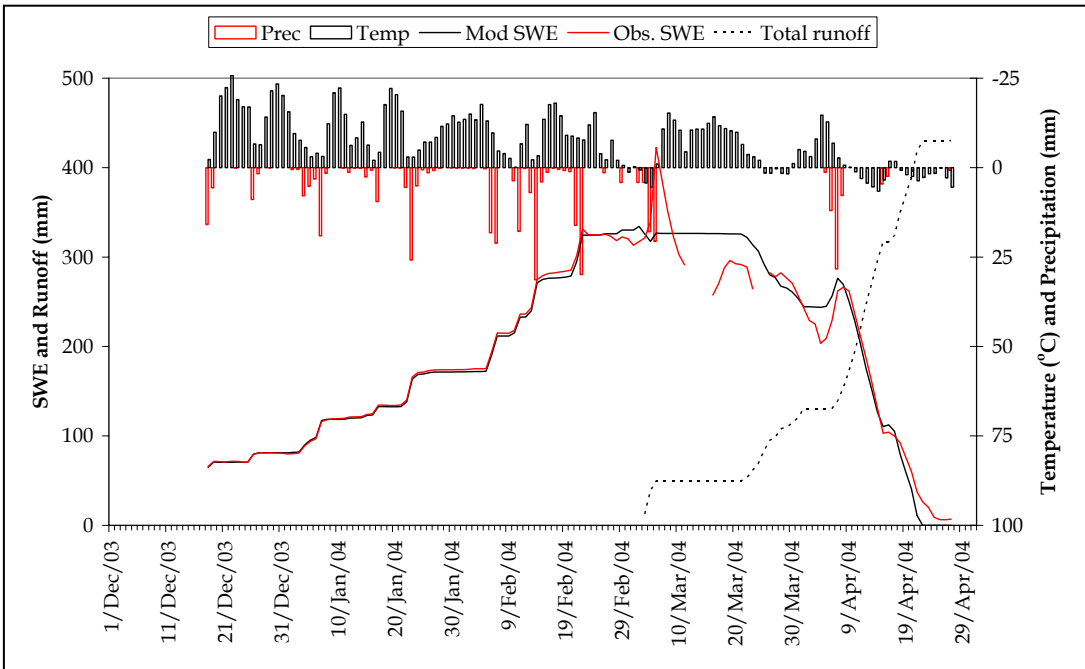
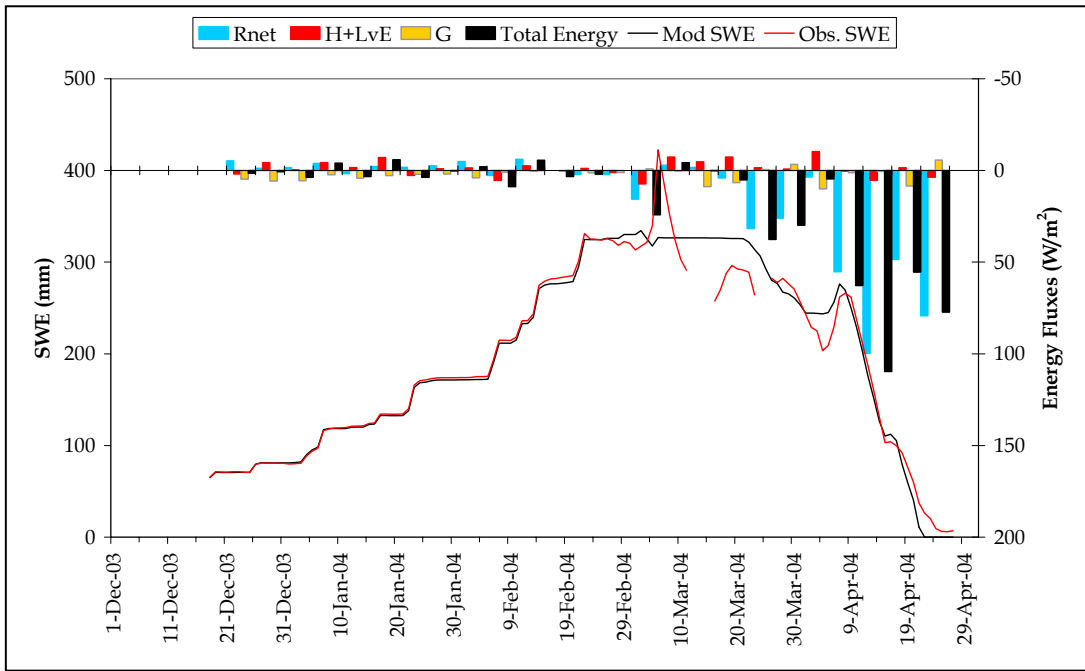


Figure 4.10 Model outputs for energy and mass balance at OVA, 2003-2004

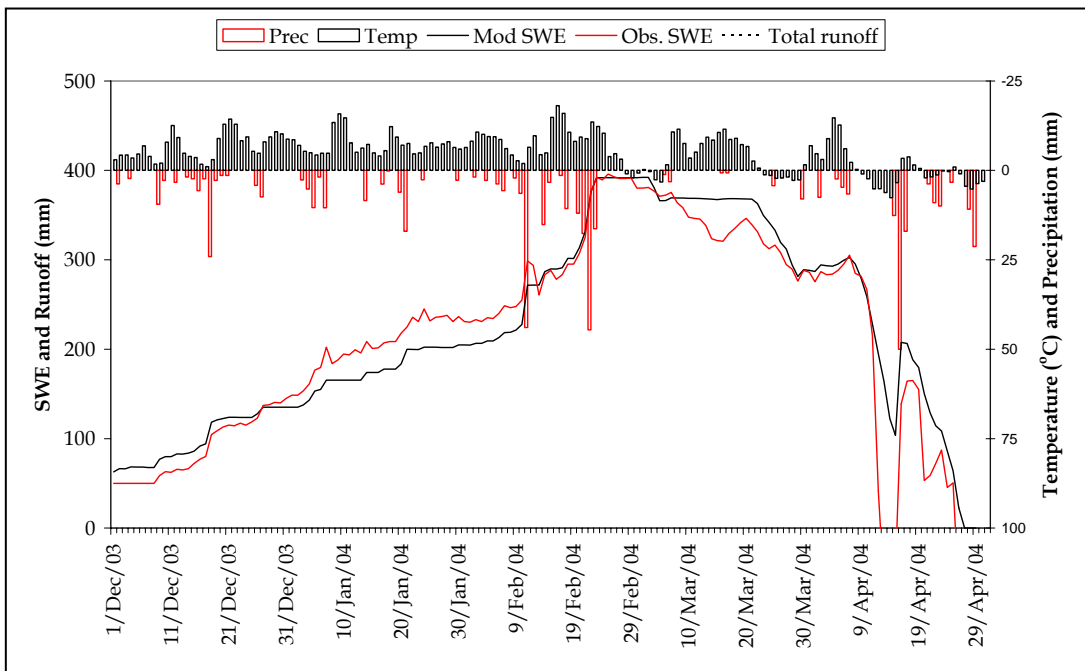
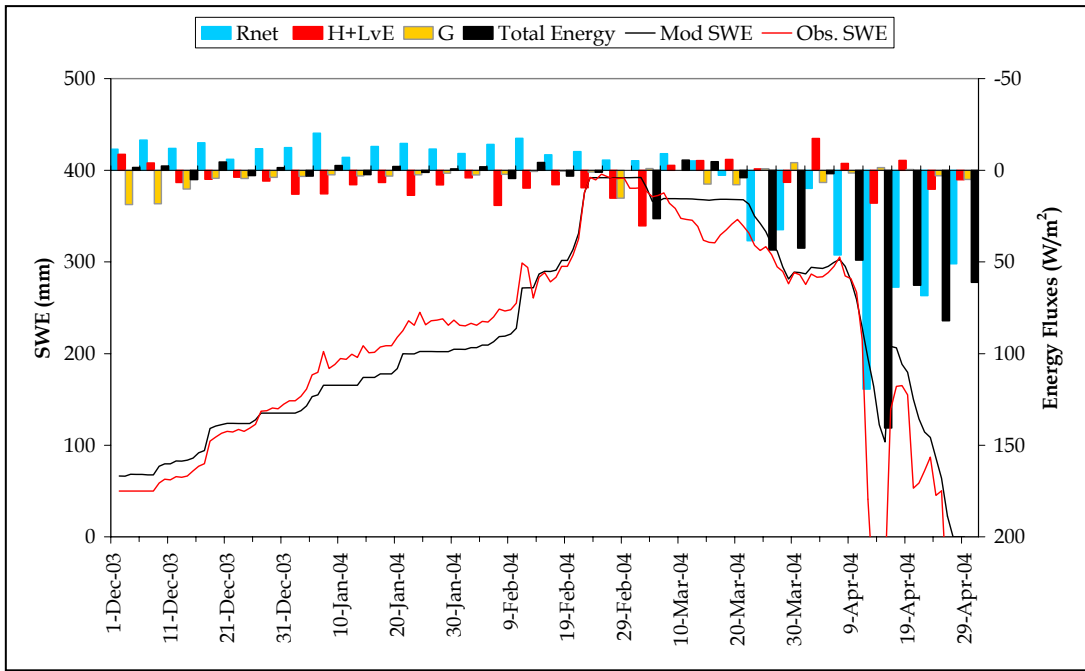


Figure 4.11 Model outputs for energy and mass balance at CAT, 2003-2004

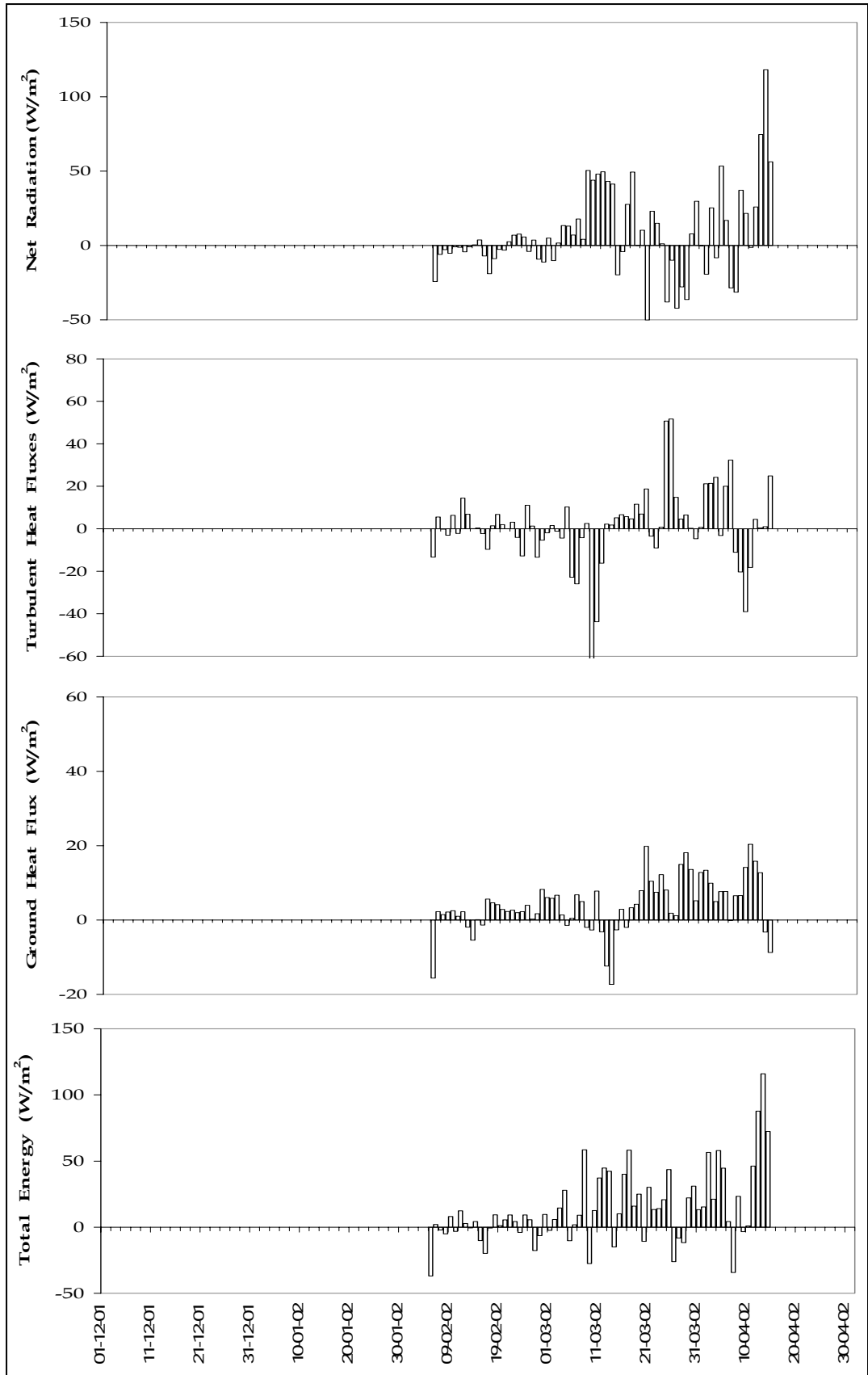


Figure 4.12 Energy flux outputs at GY, 2001-2002

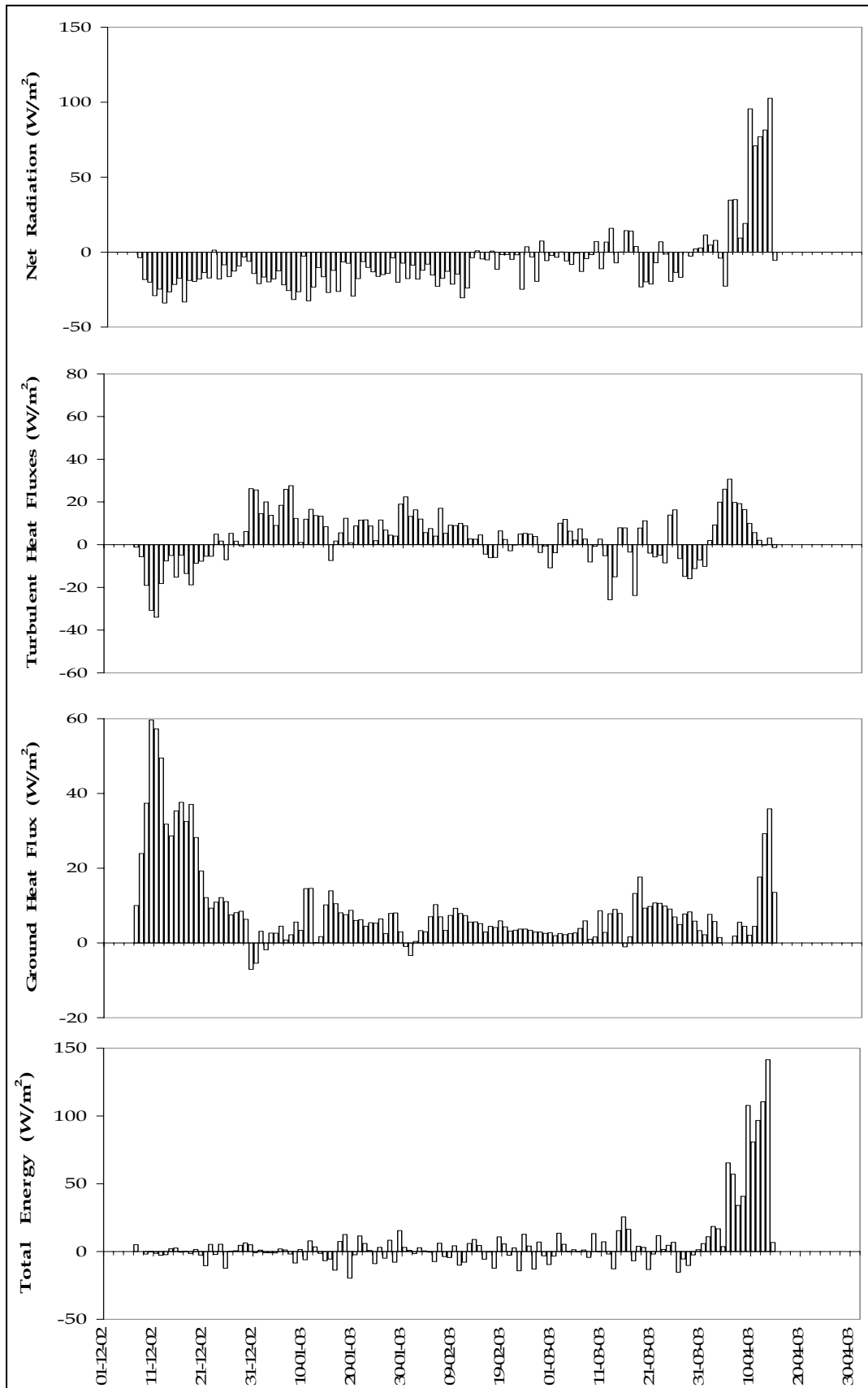


Figure 4.13 Energy flux outputs at GY, 2002-2003

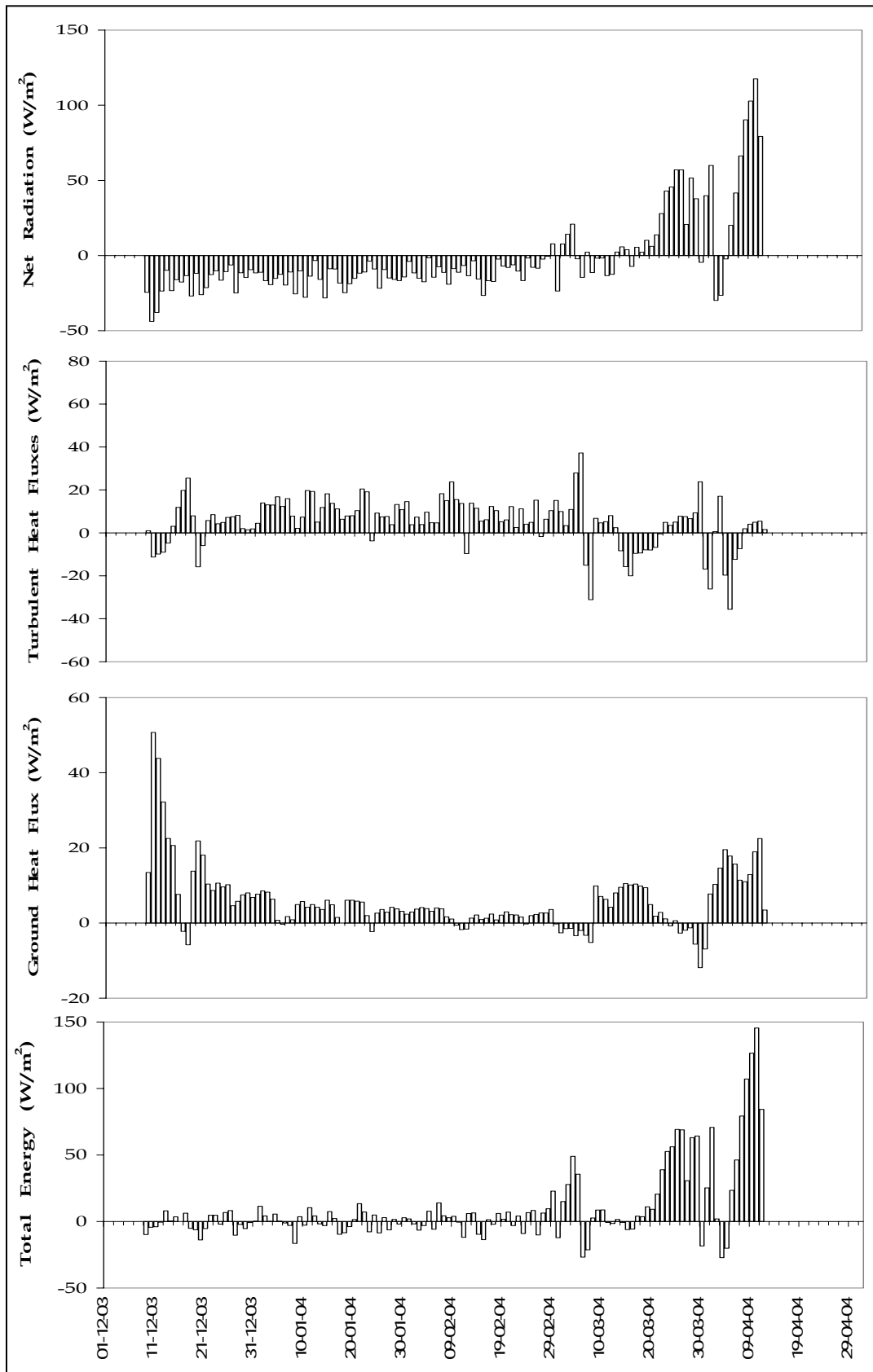


Figure 4.14 Energy flux outputs at GY, 2003-2004

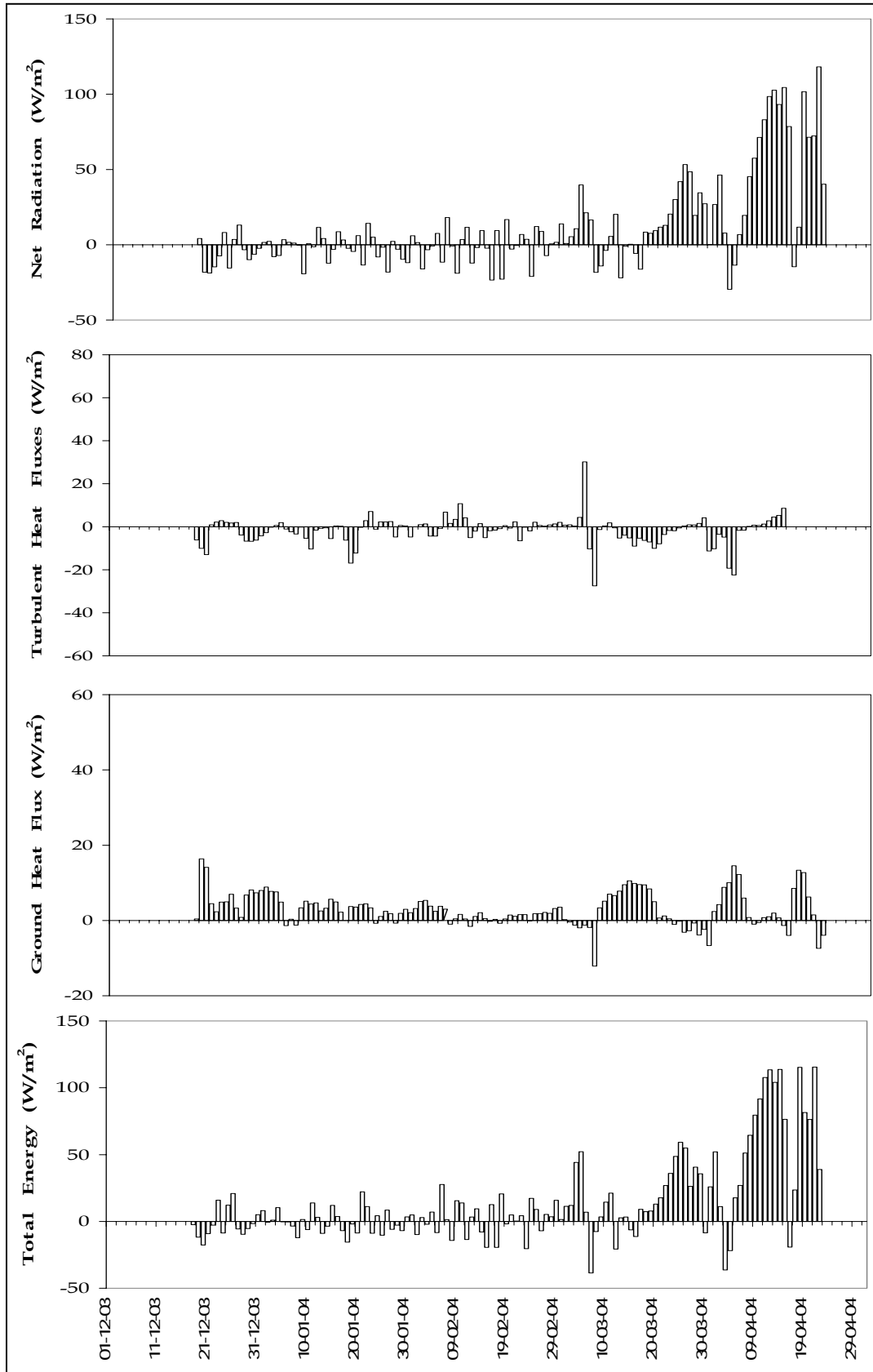


Figure 4.15 Energy flux outputs at OVA, 2003-2004

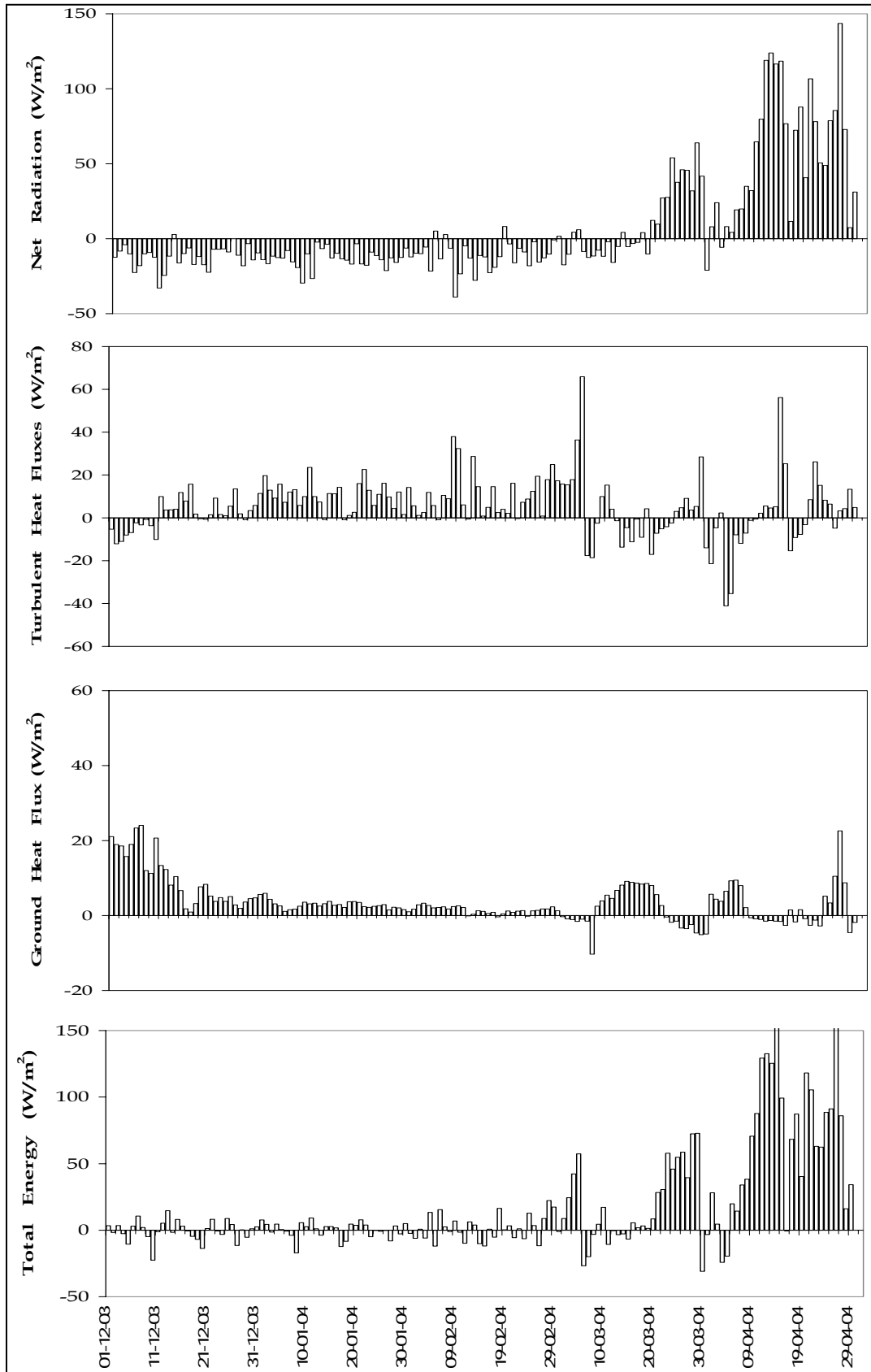


Figure 4.16 Energy flux outputs at CAT, 2003-2004

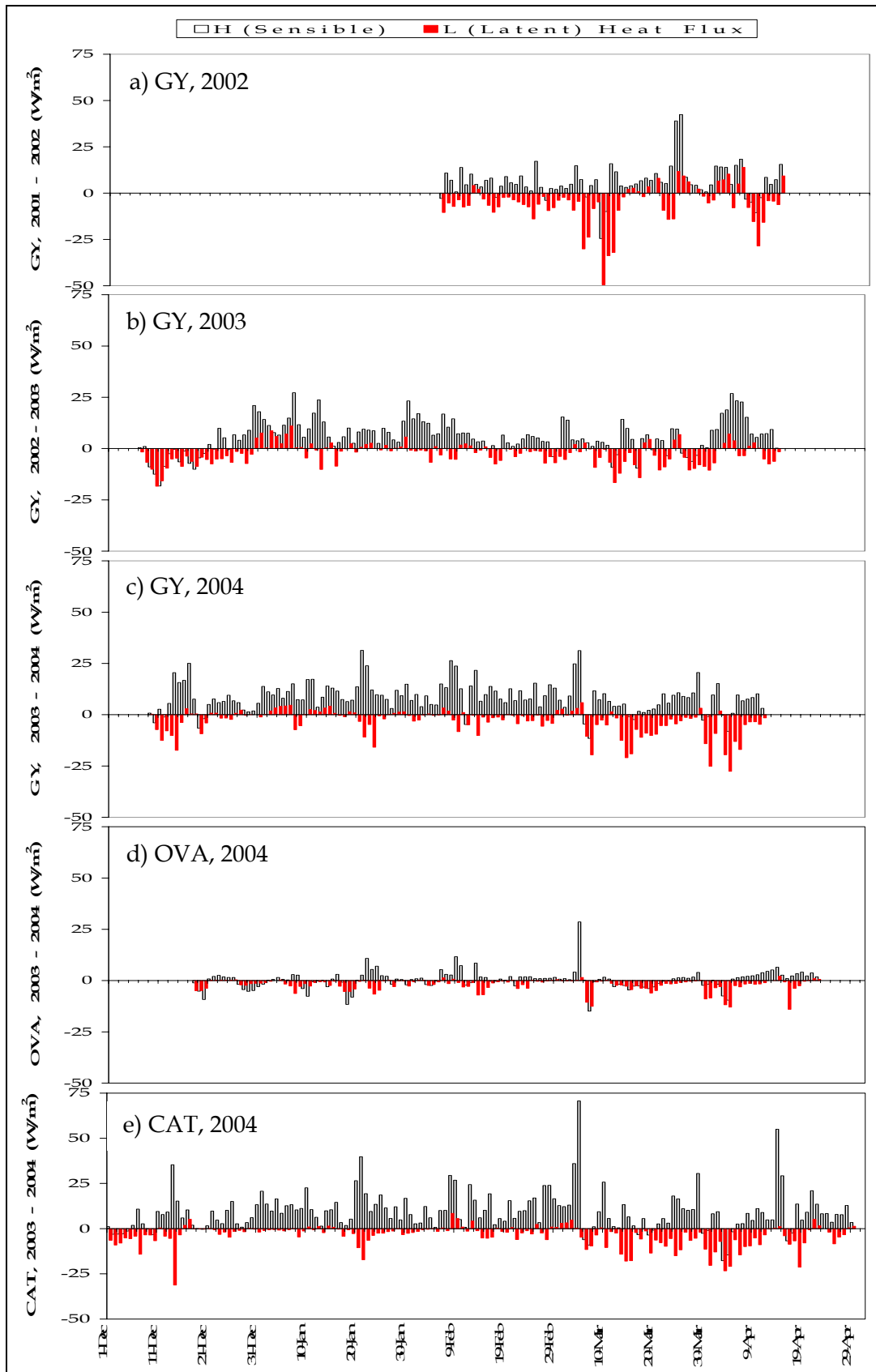


Figure 4.17 Daily average sensible and latent heat flux values

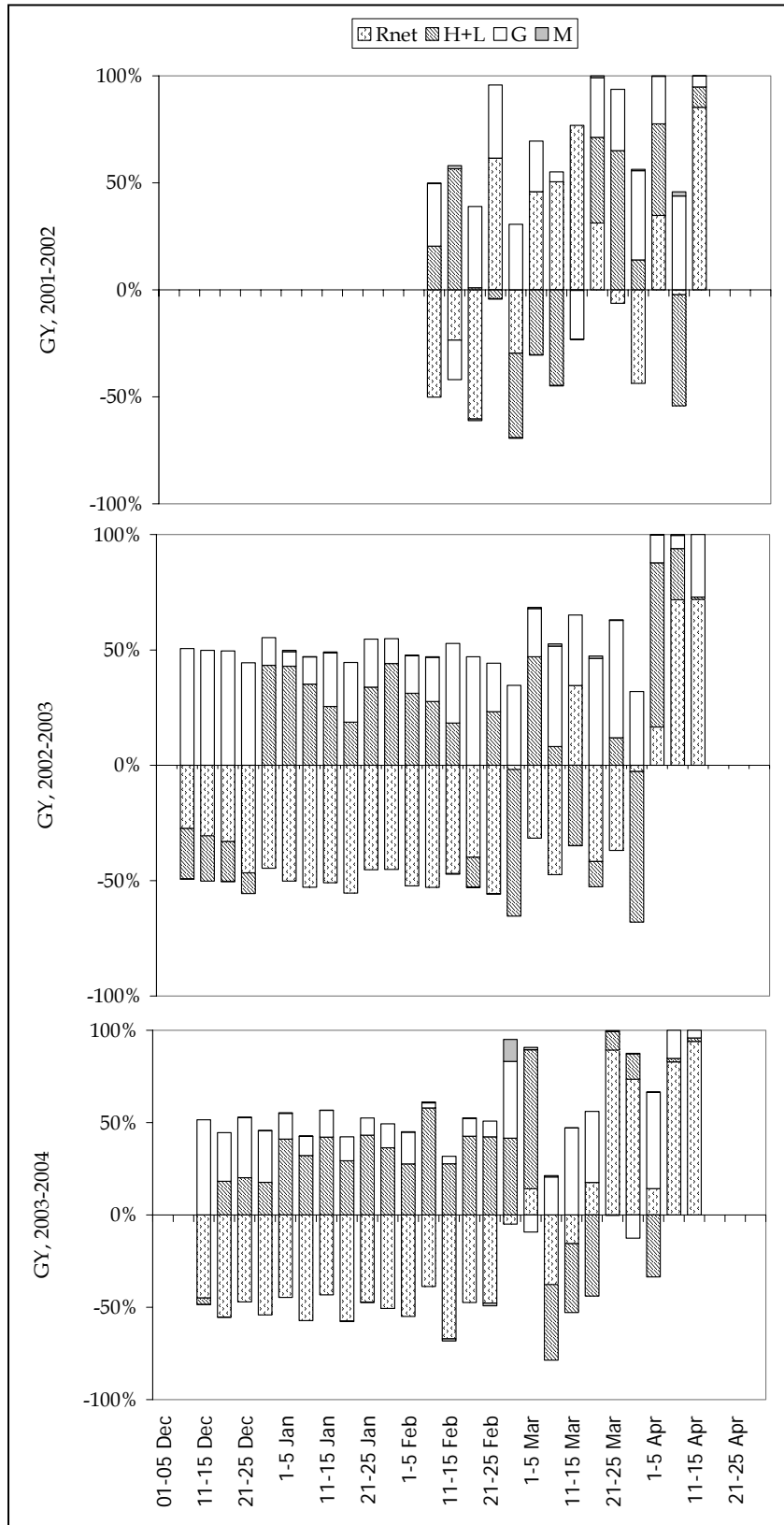


Figure 4.18 Energy percentages within the total energy, GY

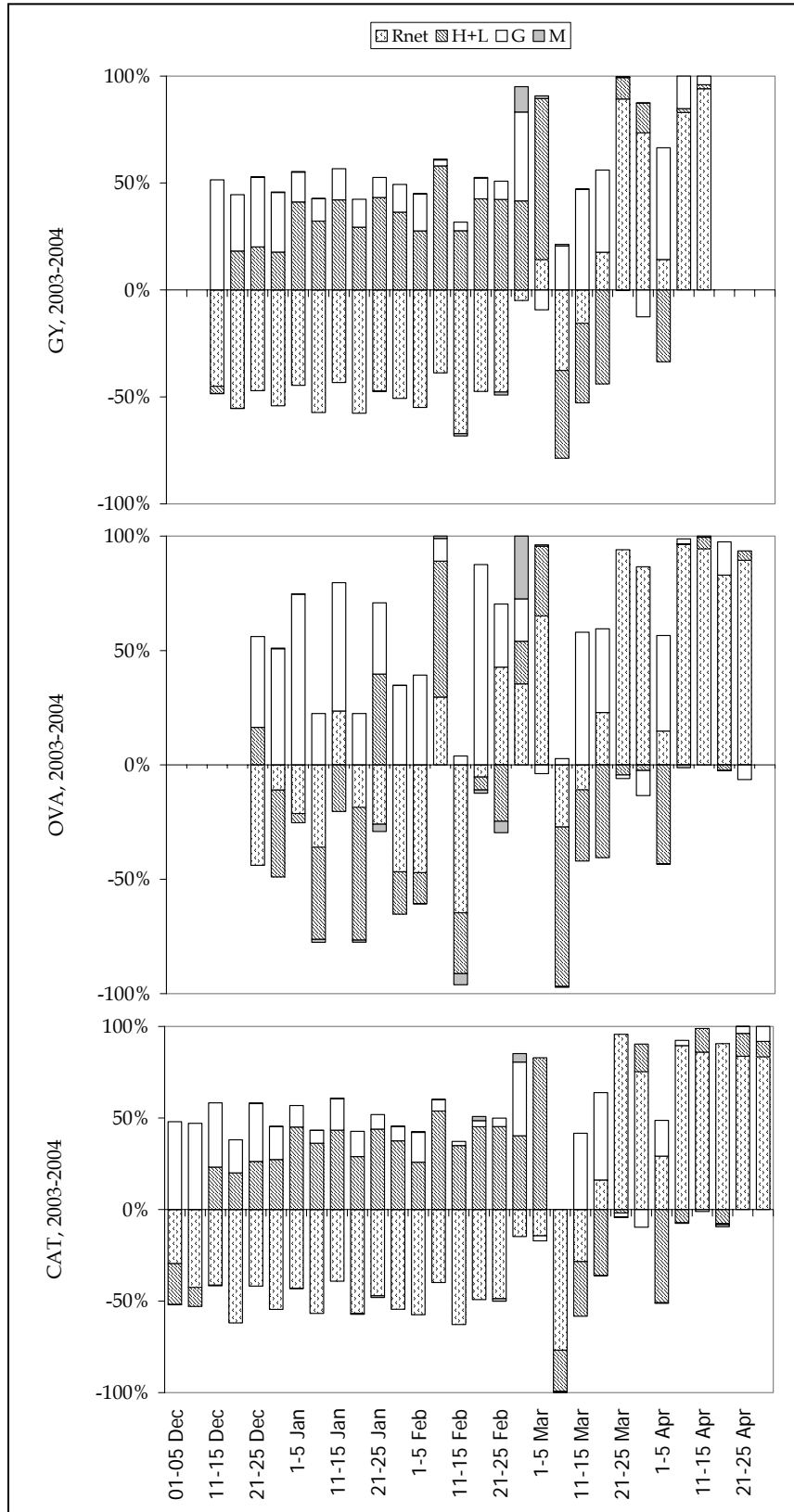


Figure 4.19 Energy percentages within the total energy (GY, OVA, CAT)

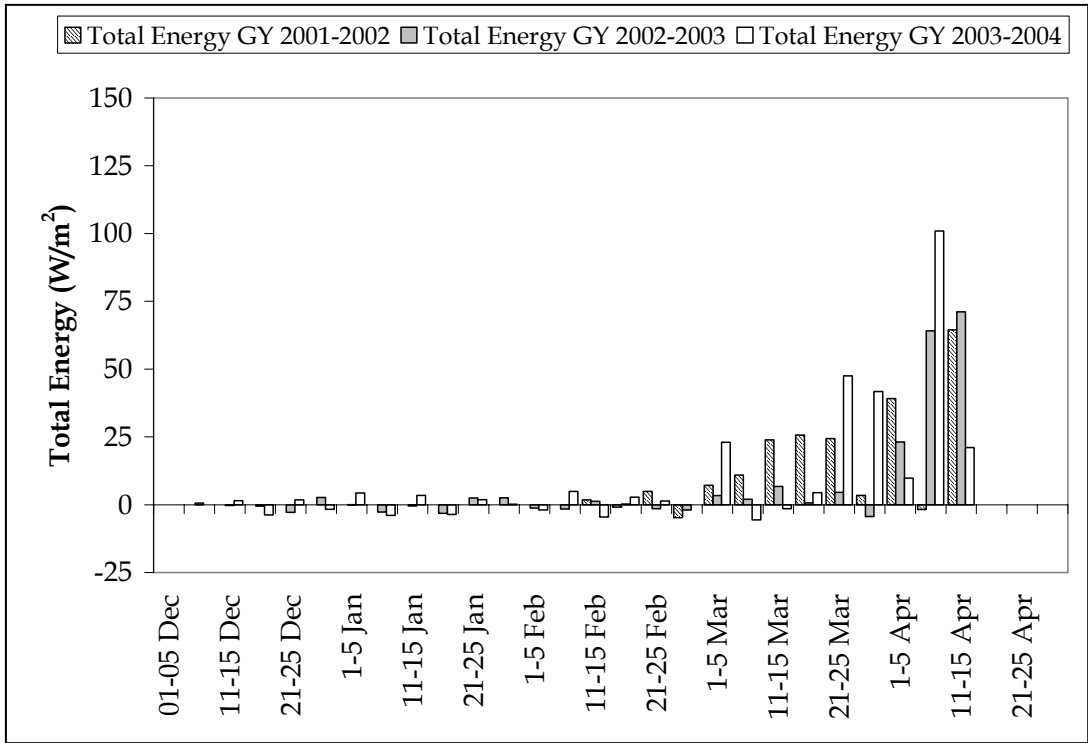


Figure 4.20 Total energy comparisons for three years, GY

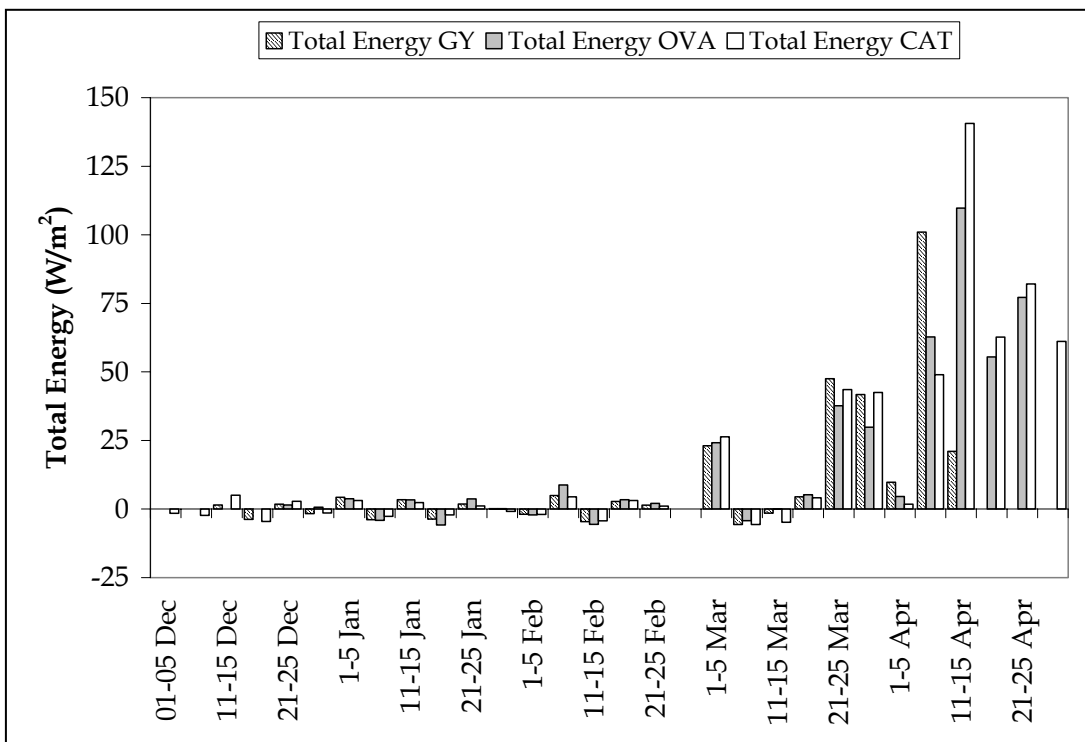


Figure 4.21 Total energy comparisons for three sites, 2003-2004

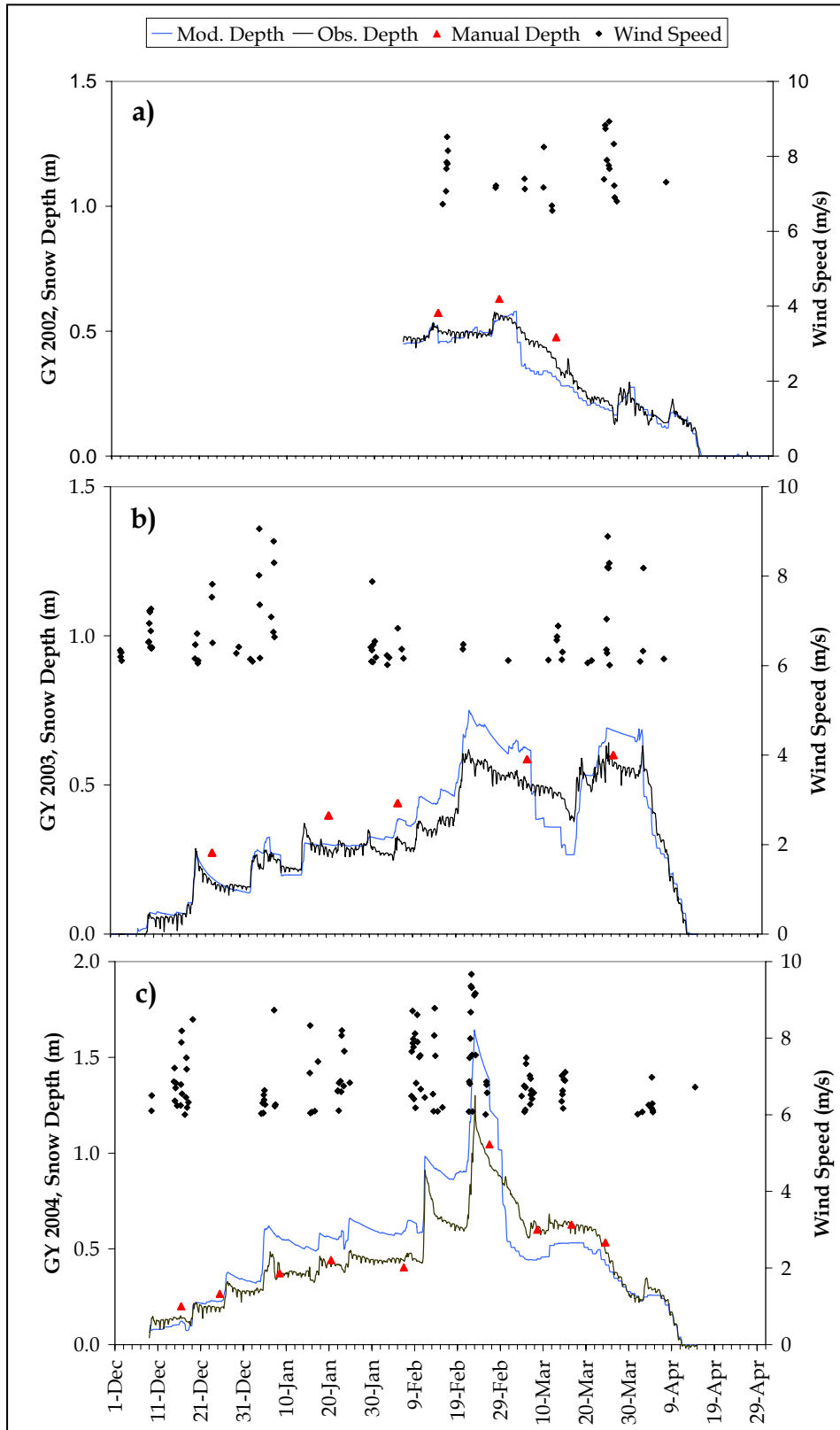


Figure 4.22 Modeled and observed snow depths, GY

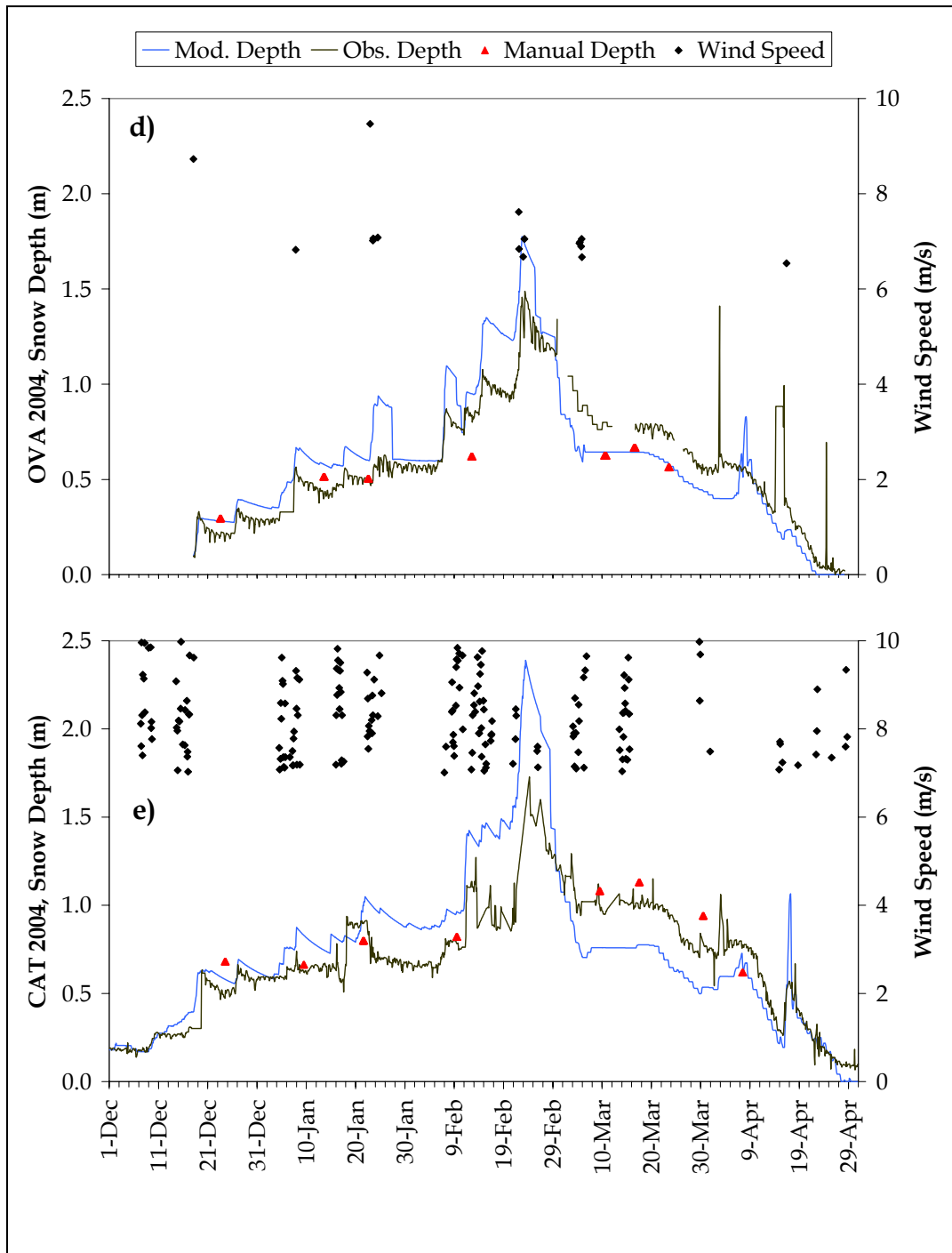


Figure 4.22 (Cont'd) Modeled and observed snow depths, OVA and CAT

4.8.1. Temporal Analysis of Model Applications

The first two snow seasons are similar to each other in terms of maximum SWE and snow depth. However, the observed maximum SWE and snow depth values of the year 2004 are almost the double those of the previous two years. Compared to the long term averages (Figure 3.6) the first two snow seasons are average years, whereas SWE values are well above average during the peak period of 2004. On the other hand, total volume of flow (EIE2154) are close to each other with 10% difference, being $361.7 \times 10^6 \text{ m}^3$ and $397.9 \times 10^6 \text{ m}^3$ (total volume of March - May, without considering baseflow) for the last two snow seasons, respectively. The main reason for this close correspondence in volume is the rainfall after snowmelt.

Even there are similarities between snow seasons in terms of SWE and snow depth, melting patterns are different at each case. The removal of snowpack from the site GY occurs within the interval of 10-15 April for all three years with different melting characteristics. However, the snow covered area images from satellites (NOAA and MODIS) indicated gradual melting for 2004 especially for the high elevation zones, in contrast to the sharp melting period observed for the year 2003.

In terms of climate data, net solar radiation amounts are generally less during the first snowmelt period (2001-2002) compared to the other years. Temperatures are generally lower for the second year, and wind speeds are slightly greater for the third year than for the other years.

4.8.1.1. Snow Cover Energy Balance

The presence of snow greatly alters the land surface energy balance; net input of solar radiation is reduced due to the high snow albedo, turbulent heat exchange is lowered due to low aerodynamic roughness of the smooth snow surface and heat flux from the ground is reduced as a result of the low thermal conductivity of snow. The SNOBAL outputs are summarized in Table 4.4-4.6 in five-day averages.

Table 4.4 The model outputs in five daily averages at GY, 2001-2002.

	R _{net}	H + L	G	M	ΔQ	Evap	Melt	Runoff
	(W/m ²)					(mm)		
6-10 Feb	-3.22	1.31	1.88	0.02	-0.01	-0.91	0.00	0.00
11-15 Feb	-1.61	3.89	-1.27	0.10	1.81	-0.44	2.06	0.00
16-20 Feb	-6.21	0.10	3.90	-0.08	-0.84	-0.58	0.00	0.00
21-25 Feb	3.99	-0.27	2.21	-0.01	4.92	-1.06	1.72	0.00
26-28 Feb	-5.16	-6.87	5.33	-0.04	-4.79	-0.60	0.24	0.00
1-5 Mar	4.98	-3.29	2.57	-0.02	7.13	-1.48	14.28	4.61
6-10 Mar	32.85	-29.09	2.97	-0.10	10.92	-3.64	15.28	6.56
11-15 Mar	22.01	-0.08	-6.53	-0.02	23.90	-1.21	31.38	18.95
16-20 Mar	7.45	9.54	6.65	0.19	25.73	0.39	42.10	36.39
21-25 Mar	-1.76	18.15	8.01	0.00	24.40	-0.41	29.08	25.04
26-31 Mar	-11.51	3.68	10.97	0.15	3.44	0.06	15.61	13.59
1-5 Apr	13.61	16.75	8.72	0.07	39.14	0.74	48.43	45.97
6-10 Apr	-0.50	-11.25	9.51	0.42	-1.79	-1.53	17.44	15.93
11-15 Apr	54.98	6.15	3.30	0.04	64.47	-0.10	76.18	77.19

Table 4.5 The model outputs in five daily averages at GY, 2002-2003.

	R _{net}	H + L	G	M	ΔQ	Evap	Melt	Runoff
	(W/m ²)					(mm)		
5-10 Dec	-14.21	-11.34	26.20	-0.02	0.62	-1.01	1.47	1.36
11-15 Dec	-24.82	-15.99	40.51	-0.01	-0.31	-1.04	0.00	0.00
16-20 Dec	-20.63	-10.73	30.94	-0.12	-0.54	-0.65	0.00	0.00
21-25 Dec	-11.69	-2.25	11.12	0.00	-2.82	-0.65	0.00	0.00
26-31 Dec	-11.07	10.74	2.99	0.00	2.66	0.06	0.00	0.00
1-5 Jan	-17.72	15.17	2.20	0.21	0.02	0.75	0.00	0.00
6-10 Jan	-23.73	15.78	5.30	0.05	-2.71	0.33	1.16	0.00
11-15 Jan	-17.79	8.92	8.11	0.11	-0.42	-0.43	0.00	0.00
16-20 Jan	-17.42	5.87	8.16	0.00	-3.17	0.02	0.00	0.00
21-25 Jan	-12.12	9.07	5.57	0.01	2.49	0.19	0.00	0.00
26-31 Jan	-11.92	11.66	2.85	0.01	2.52	0.11	0.00	0.00
1-5 Feb	-15.25	9.10	4.80	0.01	-1.20	-0.30	0.02	0.00
6-10 Feb	-19.34	10.10	6.97	0.13	-1.57	-0.14	0.11	0.00
11-15 Feb	-7.29	2.84	5.34	-0.04	1.20	-0.10	0.00	0.00
16-20 Feb	-3.73	-1.21	4.40	-0.01	0.26	-0.49	0.00	0.00
21-25 Feb	-9.11	3.80	3.43	-0.01	-1.52	-0.12	0.00	0.00
26-28 Feb	-0.14	-5.03	2.74	0.00	-1.91	-0.52	0.00	0.00
1-5 Mar	-3.59	5.34	2.37	0.05	3.37	-0.29	0.23	0.00
6-10 Mar	-4.57	0.78	4.19	0.10	1.97	-0.30	4.48	0.00
11-15 Mar	6.00	-6.04	5.30	-0.01	6.73	-1.30	7.94	4.07
16-20 Mar	-9.29	-2.44	10.32	0.24	0.68	-0.50	6.09	4.06
21-25 Mar	-6.85	2.21	9.44	0.05	4.59	-0.28	0.00	0.00
26-31 Mar	-0.46	-10.97	5.39	0.00	-4.36	-1.45	0.00	0.00
1-5 Apr	4.11	17.57	2.97	0.06	23.09	0.25	26.28	21.93
6-10 Apr	45.99	14.23	3.67	0.23	64.13	-0.07	89.30	99.50
11-15 Apr	51.10	0.74	19.26	0.00	71.10	-0.53	91.68	93.82

Table 4.6 The model outputs in five daily averages at GY, 2003-2004.

	R _{net}	H + L	G	M	ΔQ	Evap	Melt	Runoff
	(W/m ²)					(mm)		
11-15 Dec	-22.16	-1.70	25.35	-0.03	1.47	-1.39	0.00	0.00
16-20 Dec	-19.19	6.33	9.13	-0.04	-3.78	-0.17	2.15	1.72
21-25 Dec	-14.32	6.13	9.88	0.06	1.76	0.10	0.00	0.00
26-31 Dec	-13.07	4.27	6.73	0.07	-1.69	0.10	0.00	0.00
1-5 Jan	-15.03	13.84	4.69	0.11	4.33	0.43	0.00	0.00
6-10 Jan	-18.88	10.61	3.47	0.03	-3.93	-0.11	0.00	0.00
11-15 Jan	-14.02	13.65	4.71	0.02	3.44	0.40	0.00	0.00
16-20 Jan	-17.24	8.77	3.89	-0.02	-3.61	-0.02	0.00	0.00
21-25 Jan	-11.50	10.52	2.28	-0.05	1.84	-1.00	0.75	0.00
26-31 Jan	-12.51	8.98	3.20	0.01	0.17	0.05	0.00	0.00
1-5 Feb	-12.02	6.04	3.76	0.06	-1.88	-0.03	0.00	0.00
6-10 Feb	-11.56	17.27	0.83	0.13	4.92	-0.13	0.48	0.00
11-15 Feb	-13.20	5.45	0.80	-0.22	-4.57	-0.59	0.00	0.00
16-20 Feb	-10.30	9.25	2.10	0.06	2.79	-0.11	0.00	0.00
21-25 Feb	-8.56	7.59	1.54	-0.26	1.38	-0.26	0.00	0.00
26-28 Feb	-0.90	7.58	7.58	2.17	0.00	-0.25	7.88	0.00
1-5 Mar	3.36	17.89	-2.19	0.30	23.03	0.38	39.93	56.66
6-10 Mar	-5.43	-5.90	2.96	0.11	-5.64	-1.26	1.69	13.05
11-15 Mar	-2.80	-6.71	8.47	0.03	-1.49	-1.50	0.00	0.00
16-20 Mar	3.33	-8.30	7.26	0.00	4.46	-1.34	5.14	0.00
21-25 Mar	37.41	4.17	0.22	-0.10	47.51	-0.61	66.01	49.31
26-31 Mar	32.54	6.11	-5.54	0.09	41.75	-0.49	63.80	59.13
1-5 Apr	4.25	-10.00	15.58	0.01	9.77	-1.96	15.74	14.82
6-10 Apr	83.69	1.84	15.34	0.00	101.0	-0.90	124.0	120.4
11-15 Apr	19.82	0.40	0.86	0.00	21.08	-0.04	21.36	22.59

Below, simulations for each of the three years at GY are analyzed in detail.

2001-2002, GY

Net radiation and turbulent heat fluxes are around zero till the beginning of snowmelt (Figure 4.12). Sensible and latent heat transfers tend to mirror each other with opposite signs until the beginning of melting (Figure 4.17a). Snowmelt runoff is started in the 1-5 March 2002 time period with an increased net radiation effect and gradual melting continuously developed until 15 April with net radiation and turbulent heat fluxes dominating (Figure 4.7). The greatest negative net turbulent heat fluxes occurred within the period of 6-10 March. The basic reason is the climate conditions on 9 March, on which 8.25 m/s wind speed was observed, although the average wind speed for the five day period was 2.62 m/s. On this

day, the vapor pressure was very low, around 200 Pa, and the average temperature decreased by 5°C. Under these conditions both the sensible and latent heat fluxes are generally negative, since the air is both colder and less humid than the snow surface, and the high wind speed enhances this negative turbulent heat flux (Figure 4.17a). This condition occurs occasionally during winter but does not persist, as the snow surface either cools to the air temperature or the air temperature increases during a diurnal cycle (Marks and Dozier, 1992). During the period 11-15 March, air temperatures turned to positive values, and there was significant cloud cover, resulting in the highest incoming longwave radiation for the season. A sudden increase in wind speeds during 21-25 March coincided with a reaccumulation of snow and also directly affected sensible heat flux, since the air temperatures were around 0°C. During 16-25 March, both the sensitive and latent heat fluxes were generally positive during this period, since the air was warmer and more humid than the snow surface. This case occurred infrequently especially during a storm. A warm rain event during spring would be an extreme case of combined positive turbulent transfer at the snow surface. In 21-25 March, turbulent heat explains more than 50% of the total energy for snowmelt (Figure 4.18). 26-31 March interval points very low wind speeds (around zero), temperatures are below freezing with the lowest incoming longwave values. Precipitation falling as snowfall during 6-10 April, as a result of decreasing temperatures and rather high vapor pressure values, caused a sharp latent heat flux increase, which explains half of the total energy. Finally, for the last interval, ΔQ yields an amount of melt due to high net radiation, which is around 80% of the total energy.

2002-2003, GY

The second year application (Figure 4.8 and 4.13) includes 2002-2003 snow season. During the deposition of a permanent snow cover on 7 December through mid March, net snow cover energy remained at or near zero. The snow season started with low temperatures and vapor pressures, so both the sensible and latent heat fluxes are negative in sign almost until the end of December (Figure 4.17b). A sudden increase of air temperature (around 10 °C) in four days (1-5 January), besides increased wind speeds and vapor pressures to the highest values observed

during the snow accumulation period, resulted in snowfall and SWE increasing by an extensive amounts. Turbulent energy turned positive with the explained climatic conditions at the end of December. Though net turbulent radiation remains positive, negative net radiation balances the energy equation and causes total energy is to be around zero. Ground heat flux lost its effect after a permanent snow cover of 20 mm SWE formed. Sensible heat fluxes oscillated in direction during the snow season, whereas latent heat fluxes tend to be negative through the season, indicating evaporative cooling of the snow cover. Since the site is dry and cold, observed sensible and latent heat fluxes are small in amount, although the wind speeds are rather high, averaging a little over 3 m/s. In contrast to the 2001-2002 snow season, accumulation is continuous until the beginning of April 2003, and then a sharp ablation period starts on 3 April, ending on 15 April. Increases in average air temperature and wind speed from -12.67 to -0.15°C and from 2.73 to 3.95 m/s, respectively (26-31 March to 1-5 April), led to a drastic increase in sensible heat flux, which initiated the snowmelt (Table 4.5). From then on, net radiation constituted around 70% of the overall energy (Figure 4.18).

2003-2004, GY

In the third application year (Figure 4.9 and 4.14), the accumulation period continued till the end of February, with negative net radiation values balanced by positive turbulent and ground heat fluxes. An unusual flood event occurred during 29 February - 6 March 2004 due to increased turbulent flux and rain on snow (ROS). The precipitation in the form of rainfall, due to positive air temperatures, contributed to positive advective energy and more importantly, caused an increase in the specific mass of the existing snow cover. Turbulent heat flux increased to 76.31 % of the total energy, which is the maximum value of all three years (Figure 4.17c-4.18). Similarly, advective energy increased to 2.17 W/m^2 in total at the end of February. Details of the ROS event will be discussed with the contribution of the other two point applications at OVA and CAT on the forthcoming pages. Temperature and vapor pressure increased the net turbulent heat, which led to melting of the already isothermal snow. As the event ended and conditions cleared, there was a sharp drop in incoming longwave radiation. After

the cold and cloudy period, the snow melt restarted on 22 March at a much more moderate rate with the net radiation dominating. During the next five days, temperatures decreased, accompanied by high winds, resulting in rather low turbulent heat. Ground heat flux, however, caused snowmelt, and finally, with the net radiation increase snow cover disappeared on 11 April.

In summary (Figure 4.20), the year 2002 is different from the other two years, with an early melting as a result of solar radiation and an extensive melting period of approximately one and a half months. The year 2003 is distinguished by a sharp and short melting period, starting with high turbulent heat and continuing with high net radiation, ending nearly within ten days. The year 2004 is characterized by a flood due to high turbulent heat fluxes and an ROS event. The timing of snowmelt is comparable for the last two years except for the ROS event.

4.8.1.2. Snow Cover Mass Balance

Snow water equivalent-- Simulated snow cover mass is compared with measured mass in terms of both SWE (Figures 4.7-4.9) and snow depths (Figure 4.22) for model verification in two hourly time steps. The model converts rain directly to runoff, when no snow cover is present. When snow is present, runoff is the sum of melt, less the liquid water holding capacity of the snow, plus rainfall. Early in the spring, several minor melt events that do not exceed the water holding capacity of the snow pack occurred at the site (Tables 4.4-4.6). Cumulative runoff values are also given in correspondence with SWE in the Figures 4.7-4.9. Model simulation results are in close agreement with the continuous snow pillow data throughout the snow season except for some discrepancies due to accuracy issues with the snow pillow observations, as described below in Section 4.8.3.

Snow depth-- The continuous automatic depth measurements are used to validate the simulated snow cover depths (Figure 4.22). Although the total change in snow depth is modeled well over the whole snow season, there are periods when the

model seems both to over- and underestimate the snow depths. In addition, mean depth measurements recorded manually during bimonthly snow course surveys provided an additional validation data set. Although snow courses are by necessity conducted at a coarse temporal resolution, they allow direct observation in changes in SWE and depth during events. Wind speed values greater than 6.5 m/s are also plotted to show its effect on redistribution of snowfall during the accumulation phase. The biggest deviations between the model results and the measured snow depth (also SWE) start with the pronounced windy periods.

Model performance itself can be judged by visual comparison of time series of observed values and modeled output, and with quantitative measures of goodness of fit. The rate, amount and timing of snowmelt are accurately simulated according to SWE and snow depth measurements. The statistical comparisons and the goodness of fit for the model applications will be discussed later in Section 4.8.4.

Lysimeter yield-- Determinations of the amounts and the temporal distributions of snowmelt runoff require additional analysis of the storage of the snowmelt in the snowpack and transmission of the snowmelt through the snowpack. Snow lysimeters are used to provide a physical measurement for testing models of snowpack energy balance and/or meltwater production (Kattelmann, 2000). Thus, the simulated snowmelt runoff values are also compared with measured yield/discharge from the lysimeter for the years 2003 and 2004 at GY. Lysimeter yields are compared with the total outflow and SWE (Figure 4.23 and Figure 4.25); in addition, time series of observed and modeled snowmelt outflow from the base of the snowpack are shown in Figure 4.24 and Figure 4.26 for the years 2003 and 2004, respectively. The total amount of snow on the lysimeter does not match with the total amount on the snow pillow due to several reasons explained below; a plot of observed and modeled cumulative basal meltwater outflow (Figure 4.23 and Figure 4.25) clearly illustrates the differences. Therefore, lysimeter yields can only explain some part of the melt in both seasons, however, patterns are very similar.

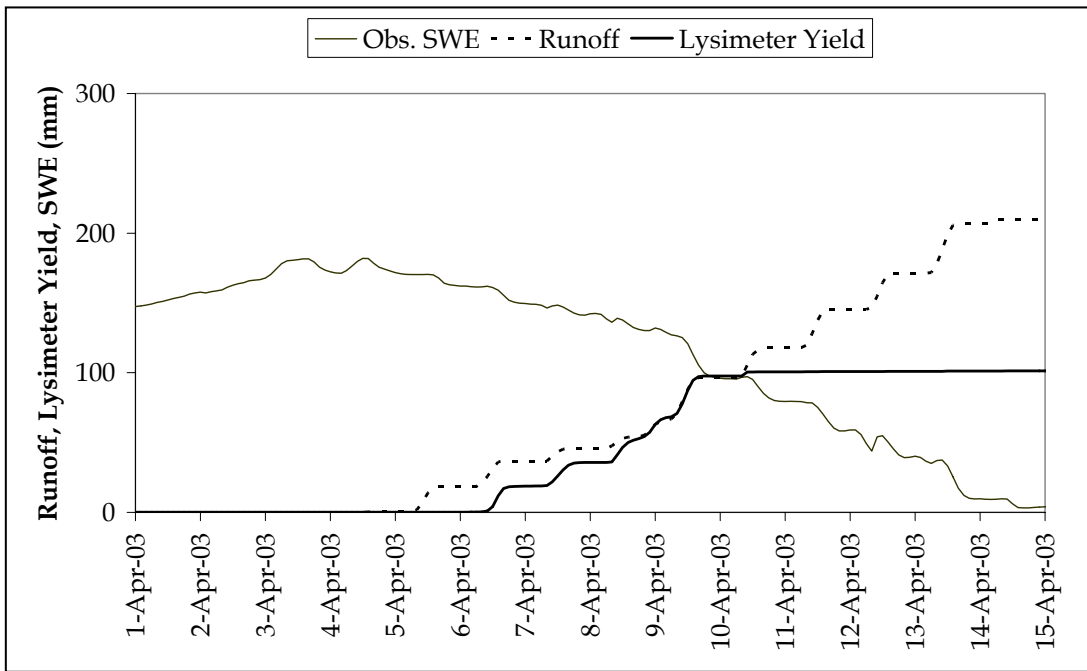


Figure 4.23 SWE, cumulative modeled runoff and lysimeter yield, 2003, GY

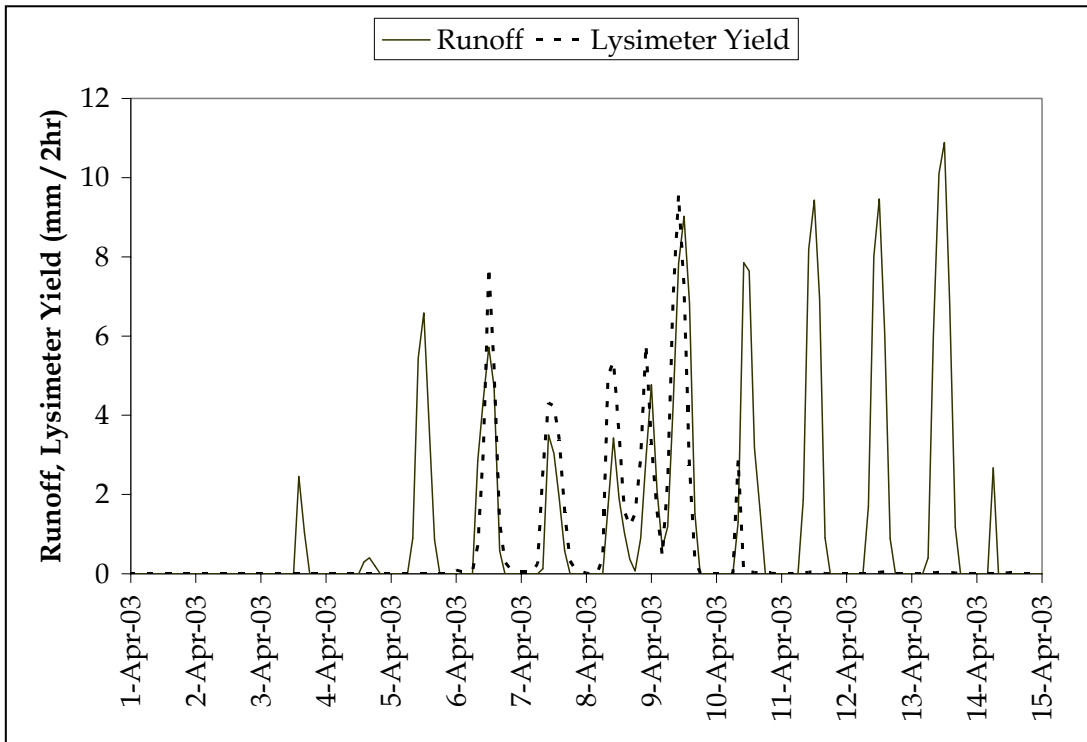


Figure 4.24 Two hourly rates of modeled runoff and lysimeter yield, 2003, GY

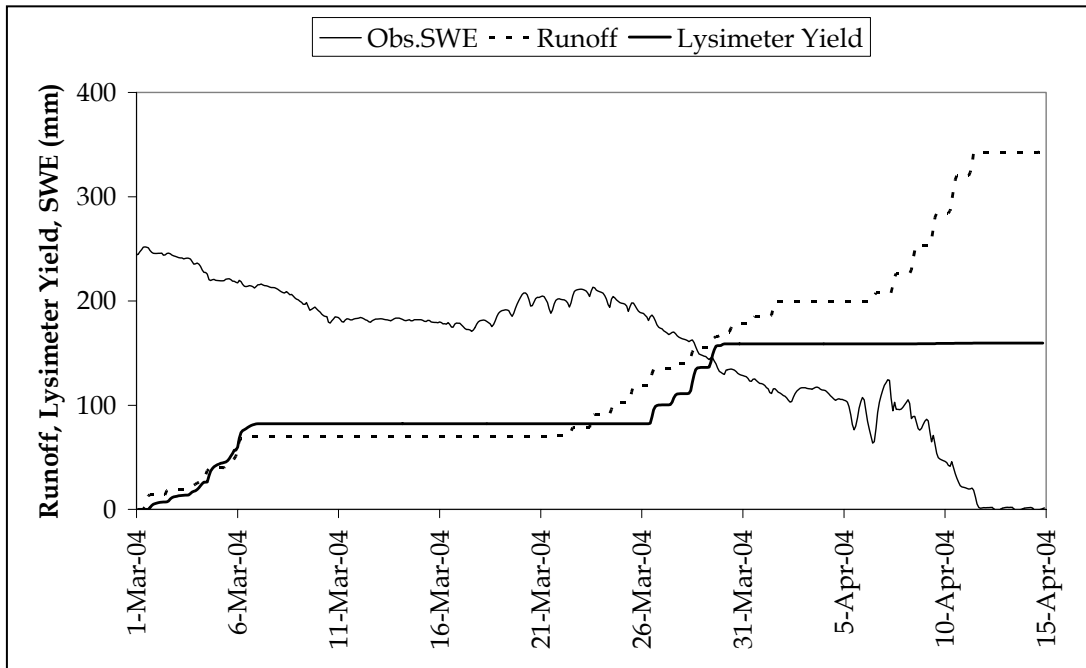


Figure 4.25 SWE, cumulative modeled runoff and lysimeter yield, 2004, GY

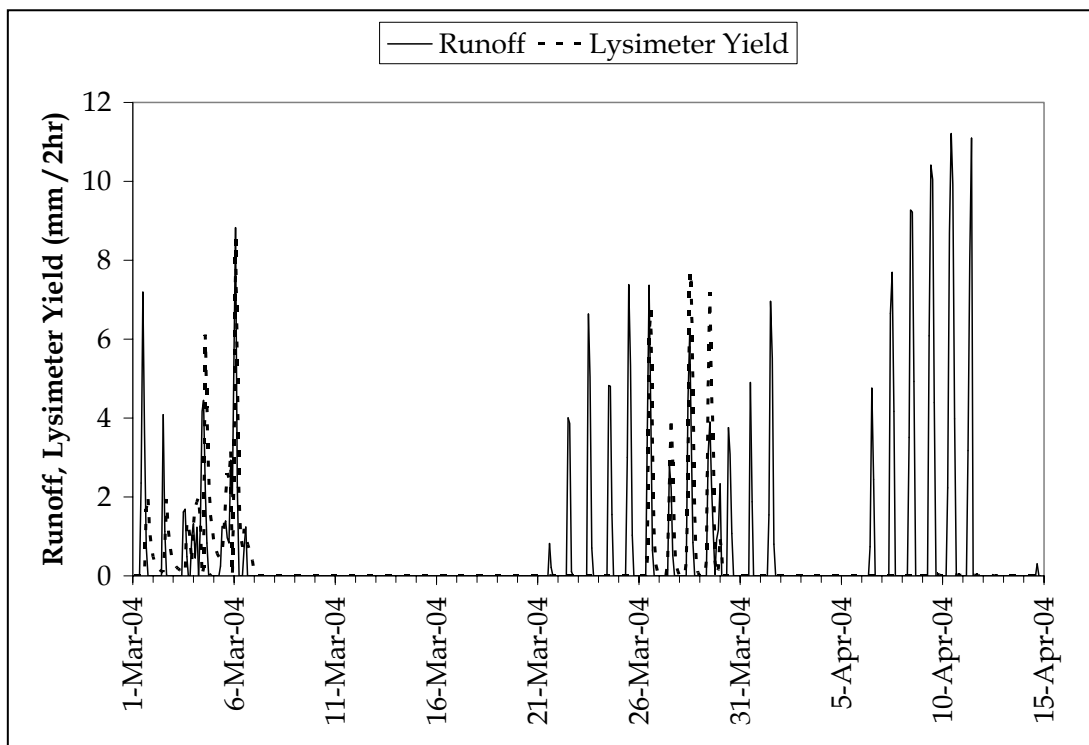


Figure 4.26 Two hourly rates of modeled runoff and lysimeter yield, 2004, GY

Two snowmelt test periods, 5-10 April 2003 (SM-I) and 11-14 April 2003 (SM-II) are examined below. During SM-I, a significant reduction in SWE occurred with an increase in lysimeter discharge. Although there is a time lag of approximately one day for the lysimeter to start yielding (due to freezing most probably) with extremely low temperature values, the melt rates are comparable to the modeled rates (Figure 4.24). Following a cold period with little melt on 4 April, daily peak outflow magnitudes rapidly increased to over 3 mm/hr, with very sharply peaked daily hydrographs. The timing of modeled outflow is generally excellent for both the peaks and troughs for the following days. There is a discrepancy, however, in the magnitudes of modeled and observed values. The model continued to underestimate outflow at all times of day compared to lysimeter outflows.

During SM-II, the lysimeter did not indicate any corresponding significant yield increase. A number of reasons can be stated for the different lysimeter responses between SM-I and SM-II. One reason may be a tipping bucket failure due to extensive melting and rainfall followed by a period of rainfall on 8-10 April. Other reasons could be: a) the non-uniformity of snow depth distribution within the snow station and the difference between the areas of the lysimeter (1.53 m²) and snow pillow (6.50 m²), thus, the lysimeter might have a snow depth that is less than the depth of snow on the snow pillow; b) the placement of the lysimeter above the ground might have led to an increased wind drift, resulting in the snow on the lysimeter to be blown away, leaving a reduced snow depth on the lysimeter; c) the difference in the material between the lysimeter (galvanized steel) and the snow pillow (hypalon) might have resulted in an increased evaporation rate (Tekeli *et al.*, 2005a).

Both the runoff and lysimeter yield start on the same date of 1 March for the last snow season 2003-2004 with the effect of increased temperatures and rainfall (Figure 4.25-4.26). Until 7 March, a comparable amount of snowmelt and rainfall occurred with both the model and lysimeter, and at the end of the ROS period, the maximum melt rate exceeded 4 mm/hr. The timing of modeled outflow is again generally excellent for both the peaks and troughs for the following days. The

second melting period started on 22 March according to the model output. No outflow was recorded by the lysimeter, however, during the first four days of this period, although the snowpack was observed to be isothermal at this time. The tipping buckets used to record lysimeter outflow, however, were exposed to the air and tended to freeze. The lysimeter again could not explain the snowmelt after 30 March, since there is no pulse from the tipping bucket under the lysimeter.

Liquid water content-- At any given time in an isothermal snowpack, the liquid water content can be viewed as consisting of the irreducible water content, plus the difference between meltwater input at the top of the snowpack and outflow from the base. This difference fluctuates rapidly and will depend not only on the amount of melt, but also snowpack depth and the rate at which the meltwater is percolating through the snowpack. As the snowpack gets thinner as the melt period progresses, the amount of water stored in this way reduces, even though the amount of melt input increases, as it is to be evacuated from the snowpack base more quickly (Fox, 2003). This pattern can be seen clearly in Figure 4.27, which shows the liquid water content of the snowpack during the second model run.

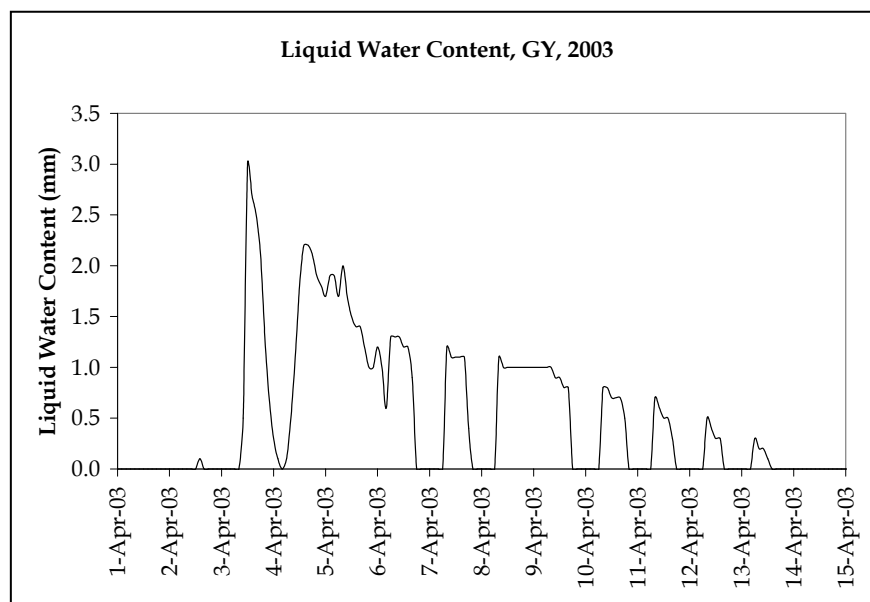


Figure 4.27 Modeled liquid water content at GY for 2002-2003 snow season

In addition to snowmelt and runoff, the model predicts evaporation from or condensation on the snow cover. Evaporation from the snow cover is shown as a negative mass flux, while condensation on the snow cover is shown as a positive mass flux. Generally, these terms are small, with a diurnal character that oscillates between day and night. The one exception to this pattern is during the rain on snow event, the condensation occurred during both day and night (Table 4.4-4.6).

4.8.2. Spatial Analysis of Model Applications

The 2003-2004 melt season included an extreme climatic event of a significant snowmelt flood that occurred during ideal ROS conditions. It provides the opportunity to investigate the effect of climate conditions prior to the event combined with the conditions that occurred during the event. To perform this analysis, the model is used with detailed data from three sites (GY, OVA, CAT) to simulate the thermodynamic processes occurring during the event.

From SWE graphs, it can be seen that the whole snow season can be broken into segments based on climatic conditions (Figure 4.28). The snow cover development occurred during the period from 1 December to 29 February. A series of cold storms deposited significant amounts of snow on 10-11 February and 21-22 February. During the latter one, about 75 mm of snowfall was observed at ERZ_CITY. 16-25 February was one of the coldest periods through the whole snow season; temperatures well below freezing (-10 to -20°C) and high wind speeds were observed at all the stations. 22-29 February was a very cold, fairly clear period.

The 29 February - 6 March, intense ROS event, was accompanied by high winds and intense rainfall. Stations ERZ, ERZ_CITY and AWS reported rainfall of about 40 to 50 mm during the event. Intense rainfall combined with rapid snowmelt contributed to the flood event. Peak flows on headwater streams and rivers draining the Upper Karasu Basin occurred on 6 March 2004, when the river rose from 10 m³/s on 29 February to 120 m³/s by 6 March (EIE2154).

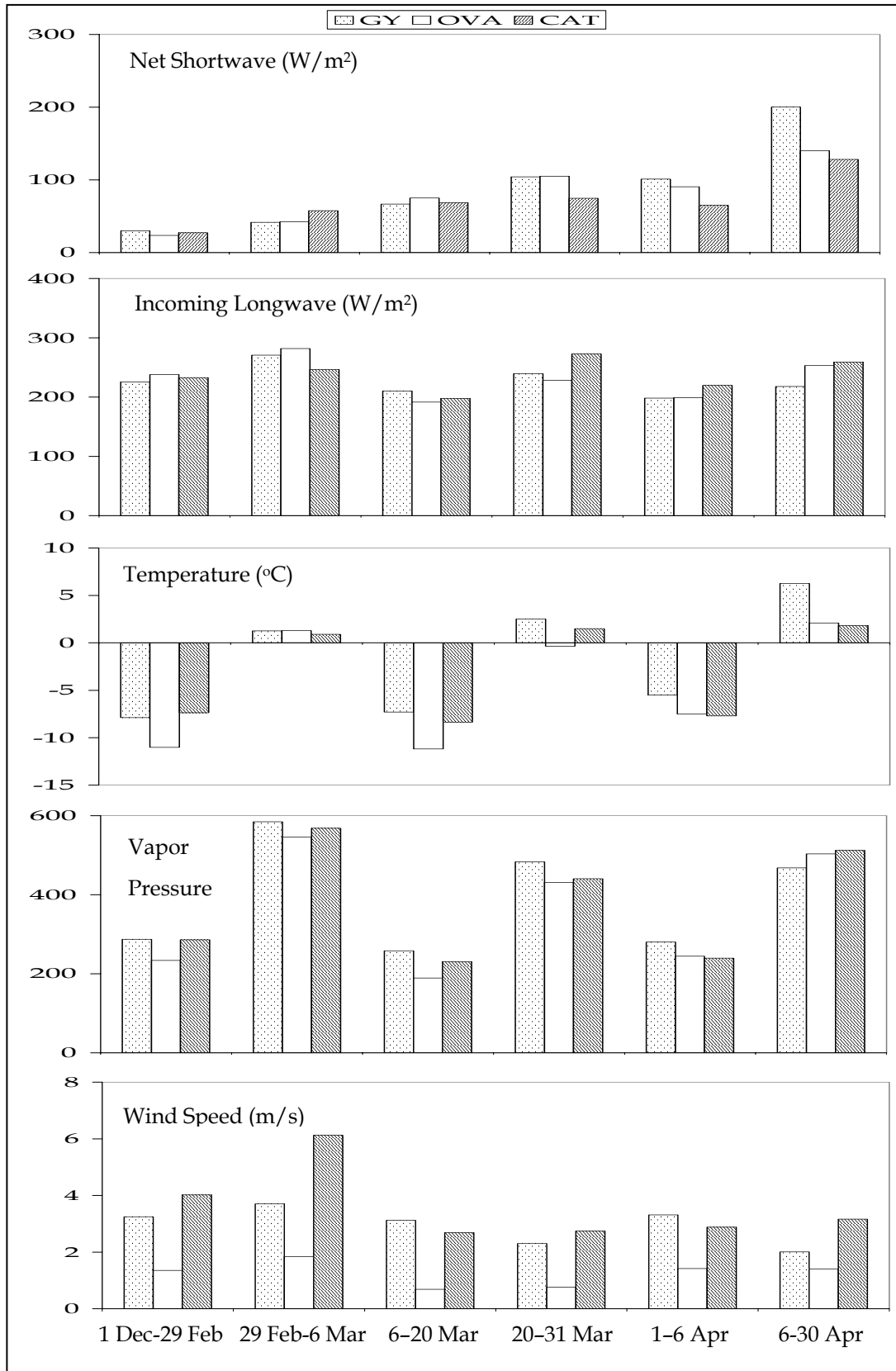


Figure 4.28 Model input categorization for 2003-2004 season evaluation

Low air temperatures, vapor pressure and solar radiation clearly indicate the period for the development of snow cover (1 December - 29 February). During the ROS event, there was a reduction in solar radiation, air temperatures were above freezing, and there was a large humidity gradient towards the snow cover at all three sites; an increase in vapor pressure to near or above the saturated vapor pressure at 0°C. The main thrust of the ROS event is followed by a cold and less humid period during 6-20 March. Snowmelt stopped at those sites that still had snow. By 16 March, flood waves in the headwater streams had passed and flows returned to normal. Then, a warm and clear period started where small and localized rainfalls occur through 20-31 March. Snowmelt continued at a much more moderate rate at those sites that still had snow. A second cold period occurred during 1-6 April with temperatures well below freezing, high winds, low vapor pressures. The extensive melting period starts with 7 April for all three sites.

For model outputs please refer to; Figures 4.9-4.11 for SWE, energy and runoff; Figures 4.14-4.17 for energy fluxes; Figures 4.19 and 4.21 for energy percentages and total energy comparison at all sites, respectively; Figure 4.22 for snow depth comparison; Figures 4.28-4.29 model input and output categorization for the spatial analysis of point based applications.

4.8.2.1. Snow Cover Energy Balance

A few minor deposition events occurred during the last week in October and the last week in November, but these melted rapidly and did not persist for more than two or three days. During the snowpack development phase until 29 February, the net turbulent flux fluctuated between 5 to 10 W/m² at GY and CAT (Figure 4.29). In contrast, it was around zero at OVA, where L_vE and H displayed the common characteristic during non-storm periods that they are of the same magnitude but opposite in sign (Figure 4.17c-e). Advective energy was effectively zero. The total energy remained around zero with the dominated negative effect of net all wave radiation during this period (Figure 4.29).

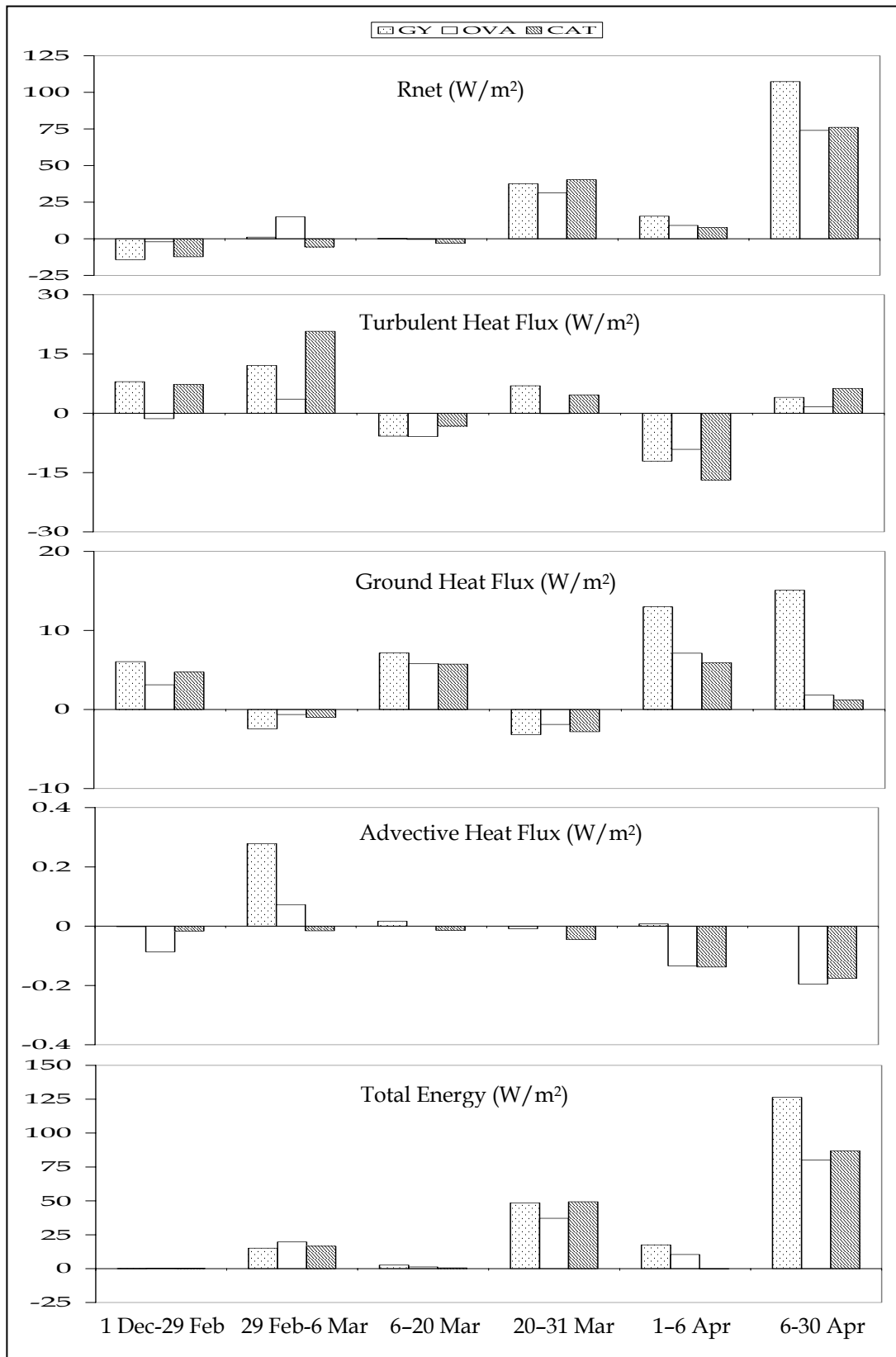


Figure 4.29 Model output categorization for 2003-2004 season evaluation

During the ROS event the snow cover energy balance is quite different, as all sites have a distinctly positive energy balance with a large input of turbulent energy; both the sensitive and latent heat fluxes were positive and combined to enhance the snow cover energy balance significantly (Figure 4.17 and Figures 4.28-4.29). Turbulent fluxes constituted around 85% of total energy at GY and CAT for the period of 1-5 March, but this value is 30% for OVA (Figure 4.19). The advective energy became effective and significant for the first time of percent of total energy (Figure 4.29). The result is that total energy is large and positive throughout the ROS event, providing a substantial amount of energy for snowmelt. Because of the influence of large volumes of 0°C melt-water percolating into the soil column, the temperature gradient between the soil and the snow is removed, and ground heat flux is unimportant (Figure 4.29).

Total energy balance was again around zero during the period immediately following the ROS event, 6 - 20 March (Figure 4.29). Although the net solar energy had an increasing trend with the progression of the season, net longwave radiation values were high but negative due to low temperatures and vapor pressures; all of these caused net all wave radiation to be zero. In addition, extreme cold conditions made both the sensitive and latent heat fluxes generally to be negative which led to enhanced negative turbulent heat fluxes. Ground heat flux values increased during this extreme weather conditions.

During the clear sky period of 20-31 March, the increased net solar radiation under clear skies dominated the energy balance and constituted around 80 to 95% of the total energy at three sites; total energy during this period was effectively well above zero (Figure 4.19-4.29). The air temperatures were well above 0°C and positive turbulent heat fluxes were observed at GY and CAT, though negative turbulent heat occurred at OVA, most probably due to negative air temperatures.

Cloudy skies with rather low temperatures and vapor pressures caused both the latent and sensible heat fluxes to be negative and constitute 50% of total energy fluxes (Figure 4.17 and 4.19) during the mixed rain and snow event on 1-6 April.

Ground heat flux began to increase as the snow cover thinned and the soil began to be heated by solar radiation, especially at GY and OVA, contributing nearly 50% of the energy for melt.

The last part (7 April and onward) is purely a snow melting period with the considerable effect of net solar radiation (Figure 4.29). Snowpack disappeared in mid-April at GY, whereas it extended until the end of April at OVA and CAT (Figure 4.9-4.11).

The total energy transfer between atmosphere-snow-ground is compared for the three sites in Figure 4.21. They look similar to each other except for the month April due to the early melting at GY compared to others.

4.8.2.2. Snow Cover Mass Balance

Data on SWE (Figure 4.9-4.11), snow depths (Figure 4.22) and lysimeter yield (Figures 4.23-4.26) are used to verify the simulated snow cover energy and mass characteristics. The two gaps in the observed records of OVA might be due to the problems related with improper functioning of the datalogger as a result of low temperatures. Simulated SWE matched observed SWE very closely, especially at GY and OVA, during the development of the snow cover, whereas there is a deviation at CAT, that can be attributable to problems related to the snow pillow itself. In the same manner, there is a mismatch for the modeled and observed SWE values after the ROS period for the GY model application for the last season. Please refer to Section 4.8.3 for further explanations related to snow pillow error issues.

The model has a tendency occasionally to overestimate maximum snow depths. The amount of overestimation of maximum snow depths by the model is not consistent between stations and is difficult to explain. There are unrealistically high accumulation records (Figure 4.22), especially at OVA. It is possible that the ultrasonic depth gauge (UDG) record is in error, and the observed inaccurate

accumulation was due to refreezing of surface meltwater that reduced the distance into the snowpack that could be detected and the UDG detecting the top of blowing snow over the snowpack surface rather than the snowpack surface itself.

Melt with associated runoff production started on the first days of March and continued over a period different for each of the sites. Maximum sustained melt rate exceeded 6 mm/hr at CAT, whereas it approached 5 mm/hr for OVA and was 5.5 mm/hr at GY. Melt rates at CAT site were comparable to the GY site; however, a substantially larger snowpack at CAT resulted in an extended ablation period, with complete ablation occurring almost two weeks later than at GY.

4.8.3. Discussion on Snow Pillow Performance

A snow pillow provides a non-destructive measurement of SWE compared to snow courses. The results can be received in real time from remote sites with the aid of automatic operation of snow pillow. In general, snow pillows function adequately, however long term experience with snow pillows demonstrates that they can yield unpredictable and erroneous results that make it difficult for water resource managers and researchers to determine what is occurring. The general explanation is given as some form of bridging of the snow over the snow pillow. The actual cause of snow pillow measurement excursion is due to the thermal and mechanical interaction of the snow pillow with the snow and ground.

There are error sources related with the snow pillow; leaking pillow, occurrence of ice bridging and connection with the snowpack outside of the snow pillow causing a reduction of the measured pressure and calculated SWE, changes in structure of the antifreeze with temperature. Another common cause of instability is air bubbles in the SWE pillow plumbing. There may be weird impacts to the snow above the pillow which are hard to evaluate or recognize because of the remote and automatic operation. In all these cases and potentially others, sensor performance is affected, and data quality is impaired (Johnson, 2001).

SWE sensor errors are most severe during the transition from a cold to a warm snow cover when the 0°C isotherm progresses from the snow surface toward the ground. The isotherm reaches the ground surface and the top of a SWE sensor at different times due to differences in the temperature of the snow over the ground and over the sensor. These temperature differences arise from the difference in thermal properties between the sensor and surrounding ground. When the isotherm reaches the ground before reaching the sensor, heat from the ground can no longer be conducted into the snow, producing a sudden increase in the snowmelt rate on the ground. This sudden snowmelt rate spike can cause a SWE sensor overmeasurement error that continues to increase until the 0°C isotherm reaches the top of the sensor, causing melt rates over the sensor and ground to stabilize. This may be the case at OVA, where a sudden jump is observed during the ROS event (Figure 4.10). When the 0°C isotherm arrives at the SWE sensor before the ground, then a SWE undermeasurement error will occur.

Either undermeasurement or overmeasurement errors may occur at critical times when the snow cover transitions from winter to spring conditions and at the start of periods of rapid snowmelt. Parameters to determine the onset of SWE sensor undermeasurement errors are defined by a negative rate of change for SWE, a negative rate of change for snow density and an increasing snow depth as explained below (Johnson and Marks, 2004).

There was an unusual circumstance in early March 2004 in which precipitation fell as rainfall (Figure 4.9-4.11) due to increased temperatures in the first several days of March. Average daily temperatures increased from -13.4 to 3.45 °C. Over the next several days, average temperatures became extremely cold, down to -10°C. Because the snow pillow alters the thermal and moisture exchange between the soil and snow and because the soil was quite moist, it can be assumed that a significant transfer of vapor from the soil to the cold snowpack, with its associated heat, would have taken place prior to the ROS event. This vapor transfer could not have occurred over the snow pillow, so it can also be assumed that the snow over the snow pillow would be colder and may have contained basal ice. Rain water

was probably retained above the snow pillow until the thermal gradient was removed and the ice layers melted (Marks et al., 1999a). At that time, a sudden reduction in SWE occurred, much like the breaking of an ice dam, which would explain the sudden catastrophic loss of SWE reported at the three stations. This caused unexpected readings from the snow pillows shown on Figures 4.9-4.11. Later manual snow samples indicated several very dense layers deep within the snowpack as well as ice lenses distributed throughout, which indicated ice bridging. The pack was not isothermal at this time and sustained melt did not occur until late March. Ultimately, this assessment must be considered to be speculation, however, the model results and manual snow course measurements at all of the sites agree on the undermeasurement of SWE values after the early melting due to the ROS. The snowpack went isothermal toward the end of March and steady melt began near March, 20.

There is a similar pattern in the 2002-2003 snow season simulation (Figure 4.8); an amount of pre-melting within the time period of 11-20 March 2003 due to net radiation resulted in ice bridging. The pack was not isothermal at this time, and sustained melt did not occur, which caused the side walls to carry the ice load, thus decreasing the pressure on the snow pillow during 26 March - 1 April 2003.

The temperature and water vapor interactions between the snowpack and soil are changed with the presence of the snow pillow and potentially changing the amount of snow over the pillow relative to snow outside the pillow. In addition, differential ground surface movement between the transducers and the pillow due to soil expansion or contraction due to excess moisture or extremely dry conditions can cause the tolerance to be exceeded without any fault on the part of the sensor. Soil expansion is a real problem at the beginning of the snow season if rainfall occurred after the calibration of a snow pillow. This might be the reason for snow pillow at CAT not working properly during the first phase of the snow accumulation (Figure 4.11). Soil expansion may also a problem causing reading SWE values bigger than zero after all the snow melts.

4.8.4. Evaluation of Model Performance

In the case of one dimensional snow process models, the level of model complexity dictates the type of validation testing possible. The simplest models may only allow the presence or absence of snow, snow depth and/or SWE to be tested (e.g. Martinec, 1975; Kondo and Yamazaki, 1990; Essery, 1997). Other models may also allow validation against other bulk snowpack properties, such as mean density and temperature, or meltwater outflow from the base of the snowpack (e.g. Wigmosta et al., 1994; Albert and Krakeski, 1998; Marks et al., 1999a). However, within snowpack temperature changes associated with nocturnal refreezing and rain-on-snow events are very difficult to represent (and thus validate) in a bulk snowpack model (Fox, 2003). Davis et al. (2001) present details of a variety of measurements used to successfully validate the physically based, energy balance model SNTHERM, where the snowpack is shallow (rarely exceeding 60 cm) and may melt completely during mid-winter thaws. Validation measurements included snow depth measured with an ultrasonic depth gauge, meltwater outflow from the base of the snowpack using lysimeters, snow density, temperature and wetness profiles measured in snow pits and snow grain size, although they identified a number of problems associated with making physical measurements of the latter (Fox, 2003). In this study, automated and manual SWE, snow depth measurements and lysimeter outflows are all used to validate the model results as presented in the model output section.

Three standard quantitative tests were used to evaluate model performance. The root mean square error (RMSE) between simulated and observed values, and the mean bias difference (MBD), or mean deviation of simulated from observed values, are presented below. The Nash-Sutcliffe coefficient or “model efficiency” (ME), which describes the variation in the observed parameter accounted for by the simulated values (Nash and Sutcliffe, 1970), is also presented for SWE. These tests were chosen to illustrate the difference between simulated and observed rather than the error, because there is a significant uncertainty in the measured

parameter. It is therefore misleading to assume that a deviation from the observed is an error (Marks et al., 1999a). The magnitude of both RMSE and MBD in all cases is small and not much more beyond the sensitivity of the snow pillow.

$$RMSE = \sqrt{\frac{1}{n} \sum_{i=1}^n (x_{\text{mod}} - x_{\text{obs}})^2} \quad (4.8)$$

$$MBD = \frac{1}{n} \sum_{i=1}^n (x_{\text{mod}} - x_{\text{obs}}) \quad (4.9)$$

$$ME = 1 - \left[\frac{\sum_{i=1}^n (x_{\text{obs}} - x_{\text{mod}})^2}{\sum_{i=1}^n (x_{\text{obs}} - x_{\text{ave}})^2} \right] \quad (4.10)$$

where x_{mod} is the modeled value, x_{obs} is the observed value and x_{ave} is the average value of the observations. RMSE and MBD are calculated for both SWE and snow depth for all the applications disregarding negative observation records for SWE at CAT; values of these validation statistics are presented in Table 4.7.

Table 4.7 Statistical model evaluation

	RMSE SWE (mm)	MBD SWE (mm)	ME SWE	Max SWE (mm)	RMSE depth (cm)	MBD depth (cm)	Max depth (cm)
2001-2002 GY	5.98	1.63	0.83	174.2	4.52	-2.22	57.7
2002-2003 GY	7.22	3.50	0.86	184.0	7.24	2.53	64.1
2003-2004 GY	26.52	15.7	0.58	273.5	16.10	6.31	130.0
2003-2004 OVA	19.05	0.56	0.80	335.0*	18.31	2.74	148.8
2003-2004 CAT	32.76	4.25	0.68	396.6	24.89	5.25	172.8

* Taken from SNOBAL result

Model performance can be evaluated as good according to the differences between observed and modeled SWE and snow depths. The better results can be achieved by ignoring the ice bridging observations of the year 2003 and especially 2004 in the computations (e.g. the exclusion of the ice bridging period from the statistical evaluation for GY application during the 2004 year, improved the results by

reducing RMSE to 15 mm and increasing ME to 0.74). Good agreement is also evident between the simulated and the manual depth measurements, demonstrating the applicability of the preprocessing algorithms at sites where detailed meteorological measurements are absent. Snow course measurements are not located in close vicinity to the sites where AWS are located, especially for OVA and CAT, but were chosen to be representative of overall snow conditions.

Although generally simple in design, lysimeters have been difficult to use in the field. Given the problems with the lysimeters, model performance is judged to be relatively good, with outflow timing, key to determine storage of water within the snowpack due to vertical percolation on a daily basis, modeled well. Unfortunately, in spite of all the effort spent for the design and installation of the lysimeter at Ovacik last year, it did not work properly. A new design should be produced for a lysimeter that could be simply and effectively inserted into the snowpack from a snow pit wall and that would cause minimum disturbance of the snowpack, avoiding convergence or divergence of vertical meltwater flow.

The pattern of snow deposition and melt is a function of exposure or shelter by topography and vegetation, leading to the development of scour sites on wind exposed areas. To simulate the hydrological processes of these areas, it is essential that wind scour, drifting and vegetation effects are accounted for. This will improve our understanding of the causes for the differences and help to define the critical parameters and processes that must be included in watershed-scale snow models (Marks and Winstral, 2001). The wind effect is more pronounced during the 2004 winter than the others, which generates a difference between observed and simulated snow depth (and also SWE) values, especially after 12 February when an increased wind speed observed with a heavy snowfall (Figure 4.22). Under these conditions, the pattern of extensive snow deposition and drifting occurred in the site should be investigated. This would indicate the relative contribution of runoff from the drifts within the basin.

SNOBAL is a step toward the development of the next generation of hydrological models. If the initial conditions and forcing data are reasonable representations of actual conditions, SNOBAL can be used to accurately estimate the timing, magnitude and source areas of snowmelt generation over a basin, drainage, or region. This and its end developer spatial distribution can provide resource managers with the information required to understand the complex interaction between water and other natural resources, recreation and changing land use as demand for these resources increases (Marks et al., 1999a).

It is acknowledged that the temporal scale at which this work was carried out means that is unlikely to be of direct practical application in water resources management. It is believed, however, that the results presented herein will be of use in the development of larger scale snowmelt models by providing an indication of how spatial variability might be parameterized at the sub-grid scale (Anderton 2002).

Having tested SNOBAL output against observed data and found good agreement, model results can be used with some confidence in further applications related with snow models (see Chapter 5). The use of snowpack energy exchange processes at a basin scale is always considered to be troublesome due to its huge amount of data requirement; therefore, the model simulation results at the index points (AWS) are related with an operation model, radiation index, and spatial distribution of the snow cover was simulated in a daily manner.

CHAPTER 5

DISTRIBUTED MODEL APPLICATION

5.1. Distributed Model Approach

Adequate representation of the most important aspects of spatial variability in snowmelt models is essential if the timing and magnitude of snowmelt runoff to be accurately simulated. One of the objectives of this thesis is, with the help of GIS tools, to develop the distributed version of the process-based snow model and test it in the headwater mountain catchment of the Euphrates Basin.

Snowmelt can be calculated in a distributed manner by means of two different approaches, namely physically based energy balance models, in which each of the relevant energy fluxes is computed, or conceptual index models (e.g. temperature or radiation index models) based on knowledge of one or few meteorological variables (see Chapter 2).

The most significant contributions in the field of snowpack energy exchange processes were developed at a point scale, whereas the use of this technique at a basin scale was always considered to be troublesome. At the same time, the problems in the accurate measurement of input variables in time and of their spatial variability were recognized to be a major constraint in snow model improvement. The progress of GIS techniques in managing distributed information and the increase of computational power give a new opportunity for a distributed modeling approach. An early attempt was made simply to extend the physically based models developed at point scale to each grid of basin representation

(Cazorzi and Fontana, 1996). Although these physically based algorithms are ultimately required to model the detailed hydrology of a region precisely, existing distributed physical models (e.g. SNOBAL) are not practical options because of their current numerical limitations and the lack of requisite input data for the study region (Hamlin et al., 1998). The variability of the energy fluxes contributing to the energy balance of the snow cover is expected to be large for mountainous environments. Therefore, due to logistical demand, it is difficult to perform a large number of measurements in complex terrain over either short or long time periods to measure the spatial variability of these fluxes (Fierz et. al., 2003).

The degree-day method is temperature index approach that equates the total daily decrease of the water equivalent of the snowpack to a temperature difference between the daily average air temperature and a base temperature as threshold. The coefficient multiplying this temperature difference is the degree-day factor. Because temperature is one of the key climate variables to be affected by climate change, the degree-day approach is easily adaptable to evaluation of various climate change scenarios associated with a temperature change (e.g. Rango and van Katwijk, 1990; Martinec and Rango, 1989). Temperature index methods have three main advantages; first, good performance at the catchment scale at daily or coarser temporal resolutions, which is not significantly outperformed by the more sophisticated physically based energy balance models (WMO, 1986), second the relatively wide availability of temperature data in contrast to data required by energy and mass balance models (radiation, wind speed, humidity and cloud cover) and third, the ease of the spatial extrapolation of temperature compared to other meteorological variables such as wind speed. The better performance in melt calculations from such simple models can be attributed to the high correlation of air temperature with other meteorological variables controlling melt.

A major drawback with this approach is that although the degree-day factor is a bulk melt factor that can provide a reasonably good measure of an average energy flux when well calibrated against prior data for a particular basin in a wide range of applications, other important melting factors like solar radiation, albedo,

topography and the turbulent energy exchange processes are not specifically taken into account. Therefore the degree day approach is unreliable under conditions when these other factors may largely dominate the melt process (Anderson, 1968), since temperature index methods imply a strong simplification of complex physical processes which have high temporal and spatial variability. The applicability of index methods is usually restricted to simulation of melt rates at daily or coarser resolution and in lumped or semi lumped manner for calculation of average melt rates over a whole basin. In addition, the spatial variation of melt rates across snow cover can only be simulated through changes in elevation associated with the air temperature lapse rate. Therefore, any improvements that can be added to the physical basis of the degree-day method will likely improve its use in both snowmelt runoff forecasting and evaluation of the effects of climate change.

Recently, an increasing need for high temporal and spatial resolution simulations of the melt rate has prompted numerous attempts to incorporate additional meteorological variables and/or more physically based expressions in the standard temperature index model. A new model would be both parsimonious enough to use in practical applications for melt estimations over large areas, as well as rigorous enough to capture the fundamental physics of melt and provide spatially explicit estimations which bridges a gap between the physical and operational models. To this end, researchers have recently attempted to produce more physically realistic results by including the significant effect of solar radiation along with air temperature to their model (Williams, 1998). Several scientists, including Cazorzi and Fontana (1996), Brubaker et al. (1996) and Pellicciotti et al. (2002) presented melt models that combine the air temperature with a radiation index.

Grid based distributed approaches, which permit a more detailed representation of spatial variability, have become more commonplace in recent years (Blöschl et al., 1991a,b; Cazorzi and Fontana, 1996; Cline et al., 1998; Davis et al., 1995; Dunn and Colohan, 1999; Hartman et al., 1999; Luce et al., 1998, 1999; Marks et al., 1999).

Generally, these incorporate some representation of spatial variability in accumulation through the use of a spatially varying initial condition (Blöschl et al., 1991a,b). Terrain-based spatial interpolation of meteorological data (Susong et al., 1999) and physically based radiation models (Dozier and Frew, 1990; Ranzi and Rosso, 1995; Varley et al., 1996) allow representation of spatial variation in the energy inputs driving snowmelt (Anderton et.al., 2002).

The aim and unique contribution of this study is to identify potential improvements to a specific aspect of the snowmelt parameterization for this mountainous region using two indexed snowmelt algorithms; a daily radiation - temperature index model applied on a landscape basis. The model indices are evaluated using physically based energy and mass balance application at representative points. The model results will be presented to demonstrate the feasibility of applying a spatially distributed snowmelt model in the mountainous basin (Garen and Marks, 2005). The model results are validated with multiple methods; using satellite data in terms of SCA, independent and continuous observations of SWE at AWS's and streamflow data at the outlet of the basin.

Air temperature is known to be a poor index of the energy available for melt when solar radiation dominates, which frequently occurs in this area (Chapter 4), hence it is expected that modeling of snowmelt in this terrain would benefit from the incorporation of a radiation term. The remainder of this thesis describes the theory, application and testing of the model, which is a method for estimating the spatial distribution of snowmelt based on point measurements and topography.

5.2. The Methodology

A more physically based snowmelt modeling by combining simplified radiation budget approach with the degree day method is applied in the present work. To achieve this, three objectives are addressed;

- 1) to improve the physical representation of the surface energy balance in the model, through separation of temperature and radiation dependent processes,
- 2) to incorporate variations in albedo into melt calculations, as albedo controls the amount of global radiation which is available for melting,
- 3) to benefit from the results of physically based model application at representative points.

The model computes melt as the sum of two components

$$M=a(T - T_c) + b(1 - \alpha)S \quad (5.1)$$

Where T is daily average air temperature ($^{\circ}\text{C}$), T_c is critical temperature as a threshold showing the temperature at which melt occurs ($^{\circ}\text{C}$), α is snow albedo and S is incoming shortwave radiation (Wm^{-2}), a and b are two empirical coefficients called respectively temperature index and radiation index ($\text{mm day}^{-1} \text{ }^{\circ}\text{C}^{-1}$) and ($\text{mm day}^{-1} (\text{Wm}^{-2})^{-1}$). The first proportion of the equation attempts to conceptualize the turbulent energy components of the energy budget, namely the sensible and latent heat exchanges and also longwave radiation through a simple index. Ohmura (2001) has recently argued that, due to strong correlation of air temperature with incoming longwave radiation, which is estimated to be one of the main energy source, the physical basis of temperature based melt index models is sounder than generally thought. The latter portion of the equation incorporates the surface radiation budget similar to that used in energy balance models.

The model is a grid-based radiation index (modified degree day) model that uses initial conditions describing the snow cover, topographic structure of the region with distributed estimates of climate variables to predict the development of melting from the snow cover as discussed in the following sections. All inputs to the model are images which exactly replicate the coordinate system and spacing of DEM grid which defines the region over which the model is run.

The most challenging aspects of spatially distributed modeling are in generating the climate forcing surfaces, correcting these for atmospheric effects and developing appropriate spatial methods for model assessment (Marks et al., 1999). The model calculates parameterized daily mean energy fluxes at the snow surface within a complex topography as given by DEM. The parameterizations are chosen in such a way that they are applicable with cloud cover observations and simple meteorological input data extrapolated from AWS measurements.

In complex terrain, the shortwave radiation balance is spatially variable which includes both the contribution from the sky and that reflected from the surrounding topography (Marsh, 1999). The global radiation (Section 5.2.3) was first calculated for clear sky conditions then corrected for the cloud cover effect. Snow albedo (Section 5.2.4) was determined by an empirical power law decay model based on time since last snowfall, using observed albedo values at two sites (GY and OVA). Through the inclusion of albedo, the new index model is able to calculate the increase in melt rate associated with snow metamorphism and with the transition from snow to land. In addition, the over-sensitivity to temperature fluctuations, which is typical of the more empirical melt models, is considerable reduced with this more physically based formulation (Pellicciotti et al., 2002).

Combination of the three point applications of energy and mass balance of snow cover in the pilot basin provides a picture of the spatial variability of melt rates and driving meteorological variables associated with along- and across-snow changes in topography and surface conditions. The comparisons showed that there is a good agreement between the energy balance simulations and the measurements (Chapter 4) which means that the energy balance simulations can be confidently used as reference melt rates.

Figure 5.1 shows a conceptual flow diagram of the modeling procedure. The model is base on the fact that snowmelt is an energy driven process and that the energy available for melt is primarily dependent upon solar radiation and air temperature, which are both functionally related to topography. Solar radiation is a function of

slope, aspect and shading, while air temperature is commonly considered to be a function of elevation (Dingman, 1994). Therefore, the model requires a digital elevation model from which elevations, slopes and aspects are calculated for each grid cell in the watershed. The slopes and aspects are used to calculate the amount of exoatmospheric radiation that each point in the watershed receives during a given time step. The radiation data are corrected for cloud effect in each day. Next, Figure 5.1 shows that the model requires distributed SWE values for the initial snow cover determination and distributed temperature data for the first part of Equation 5.1. Albedo values are modeled using a decay function depending on cumulative daily maximum temperatures distributed over whole basin. All of these distributed data are provided with an algorithm developed by Garen (1995), solar radiation model and observed measurements at sites. The model requires the calibration of temperature and radiation indices using the calculated melt amounts with physically based energy and mass balance of snowpack at a number of topographically unique locations (measurement sites or index points) throughout the watershed. A sufficient number of melt must be computed within the watershed to obtain a sound calibration of Equation 5.1.

Then, using the elevations from the DEM and the calculated indices and variables, the melt is estimated from Equation 5.1 for all unmeasured points in the watershed that are still covered with snow, as indicated by the current map of snow-covered area. The model shown in this thesis is a valuable practical method for estimating melt, but it cannot perform all of the functions of a full energy balance model.

Finally, these estimates of melt may be used as inputs to a flow-routing module, which is used to generate a prediction for streamflow. This is usually the quantity of interest (Williams, 1998).

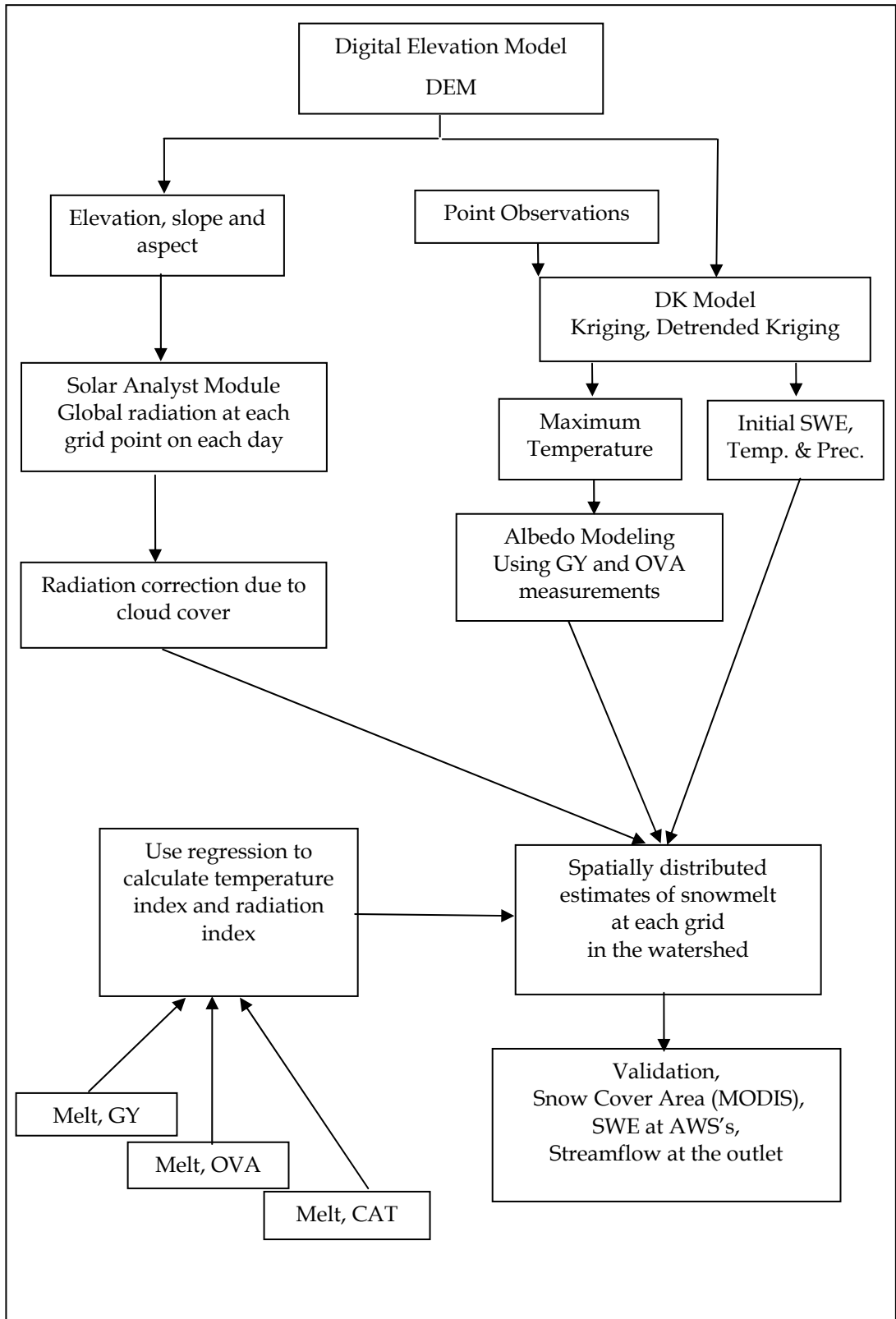


Figure 5.1 Flow chart of the distributed model application

5.2.1. GIS and Topographic Data

Recent advances in GIS technology allow powerful integration of GIS analytical and visualization tools with physically based hydrologic models and give impulse to the distributed approach. In the field of snowmelt modeling, such integration provides valuable basis for better understanding of snow accumulation and snowmelt runoff processes within the catchment, as well as for incorporating the spatial variability of hydrological and geographical variables and their impacts on catchment responses (Parajka et al., 2000).

GIS is used to provide the spatially distributed meteorological input data, additional spatial inputs, namely DEM, slope, aspect maps and map of incoming solar radiation. The DEM was the base for all elaboration and it is derived from 1/25,000 scale contour maps. GIS layers are composed of raster maps of elevation, aspect and slope, each composed of 11270 elements of 500 m x 500 m. Elevation and aspect play different roles in snow melt phenomena, the former affecting air temperature, and the latter influencing energy supply by solar radiation.

Practical scales of application for distributed snow models are determined by the resolution of the data available for model parameterization and by computational requirements, especially for larger catchments (Anderton et al., 2002). The grid size of 500 m is used in all selected raster maps. This spatial resolution is also in accordance with remote sensing data (Section 5.4.1).

5.2.2. Initial Snow Cover, Temperature and Precipitation

The index models require estimates of distributed SWE accumulation as an input for the beginning of the model run. There is no universally accepted method to estimate SWE and methods of doing so continue to be a major area of research. Areal SWE can be estimated either from the point records and distributed spatially by Thiessen Polygons, kriging and detrended kriging or similar methods under the

assumption that spatial snow variability is constant across an extent of the area. Rango and Martinec (1982) showed that basin wide SWE can be calculated using snow cover depletion curves of SCA using accumulated degree-days as the response variable. This approach incorporated SCA depletion processes into estimates of SWE but the estimates are still empirical estimates of SWE. Cline et al. (1998) showed that snow cover depletion data from remotely sensed imagery can be used in conjunction with estimates of energy balance variables to back calculate SWE on a pixel-by-pixel basis throughout the melt season. Elder and Cline (1998) simulated SCA and SWE and the spatial variability of SWE was reconstructed with some success using a GIS linked decision tree. At present, there are very few studies to draw on, because of the effort and the time labor in doing detailed spatial snow surveys. Even if it is done, it covers only a very small area for a specified time of year. The alternative of spatial data distribution beside remote sensing techniques and simulated studies from topographic variables is to model it in a statistical way. It involves statistical assumptions about the spatial snow parameterization without reference to actual locations, so it is most applicable for semi-distributed models with relatively large subareas.

Although slopes and aspects play important role in the spatial distribution of snow cover at the beginning of the winter, at the time of maximum accumulation elevation gradients seem to have dominant effect on spatial distribution of snow. In this research we attempt to add to the aforementioned studies by computing initial SWE distribution with Detrended Kriging (DK) method, (Section 5.3.1) and comparing the result with satellite data of SCA (Molotch et al., 2001).

Ideally, the lapse rate used in spatially distributed snow process models should vary in accordance with the observed variation, possibly in response to synoptic scale weather information. The most models used a fixed lapse rate value, which may lead to considerable error when air temperatures are extrapolated over a large altitude range (Blöschl, 1991). In this model application, however, the lapse rate changes spatially with the usage of DK model explained below. Initial SWE values

as of March 23, 2004, daily average and maximum temperatures and precipitation values are all distributed with the help of DK model.

The Model DK

The purpose of this program is to estimate spatial fields of precipitation, temperature and snow water equivalent by interpolating among point measurements from standard surface stations. The algorithm is based on detrended kriging and is documented in Garen et al. (1994) and Garen (1995). It has found use in several studies, including Garen and Marks (1996), Schumann and Garen (1998), and Susong et al. (1999).

The overall aim of this program was to create a better way of calculating mean areal inputs for spatially lumped hydrologic simulation models and to create a method for estimating spatial fields of these inputs for spatially distributed models, especially in mountainous areas. Traditional methods, such as Thiessen polygons and other station weighting procedures, do not adequately account for orographic effects nor do they make use of modern spatial estimation (geostatistical) techniques. This program is an attempt to account for the most important factors affecting hydrometeorological variables, taking advantage of topographic information and to create usable software for operational applications.

The program is most appropriate for meso-scale watersheds, approximately 100-10000 km². The implicit assumption is that there is a homogeneous relationship between the hydrometeorological variable and elevation within the domain, hence other factors such as slope, aspect, differing orographic regimes, etc. are not considered.

Spatial fields on a grid cell basis for daily precipitation, temperature and SWE are calculated by interpolating point measurements at hydrometeorological stations. Spatial interpolation is done by detrended kriging, which carries out the interpolation by dividing the variability into a vertical (elevation) and a horizontal

(spatial) component. The vertical component is described by time-varying linear relationships between the hydrometeorological quantity and elevation. The detrending is then accomplished by subtracting the line from the observations, thus yielding the residuals, which are used in the kriging calculations. Ordinary kriging is a spatial interpolation procedure that estimates a quantity at an unmeasured site as a weighted sum of nearby measurements, taking into consideration the spatial correlation structure of the quantity, which is represented by the semivariogram. A linear semivariogram greatly speeds up the calculations and does not require the estimation of a semivariogram for each time step, but rather the kriging weights become constant over the entire simulation period. Kriging weights are calculated from the distances among stations and distances between stations and grid cells.

There are constraints placed on the detrending lines; for precipitation, the slope of the line must be positive, otherwise it is set to zero. This is to ensure that the detrending is in fact dealing with orographic influences, for which precipitation increases with elevation. By setting the slope to zero if it is negative, the detrending step is in effect not done, thereby saying that there is no trend with elevation, and the interpolation consists only of kriging in the horizontal. Similarly, for temperature, the slope of the regression line must be negative, otherwise it is set to zero. The program deals only with the normal cooling with elevation and hence does not handle temperature inversions or other unusual atmospheric conditions that would cause temperature to increase with elevation. Here again, a zero slope reduces the interpolation to purely kriging in the horizontal.

Detrending for SWE is handled like precipitation, except that the program takes an extra step to identify an approximate snow line elevation and do the detrending only for stations above this elevation. This is particularly important early and late in the snow season, when the lower elevations are snow-free. For each day, SWE measurements are examined, in the order of low to high elevation, to identify the first nonzero value. The elevation at which this line predicts zero SWE is the estimated snow line. No detrending is used for stations or grid cells below this

snow line. Users should be cautioned that during the initial snow accumulation period and during the latter part of the melt period, the detrending can be unstable due to stations switching from snow-free to snow-covered and vice versa. This causes stations to enter or leave the group used for detrending, which usually causes an abrupt change in the detrending line, especially when the station number is limited. During the main part of the winter, after the snowpack is well-established, the interpolation algorithm performs well (Garen et al., 1994).

For estimating the detrending line, the program can use either the usual least squares regression, or it can use least absolute deviations regression (algorithm taken from Press et. al., 1988). The latter is a robust regression technique that is less influenced by so-called “outliers”, that is, values that are significantly different from most of the others in the regression data set. From the modeler’s experience, least absolute deviations regression is preferable for daily precipitation data. For temperature, the method least squares generally performs fine. Either method can be successfully applied for SWE.

5.2.3. Spatial Solar Radiation Model

Based on the concept of hemispherical fractions of both unobstructed and obstructed sky by terrain (Kondryatev, 1969), the modeling of the distributed solar radiation fluxes includes shading effects and emission by the surrounding topography. Spatial representation of incoming solar radiation is computed with the algorithms, the one described below is called as Solar Analyst (<http://www.fs.fed.us/informs/solaranalyst>), considering topographical shading of neighboring terrain. Unlike the traditional approach used to calculate the flux of shortwave radiation only incident to the earth’s surface, a method is applied to improve the results by moderating the extra-terrestrial flux by the daily cloud cover observations which will be explained in application part.

Solar Analyst

Incoming solar radiation (insolation) is the primary driver for our planet's physical and biological processes (Geiger 1966, Gates 1980, Dubayah and Rich 1995, 1996). At a global scale, the latitudinal gradients of insolation, caused by the geometry of Earth's rotation and revolution about the sun, are well known. At a landscape scale, topography is the major factor modifying the distribution of insolation. Variability in elevation, surface orientation (slope and aspect) and shadows cast by topographic features create strong local gradients of insolation. This leads to high spatial and temporal heterogeneity in local energy and water balance, which determines micro-environmental factors such as air and soil temperature regimes, evapotranspiration, snowmelt patterns and soil moisture.

Spatial insolation models can be categorized into two types: point specific and area based. Point-specific models compute insolation for a location based upon the geometry of surface orientation and visible sky. The local effect of topography is accounted for by empirical relations, by visual estimation, or, more accurately, by the aid of upward-looking hemispherical photographs. Point-specific models can be highly accurate for a given location, but simple interpolation and extrapolation of point-specific measurements to areas are generally not meaningful because most locations are affected by strong local variation. Spatial solar radiation models provide a cost-efficient means for understanding the spatial and temporal variation of insolation over landscape scales (Dubayah and Rich 1995, 1996). Such models are best made available within a GIS platform, whereby insolation maps can be conveniently generated and related to other digital map layers, and compute insolation for a geographical area, calculating surface orientation and shadow effects from a DEM (Hetrick et al. 1993a, 1993b, Dubayah and Rich 1995, 1996, Rich et al. 1995, Kumar et al. 1997).

The program, *Solar Analyst*, draws from the strengths of both point-specific and area-based models. In particular, it generates an upward-looking hemispherical viewshed, in essence producing the equivalent of a hemispherical photograph

(Rich 1989, 1990) for every location on a DEM. The hemispherical viewsheds are used to calculate the insolation for each location and produce an accurate insolation map. The model can calculate insolation integrated for any time period. They account for site latitude and elevation, surface orientation, shadows cast by surrounding topography, daily and seasonal shifts in solar angle, and atmospheric attenuation. It is implemented as an GIS extension with the following advantages over previously developed models: the model calculates direct, diffuse, global radiation and direct radiation duration, sunmaps, skymaps, and viewsheds; requires only DEM, atmospheric transmittivity and diffuse proportion (latter two parameters calculated from nearby weather stations or using typical values); calculates insolation for any specified period (instantaneous, daily, monthly, etc) and any region (whole DEM, restricted areas, or point locations); allows specification of receiving surface orientation (from DEM, field survey, or orientations of surfaces such as sensors or leaves); uses advanced viewshed algorithm for calculations; accounts for viewshed (sky obstruction by near-ground features), surface orientation, elevation and atmospheric conditions. One may refer to Solar Analyst Manual (2000) for the detailed information on the theory.

Diffuse proportion is provided for the global normal radiation flux that is diffuse. Values range from 0 to 1. This value should be set according to atmospheric conditions. Typical values are 0.2 for very clear sky conditions and 0.3 for generally clear sky conditions. Transmittivity value is the transmittivity of the atmosphere (averaged over all wavelengths), expressed as the proportion of exoatmospheric radiation transmitted as direct radiation along the shortest atmospheric path (i.e., from the direction of the zenith). Values range from 0 (no transmission) to 1 (full transmission). Because the model corrects for elevation effects, transmittivity should always be given for sea level. Typical values are 0.6 or 0.7 for very clear sky conditions and 0.5 for generally clear sky. Note that transmittivity has an inverse relation with the diffuse proportion parameter (Solar Analyst, 2000).

5.2.4. Albedo

Albedo determines the amount of global radiation that is available for conversion to melt energy at the snow surface and thus exerts a strong influence upon the spatial and temporal evolution of melt rates. It is well known that albedo variations associated with snow metamorphism alone are a significant control on the surface melt rate and in particular that summer snowfall events are of great importance to the summer energy balance (Brock et al., 2000a). Indeed, the importance of taking into account albedo in melt computations through temperature-index models has been emphasized by Lang and Braun (1990).

In many cases, limited data sets must be combined with the use of models to fully appreciate the spatial variability in energy fluxes (Marsh, 1999). Additionally, albedo variations on snow can be largely explained by temperature (Brock et al., 2000b) and may be parameterized purely as a function of temperature and/or age of the snow surface (US Army, 1956; Brock et al., 2000a) and hence may be incorporated into a temperature-index model without the need for additional data (Pellicciotti et al., 2002). In this study, the albedo exponential decay function is obtained from observed albedo values and cumulative maximum temperatures at AWS since last snowfall (see Section 5.3.3).

5.3. Distributed Model Application

A process based representation of external energy balance of the snowpack is included in the grid scale model. Spatial variability is introduced into the model in two ways: first, through specifying spatially variable initial conditions, second through the intrusion of meteorological factors in a distributed manner. Global irradiance and temperature are input via a distributed pre-processor (explained above). The clear sky irradiance is then corrected for the effects of cloud cover. Snow albedo values are computed by an empirical power law decay model based

on cumulative daily maximum air temperatures since last snowfall depending on the melting stage (Anderton et al., 2002).

Using a combination of meteorological data from basically four snow-meteorological stations (ERZ, GY, OVA, CAT), DEM, the model DK and an atmospheric radiative transfer model, the snowmelt is modeled for the ablation period of 23 March-26 April 2004. Although the early melt takes place between 29 February and 6 March 2004 with ROS event, the distributed model application is started from the second melting period because of lack of detailed information during this period and as well the fact that there are more field data on SWE to determine initial snow cover on March 23, 2004 (Section 5.3.1). Because of the importance of accurate SWE at the beginning, using ground based observations of SWE, the ability of the approach to represent the distribution model of SWE is qualitatively evaluated. The snow products of MODIS are used to construct SCA images across the basin to check the model performance. Finally, observed SWE values at AWS's are compared with the modeled ones and streamflow data is presented with the comparison of computed average snow melts in each day.

5.3.1. Distributed Snow Cover, Temperature and Precipitation

The use of observed SWE values is preferred to the alternative approaches consisting in the initialization of the model with the SWE at the beginning of the melt season (Blösch et al., 1991). GY (2065 m), OVA (2130 m), CAT (2340 m) and ERZ (1758 m) station data are used besides field data carried out on March 23 and 25, 2004 by the research team to distribute initial SWE data with DK model presented in Section 5.2.2.

Researchers studying on hydrological modeling have a keen interest on the temporal and spatial distribution of albedo values and also consistency between MODIS retrieved albedo values with in-situ observations. On behalf of this, a field work was carried out for a special study, detailed snow survey work carried out in the catchment; in addition to automated snow and weather station at GY, in-situ

data collected for both albedo and SWE values during two days provide the ground based measurements. SWE values have been observed at 20 different points in an approximately 25 km² area around GY station on 23rd and 24th March 2004 during clear sky days. Therefore, five extra points are used in DK model in order to distribute SWE data in a more sound manner. These points are selected from different elevations (2112-2348 m), aspects and slopes. The resulted SWE map is shown in Figure 5.2, consistency of the map with the satellite image obtained from MODIS will be discussed later in the subsection of 5.4.1.

ERZ, GY, OVA and CAT stations are used to distribute average daily temperature data. Temperature values of OVA site are not included generally since an inverse relation occurs at this station. All of the stations are used to distribute daily maximum temperature data in order to model the albedo values. Precipitation data is distributed as SWE on April 18, 2004 and added to the image of resulting SWE.

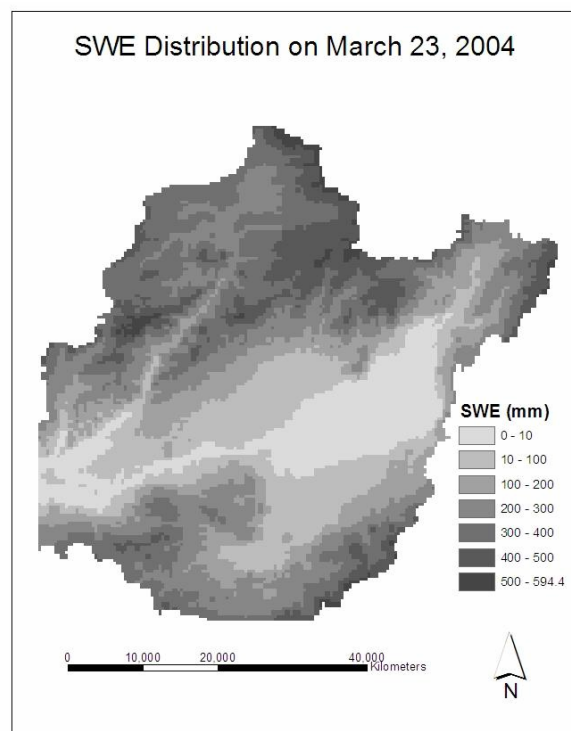


Figure 5.2 Initial snow cover including SWE values on 23 March 2004

5.3.2. Distributed Solar Radiation

Solar radiation tends to be the principal component in the energy balance of the melting snowpack, with turbulent transfer of sensible heat playing a secondary role (Diez Monux, 1991). Distributed solar irradiance values are computed using Solar Analyst extension of ArcGIS as discussed earlier in Section 5.2.3 in a daily manner during the application period with the parameters of 0.25 for diffuse proportion and 0.4 transmittivity. The values are obtained by comparing global radiation measurements on clear days against the corresponding values given by the model. The value giving the closest agreement between measured and modeled fluxes is adopted. The modeled and observed total global radiation ($\text{W}\cdot\text{hr}/\text{m}^2$) values are shown at stations with respect to cloud cover at ERZ in Figure 5.3.

The atmospheric reduction factors are widely variable, as they are linked to weather, specifically to cloud cover. It is virtually impossible to account for these variations in the absence of radiation measurements (Cazorzi and Fontana, 1996). Escher-Vetter (2000) scaled measured values of incoming shortwave radiation using the ratio of measured shortwave to potential shortwave radiation at the model grid cell in which measurements were made. Unlike the traditional approach used to calculate the flux of shortwave radiation incident to the earth's surface, the method improves the results by moderating the extra-terrestrial flux by the daily cloud cover observations. In order to achieve an accurate estimate of the spatial variability in solar irradiance, the global radiation values measured at the meteorological stations are used to correct distributed model results with daily cloud cover data that are available at ERZ. Since the cloud cover percentages give similar relations with observed to modeled global radiation ratio at individual sites (Figure 5.4) the cloud cover is applied uniformly across the model domain. Therefore, the cloud correction factor is input to the model used and considered as constant over the calculated grids in a daily basis. The cloud corrected and observed total global radiation values are compared in Figure 5.5. The corrected total global radiation values are divided by solar duration values in order to be used in the model as daily global radiation in W/m^2 units.

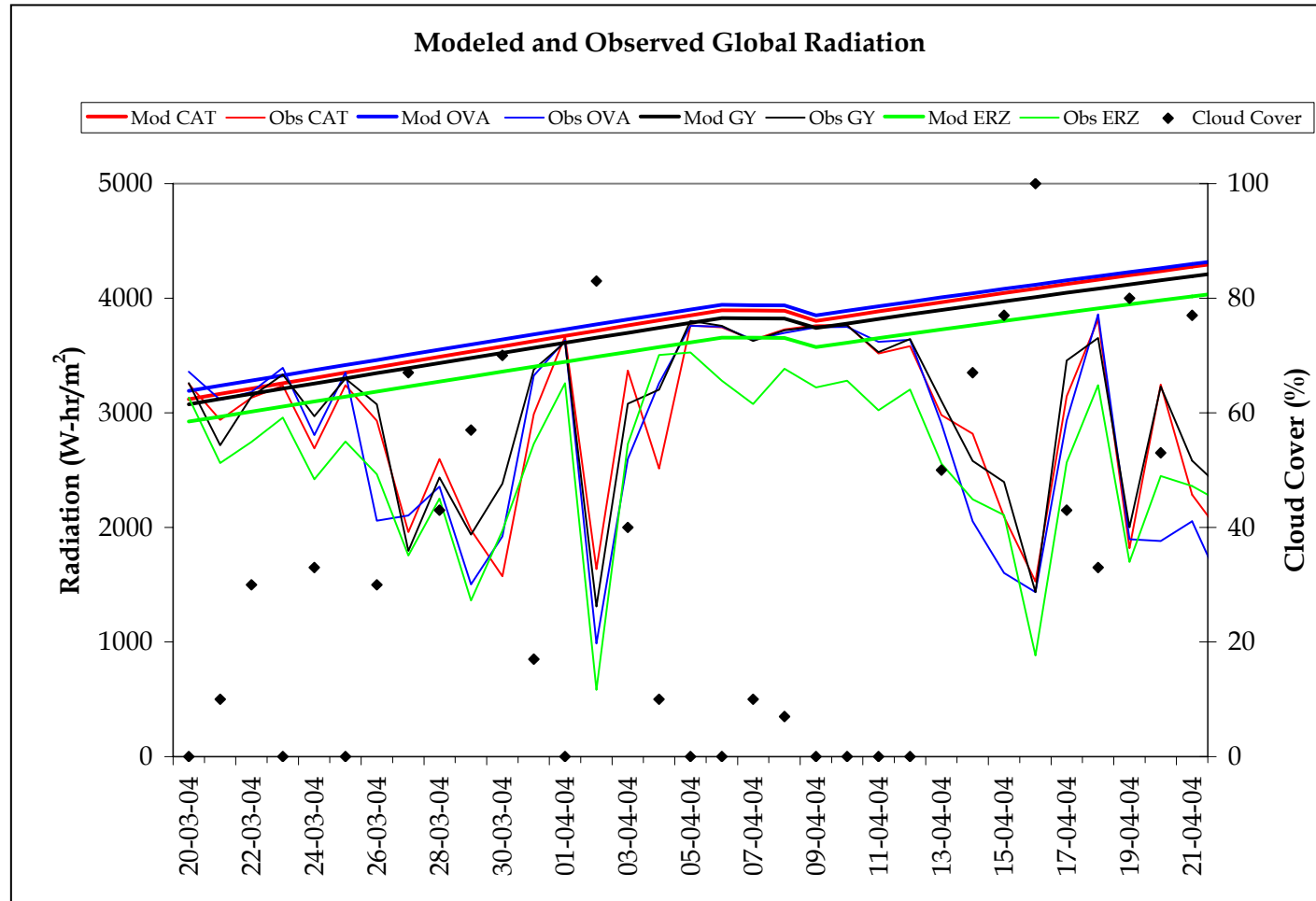


Figure 5.3 - Modeled and observed total global radiation at four stations and cloud cover percentages at ERZ station

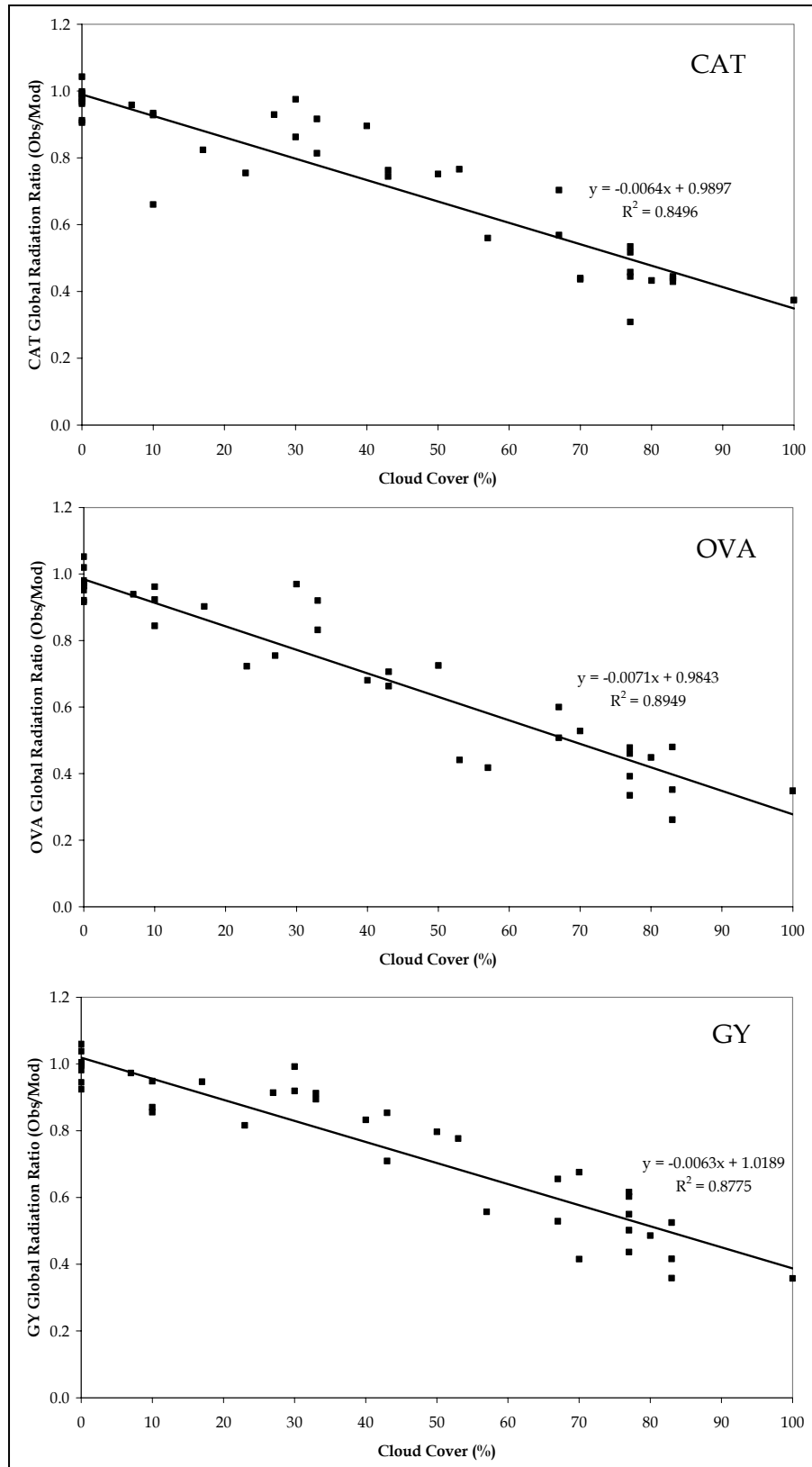


Figure 5.4 Observed to modeled global ratio in relation to cloud cover at each site

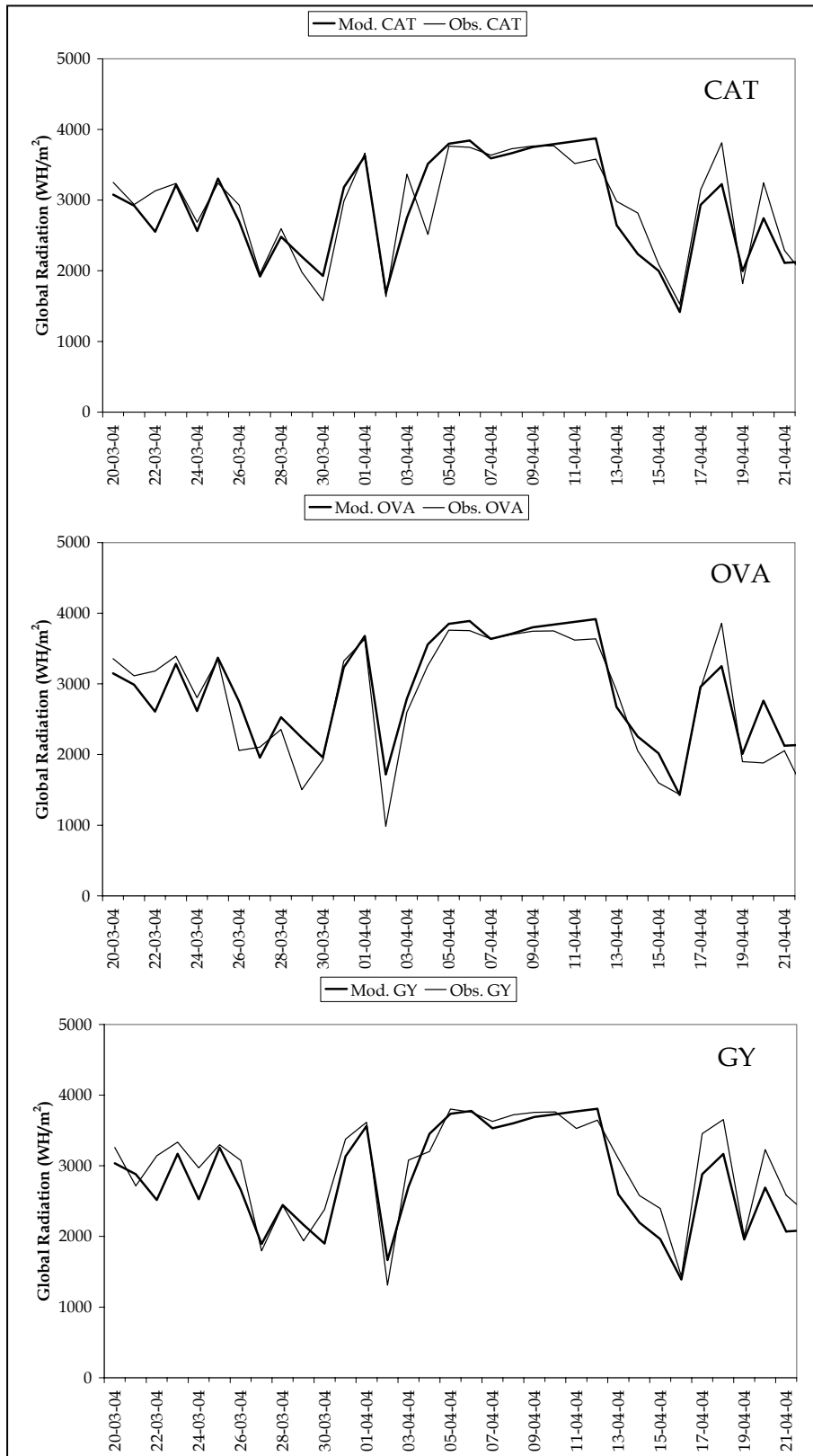


Figure 5.5 Cloud corrected radiation model results and comparison with observations at three sites

5.3.3. Distributed Albedo

Spatial albedo model is constructed according to the relation of albedo and cumulative daily maximum air temperatures. The snow cover was ripe already; therefore, the modeling does not start from the maximum observed albedo. Parameterization albedo independently from snow cover properties leads to large errors in particular after snow falls on an otherwise ripe snow cover (Fierz et al., 2003). In order to avoid these errors, albedo modeling is considered in three different melt periods, see Figure 5.6. The first period starts from March 23 and continues till April 1 (Period_1), the second period starts on April 2 and ends on April 15 (Period_2) and finally the last period is in between April 16-26 (Period_3). Each period is modeled with the observed data at GY and OVA; for Period_1, both stations were concerned together and the exponential decay coefficient is 0.0051; for Period_2, since the snow cover amounts are very different at two stations, albedo models are constructed for two classes with 2100 m elevation threshold, for the lower class the coefficient is 0.0120 and for the other 0.0057; for Period_3, since the snow cover was already disappeared from GY, albedo model is derived from observed values at OVA and the decay coefficient is 0.0223 (Figure 5.7).

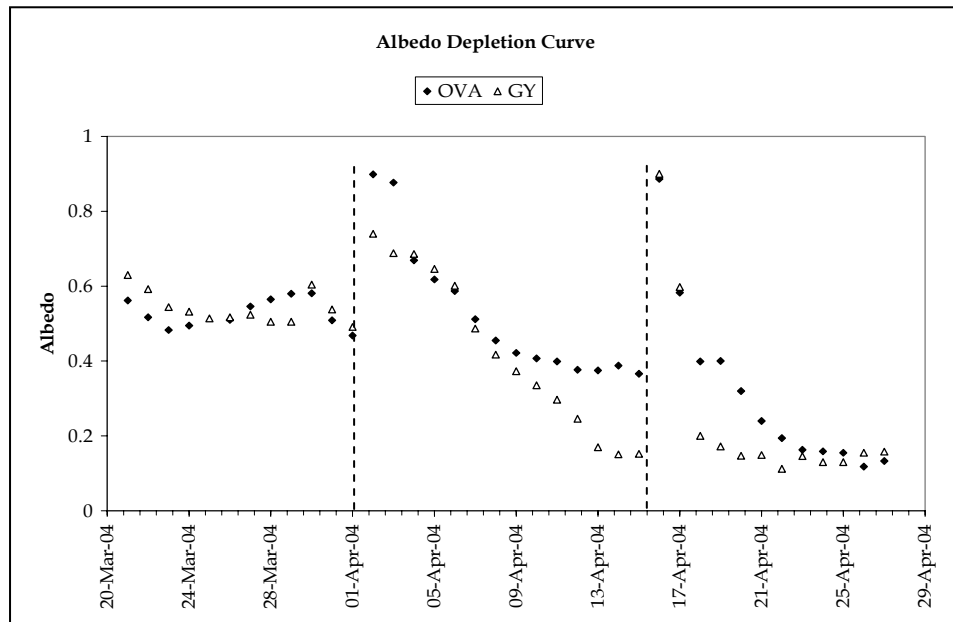


Figure 5.6 Albedo depletion curve at observation sites

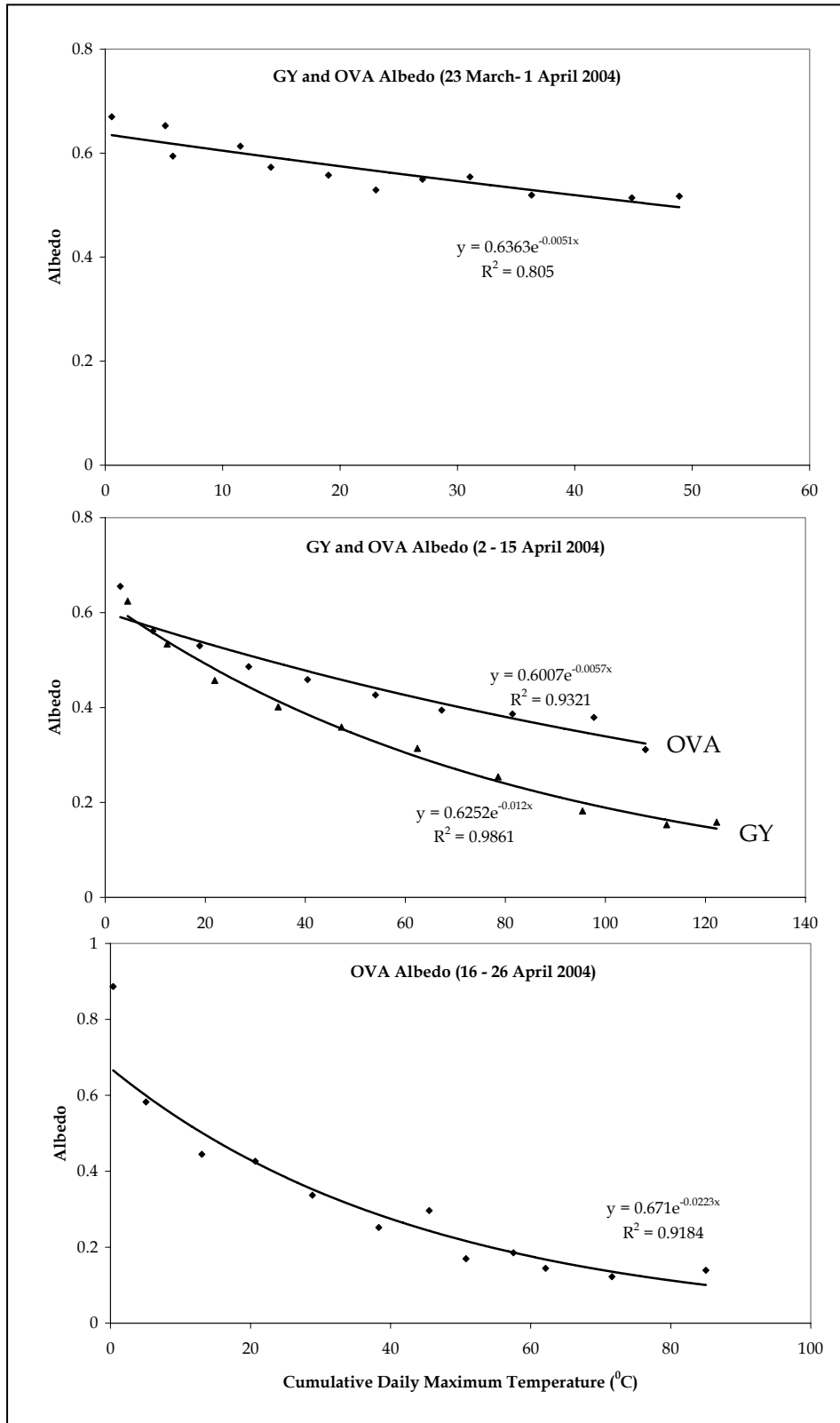


Figure 5.7 Albedo modeling for three different melting periods

5.3.4. Calibration of Radiation Index Model Parameters

Both the initial snow cover and meteorological variables are prepared to run the radiation index model (Equation 5.1), at this step of the application, the model coefficients of temperature index, a ($\text{mm}/^{\circ}\text{C}/\text{day}$) and radiation index, b ($\text{mm}/(\text{Wm}^{-2})/\text{day}$) have to be determined. Due to the large relative errors associated with direct measurements of surface lowering over short time scales, daily melt rates are modeled by an energy and mass balance model, rather than measured melt rates (Pellicciotti et al., 2002).

It is possible to calibrate the model coefficients satisfactorily with limited operational data using minimized root mean squared errors (RMSE) or maximized model efficiency in the observed and predicted melt rates as a measure of calibration success (Hamlin et al., 1998). The values of the efficiency criterion R^2 computed at each weather station for each melt period are listed in Table 5.1.

The parameter values, which range from 1.359 - 3.211 ($\text{mm}/^{\circ}\text{C}/\text{day}$) for a , and 0.005479 - 0.12935 ($\text{mm}/(\text{Wm}^{-2})/\text{day}$) for b , were estimated by means of statistical criteria of model efficiency. For the evaluation, the data set is divided into three periods. The both model coefficients are in close agreement with elevation bands in the first melting period, therefore, elevation band categorization is used to express distribution of model indices. On the other hand, there is no elevation relation in the second part, thus, spatially invariant model coefficients are used for the second and third melting periods where there are only two data sets are available (Table 5.1, the bold ones are used in the model application). The lowest values were found for the first period, characterized by early melt and therefore with a relatively young snowpack, moderate metamorphism and high albedo. In contrast, for the last period, when melt began to be late, the highest values correspond to a highly metamorphosed snowpack. The critical temperature (Equation 5.1) is set to -1.0°C since it provided the best model efficiencies during the model parameter calibrations.

The energy and mass balance model results are synthesized in the scattergraph with index model results in Figure 5.8, the regression lines are very close to the 1:1 line and the point spread is maximum for the lowest values of SWE corresponding to which spatial heterogeneity increases, also because of redistribution factors neglected by the model (Cazorzi and Fontana, 1996).

Table 5.1a Calibrated model coefficients (Equation 5.1) for Period_1

	Period I (23 March - 1 April)		
	GY	OVA	CAT
Temperature Index a (mm/°C/day)	1.359	1.840	3.836
Radiation Index b (mm/W/m ² /day)	0.08119	0.07621	0.05479
Model Efficiency R ²	0.82	0.71	0.83

Table 5.1b Calibrated model coefficients for Period_2

	Period II (6 April - 15 April)		
	GY	OVA	CAT
Temperature Index a (mm/°C/day)	3.051	2.077	3.233
Radiation Index b (mm/W/m ² /day)	0.10565	0.12606	0.13001
Model Efficiency R ²	0.94	0.84	0.96
All	a= 2.778 b= 0.10517 R²= 0.88		

Table 5.1c Calibrated model coefficients for Period_3

	Period III (16 April - 26 April)		
	GY	OVA	CAT
Temperature Index a (mm/°C/day)	NA	3.449	4.156
Radiation Index b (mm/W/m ² /day)	NA	0.10537	0.12752
Model Efficiency R ²	NA	0.93	0.89
All	a= 3.211 b= 0.12935 R²= 0.86		

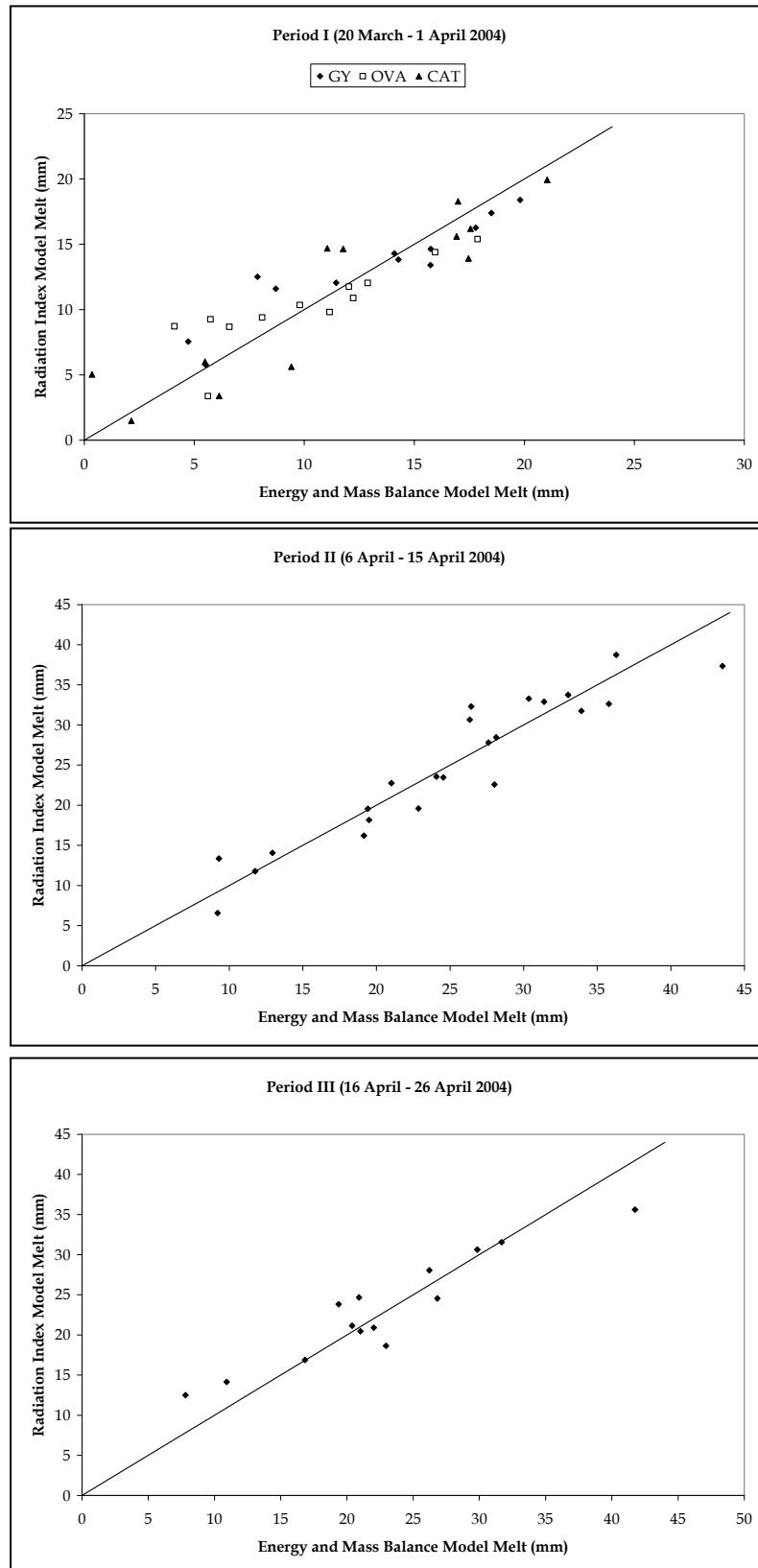


Figure 5.8 Snowmelt comparison at AWS using index and energy balance models

5.4. Model Results and Verification

Three important catchment scale variables namely, average SWE, snow covered area (SCA) and average melt rate, provide useful summary information on model performance over time. For SWE, model results are discussed against values derived from AWS's; for SCA, model results are compared with satellite images. Simulated melt rates are also compared against runoff, but in order to eliminate discrepancies in values arising from the omission of routing (time travel) effects, only the timing is considered in the streamflow (Anderton et al., 2002).

Spatial distribution in the timing of snow disappearance has specifically been chosen as the primary indicator of model performance, since it is the integrated consequence of spatial variability in both initial SWE and simulated melt rates (Anderton et al., 2002). The accuracy and short term consistency of the process based operational model result, SCA, is assessed by using MODIS (Version 4) daily snow product in the Upper Karasu Basin. The objective for this part of the study is to address the questions a) is the model statistically consistent with the observed snow cover of MODIS, b) what is the bias for the misclassification of the products?

The ability of the model to represent the spatial distribution of the melt process was analyzed by comparing the maps of simulated SWE with the observed maps. Melt is lower at the start of the season due to the high snow albedo and lower temperature, and increases over the course of the ablation season with increasing temperature and decreasing albedo.

As melt continues, any spatial variation in remaining SWE will be a function of both initial accumulation and subsequent melt rates. Given the variations in both these processes already discussed, a topographically controlled pattern of snow covered and snow free areas should develop at the micro- and meso-scales discussed above (Fox, 2003).

5.4.1. Comparison of Snow Cover Area with Satellite Data

As water supply forecasting in the eastern Turkey relies heavily on the accurate estimation of snowpack including both SWE and Snow Areal Extent (SAE) or Snow Cover Area (SCA), reliable spatial information on snow cover/non-snow cover can help screening model outputs.

Snowmelt models are traditionally calibrated by comparing simulated and observed discharges at the basin outlet. The latter are usually the only available data, so that the comparison is normally the only approach. It should, however, be observed that in substance this makes a true validation of snow processes simulation not quite reliable. The spatial distribution congruency of the simulation should be verified. The availability of SCA maps and reference values of SWE allowed the snow processes to be modeled independently of other hydrological aspects. The improved capability of MODIS daily product in classifying snow in topographically complex watersheds is to be of greatest interest to hydrologic modeling and water supply forecast. These validation and evaluation activities are mainly focused on the MODIS daily snow cover product (Zhou et al., 2005).

The basin is sufficiently large for the medium resolution of the MODIS data but small enough for the management of data retrieval (Zhou et al., 2005). Forest stand area in the basin is negligible which makes terrestrial recognition of snow covered areas easier. No measurements were ever made at elevations higher than 2400 m, owing to difficulty of reaching such impervious areas and the risk of avalanches.

During the melting period of 35 days from 23 March-26 April 2004 there are 11 number of MODIS scenes that can be compared with the model results. Though subjective, the visual comparison between the maps provides a great immediacy and allows one to grasp the global cover pattern (Figure 5.9 includes eight MODIS and four NOAA images). Comparisons with observed SCA demonstrate that the distributed SWE model gave the realistic simulation of SCA depletion for the melt season, although the rate at which this occurred is somewhat overestimated.

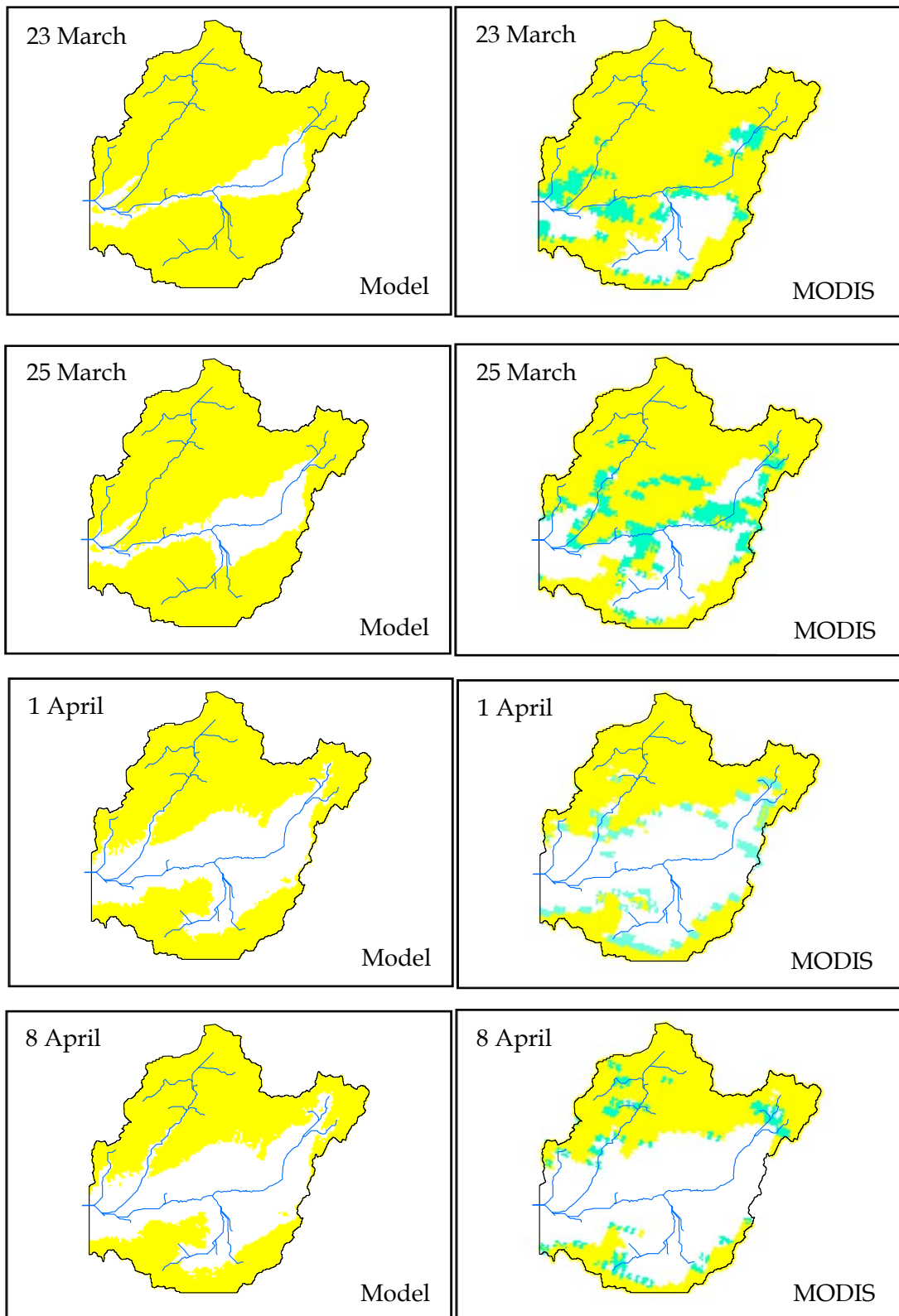


Figure 5.9 Visual comparison of snow cover area of the model and MODIS (Yellow: snow cover, blue: cloud or unclassified pixels, white: land cover)

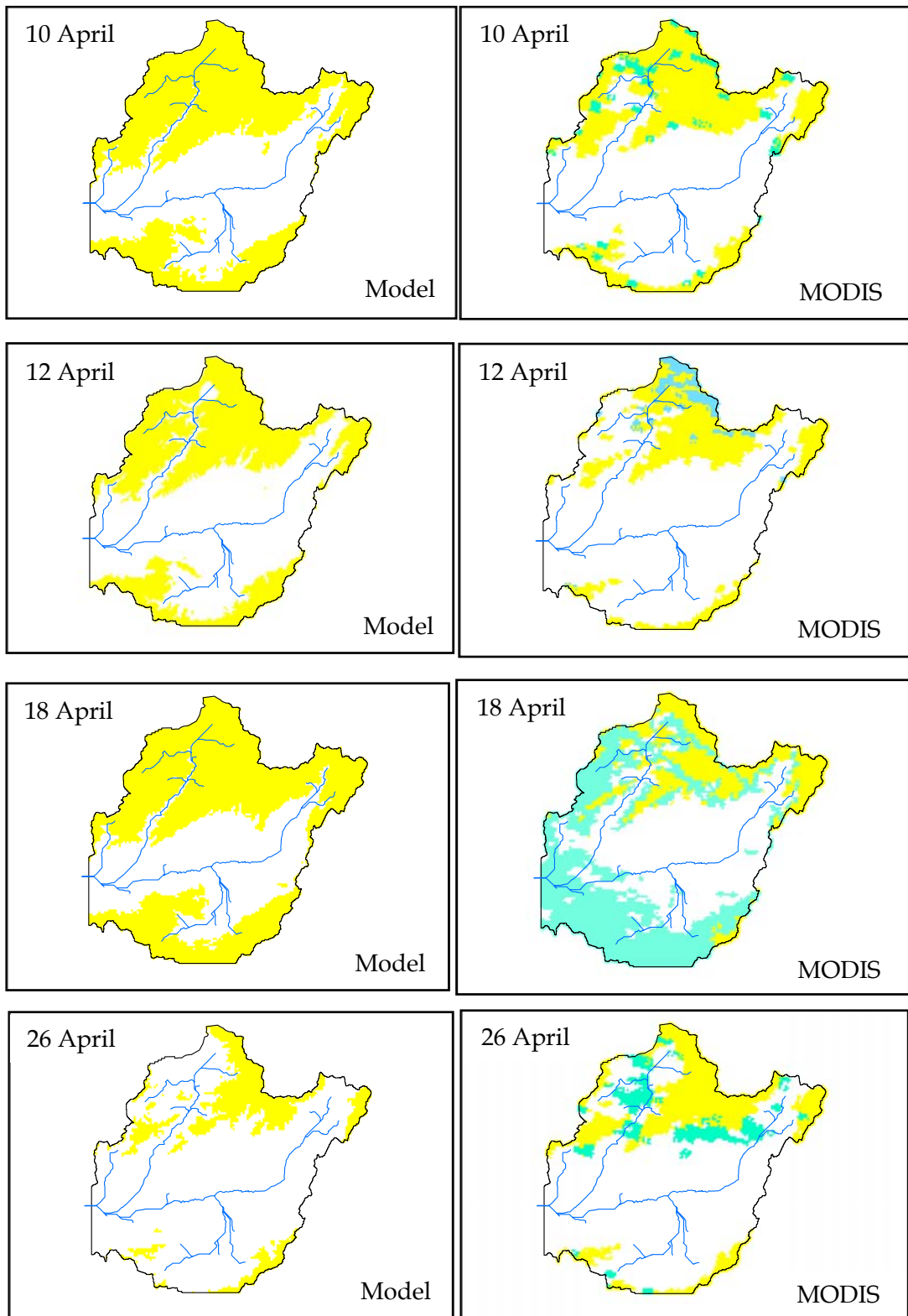


Figure 5.9 (cont'd) Visual comparison of snow cover area of the model and MODIS (Yellow: snow cover, blue: cloud or unclassified pixels, white: land cover)

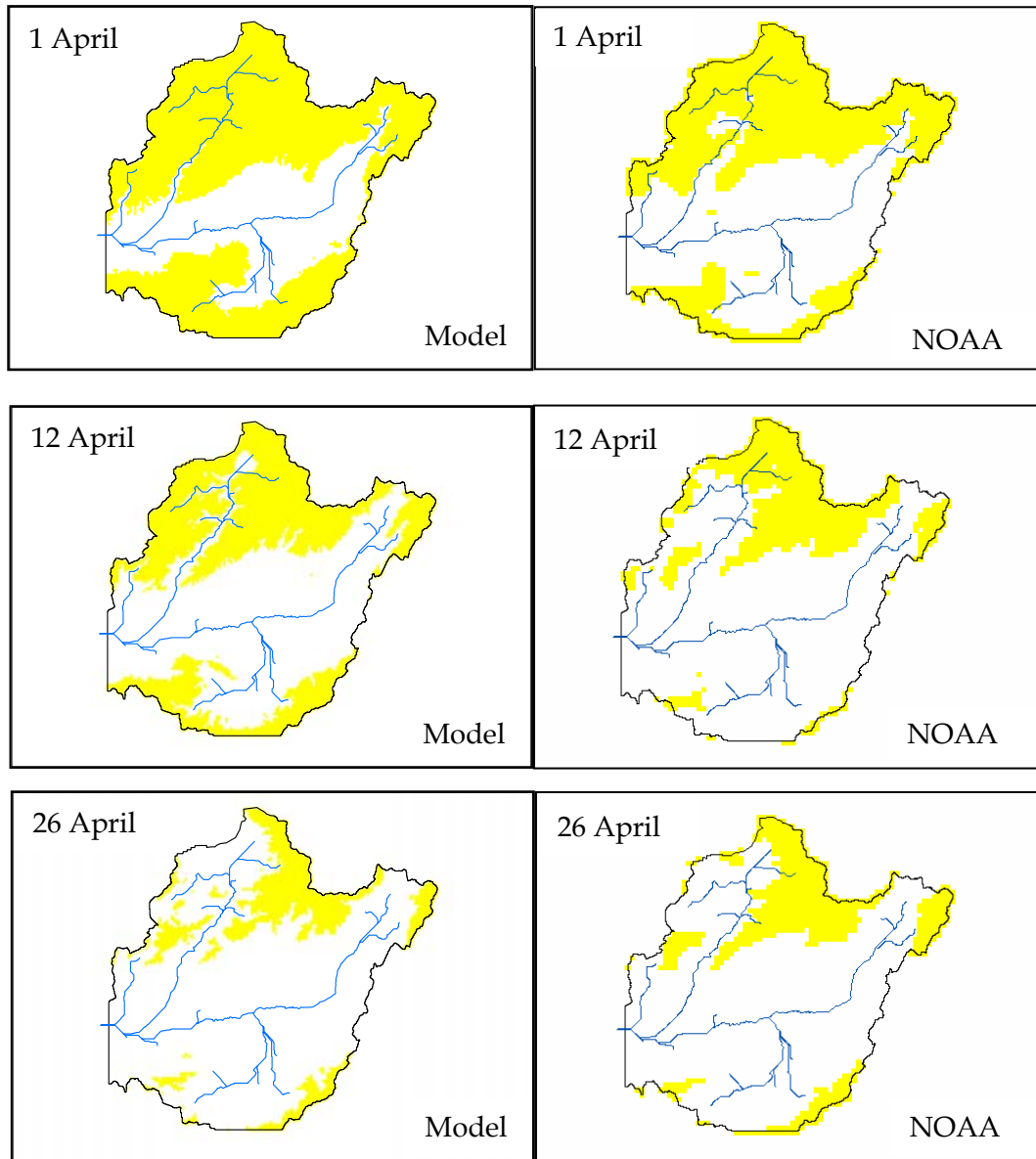


Figure 5.9 (cont'd) Visual comparison of observed and modeled snow cover areas (Yellow: snow cover, blue: cloud or unclassified pixels, white: land cover)

Daily snow covered area product of NOAA/AVHRR has a coarser spatial resolution of 1.1 km compared to that of MODIS/Terra product which has 500 m resolution. Moreover, since there are advantages of MODIS products over NOAA as explained in Chapter 3, and due to the fact that SCA products of NOAA are consisted with MODIS products (Figure 5.9), NOAA images were not considered in the statistical evaluations.

For March 23, 2004, starting date for initial SWE, model outputs provided more snow than that is observed at MODIS (Figure 5.9). The difference between modeled and observed SCA for March 25 is shown in the center of Figure 5.10 with overall consistent (match) and inconsistent (omission, model estimates land - MODIS estimates snow, and commission, model estimates snow - MODIS estimates land) areas. MODIS March 25 product is preferred to be analyzed due to the problem of improper cell size for March 23 image. The primary area of disagreement between the initial model of snow areal extent and satellite data within the study area is at the southern portion of the basin and around city center of Erzurum where the model shows complete snow cover whereas MODIS identifies land (commission error). The city center detected as snow covered with model since the station at the city (ERZ_CITY) was excluded in the initial snow cover computation in order to eliminate the urban micro-climate effect in the spatial analysis. Moreover, the detrended kriging method basically depends on elevation gradient and the snow line elevation will increase to 1869 m if ERZ_CITY, where no snow was observed on March 23, is included in the computations. This scenario will be analyzed in detail in the next paragraphs.

On the other hand, the commission error around the southern portion, especially around Ilıca, can be explained by the early melting. The Ilıca district was the main contributor to the flooding observed at the basin between 29 February and 6 March 2004. The concurrent action of high wind speeds (averaging to 7 m/s) from south and south west direction and increased temperatures resulted in snow redistribution and melting at that portion of the terrain basin during 4-6 March since the site is located in the lower elevation classes (Figure 5.10). The commission error can be eliminated with the inclusion of SWE information from this region in the initial snow cover distribution. The omission error is observed especially at the land use types of high ground water and irrigation (Figure 5.10); this is reasonable because the MODIS reflectance is affected by wetness which led it to discriminate these portions as snow covered. This phenomenon is more pronounced at March, 23, however, the cloud or unclassified mixed pixels were observed in the next couple of days and omission errors are minimized.

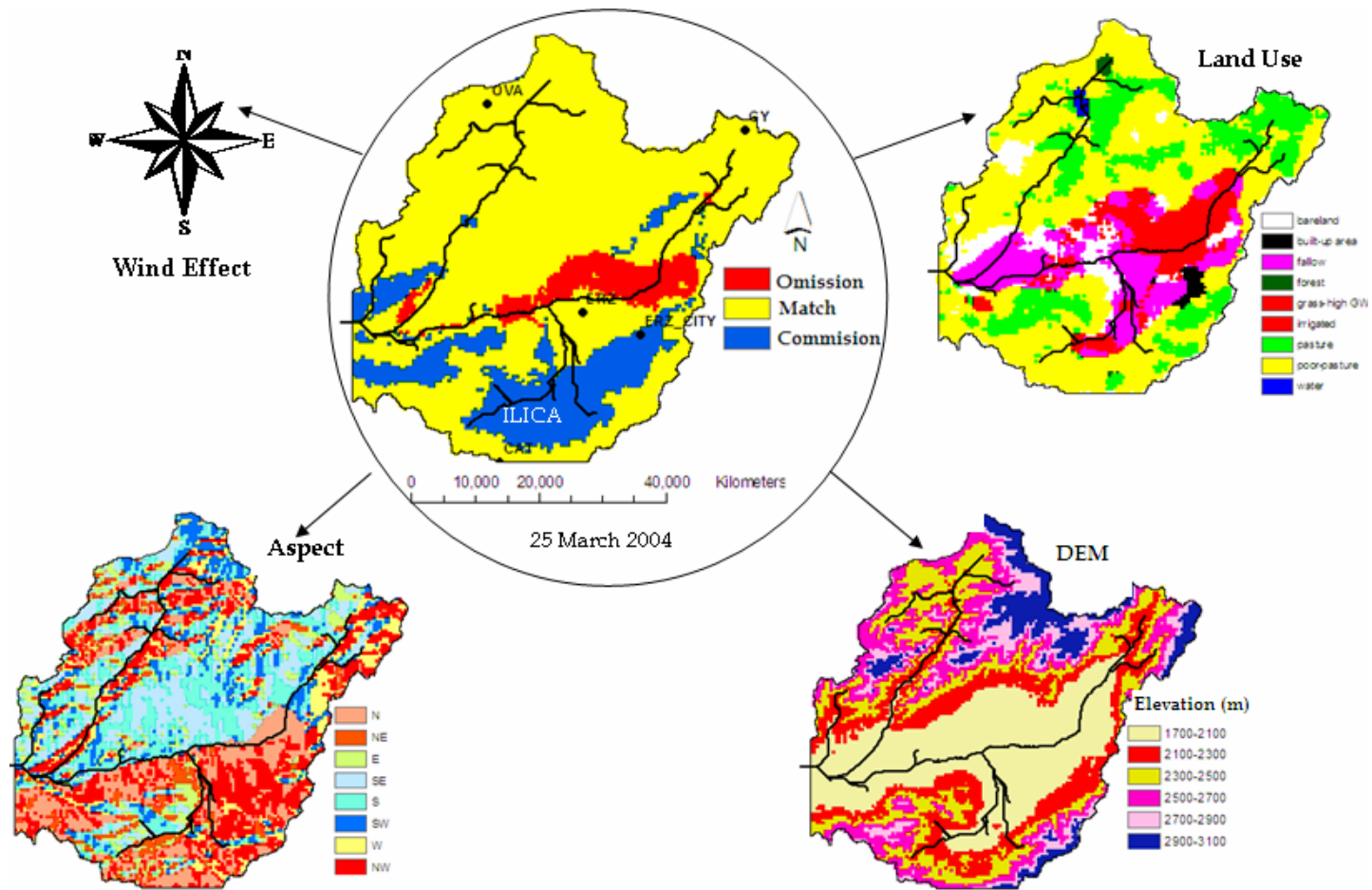


Figure 5.10 The comparison of model result and MODIS with respect to different thematic maps

The modeled initial snow covered area percentage can be decreased by the usage of additional observation at ERZ_CITY as explained above, but this was not preferred owing to urban micro-climate effect included in the observations at that station (Figure 5.11). Although modeling with this scenario resulted in rather lower melt rates in the first melting period due to decreased SCA, overall snow cover mapping and SWE values were very similar at the end of the period April 1, 2004 (Figure 5.12). The main reason for this is the snow's areal extent in horizontal plane rather than its existence in vertical plane for the initial snow cover simulation.

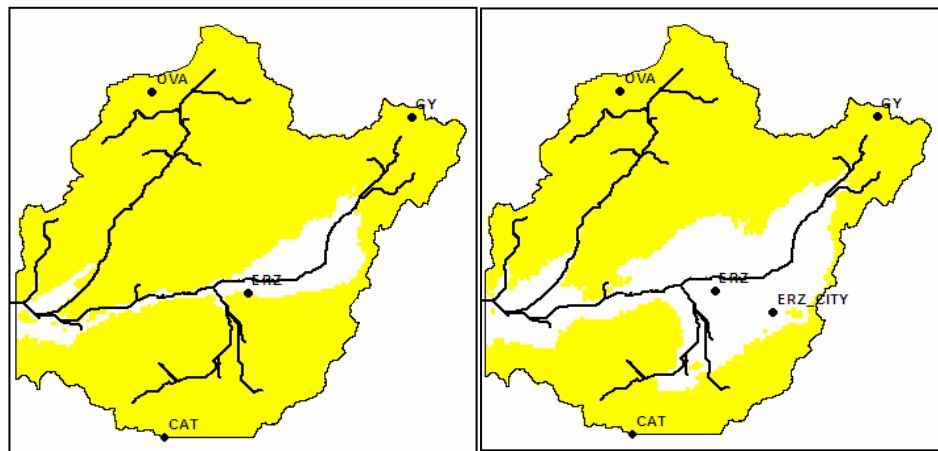


Figure 5.11 Initial snow cover a) used in the application b) including ERZ_CITY

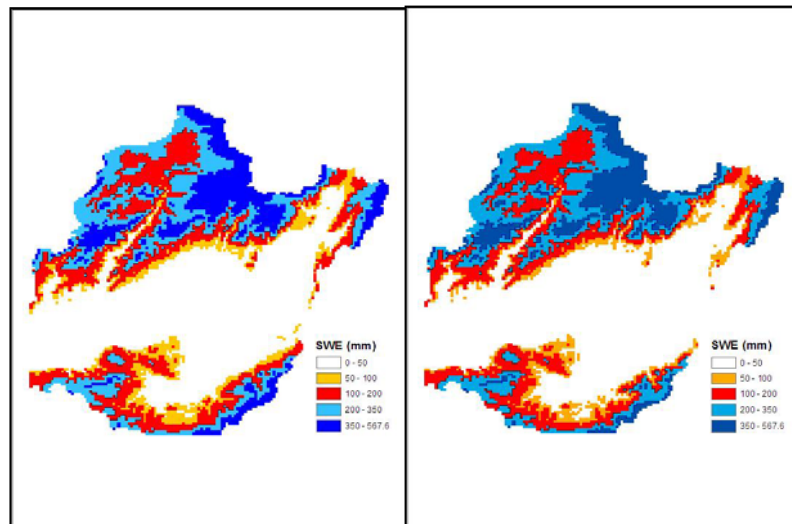


Figure 5.12 SWE map (1 April) a) model result b) alternative result with ERZ_CITY

A detailed analysis was conducted to see the consistency of model results with MODIS daily product under different land use types and further under the sub-classification of aspect within elevation classes for March 25 (Table 5.2 and 5.3) and April 9 (Table 5.4 and 5.5). First, the inconsistencies of snow-land (model to MODIS) for the snow cover on March, 25 are concentrated on the first two DEM classes, where edge cells appear, and north and north-west pixels, which constitute most of the portions that were explained before (Table 5.2). The inconsistencies of land-snow are all in the first elevation class and correspond to high groundwater and irrigated areas of which 76% is in the first DEM class; bareland and fallow are secondary dominating land use types (Table 5.3). Furthermore, in order to see the distribution of compared pixels further in the melting stage, April 9 was also analyzed in detail. Since the snow line elevation increased, the inconsistencies appeared in the second and third elevation classes instead of the first one (Table 5.4). Although the model estimates snow free areas at northern and eastern parts, since it does not account for aspect, MODIS discriminates snow over these areas (Table 5.4). The dominating land use for the inconsistent areas is poor pasture and pasture that constitute two third of the basin (Table 5.5). The high omission and commission errors are marked bold in the tables.

As would be expected, snow disappeared first from the lowest lying, sunniest areas and last from the highest, shadiest areas. However, deep snow in ridge cornices in the higher parts of catchment persisted, so that 15-20% of the catchment was still snow covered by the end of the simulation, with grid element SWE values ranging from 0- 477 mm read from last image (March 26). This occurred because the locations that favor deep snow accumulation, hollows, gullies and ridge cornices are often those that have lower than average radiation inputs or air temperature (Anderton et al., 2002).

Overall statistical evaluation of modeled to observed SCA through satellite are provided in graphical forms in Figure 5.13 as a linear regression and Figure 5.14 as a SCA depletion. Consequently, in Figure 5.13, generalized overestimation of SCA of almost 10% can be noted.

Table 5.2 Comparison of model results with MODIS for DEM and aspect classes on March 25, 2004

DEM-ASPECT	MODIS (March, 25)			
Model	Land-Land	Snow-Land	Land-Snow	Snow-Snow
1700-2100 m (Class 1)	(%)	(%)	(%)	(%)
N	28.79	8.86	27.94	0.5
NE	5.61	3.84	0.99	0.28
E	3.61	3.58	2.27	0.68
SE	9.62	4.41	24.96	3.65
S	15.40	3.32	25.53	3.64
SW	7.22	1.4	5.53	1.16
W	6.26	4.2	4.54	0.87
NW	23.50	11.25	8.23	0.87
2100-2300 m (Class 2)				
N		8.24		1.29
NE		3.37		0.87
E		3.42		1.25
SE		5.6		3.87
S		3.68		2.95
SW		2.18		1.06
W		3.21		1.77
NW		10.94		2.19
2300-3100 m (Class 3-6)				
N		3.88		8.8
NE		1.19		4.28
E		1.14		5.62
SE		1.25		11.05
S		2.02		8.45
SW		1.81		6.07
W		2.5		6.28
NW		4.71		10.89

Table 5.3 Comparison of model results with MODIS for land use on March 25, 2004

Land Use	MODIS (March, 25)			
Model	Land-Land (%)	Snow-Land (%)	Land-Snow (%)	Snow-Snow (%)
bareland	10.34	10.84	17.39	6.44
poor pasture	10.90	50.26	5.43	61.12
grass-highGWT	10.98	1.35	14.67	0.78
built-up area	1.99	3.11		
forest	0.00	0.21	0.14	0.49
pasture	1.11	12.03	0.14	23.64
fallow	40.89	17.17	24.46	5.88
irrigated	23.79	5.03	37.77	1.59

Table 5.4 Comparison of model results with MODIS for DEM and aspect classes on April 9, 2004

DEM-ASPECT	MODIS (April, 9)			
Model	Land-Land	Snow-Land	Land-Snow	Snow-Snow
2100-2300 m (Class 2)	(%)	(%)	(%)	(%)
N	5.28	3.55	11.11	0.26
NE	1.32	1.95	13.89	0.10
E	0.63	2.21	5.56	0.13
SE	0.84	4.68	2.78	0.23
S	2.31	2.43	0.00	0.18
SW	1.89	1.26	0.00	0.05
W	0.74	1.47	5.56	0.08
NW	1.29	3.94	5.56	0.15
2300-2500 m (Class 3)				
N	2.29	7.24	0.00	3.86
NE	0.00	3.86	5.56	1.64
E	0.00	4.98	22.22	2.43
SE	0.05	12.05	2.78	2.84
S	0.17	8.75	5.56	1.76
SW	0.10	4.51	2.78	1.61
W	0.04	5.16	5.56	1.58
NW	0.10	10.10	11.11	3.32
1700-1900 (Class 1) & 2500-3100 m (Class 4-6)				
N	58.17	1.21		12.63
NE	6.38	0.78		5.01
E	1.44	1.78		5.57
SE	1.50	3.86		11.15
S	5.44	5.11		9.56
SW	5.89	2.69		9.43
W	2.02	2.47		10.89
NW	2.13	3.99		15.54

Table 5.5 Comparison of model results with MODIS for land use on April 9, 2004

Land Use	MODIS (April, 9)			
Model	Land-Land (%)	Snow-Land (%)	Land-Snow (%)	Snow-Snow (%)
bareland	14.50	2.28	4.62	3.85
poor pasture	27.44	71.95	66.15	65.64
grass-highGWT	6.52	0.00	0.00	0.00
built-up area	1.70	0.00	0.00	0.00
forest	0.10	0.00	0.00	0.95
pasture	5.29	25.50	29.23	28.68
water	0.00	0.26	0.00	0.87
fallow	28.76	0.00	0.00	0.00
irrigated	15.70	0.00	0.00	0.00

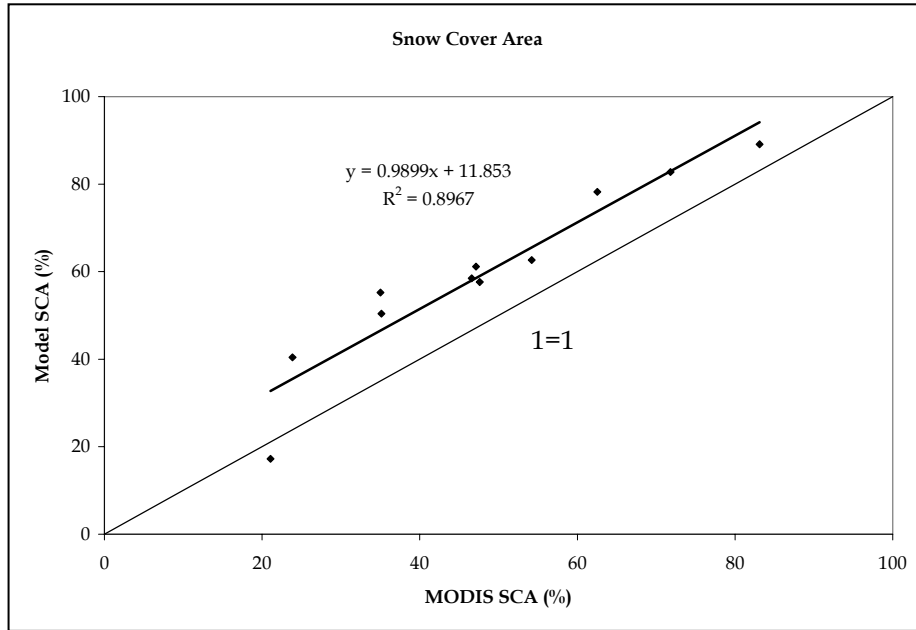


Figure 5.13 Linear regression between modeled and observed SCA

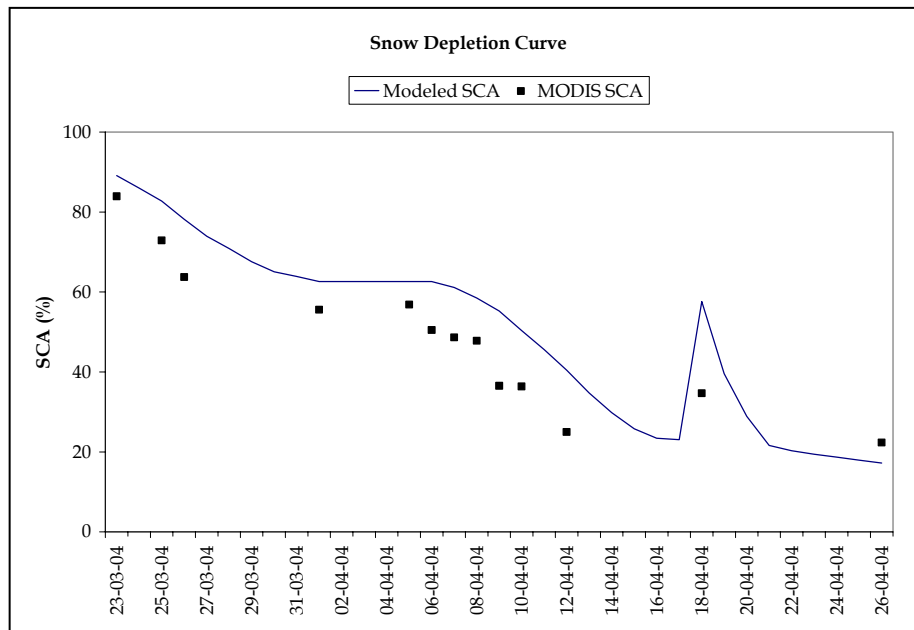


Figure 5.14 Modeled snow cover depletion curve and its consistency with MODIS

There is a clear indication that the model overestimates SCA in this environment. Later in the melting season, the simulated SCA and that from the model result coincide closely with one another. The consistency of model results with MODIS daily products are assessed, the one of the objectives of the study was to evaluate the bias for the misclassification of these satellite product and model outcomes. A comprehensive comparison of presence-absence of snow on per pixel basis was conducted. A grid by grid comparison of modeled and observed snow cover showed systematic deviations. Elevation seemed to explain more of the differences, with more snow at high altitudes in the model. Table 5.6 displays the percent of grid cells in agreement between model and the satellite as to the designation of the consistency and inconsistency.

Table 5.6 Error matrix for the intercomparison between the model results and MODIS product integrating cloud pixels

Data Sets	Overall Consistency (%)	Cloud Area (%)	Model (%) Area	Land type identified by the model	MODIS	
					Snow	Land
23-Mar-04	77.16	8.5	89.1	Snow	83.8	16.2
			10.9	Land	77.3	22.6
25-Mar-04	76.64	11.7	82.8	Snow	79.3	20.7
			17.2	Land	36.1	64.0
26-Mar-04	71.10	12.5	78.2	Snow	71.5	28.5
			21.8	Land	30.3	69.7
01-Apr-04	87.37	7.4	62.6	Snow	83.2	16.8
			37.4	Land	5.6	94.3
07-Apr-04	83.96	5.5	61.1	Snow	75.5	24.5
			38.9	Land	2.7	97.2
08-Apr-04	85.03	5.3	58.5	Snow	77.0	22.9
			41.5	Land	3.7	96.3
09-Apr-04	79.16	5.3	55.2	Snow	62.9	37.2
			44.8	Land	0.7	99.2
10-Apr-04	83.44	4.0	50.4	Snow	68.4	31.5
			49.6	Land	1.3	98.7
12-Apr-04	80.85	3.5	40.4	Snow	55.9	44.2
			59.6	Land	2.2	97.8
18-Apr-04	77.30	39.2	57.6	Snow	78.4	21.7
			42.4	Land	24.1	75.8
26-Apr-04	91.84	8.0	17.3	Snow	87.3	12.6
			82.7	Land	7.2	92.8

The percent agreement starts out low, increases during the active melt period. Similarly, toward the end of the snowmelt period, most grid cells are snow free and both methods identify this. The agreement is rather low in days with more cloud cover obstruction or unclassified pixels, though no direct conclusion can be inferred if the pixel is covered with cloud or unclassified, these pixels are assigned the most probable class concerning the previous and next images. These pixels are generally considered as snow; however, it is not thought as a serious situation since the cloud percentage is generally well below 10%. The high cloud percentage belonging to date April 18 is expected since there was snowfall on that date which is also considered in model application. Nevertheless, the percent agreement was always high, with most values falling in the 77-92% range. This high degree of agreement in designating snow cover is a positively confirming result indicating the good correspondence between the model outcomes and the satellite images.

An analytical verification is done on pixel by pixel basis by comparing observed and simulated maps. At the beginning of the season, the comparison is biased by the presence of a wide portion of the basin where melt processes have not yet begun. The grid-by-grid analysis was performed for each pair of maps, analyzing error frequency by elevation and aspect classes as presented in Tables 5.7 and 5.8. A marked increase of the omission and commission errors occur at the edges of snow covered areas. The accuracies of classifying snow (MODIS) as snow (Model) and land (MODIS) as land (Model) by the MODIS daily product algorithm are generally high. From the point of view of, the omission errors of classifying snow (MODIS) as land (Model) are generally low, however, the model results have higher commission error than omission error. As there is no ground truth data for cloud condition at the AWS sites, these data added to snow and land cover according to their spatial distribution within the elevation bands suggested by Zhou et al. (2005).

Table 5.8 is a representation of the distribution of snow cover as a function of exposure (in eight directions) for the application period. The south/south-east and the north/north-west aspect constitute 33.3% and 34.9% of the basin, respectively.

Table 5.7 Grid by grid comparison of model percent omission and commission errors in different elevation bands

			Class-1	Class-2	Class-3	Class-4	Class-5	Class-6						
		Zone (m)	1640-2100	2100-2300	2300-2500	2500-2700	2700-2900	2900-3100						
		Area (%)	31.95	16.95	18.93	15.42	9.11	7.64						
		MODEL	MODIS											
	% Area		Snow	Land	Snow	Land	Snow	Land	Snow	Land	Snow	Land	Snow	Land
23-Mar-04	89.1	Snow	14.98	8.66	13.82	5.20	19.34	1.90	16.89	0.40	10.21	0.02	8.58	0.00
	10.9	Land	77.35	22.63	0.00	0.00	0.00	0.00	0.00	0.00	0.00	0.00	0.00	0.00
25-Mar-04	82.8	Snow	9.29	8.51	12.07	8.40	19.87	2.99	17.87	0.74	10.93	0.08	9.23	0.00
	17.2	Land	36.07	64.03	0.00	0.00	0.00	0.00	0.00	0.00	0.00	0.00	0.00	0.00
26-Mar-04	78.2	Snow	6.20	6.89	8.33	13.26	17.50	6.71	18.24	1.46	11.47	0.18	9.77	0.00
	21.8	Land	30.00	69.65	0.33	0.00	0.00	0.00	0.00	0.00	0.00	0.00	0.00	0.00
01-Apr-04	62.6	Snow	0.00	0.00	7.07	11.36	25.31	4.93	24.10	0.51	14.55	0.01	12.21	0.00
	37.4	Land	2.89	82.55	2.73	11.75	0.00	0.00	0.00	0.00	0.00	0.00	0.00	0.00
07-Apr-04	61.1	Snow	0.00	0.00	3.09	13.41	21.63	9.31	23.54	1.67	14.76	0.16	12.51	0.00
	38.9	Land	0.80	81.36	1.80	15.86	0.07	0.00	0.00	0.00	0.00	0.00	0.00	0.00
08-Apr-04	58.5	Snow	0.00	0.00	3.14	9.89	21.71	10.24	23.91	2.43	15.20	0.38	13.06	0.00
	41.5	Land	0.34	76.66	2.95	19.52	0.45	0.13	0.00	0.00	0.00	0.00	0.00	0.00
09-Apr-04	55.2	Snow	0.00	0.00	0.74	8.07	11.98	21.01	20.84	7.07	15.53	0.98	13.81	0.03
	44.8	Land	0.00	71.33	0.32	26.66	0.40	1.21	0.00	0.00	0.00	0.00	0.00	0.00
10-Apr-04	50.4	Snow	0.00	0.00	0.51	2.34	13.12	20.18	22.75	7.82	16.97	1.11	15.07	0.09
	49.6	Land	0.00	64.43	0.45	30.83	0.89	3.44	0.00	0.00	0.00	0.00	0.00	0.00
12-Apr-04	40.4	Snow	0.00	0.00	0.00	0.00	4.02	16.85	15.73	21.99	17.57	4.99	18.54	0.37
	59.6	Land	0.00	53.62	0.28	28.16	1.82	15.80	0.07	0.21	0.00	0.00	0.00	0.00
18-Apr-04	57.6	Snow	0.00	0.00	4.36	6.98	21.63	11.23	23.71	3.04	15.41	0.42	13.27	0.00
	42.4	Land	18.23	57.12	5.86	18.71	0.00	0.00	0.00	0.00	0.00	0.00	0.00	0.00
26-Apr-04	17.3	Snow	0.00	0.00	0.00	0.00	0.00	0.00	3.03	2.15	41.30	9.18	42.94	1.23
	82.7	Land	0.00	38.64	0.01	20.49	0.70	22.19	6.21	11.33	0.32	0.14	0.00	0.00

Table 5.8 Grid by grid comparison of model percent omission and commission errors in different aspect classes

		Aspect	N		NE		E		SE		S		SW		W		NW		
		Area (%)	16.49		5.94		7.28		17.57		15.71		8.57		9.99		18.44		
		% Area	MODEL	MODIS															
				Snow	Land	Snow	Land	Snow	Land	Snow	Land	Snow	Land	Snow	Land	Snow	Land	Snow	Land
23-Mar-04	89.1	Snow	10.51	3.95	4.81	1.52	6.84	1.07	17.05	0.87	14.42	1.01	7.91	0.61	9.14	1.26	13.14	5.89	
	10.9	Land	27.52	5.54	0.90	1.87	1.22	0.98	12.78	1.79	13.84	4.23	6.43	2.61	4.56	2.04	10.10	3.58	
25-Mar-04	82.8	Snow	9.62	4.35	4.62	1.74	6.46	1.69	15.76	2.32	13.15	1.86	7.86	1.11	8.84	2.05	12.95	5.59	
	17.2	Land	10.11	18.47	0.36	3.61	0.83	2.27	8.93	6.14	9.18	9.91	2.01	4.64	1.65	4.02	2.99	14.96	
26-Mar-04	78.2	Snow	9.27	4.65	4.31	2.21	5.99	2.21	13.73	4.19	11.00	3.90	6.93	2.20	8.33	2.63	11.94	6.49	
	21.8	Land	7.86	17.83	0.33	3.54	0.85	3.13	6.80	9.44	6.31	12.34	2.04	4.52	2.40	4.11	3.75	14.74	
01-Apr-04	62.6	Snow	12.38	2.24	5.57	1.06	7.23	1.23	13.96	3.30	10.33	3.12	8.28	1.55	9.95	1.19	15.52	3.12	
	37.4	Land	0.74	18.89	0.12	4.67	0.62	4.70	1.12	16.92	0.93	18.58	0.36	6.12	1.00	7.07	0.76	17.35	
07-Apr-04	61.1	Snow	11.94	2.80	5.36	1.29	6.42	1.98	11.37	5.74	8.98	4.39	7.65	2.31	9.19	2.03	14.61	4.01	
	38.9	Land	0.48	18.75	0.14	4.70	0.37	5.18	0.46	17.80	0.09	19.32	0.11	6.27	0.21	7.85	0.82	17.34	
08-Apr-04	58.5	Snow	11.30	3.47	5.05	1.65	7.01	1.40	13.09	3.81	9.83	3.52	8.03	2.02	8.95	2.31	13.76	4.76	
	41.5	Land	0.09	18.82	0.21	4.66	0.51	5.20	0.98	17.49	0.47	18.58	0.26	6.24	0.56	7.66	0.66	17.66	
09-Apr-04	55.2	Snow	10.53	4.49	4.24	2.44	5.11	3.33	8.94	7.60	7.23	6.08	6.98	3.15	7.89	3.39	11.96	6.69	
	44.8	Land	0.08	18.22	0.14	4.89	0.20	5.67	0.04	18.76	0.04	18.64	0.02	6.64	0.08	8.32	0.12	18.07	
10-Apr-04	50.4	Snow	10.41	4.97	4.45	2.20	5.85	2.32	10.83	5.21	8.54	4.63	7.91	2.45	8.33	3.08	12.11	6.67	
	49.6	Land	0.09	17.53	0.14	5.08	0.27	6.12	0.36	18.73	0.09	18.21	0.13	6.64	0.16	8.39	0.11	17.98	
12-Apr-04	40.4	Snow	8.59	7.36	2.94	3.34	3.80	4.02	7.80	7.10	7.16	5.95	7.25	3.49	8.22	4.00	10.10	8.94	
	59.6	Land	0.13	16.72	0.19	5.52	0.28	6.64	0.36	19.00	0.28	17.20	0.39	6.72	0.25	8.23	0.28	17.75	
18-Apr-04	57.6	Snow	13.60	0.99	5.92	0.72	6.90	1.46	10.77	5.78	8.41	4.98	7.55	2.57	9.34	2.31	15.89	2.85	
	42.4	Land	4.77	14.30	2.18	2.83	1.99	3.81	3.31	15.61	3.31	15.57	1.61	4.86	2.05	5.69	4.88	13.17	
26-Apr-04	17.3	Snow	12.82	2.10	3.95	1.08	5.08	0.51	10.62	1.03	11.75	1.44	12.11	1.23	14.31	1.85	16.62	3.33	
	82.7	Land	0.89	15.93	0.50	5.63	0.88	6.76	1.50	17.29	0.78	15.46	0.75	6.83	0.78	7.92	1.15	16.98	

5.4.2. Comparison of Snow Water Equivalent

One way to assess the validation of the snow model results is to compare observed SWE at a AWS with simulated values for the grid cells in which the meteorological stations are located, Figure 5.15 shows this comparison at two stations. Unfortunately, a strict comparison is not possible, for two reasons (Garen and Marks, 2004). First, the observations are essentially point measurements, taken by registering the pressure in fluid filled snow pillows. The simulated values, however, represent an average for the respective grid cell, which in this case is 500 m x 500 m. There are times during the snowmelt period when the simulated SWE tracks the observations very closely; other times, the snowmelt gets a bit off track at some point, then it parallels the observations. Despite the small discrepancies, it is felt that this correspondence is quite good, especially considering the issues in making this comparison. In Figure 5.15, the negative values observed at CAT snow pillow are replaced with the values computed from energy and mass balance model application.

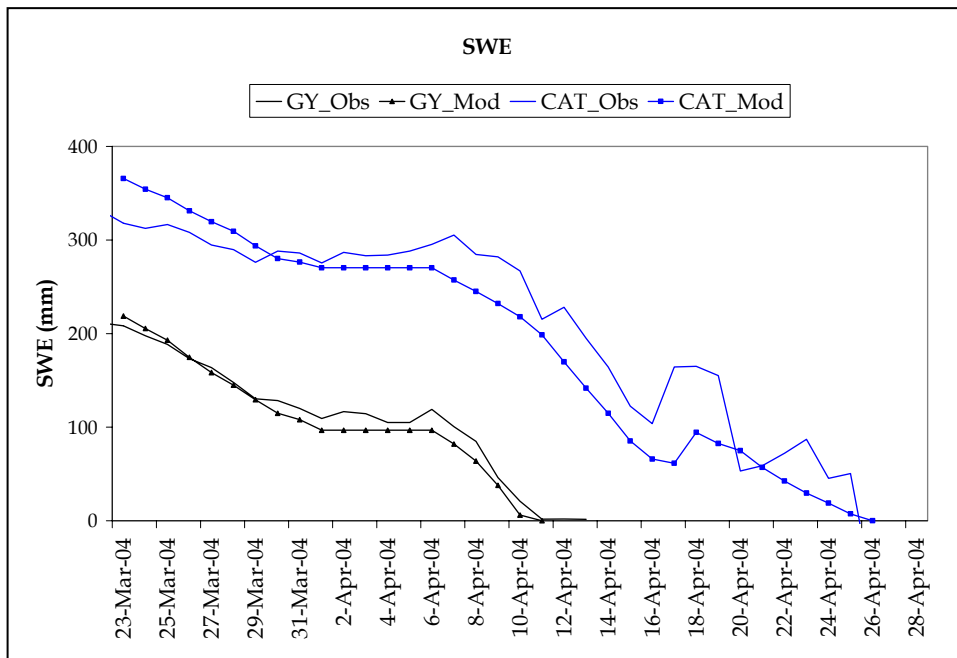


Figure 5.15 Comparison of modeled and observed snow

water equivalents

5.4.3. Comparison of Discharge with Daily Modeled Melt

As SCA is not a quantity that directly characterizes the water storage within a snowpack, rate and timing of the snowmelt should also be determined. Although the comparison between observed and simulated SWE by itself supports the reliability of snowmelt volume simulation, a definitive validation should be performed integrating the snowmelt model in a hydrological model and using discharge data at the basin outlet. The snow model structure, its limited data requirement and the easy link with a GIS are expected to make the model suitable for use in operative purposes. A detailed modeling of snowmelt with routing and infiltration routines is not in the scope of this study, however, average melt rates will be used to derive modified depletion curve of the basin (Figure 5.16) and to show the consistency with streamflow data at the basin outlet station 2154.

Catchment wide modeled snowmelt is compared with observed discharge (Figure 5.16). There is an apparent time lag between snowmelt and the observed discharge, therefore average daily snowmelt data are shifted by two days in Figure 5.17 at the beginning (25 March-3 April) and another three days in the second melting period (10 April-27 April) since snow covered area is decreased through the higher elevations at the boundaries of the catchment. Flow rate generally declined after snow disappeared from the catchment, non-melting period between 1-6 April can also be observed from the discharge data. Intense rain storms at lower altitudes produced peak values in streamflow together with snowmelt on 30-31 March, 16-17 April and 22-23 April 2004.

A saturated flow model able to store and route meltwater output from the distributed snow process model through the snowpack should be selected, further developed and tested.

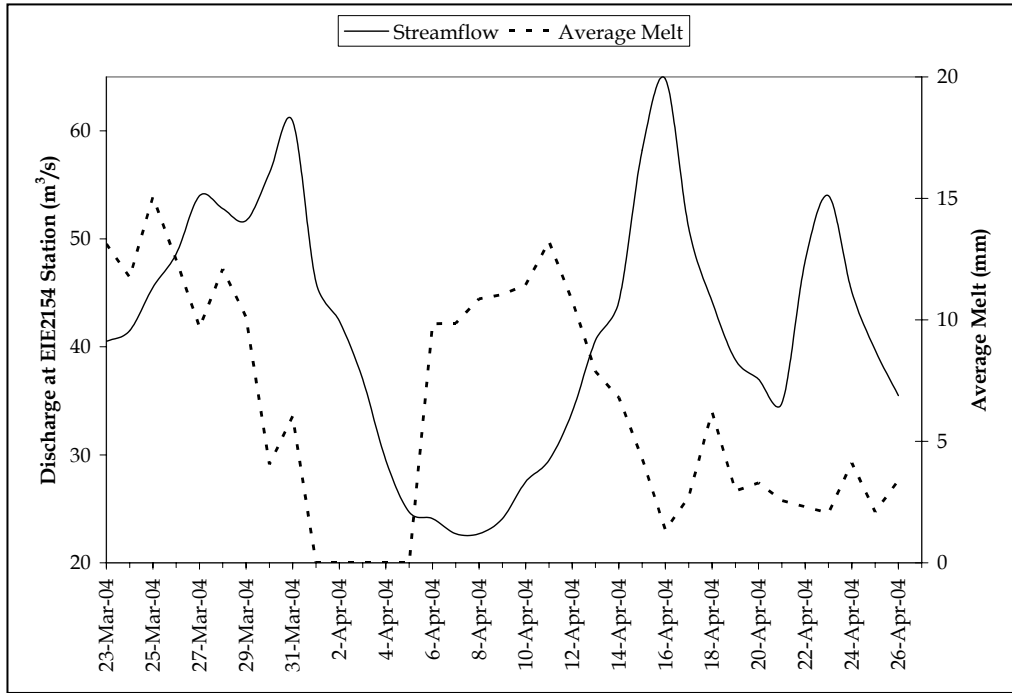


Figure 5.16a Comparison of average daily snowmelt and observed discharge

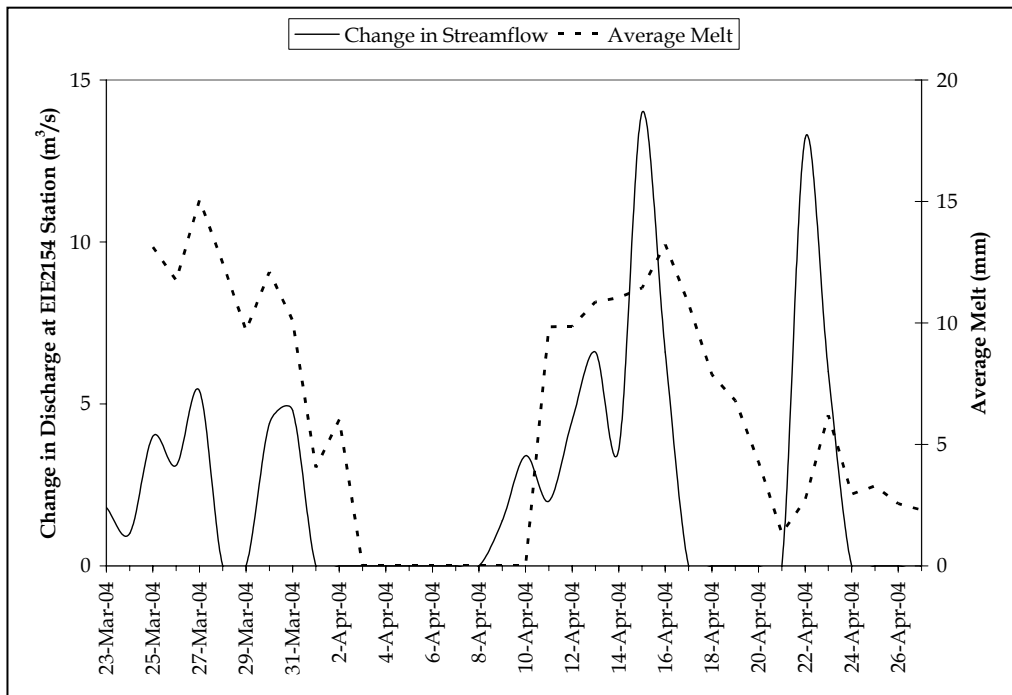


Figure 5.16b Comparison of average daily snowmelt and change in observed discharge

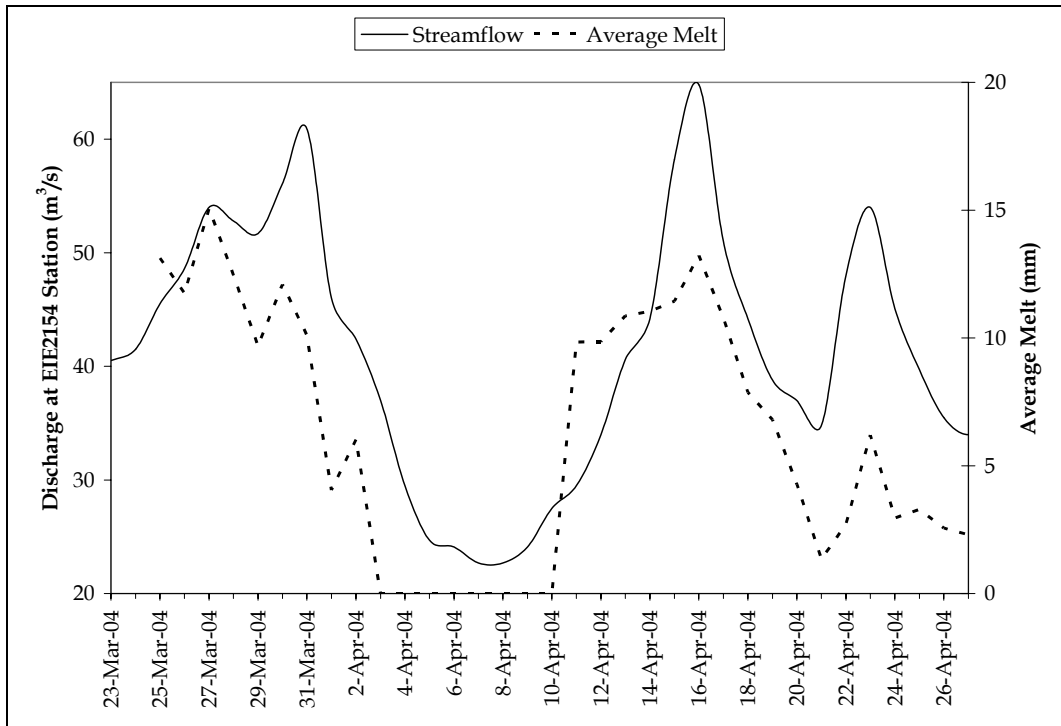


Figure 5.17 Comparison of lagged daily average snowmelt and observed discharge

CHAPTER 6

CONCLUSIONS and RECOMMENDATIONS

6.1. Introduction

This chapter first summarizes the main results of the preceding chapters, addresses the questions on how successfully the aims outlined in Chapter 1 have been addressed. The implications of these results are then discussed in the context of existing global and national snow hydrology literature. A few of the more important limitations faced by this work are outlined and suggestions on to how they might be improved, and additional recommendations for future work are put forward.

The two major aims initially identified in Chapter 1 were:

- a) To use theoretical understanding of snow processes and previous work to select, further develop and test a physically based snow process model of snowpack at a point scale,
- b) To implement and test this physically based snow process model in a spatially distributed conceptual framework across the mountainous pilot basin.

These aims were accomplished through a combined monitoring and modeling approach, within the general framework of numerical model application in hydrology. The extent to which these objectives have been achieved, and the main results arising from the work presented in this thesis are discussed below.

6.2. Summary

6.2.1. Physically Based Snow Process Model

SNOBAL was selected as a suitable physically based layered snow process model as it provides the necessary level of complexity to accurately simulate the timing and rate of meltwater outflow from the base of the snowpack with energy and mass balance approach (Chapter 4). The point model and its distributed version has used in a variety of studies (Susong et al., 1999; Marks et al., 1998; Marks et al., 1999; Garen and Marks, 2005). The task of accurately simulating the timing and magnitude of snowmelt runoff is greatly complicated by the great temporal and spatial variability in snow processes in mountain areas and the need to represent this in models (Kirnbauer et al., 1994; Blöschl, 1999). Therefore, the model outcomes were interpreted both under temporal and spatial variability using three year's data at one AWS and a year's data at three AWS (Chapter 4).

Applications of physically based models are usually conducted at the scale of small experimental basins, well equipped for input and output variable measurements. In order to provide this, automated weather stations were installed and upgraded with the great effort of people working in snow hydrology group at METU, Water Resources Division and DSI, General Directorate and Erzurum VIII Region District which collect high quality data with automated transfer (Chapter 3).

Since the overall objective of this part of the study has been to investigate the effect of each energy flux on snow cover both during accumulation and ablation the model necessarily had to have high temporal resolution, which was set to two hour time-steps. Net radiation fluxes were found to dominate the surface energy balance, representing about two thirds of energy input to the snowpack most of the time (section 4.8). This emphasizes the importance of correct estimation of longwave and albedo when modeling melt. Results from the point model applications showed clearly that the surface energy balance was secondly

dominated by the turbulent heat flux. This study, therefore, is in agreement with earlier investigations (Arnold et al., 1996) and can be added to a number of previous studies in mountainous areas that found net radiation fluxes and turbulent fluxes to account for approximately 70% and 30% of melt respectively (e.g. Munro, 1990; Marks and Dozier, 1992; Hock and Holmgren, 1996; Cline, 1997; Fox, 2003). Cumulative latent heat transfer during the modeled period was found to balance the positive sensible heat flux for the cases other than the rainfall and extreme weather conditions. Although the high wind speeds are observed especially at GY and CAT, extreme weather conditions decreased the effect of turbulent heat fluxes, however the ROS event observed at 2004 emphasized the effect of turbulent heat fluxes (sensible and latent heat) as reported elsewhere (e.g. Marks and Dozier, 1992; Cline, 1997; Anderton et al., 2002).

Two main adaptations were made to SNOBAL for the use of it at the Upper Karasu Basin in Turkey. The first was an approximation to incorporate the snow surface temperatures depending on manual measurements that is tested by longwave observations at OVA (section 4.7.3). The second was the replacement of the physically based albedo algorithm, when there is a lack of observation, with an empirically derived albedo scheme that has been developed at GY (section 4.7.3).

Having established the dominance of net radiation flux in the surface energy balance, receipt of shortwave radiation would be expected to be a key control over melt rates. One of the main factors which affect shortwave radiation receipt is albedo. Given the large temporal variation in albedo observed during this study and others, particularly the transition between the contrasting values for seasonal snow, the ability to simulate temporal variation in albedo would seem to be crucial. Ideally, this should be done through an understanding of the physical controls on snowpack albedo (i.e. grain size, solar angle and impurity concentrations). This study suggests that the importance of accurately simulating albedo in any energy balance based snowmelt model cannot be underestimated. However, as with all empirically derived model parameters, the applicability of the developed scheme to other glaciers in different environments is uncertain. The

importance of incoming longwave modeling was clearly illustrated by contrasting general model performances of the developed longwave scheme with the empirically derived SNOBAL algorithm (section 4.7.3).

Model performance was tested against continuous records of SWE with snow pillows and change in snow depths measured with ultra sonic depth sensor, manual measurements of SWE and snow depths through snow courses, and water yield collected from snow lysimeters (sections 4.8.1 and 4.8.2). The results were encouraging, because not only did simulated melt track measured runoff, but the model showed how sensitive the melt process is to changes in climate conditions. The model was found to effectively simulate rates of seasonal snowpack ablation; there was very good agreement in the timing of observed and modeled SWE, except for the times of ice bridging (section 4.8.3). On the other hand, the model seemed to overestimate water fluxes from the base of the snowpack overall when compared to lysimeter yields. Given the good agreement between observed and modeled SWE and snow depth, this was surprising; a possible explanation could be overflowing of tipping bucket under lysimeter and non-uniform distribution of snow on the lysimeter and snow pillow. It had been anticipated that some improvements on the measurement of snowmelt yield from the lysimeter would be required. However, beyond determining surface roughness values which may be site specific, the model were found to work well. This points towards model robustness as it is not dependent upon site-specific parameter values.

These verify that the model is functional during both the cold, snow cover development period, during the mixed climatic conditions of early spring and during the ablation period of late spring and early summer. Statistical evaluation of model performance can be referred in section 4.8.4. Thus the first stated objective appears to have been achieved, and represents a successful application of SNOBAL. This was the first time to apply fully physically based model for snow hydrology modeling during both accumulation and ablation in eastern Turkey. Most of the previous studies have been restricted to conceptual model applications during spring melt period.

After establishing that SNOBAL seemed to perform well it can be used in further investigations of liquid water storage, meltwater runoff and surface energy balance at different observation points within the catchment. Validation was done against three data sets (SWE, snow depth, lysimeter yield), including internal state variables and this indicated a high level of model performance, and made the model a suitable candidate for incorporation into a distributed model, which is discussed below.

6.2.2. Distributed Radiation Index Model

The snowmelt modeling literature points to the need for a model that is both simple enough to use in practical applications for melt estimations over large areas, as well as rigorous enough to capture the fundamental physics of melt and to provide spatially explicit estimations. Therefore, one of the goals of this study is to explore some of the modules and apply a melt model with comparatively less data requirement but a stronger physical basis than current temperature-index models. This thesis has described the radiation index model, which is a new method for estimating the spatial distribution of snowmelt based on point model applications and topography (Chapter 5).

Once the SNOBAL had been thoroughly tested, it was incorporated into a distributed structure to allow its application across the whole basin. This was undertaken using a standard approach, disaggregating the model domain into 500 x 500m grid cells based on the underlying DEM, and running the model for each cell. One of the benefits of a fully distributed model is that it can produce maps of modeled output. Distributed model was used to investigate temporal variation in spatial patterns of SWE, albedo, melt rates and peak-to-peak delay times.

It was the first time for grid based snow model application in the eastern part of Turkey. Early and recent studies for the same region include HEC, HBV and SRM model applications with snow routines for the former two. In SRM, the only spatial

subdivision is elevation zones, in HBV, the subdivision is again elevation zones but it also allows parameter representation for different land use types; however neither model is fully distributed.

Representation of spatial variability was achieved through varying initial input conditions and meteorological driving variables for each cell. Spatially varying initial inputs included SWE and DEM. Shading across the basin was calculated using a DEM of the surrounding mountain topography. Detrended kriging approach was used to extrapolate air temperature and SWE from AWS and snow survey on 23 and 25 March 2004 for the case of SWE on the basin (section 5.3.1). Slope and aspect for individual model cells were used to model solar radiation receipt which is then corrected for cloud cover. The albedo values are computed according to the scheme of exponential decay function based on cumulative air temperatures.

The initial SWE distribution was more important than spatial variation in meteorological driving variables in determining the final SWE distribution at the end of the modeled period (Luce et al., 1998; 1999; Dunn and Colohan, 1999; Hartman et al., 1999). This suggests that small-scale variation in SWE needs to be taken into account in catchment scale snowmelt modeling, either explicitly as in this study, or implicitly through some sort of sub-catchment parameterization in lumped models. This investigation serves to highlight the importance of continuing efforts to improve ways to measure and model SWE distribution in alpine catchments given the important impact on a number of key processes in snowmelt and runoff modeling (Blöschl and Kirnbauer, 1992; Copland, 1998; Elder et al., 1998). Some progress is being done in modeling (Pomeroy et al., 1997; Elder et al., 1998) and it may possible to use parameterization of topographic influences on the SWE distribution. Scale differences between field and earth observation data, model grid spacing and the true spatial variability of SWE can introduce bias to models (Blösch, 1999).

In this study, estimates of SWE distribution in the catchment were derived from a limited number of AWS and detailed field surveys on 23 and 25 March 2004 around 25 km² area. While intensive snow surveys might be possible in a research context for small experimental catchments, they are not practical for operational use for large areas. Furthermore, no remote sensing alternative currently exists for the derivation of the fine scale distribution of SWE for mountainous areas. It is likely that the characterization of SWE distribution for large mountain catchments will remain a pertinent research issue for some time to overcome (Anderton et al., 2002).

The sensitivity of distributed model to spatial variation in model input variables was tested by running the model for one additional scenario (section 5.4.1); changing the initial snow cover by concerning an additional input for the initial snowpack conditions. It was clear that initial SWE distribution was a more important control over final SWE distribution than spatial variation in meteorological variables. Melt may be overestimated over large parts of the lower elevations at early stages of process. This highlights the importance of using 'internal' validation measurements when testing distributed models.

Being a relatively powerful predictor of melt rates, elevation supports the wide number of model studies that have employed elevation zonation as a means to explicitly represent spatial variation in snow processes (e.g. Martinec, 1975; Blöschl et al., 1990; Bell and Moore, 1999; Turpin et al., 1999; Fox 2003). The air temperature distribution of the model has a direct impact on melt rates through variation in sensible heat transfer. Detrended kriging algorithm was preferred to be used instead of a single, fixed air temperature lapse rate, since it is well known that this can vary considerably in alpine environments, dependent upon micro- and mesoscale climatological conditions (e.g. Barry, 1992). The algorithm provides a more physically reasonable distribution of lapse rate both in vertical and horizontal dimensions according to the observations.

On the other hand, in terms of distributed snowmelt modeling overall, the analysis of surface energy balance and controls on melt rates clearly illustrates the importance of net radiation flux and highlights the need to accurately simulate spatial and temporal variations in global shortwave and albedo. Therefore, two main adaptations were made to radiation index model for use at the Upper Karasu Basin. The global radiation values distributed with a spatial solar algorithm was corrected for cloud cover, the results of which clearly illustrates the improvement in the model input variable of global radiation (section 5.3.2); the albedo parameterization algorithm was developed in accordance with observed values at two sites with respect to different melting patterns instead a uniform constant albedo scheme (section 5.3.3).

In distributed radiation index it seems that much of the elevational variation in melt rates results from the strong co-variation between elevation and albedo, which results from the dependence of the albedo algorithm on accumulated maximum daily air temperatures, variation in which is obviously controlled by the air temperature lapse rates employed by the model (Fox, 2003). Slope, aspect and shading all play smaller, but still significant roles in controlling variation in melt rates. However, caution should be exercised in attempting to extrapolate these results in particular to other catchments.

The model results indicate that the interpolation methods do a good job of estimating the spatial fields of the relevant meteorological input variables. Albedo and elevation were found to have the strongest control over melt rates, with the surface energy balance dominated by net shortwave radiation fluxes. The quality of the fit between observed SCA from MODIS and NOAA daily products and modeled SCA was very good (section 5.4.1) although the model did tend to over-estimate SCA. Unfortunately, due to the good weather requirements, the number of SCA measurements available for testing was more limited than for SWE.

The advent of DEM data and GIS tools has enabled researchers to investigate correlations at grid scale between presence of snow, its SWE with respect to

influencing topographic variables as slope, aspect, gradient as well as elevation, because they influence the deposition of snow and its redistribution by wind and affect radiation melt through incidence and shadow due to shading. Detailed statistical analysis and comparison between the MODIS snow cover products and the radiation index model results have been carried out in section 5.4.1. The overall accuracy of the model in comparison with MODIS increases, if the cloud or unclassified percentages are equal or less than 5%. Comparison between the modeled and observed SCA product shows that the classification accuracy (for omission) of land (model) to snow of the MODIS daily product is much higher than that of (for commission) the snow (model) to land (MODIS). The reasons for the omission and the commission errors, especially observed during the initial snow cover, were explained by detailed analysis concerning elevation, aspect and land use classifications. Elevation was found to be the most important control over the accuracy since the errors were concentrated on snow line transition zones which shift to high elevations during melting period. Land use was the main reason of omission errors for the initial snow cover. Aspect was helpful both to explain wind induced melting effect during ROS event and to show the general distribution of snow existence pixels. Table 5.8 was obtained by subdividing the watershed into aspect categories and measuring the percentage of SCA of each single category. Aspect proves to play a dominant role; although the north/north-west area equals to south/south-east area in the basin snowmelt begins on southern slopes where bare land and fallow surfaces appear earlier.

The model accuracy was also tested in terms of SWE values at AWS and this analysis yielded promising results (section 5.4.2). Another important affect of SWE that emerges from this investigation is its impact on the delay in runoff, and short-term storage of meltwater as it percolates down, as expressed in terms of peak-to-peak delay times. An analysis of the controls over peak-to-peak delay times suggested there was an interaction between melt rates and streamflow, and there is an inverse relationship between daily melt input magnitudes and delay time (section 5.4.3). SWE was shown to be highly significant; where the snowpack is

deep, peak streamflow outflow from its base can be delayed by over 24 hours from the time of maximum melt outputs from the basin.

The second objective of this work has, therefore, been achieved, and a physically based model has been successfully implemented into a spatially distributed framework across the mountainous basin. Tests of model performance showed that it was capable of providing accurate simulations of melt rates along the basin and, when a saturated flow model able to store and route meltwater are combined with outputs from the distributed snow process model through the snowpack the results would seem to be encouraging.

6.3. Implications of Results

The results and discussions found in the preceding chapters contain ideas with implications for three broad areas of snow hydrology -surface energy balance, the importance of SWE and SCA distribution and meltwater outflow from the basin. The work contained in this thesis has evolved directly from previous hydrology research, and it occupies a position at the boundary between climate monitoring and modeling in the snow hydrology sciences.

In the first part of the study, the physically based model results both in terms of temporal and spatial evaluation provided the understanding of the key processes that have major impact on the snow simulation during accumulation and ablation in two-hourly timesteps. The model was accurately simulated the snowpack under different climate conditions. To authors knowledge this is the first time a physically based modeling based on validated model results has attempted to quantify the magnitude of the meltwater outflow, and this result is potentially important to those interested in the water balance of snow systems and its impact on water resources. Since they are 'research tools', unlikely to be of direct practical application for water resources management; however, the development of physically based models at the high temporal and spatial resolution necessary to

develop further modeling approaches and algorithms to simulate discharge at a point. This should help to illustrate how small scale spatial variability (at representative points) may potentially affect catchment-scale models.

In the second part, the results indicated that the radiation index model can be an accurate, efficient way to predict the spatial distribution of snowmelt in a rugged, mountainous watershed. Because of the model's simplicity and accuracy, it could replace more traditional methods for modeling snowmelt in many applications.

Though energy balance models will always be required for some applications, there are many practical uses for the simpler radiation index model. Flood forecasters as well as reservoir operators, who traditionally use simpler lumped index models, would benefit from the improved accuracy over the entire range of possible weather conditions provided by a more physically-realistic model. Researchers could employ the model to efficiently and accurately calculate the spatial distribution of water inputs to large watersheds. The main advantages include simple data requirements, computationally efficient algorithm for rapid simulations of large basins compared to fully physically based models and realistic spatial melt simulations. This would be useful for basin response modeling in the eastern Turkey where snow melting contributes large volume of runoff to the existing reservoirs.

The point of this study has been to demonstrate that is feasible to use a spatially distributed snowmelt model in a real world setting that is using data from meteorological stations in an existing network and for a basin that is actively managed. With continued work, it is envisioned that spatially distributed modeling of this type will form the basis of the next generation of models for water resource management (Garen and Marks, 2005). Comparison of a time series of modeled surface melt outflows illustrated that incorporating routing and soil storage model can move the timing of daily peak discharge back by several hours, and made it comparable with the timing and rate of observed daily peak values in

the observed stream discharge record. This highlights the benefits for snowmelt and runoff models to be incorporated together at least during the melt period.

In addition to providing accurate simulations of snowmelt runoff for operational forecasting purposes, such distributed, physically based models are potentially useful tools for assessing the impact of possible future climate change on snowmelt runoff or analyzing the effects of changing spatial distributions of snow processes on geomorphologic, chemical and biological systems (Hardy et al., 1999).

6.4. Limitations of the Work Presented

6.4.1. Data Acquisition

It is common that the most severe problems found in distributed, physically based modeling in hydrology are related to acquiring reliable and sufficient length of data to run and test the models (e.g. Beven, 1989; 2001). This is certainly the case in snow hydrology, and is often compounded by the necessity to obtain data in harsh, mountainous areas, where equipment failure can almost be expected due to extreme weather conditions. For this study in particular, meltwater freezing onto instruments exposed in the instrumented site caused loss of data, for example in the early part of the lysimeter record, and also caused uncertainty in the accuracy of the precipitation record. It is difficult to see how these problems can be overcome without large investment in infrastructure, which is beyond the scope of this project. However, the biggest problems reflect the difficulties in trying to measure the spatial variation in snowpack properties, both to initialize the model and to test its performance. This is particularly important for models with high input data requirements. The spatial coverage of the snow depth survey, and the number of snow course, was strictly limited by the number of field personnel. Remote sensing, especially for remote mountainous areas, giving quantitative values rather than existence of snow cover, would have been valuable to improve model validation, especially for the performance of distributed radiation index.

Another limitation is related with the MODIS snow mapping algorithm, as it is designed at 500 m spatial resolution, is that it is a binary algorithm (snow or no snow). The binary MODIS snow-mapping algorithm will map snow cover if 50% of the 500 m pixel is snow covered. In this case where the snow is patchy within each 500 m pixel, the MODIS snow map will overestimate the snow cover. Several algorithms are under development for mapping fractional snow cover using MODIS data (Barton et al., 2000; Appel and Salomonson, 2002; Hall et al., 2002; Tekeli et al., 2005b).

6.4.2. Model Limitations

The main uncertainty of the physically based snowmelt modeling at representative points is the exclusion of wind drifting subroutine, which is also worrying issue in the distribution of SWE values as an initial input across the basin. The uncertainty as a result of wind redistribution to the drifting is unknown, but could be considerable (Marks and Winstral, 2001; Luce et al., 1999).

Radiation index is well validated model, and its performance is limited to initial input of SWE and the implementation of physically based model melt rates at AWS. The exception to this is perhaps in the algorithms used to extrapolate the meteorological driving variables. There are some issues to resolve before the model is feasible to use in an operational environment. The data preparation is time consuming and difficult to automate. With respect to data collection, it is feasible to install and collect data from extra sensors needed for the energy balance approach at remote mountain sites. This places an additional burden on field personnel for instrument installation and maintenance and for data quality control, in addition to the obvious costs incurred in purchasing the instruments. Even though it is generally accepted that these extra data are valuable and probably worth the investment, there are political and budget constraints that must be resolved before one can implement a plan for collecting these data on a widespread and routine basis.

Despite these issues, the potential value of this kind of modeling can be envisioned. One clear advantage of such modeling would be the more accurate prediction of streamflow for water management or flood prediction. The spatially distributed nature of the snowmelt and water balance models lends itself to the generation of new kinds of spatial informational products depicting things like snow depth, SWE, soil moisture or evapotranspiration (Garen and Marks, 2005).

6.5. Recommendations for Future Work

Several operational snowmelt-runoff modeling studies have been carried out for this basin at several scales. These studies provide insights for the present evaluation study and results from the present study provide insights for future snowmelt-runoff modeling (Zhou et al., 2005). These include:

_ The hydroclimate data monitoring and transferring in real time is essential for any kind of hydrological modeling. The physically based snow hydrology studies depend heavily on high quality data with high temporal and spatial distribution. Monitoring of snow and meteorological data in their natural conditions is a challenging issue in remote mountainous areas as in eastern Turkey. In order to achieve near real time, accurate and reliable results from a model, design and installation of automated weather stations is a must which is accomplished during this study. However, the operation and maintenance of these AWS and additional ones require continuance man power and finance which is difficult to be supplied by individuals and universities. Therefore, it is an urgent issue to develop governmental policies to create a national climate database that can be operational for a model study, if we would like to improve our knowledge about the water resources potential through snow accumulation in the eastern Turkey.

_ It has been stressed that the models described in this thesis are designed for seasonal snowpacks overlying mountainous basin. For it to be applied in other catchments, more experiments would be required.

_ A topographic index describing the relative exposure of a point to wind can be the most important predictor of snow depth, thereby it would be suggested that the modeling of redistribution by wind for snow distribution in a high mountain environment is a crucial study. In most cases nonuse of wind fields can probably be ascribed to error in the regression tree models of snow depths used to provide the initial SWE condition (Anderton et al., 2002).

_ In common with many areas of hydrology (Anderson and Burt, 1990), an alternative and complementary approach to hydrology research has been the adoption of distributed, physically based modeling strategies with the aim of explaining and ultimately predicting how hydrological systems function when covered with snow. Results have shown that a realistic representation of the initial SWE distribution, especially at the maximum snow water equivalent stage, is essential for producing a realistic representation of snow disappearance patterns. However, some shortcomings in model performance are evident. These stemmed from a combination of error in the definition of the initial SWE distribution and error in the performance of the distributed melt model (Anderton et al., 2002). Improvements of the forecast are possible through a better determination of spatial input parameters to the models.

Attempts were made to distribute SWE, but most of them were only partially successful and despite a considerable time to design a suitable methodology to do this, no satisfactory technique could be developed. Overall the distributed initial SWE models are successful in producing the conditions observed at the catchment and the model results presented in this work give some idea of the range of magnitudes to be expected, and this will help any new designs in the future.

_ Distributed radiation model was used only during the early melt season in this project, so it was primarily designed to only simulate the ablation of a seasonal snowpack. However, it was shown that it simulated the ablation of snow well, so could potentially be run for an entire melt season. However, to do this successfully

the model would have to include accumulation processes. The model can simulate accumulation with given accurate precipitation input, but the problem arises in how best to simulate spatial variation in precipitation, and perhaps more importantly, redistribution of snow by wind. However, the recent development of physically based blowing snow models which use simulated wind fields (e.g. Essery et al., 1999) also offers the possibility of investigating the affects of using spatially distributed wind speeds to improve estimates of spatial variability in turbulent fluxes.

_ Further field surveys and analysis of spatial variation in snow parameters as SWE and SCA in different environments (climate and topography) would clearly be useful for further model developments. In the future, microwave data will be combined with the optic data to achieve improved snow maps that will not be restricted by weather conditions and that will contain some information on snow depth even on SWE (Hall et al., 2002).

_ The assumption of uniform surface energy balance across the model domain means it is not necessary to explicitly represent the *spatial* distribution of SWE at all, with two recent studies showing that knowledge of the *frequency* distribution of initial sub-grid scale SWE and average grid scale energy exchange is sufficient to predict depletion of grid-scale SCA (Liston, 1999; Luce et al., 1999). However, whether either explicit, spatial distributions of SWE or sub-catchment frequency distributions of SWE are used it is important to simulate this accurately because SWE has important affects on albedo, and thus melt rates, and on meltwater storage. Therefore, there must be a note of caution in any conclusion based on the sensitivity analysis that strongly suggests that spatial variation in initial SWE is much important in determining final SWE distributions than any variation in meteorological driving variables and thus melt rates. However, while the results presented here and in the other recent studies cited earlier are encouraging in suggesting that the sub-grid parameterization of snow processes can be simplified, considerable obstacles remain to parameterizing SWE at the sub-grid scale. Possibly the most serious is that of data acquisition.

- A review of the most pertinent literature (Chapter 2) revealed that whilst there were a number of layered, snow process models capable of simulating surface melt, there seemed to be much less previous work on how to simulate the discharge from a basin for a distributed physically based model. Therefore, it was proposed to develop a methodology to couple a hydrologic model, concerning the routing and infiltration, to the meltwater outflow from a snow process model.

REFERENCES

- Abbot, M.B., Bathurst, J.C., Cunge, J.A., O'Connell, P.E. and Rasmussen, J. (1986) An introduction to the European Hydrological System - Sytème Hydrologique Europeen, 'SHE', 1: History and philosophy of a physically-based, distributed modeling system. *Journal of Hydrology*, 87, 45-59.
- Akyürek, Z. and Şorman, A.Ü. (2002) Accuracy Assesment of a Landsat Assisted Landcover Mapping Case Study: City of Erzurum and Its Vicinity-Turkey, 3rd International Remote Sensing Semposium of Urban Rivers, Istanbul, Turkey, 11-13 June 2002, Vol 2, 529-536.
- Albert, M. and Krakeski, G. (1998) A fast, physically based point snowmelt model for use in distributed applications. *Hydrological Processes*, 12 (10-11), 1809- 1824.
- Altınbilek, D. (2004) Development and management of the Euphrates-Tigris Basin, *International Journal of Water Resources Development*, Vol. 20, No:1.
- Ambach, W.M., Blumthaler, M. and Kirchlechner, P. (1981) Applications of the gravity flow theory to the percolation of melt water through firn, *Journal of Glaciology*, 27, 67-75.
- Anderson, E.A. (1976) A point energy and mass balance model of a snow cover, *US National Oceanic and Atmospheric Administration*, Silver Spring, Maryland.
- Anderson, E.A. (1968) Development and testing of snow pack energy balance equations, *Water Resources Research*, 4(1), 19-37.
- Anderson, M.G. and Burt, T.P. (1990) *Process Studies in Hillslope Hydrology*, Chichester, John Wiley and Sons.
- Anderton, S.P., White, S.M. and Alvera, B. (2002) Micro-scale spatial variability and the timing of snow melt runoff in a high mountain catchment, *Journal of Hydrology*, 268, 158-176.
- Andreas, E. L. (1987) A theory for the scalar roughness and the scalar transfer coefficients over snow and sea ice, *Boundary Layer Meteorol.*, 38, 159-184.
- Appel, I.L. and Salomonson, V.V. (2002) Estimate of fractional snow cover using MODIS data, *Proceedings of IGARSS 2002*, Toronto, Canada.

- Arnold, N., Richards, K.S., Willis, I.C. and Sharp, M.J. (1998) Initial results from a distributed, physically based model of glacier hydrology. *Hydrological Processes*, 12, 191-219.
- Arnold, N.S., Willis, I.C., Sharp, M.J., Richards, K.S. and Lawson, W.J. (1996) A distributed surface energy balance model for a small valley glacier. I. Development and testing for Haut Glacier d'Arolla, Valais, Switzerland, *Journal of Glaciology*, 42, 77-89.
- ASCE - American Society of Civil Engineers - (1996) 2nd ed., *Hydrology Handbook*, The Society, New York.
- Bales, R.C. and Harrington, R.F. (1995) Recent progress in snow hydrology, *Reviews of Geophysics Supplement*, 1011-1020.
- Barnes, W.L., Pagano, T.S. and Salomonson, V.V. (1998) Prelaunch characteristics of the Moderate Resolution Imaging Spectroradiometer (MODIS) on EOS-AM1, *IEEE Transactions on Geoscience and Remote Sensing*, 36(4), 1088-1100.
- Bartelt, P. and Lehning, M. (2002) A physical SNOWPACK model for the Swiss avalanche warning Part I: numerical model, *Cold Reg. Sci. Tech.* 35(3), 123-146.
- Barton, J.S., Hall, D.K. and Riggs, G.A. (2000) Remote sensing of fractional snow cover using Moderate Resolution Imaging Spectroradiometer (MODIS) data, *Proceedings of the 57th Eastern Snow Conference*, Syracuse, NY, 171-181.
- Barry, R.G. (1992) *Mountain Weather and Climate*, London, Routledge.
- Bell, V.A. and Moore R.J. (1999) An elevation-dependent snowmelt model for upland Britain, *Hydrological Processes*, 13 (14-15), 1887-1903.
- Bergstrom, S. (1991) Principles and confidence in hydrological modeling, *Nordic Hydrology*, 22, 123-136.
- Bergstrom, S. (1975) The development of a snow routine for the HBV-2 model, *Nordic Hydrology*, 6, 73-92.
- Bernier, M., Fortin, J.P., Gauthier, Y., Gauthier, R., Roy, R. and Vincent, P. (1999) Determination of snow water equivalent using RADARSAT data in eastern Canada, *Hydrological Processes*, 13, 3031-3042.
- Beven, K.J. (2001) Calibration, validation and equifinality in hydrological modeling: a continuing discussion, *Calibration, validation and equifinality in hydrological modelling: a continuing discussion*, M. G. Anderson and P. D. Bates (eds.), Chichester, UK, John Wiley and Sons Ltd., 43-55.

- Beven, K.J. (1993) Prophecy, reality and uncertainty in distributed hydrological modeling, *Advances in Water Resources*, 16, 41-51.
- Beven, K.J. (1989) Changing ideas in hydrology - the case of physically-based models, *Journal of Hydrology*, 105 (1-2), 157-172.
- Blöschl, G. (1999) Scaling issues in snow hydrology, *Hydrological Processes*, 13 (14-15), 2149-2175.
- Blöschl, G. (1991) The influence of uncertainty in air temperature and albedo on snowmelt, *Nordic Hydrology*, 22 (2), 95-108.
- Blöschl, G. and Sivapalan M. (1995) Scale issues in hydrological modeling: a review, *Hydrological Processes*, 9 (3-4), 251-290.
- Blöschl, G. and Kirnbauer, R. (1992) An analysis of snow cover patterns in a small alpine catchment, *Hydrological Processes*. 6 (1), 99-109.
- Blöschl, G. and Kirnbauer, R. (1991) Point snowmelt models with different degrees of complexity - internal processes, *Journal of Hydrology*, 129 (1-4), 127-147.
- Blöschl, G., Gutknecht, D. and Kirnbauer, R. (1991a) Distributed snowmelt simulations in an alpine catchment, 2. Parameter study and model predictions, *Water Resources Research*, 27 (12), 3181-3188.
- Blöschl, G., Kirnbauer, R. and Gutknecht, D. (1991b) Distributed snowmelt simulations in an alpine catchment I. Model evaluation on the basis of snow cover patterns, *Water Resources Research*, 27 (12), 3171-3179.
- Blöschl, G., Kirnbauer, R. and Gutknecht, D. (1990) Modeling snowmelt in a mountainous river basin on an event basis, *Journal of Hydrology*, 113 (1-4), 207-229.
- Brandt, R.E. and Warren, S.G. (1993) Solar heating rates and temperature profiles in antarctic snow and ice, *Journal of Glaciology*, 39 (131), 99-110.
- Braun, L.N., Brun, E., Durnad, Y., Martin, E. and Tourasse, P. (1994) Simulation of discharge using different methods of meteorological data distribution, basin discretation and snow modeling, *Nordic Hydrology*, 25, 129-44.
- Braun, L.N. and Lang, H. (1986) Simulation of snowmelt runoff in lowland and lower Alpine regions of Switzerland, *Modeling snowmelt-induced processes*, Budapest, IAHS.
- Brock, B.W., Willis, I.C. and Sharp, M.J. (2000a) Measurement and parameterisation of albedo variations at Haut Glacier d'Arolla, Switzerland, *Journal of Glaciology*, 46 (155), 675-688.

- Brock, B.W., Willis, I.C., Sharp, M.J. and Arnold, N.S. (2000b) Seasonal and spatial variations in the surface energy balance of Haut Glacier d'Arolla, Switzerland, *Annals of Glaciology*, 31, 53-62.
- Brubaker, K., Rango, A. and Kustas, W. (1996) Incorporating radiation inputs into the Snowmelt Runoff Model, *Hydrological Processes*, 10, 1329-1343.
- Bruland, O. (2002) *Dynamics of the seasonal snowcover in the arctic*, Ph.D. dissertation, Faculty of Engineering Science and Technology, Norwegian University of Science and Technology, Trondheim, Norway.
- Brun, E., Durand, Y., Martin, E. and Braun, L. (1994) Snow modeling as an efficient tool to simulate snow cover evolution at different spatial scales, *Snow modeling as an efficient tool to simulate snow cover evolution at different spatial scales*, H. G. Jones, T. D. Davies, A. Ohmura and E. M. Morris (eds.) Wallingford, IAHS: 163-174.
- Brun, E., David, P., Sudul, M., Brunot, G. (1992) A numerical model to simulate snow cover stratigraphy for operational avalanche forecasting, *Journal of Glaciology*, 38, 13-22
- Brun, E., Martin, E., Simon, V., Gendre, C. and Coleou, C. (1989) An energy and mass model of snow cover suitable for operational avalanche forecasting, *Journal of Glaciology*, 35 (121): 333-342.
- Brunt, D. (1932) Notes on radiation in the atmosphere I. *Quarterly Journal of the Royal Meteorological Society*, 58, 389-420.
- Brutsaert, W. (1975) On a derivable formula for long-wave radiation from clear skies, *Water Resources Research*, 11, 742-744.
- Budd, W.R., Dingle, R. Radok, U. (1966) The Byrd snowdrift project: outline and basic results, *Studies in Antarctic Meteorology*, American Geophysical Union, Antarctic Research Service, 9, 71-134.
- Cazorzi, F. and Fontana, G.D. (1996) Snowmelt modeling by combining air temperature and a distributed radiation index, *Journal of Hydrology*, 181 (1-4), 169-187.
- Cline, D.W. (1997) Snow surface energy exchanges and snowmelt at a continental, mid-latitude Alpine site, *Water Resources Research*, 33 (4), 689-701.
- Cline, D. (1995) Snow surface energy exchanges and snowmelt at a continental alpine site, *Snow surface energy exchanges and snowmelt at a continental alpine site*, K.A. Tonnessen, M.W. Williams and M. Tranter (eds.) Wallingford, U.K., International Association of Hydrological Sciences. No. 228, 157-166.

Cline, D., Elder, K. and Bales, R. (1998a) Scale effects in a distributed snow water equivalence and snowmelt model for mountain basins, *Hydrological Processes*, 12 (10-11), 1527-1536.

Cline, D.W., Bales, R.C. and Dozier, J. (1998b) Estimating the spatial distribution of snow in mountain basins using remote sensing and energy balance modeling, *Water Resources Research*, 34 (5), 1275-1285.

Colbeck, S.C. (1982) An overall seasonal metamorphism, *Reviews of Geophysics and Snow Physics*, 20, 45-61.

Colbeck, S.C. and Davidson, G. (1973) *Water percolation through homogeneous snow*, The role of snow and ice in hydrology, UNESCO-WMO-IASH.

Conway, H. and Benedict, R. (1994), Infiltration of water into snow, *Water Resources Research*, 30 (3), 641-649.

Copland, L. (1998) The use of terrain analysis in the evaluation of snow cover over and an alpine glacier, *The use of terrain analysis in the evaluation of snow cover over and an alpine glacier*, (S.N. Lane, J.H. Chandler and K.S. Richards). Chichester, John Wiley and Sons.

Cullen H.M. and deMenocal P.B. (2000) North Atlantic influence on Tigris-Euphrates streamflow, *International Journal of Climatology*, Vol. 20, 853-863.

Daly, S.F., Davis, R., Ochs, E. and Pangburn, T. (2000) An approach to spatially distributed snow modeling of the Sacramento and San Joaquin basins, California. *Hydrological Processes*, 14, 3257-3271.

Davis, R.E., Jordan, R., Daly, S. and Koenig, G. (2001) Validation of Snow Models, *Validation of Snow Models*, M.G. Anderson and P.D. Bates (eds.) Chichester, UK, John Wiley and Sons Ltd., 261-292.

Davis, R.E., McKenzie, J.C. and Jordan, R. (1995) Distributed snow process modeling: an image processing approach, *Hydrological Processes*, 9 (8), 865- 875.

Davis, R.E., Dozier, J. and Marks, D. (1984) Micrometeorological measurements and instrumentation in support of remote sensing observations of an alpine snow cover, *Proceedings of the Western Snow Conference*, 52, 161-164.

de Quervain, M.R. (1973) Snow structure, heat and mass flux through snow, *Snow structure, heat and mass flux through snow*, Banff, Alberta, UNESCO-WMOIAHS: 203-226.

Dickenson, R.E., Henderson-Seller, A. and Kennedy, P.J., (1993) *Biosphere-Atmosphere Transfer Scheme (BATS) Version 1e as coupled to the NCAR Community*

Climate Model, Tech. Note NCAR/TN-387+STR, 72 pp. Natl. Cent. For Atmos. Res., Boulder, Colo.

Diez Minox, J.C. (1991) *Study and parameterization of the energy exchange between the atmosphere and the snowpack during the melt season, Izas experimental catchment, Central Pyrenees*, Ph.D. Dissertation, Universidad de Zaragoza, 167 pp.

Dingman, S.L. (1994) *Physical Hydrology*, Prentice-Hall, New Jersey. 575 p.

Douville, H., J.F. Royer and Mahfouf J.F. (1995) A new snow parameterization for the Météo-France climate model, *Climate Dynamics*, 12, 21-35.

Dozier, J. (1992) Opportunities to improve hydrologic data, *Reviews of Geophysics*, 30 (4), 315-331.

Dozier, J. (1987) Recent research in snow hydrology, *Reviews of Geophysics*, 25 (2), 153-161.

Dozier, J. (1980) A clear sky spectral radiation model for snow-covered mountainous terrain, *Water Resources Research*, 16, 709-718.

Dozier, J. and Frew, J. (1990) Rapid calculation of terrain parameters for radiation modeling from digital elevation data. *IEEE Transactions on Geoscience and Remote Sensing*, 28, 963-969.

Dubayah, R. and Rich, P.M. (1996) GIS-based solar radiation modeling, *GIS and Environmental Modeling*, M.F. Goodchild, L.T. Steyaert and B.O. Parks (eds.), pp. 129–134, John Wiley & Sons, New York.

Dubayah, R., and Rich, P.M. (1995) Topographic solar radiation models for GIS, *International Journal of Geographical Information Systems*, 9, 405-419.

Dunn, S.M. and Colohan, R.J.E. (1999) Developing the snow component of a distributed hydrological model: a stepwise approach based on multi-objective analysis, *Journal of Hydrology*, 223, 1-16.

Dyunin, A.K. (1959) *Fundamentals of the theory of snow drifting Iozest*, Sibirsk, Otdel. Akad. Nauk. USSR. No 12, 11-24.

Elder, K., Rosenthal, W. and Davis, R.E. (1998) Estimating the spatial distribution of snow water equivalence in a mountain watershed, *Hydrological Processes*, 12 (10-11), 1793-1808.

Elder, K. and Cline, D. (1998) Spatial properties of snow in an alpine basin, Colorado Front Range, *Int. Conf. Snow Hydrology*, Vermont, USA, Oct 5-9, 1998, IAHS, US Army Corps of Engineers Rpt, 98-10.

- Elder, K., Dozier, J. and Michaelsen, J. (1991) Snow accumulation and distribution in an alpine watershed, *Water Resources Research*, 27 (7), 1541-1552.
- Elligson, R.G., Ellis, J. and Fels, S. (1991) The intercomparison of radiation codes used in climate models: Longwave results, *Journal of Geophysical Research*, 96, 8929-8953.
- Engman, E.T., Gurney, R.J. (1991) *Remote Sensing in Hydrology*, Chapman and Hall, New York.
- Escher-Vetter, H. (2000) Modeling meltwater production with a distributed energy balance method and runoff using a linear reservoir approach - results from Vernagtferner, Oetztal Alps, for the ablation seasons 1992 to 1995. *Zeitschrift für Gletscherkunde und Glazialgeologie*, 21, 397-402.
- Essery, R. (1997) Seasonal snow cover and climate change in the Hadley Centre GCM. *Annals of Glaciology*, 25, 362-366.
- Essery, R. and Yang, Z.L. (2001) *An overview of models participating in the snow model intercomparison project (SNOWMIP)*, SnowMIP Workshop, 11 July 2001, 8th Scientific assembly of IAMAS, Innsbruck.
- Essery, R., Li, L. and Pomeroy, J. (1999) A distributed model of blowing snow over complex terrain, *Hydrological Processes*, 13, 2423-2438.
- Ferguson, R.I. (1999). Snowmelt runoff models, *Progress in Physical Geography*, 23 (2), 205-227.
- Ferguson, R.I. (1986) Parametric modeling of daily and seasonal snowmelt using snowpack water equivalent as well as snow covered area, *Modeling snowmelt-Induced Processes*, Budapest, International Association of Hydrological Sciences. Publ. No. 155: 151-161.
- Fierz, C., Riber, P., Adams, E.E., Curran, A.R., Föhn, P.M.B., Lehning, M. and Plüss, C. (2003) Evaluation of snow surface energy balance models in alpine terrain, *Journal of Hydrology*, 282, 76-94.
- Flerchinger, G.N., Cooley, K.R. and Deng, Y. (1994) Impacts of spatially and temporally varying snowmelt on subsurface Flow in a mountainous watershed: 1. Snowmelt simulation, *Hydrological Sciences*, 39, 507- 519.
- Flerchinger, F.N., Saxton, K.E. (1989) Simultaneous heat and water model of a freezing snow-residue-soil system I. Theory and development, *Transactions of the ASCE*, 32, 565-571.
- Forrer, J. and Rotach (1997) On the turbulence structure in the stable boundary layer over the Greenland ice sheet, *Boundary Layer Meteorology*, 85, 111-136.

- Fox, A.M. (2003) *A distributed, physically based snowmelt and runoff model for alpine glaciers*, Ph.D. Dissertation, St. Catherine's College.
- Frew, J.E. (1990) *The Image Processing Workbench*, Ph.D. Thesis, Department of Geography, University of California: Santa Barbara, CA: 382 pp.
- Garen D. (1995) Estimation of spatially distributed values of daily precipitation in mountainous areas. In *Proceedings of Canadian Water Resources Association Conference, Mountain Hydrology: Peaks and Valleys in Research and Applications*, Vancouver, British Columbia: pp. 237-242.
- Garen, D.C., and Marks, D. (2005) Spatially distributed energy balance snowmelt modelling in a mountainous river basin: Estimation of meteorological inputs and verification of model results, *Journal of Hydrology* (accepted).
- Garen, D.C. and Marks, D. (1996) Spatially distributed snow modeling in mountainous regions: Boise River application. In: *HydroGIS'96; Application of Geographic Information Systems in Hydrology and Water Resources Management*, (proceedings of Vienna Conference) IAHS Publication No: 235, 421-428.
- Garen, D.C., Johnson, G., Hanson, C. (1994) Mean areal precipitation for daily hydrologic modeling in mountainous regions, *Water Resources Bulletin*, 30, 481- 491.
- Gates, D.M. (1980) *Biophysical Ecology*, Springer, New York.
- Geiger, R. (1966) *The Climate Near the Ground*, Harvard University Press, Cambridge.
- Glendinning, J.H.G. and Morris, E. M. (1999) Incorporation of spectral and directional radiative transfer in a snow model, *Hydrological Processes*, 13 (12- 13), 1761-1772.
- Goodison, B.E. and Walker, A.E. (1995) Canadian development and use of snow cover information from passive microwave satellite data, In B.J. Choudhary, Y.H. Kerr, E.G. Njoku, and P. Pampaloni (Eds.), *Passive Remote Sensing of Land-Atmosphere Interactions*, 245-262, Utrecht, The Netherlands: ESA/NASA International Workshop.
- Granger, R.J. and Gray, D.M. (1990) A net radiation model for calculating daily snowmelt in open environments, *Nordic Hydrology*, 21, 217-234.
- Groffman, P.M., Hardy, J.P., Nolan, S., Fitzhugh, R.D., Driscoll, C.T. and Fahey, T.J. (1999) Snow depth, soil frost and nutrient loss in a northern hardwood forest, *Hydrological Processes*, 13 (14-15), 2275-2286.

- Gusev, Ye.M., and Nasonova, O.N. (1998) The land surface parametrization scheme SWAP: description and partial validation, *Global and Planetary Change*, 19, 63-86.
- Hall, D.K., Riggs, G.A., Salomonson, V.V., DiGirolamo, N.E. and Bayr, K.J. (2002) MODIS Snow-Cover Products, *Remote Sensing of Environment*, 83, 181-194.
- Hamlin, L., Pietroniro, A., Prowse, T., Soulis, R. and Kouwen, N. (1998) Application of indexed snowmelt algorithms in a northern wetland regime, *Hydrological Processes*, 12, 1641-1657.
- Hardy, J.P., Albert, M.R. and Marsh, P. (1999) Preface: International Conference on Snow Hydrology: The Integration of physical, chemical and biological systems, *Hydrological Processes*, 13 (14-15), 2115-2116.
- Hartman, M.D., Baron, J.S., Lammers, R.B., Cline, D.W., Band, L.E., Liston, G.E. and Tague, C. (1999) Simulations of snow distribution and hydrology in a mountain basin, *Water Resources Research*, 35, 1587-1603.
- Hastings, D. and Emery, W. (1992) The Advanced Very High Resolution Radiometer (AVHRR): a brief reference guide, *Photogrammetric Engineering and Remote Sensing*, 58(8), 1183-1188.
- Hetrick, W.A., Rich, P.M., Barnes, F.J. and Weiss, S.B. (1993a) GIS-based solar radiation flux models, *American Society for Photogrammetry and Remote Sensing Technical Papers*, 3, *GIS Photogrammetry and Modeling*, 132-143.
- Hetrick, W.A., Rich, P.M. and Weiss, S.B. (1993b) Modeling insolation on complex surfaces, *Thirteen Annual ESRI User Conference*, 2, 447-458.
- Hock, R. (2003) Temperature index melt modeling in mountain areas. *Journal of Hydrology*, 282.
- Hock, R. (1999) A distributed temperature-index ice- and snowmelt model including potential direct solar radiation, *Journal of Glaciology*, 45 (149), 101-111.
- Hock, R. and Noetzli, C. (1997) Aral melt and discharge modeling of Storglaciären, Sweden, *Annals of Glaciology*, 24, 211-217.
- Hock, R. and Holmgren, B. (1996) Some aspects of energy balance and ablation of Storglaciären, Northern Sweden, *Geografiska Annaler*, 78A (2-3), 121-131.
- Idso, S.B. (1981) A set of equations for full spectrum and 8-14 micrometres and 10.5-12.5 micrometres thermal radiation from cloudless skies, *Water Resources Research*, 17, 295-304.

IPW, <http://cirque.ars.pn.usbr.gov/~ipw>, Image Processing Workbench, Dec 2004.

Jordan, R.E. (1991) *A one-dimensional temperature model for a snow cover*, Technical documentation for SNTHERM.89. Hanover, New Hampshire, US Army Corps of Engineers.

Johnson, J.B. (2001) The physical causes of snow pillow measurement errors, *US Army ERDC-Cold Regions Research and Engineering Laboratory, Alaska Section AWRA, Northern-Region Brown-Bag Presentation*, Alaska Department of Natural Resources.

Johnson, J. and Marks, D. (2004) The detection and correction of snow water equivalent pressure sensor errors, *Hydrological Processes*, 18 (18), 3513-3525.

Justice, C. O., Vermote, E., Townshend, J. R. G., Defries, R., Roy, D. P., Hall, D. K., Salomonson, V. V., Privette, J. P., Riggs, G., Strahler, A., Lucht, W., Myneni, R. B., Knyazikhin, Y., Running, S. W., Nemani, R. R., Wan, Z., Huete, A., Leeuwen, W., Wolfe, R. E., Giglio, L., Muller, J. P., Lewis, P., & Barnsley, M. J. (1998). The moderate resolution imaging spectroradiometer (MODIS): Land remote sensing for global research. *IEEE Trans. Geosci. Remote Sens.*, 36, 1228- 1249.

Kaya, I. (1999) *Application of snowmelt runoff model using remote sensing and geographic information systems*, Ms. Thesis, Department of Civil Engineering, Middle East Technical University

Kattelmann, R. (2000) Snowmelt lysimeters in the evaluation of snowmelt models, *Annals of Glaciology*, 31, 406-410.

Kirnbauer, R., Blöschl, G. and Gutknecht, D. (1994) Entering the era of distributed snow models, *Nordic Hydrology*, 25 (1-2), 1-24.

Kite, G.W. (1995) Scaling of input data for macroscale hydrologic modeling, *Water Resources Research*, 31 (11), 2769-2781.

Kite, G.W. and Pietroniro, A. (1996) Remote sensing applications in hydrological modelling, *Hydrological Science Journal*, 41(4), 563-591.

Klein, A.G., Hall, D.K., and Riggs, G.A. (1998) Improving snow cover mapping in forests through the use of a canopy reflectance model, *Hydrological Processes*, 12 (10-11), 1723-1744.

Kondratyev, K.Y. (1969) *Radiation in the atmosphere*, Academic, New York.

Kondo, J. and Yamazaki, T. (1990) Prediction model for snow melt, snow surface temperature, and freezing depth using a heat balance method, *Journal of Applied Meteorology*, 29 (5), 375-384.

- Konzelmann, T., van de Wal, R.S.W., Gruell, W., Bintanja, R., Henneken, E.A.C. and Abe-Ouchi, A. (1994) Parameterization of global and longwave incoming radiation for the Greenland ice sheet, *Global Planetary Change*, 9 (1-2), 143- 164.
- Kouwen, N., Soulis, E.D., Pietroniro, A., Donald, J.R., and Harrington, R.A. (1993) Grouped response units for distributed hydrologic modeling, ASCE, *J. Wat. Resour. Plan. Mgmt*, 119, 289-305.
- Kumar, L., Skidmore, A.K. and Knowles, E. (1997) Modeling topographic variation in solar radiation in a GIS environment, *International Journal of Geographic Information Science*, 11, 475-497.
- Kustas, W.P. and Rango, A. (1994) A simple energy budget algorithm for the snowmelt runoff model, *Water Resources Research*, 30 (5), 1515-1527.
- Lacroix, M. and Martz, L.W. (1997) *Integration of the TOPAZ landscape analysis and the SLURP hydrologic models*, Proc. Scientific Meeting, Canadian Geophysical Union, Banff, Alberta, 208.
- Lang, H. and Braun, L. N. (1990) On the information content of air temperature in the context of snow melt estimation. In *Hydrology of mountainous areas* (ed. Molnar, L.), International Association of Hydrological Sciences, 190, 347-354.
- Leavesley, G.H. (1989) Problems of snowmelt runoff modeling for a variety of physiographic and climatic conditions, *Hydrologic Science Journal*, 105, 205- 223.
- Leavesley, G.H., Lumb, A.M., Saindon, L.G. (1987) *A microcomputer based watershed modeling and data-management system*, Proceedings, 55th Annual meeting, Western Snow Conference, Western Snow Conference, Vancouver, British Columbia, Canada, 108-117.
- Leavesley, G.H., Litchy, R.W., Troutman, M.M., Saindon, L.G. (1983) *Precipitation-runoff modeling system: User's manual*, Water Resources Investigations Report: US Geological Survey: 207 pp.
- Lettau, H. (1969) Note on aerodynamic roughness-parameter estimation on the basis of roughness element description, *Journal of Applied Meteorology*, 8 (5), 828-832.
- Link, T. (1998) *Seasonal Snowcover Dynamics Beneath Boreal Forest Canopies*. M.S. Thesis, Department of Geosciences, Oregon State University: Corvallis, OR: 58 pp.
- Link, T.E. and Marks, D. (1999) Distributed simulation of snow cover mass- and energy balance in boreal forest, *Hydrological Processes*, 13 (14-15), 2439- 2452.

Liston, G.E. (1999) Interrelationships among snow distribution, snowmelt and snow cover depletion: implications for atmospheric, hydrologic and ecologic modeling, *Journal of Applied Meteorology*, 38, 1474-1487.

Liston, G.E., Pielke Sr., R.A. and Greene E.M. (1999) Improving first-order snow related deficiencies in a regional climate model, *Journal of Geophysical Research*, 104 (D16), 19559-10567.

Liston, G.E. and Sturm, M. (1998) A snow-transport model for complex terrain, *Journal of Glaciology*, 44, 498-516.

Longley, K., Jacobsen, D., Marks, D. (1992) *Supplement to the Image Processing Workbench (IPW): Modifications, Procedures, and Software Additions*, November 1989 to June 1992 (Revision 2.0). Technical Report, US EPA, Environmental Research Laboratory: Corvallis, OR.

Longley, K. and Marks, D. (1991) *Supplement to the Image Processing Workbench (IPW), Volume 1.0: Modifications, Procedures, and Software Additions* November, 1989 to October, 1991. Technical Report, US EPA Environmental Research Laboratory: Corvallis, OR.

Luce, C.H., Tarboton, D.G. and Cooley, K.R. (1999) The influence of the spatial distribution of snow distribution for an energy and mass balance snow cover model, *Hydrological Processes*, 13 (14-15), 1921-2133.

Luce, C.H., Tarboton, D.G. and Cooley, K.R. (1998), The influence of the spatial distribution of snow on basin-averaged snowmelt, *Hydrological Processes*, 12, 1671-1683

Male, D.H. and Granger, R.J. (1981) Snow surface energy exchange, *Water Resources Research*, 117 (3), 609-627.

Male, D.H. and Grey, D.M. (1981), Snow cover ablation and runoff, *Snow cover ablation and runoff*, D.H. Male and D.M. Grey (eds.). Toronto, Ontario, Pergamon Press: 360-436

Marks, D. (1988). *Climate, energy exchange and snowmelt in Emerald Lake watershed, Sierra Nevada*. Ph.D. Thesis Geography and Mechanical Engineering, University of Santa Barbara, CA: 158.

Marks, D. and Winstral, A. (2001) Comparison of snow deposition, the snow cover energy balance and snowmelt at two sites in a semiarid mountain basin, *Journal of Hydrometeorology*, 2(3), 213-227.

Marks, D., Domingo, J., Susong, D., Link, T. and Garen, D.C. (1999a) A spatially distributed energy balance snowmelt model for application in mountain basins. *Hydrological Processes*, 13 (12-13), 1935-1959.

- Marks, D., Domingo, J. and Frew, J. (1999b) Software tools for hydro-climatic modeling and analysis: Image Processing Workbench, ARS - USGS Version 2, *ARS Technical Bulletin 99-1*, NWRC, USDA Agricultural Research Service, Boise, Idaho.
- Marks, D., Kimball, J., Tingey, D. and Link, T. (1998) The sensitivity of snowmelt processes to climate conditions and forest cover during rain-on-snow: a case study of the 1996 Pacific Northwest flood, *Hydrological Processes*, 12, 1569- 1587.
- Marks, D. and Dozier, J. (1992) Climate and energy exchange at the snow surface in the alpine region of the Sierra Nevada. 2. Snow cover energy balance, *Water Resources Research*, 28 (11), 3043-3054.
- Marks, D. and Dozier, J. (1979) A clear sky longwave radiation model for remote alpine areas, *Arch. Meteorol., Geophys. Bioclimatol. Ser. B*, 27, 159-187.
- Marsh, P. (1999) Snowcover formation and melt: Recent advances and future prospects, *Hydrological Processes*, 13 (14-15), 2117-2134.
- Marshall, S.E. and Warren, S.G. (1987) *Parameterization of snow albedo for climate models*. B.E. Goodison, R.G. Barry and J. Dozier (eds.). Wallingford, UK, International Association of Hydrological Sciences, IAHS-AIHS Publication 166: 43-50.
- Martinec, J. (1989) *Hour-to-hour snowmelt rates and lysimeter outflow during an entire ablation period*, S.C. Colbeck, IAHS. Pub. no. 183, 19-28.
- Martinec, J. (1975) Snowmelt runoff model for river flow forecasts., *Nordic Hydrology*, 6, 145-154.
- Martinec, J., Rango, A. and Roberts, R., (Eds.) (1994) *The Snowmelt Runoff Model (SRM) User's Manual*, Geographica Bernensia. Berne, Switzerland, Department of Geography, Univ. of Berne.
- Martinec, J.H. and Rango, A. (1989) Merits of statistical criteria for the performance of hydrological models, *Water Resources Bulletin* 25(2), 421-432.
- Martinec, J. and de Quervain, M.R. (1975) *The effect of snow displacement by avalanches on snow melt and runoff*, Snow and Ice Symposium, Moscow, IAHS.
- Masuoka, E., Fleig, A., Wolfe, R.E. and Patt, F. (1998) Key characteristics of MODIS data products, *IEEE Transactions on Geoscience and Remote Sensing*, 36, 1313-1323.
- Maurer, E.P., Rhoads, J.D., Dubayah, R.O. and Lettenmaier, D.P. (2003), Evaluation of the snow covered area data product from MODIS, *Hydrological Processes*, 17, 59-71.

- Melloh, R.A. (1999) *A Synopsis and Comparison of Selected Snowmelt Algorithms*, Hanover, New Hampshire, US Army Corps of Engineers, Cold Regions Research and Engineering Laboratory, CRREL Report 99-8
- Melloh, R.A., Daly, S.F., Davis, R.E., Jordan, R.E. and Koenig, G. (1997). *An operational snow dynamics model for the Sava River, Bosnia*, Eastern Snow Conference, 4-8 May, Banff, Alberta, Canada.
- Molotch, N.P., Fassnacht, S.R., Colee, M.T., Bardsley, T., and Bales, R.C. (2001) A comparison of spatial 35 statistical techniques for the development of a validation dataset for mesoscale modeling of snow water equivalence. *EOS Trans., AGU, Fall Meet. Suppl.*, 82 (47), F553.
- Moore, R. D. (1983) On the use of bulk aerodynamic formulae over melting snow, *Nordic Hydrology*, 14(4), 193-206.
- Morris, E.M. (1991) *Physics-Based Models of Snow*, D.S. Bowles and P.E. O'Connell (eds.), Netherlands, Kluwer Academic Publishers: 85-112.
- Morris, E.M. (1989) Turbulent transfer over snow and ice, *Journal of Hydrology*, 105 (3-4), 205-223.
- Morris, E.M. (1985) *Snow and Ice*, M.G. Anderson and T.P. Burt (eds.). Chichester, UK, John Wiley and Sons: 153-182.
- Morris, E.M. (1983) Modeling the flow of mass and energy within a snowpack for hydrological forecasting, *Annals of Glaciology*, 4, 198-203.
- Morris, E.M. (1982) Sensitivity of the European Hydrological System snow models. *Hydrological aspects of alpine and high-mountain areas; proceedings of a symposium held during the first scientific general assembly of the International Association of Hydrological Sciences*, IAHS Publ. No. 138, 221-231
- Morris, E.M., Anderson, P.S., Bader, H.P., Weilenmann, P. and Blight, C. (1993) *Modeling mass and energy exchange over polar snow using the DAISY model*, in: *Snow and ice covers: interactions with the atmosphere and ecosystems*. Proc. symposia, Yokohama, 223, 53-60.
- Munro, D.S. (1990) Comparison of melt energy computations and ablatometer measurements on melting ice and snow, *Arctic and Alpine Research*, 22(2), 153-162.
- Munro, D.S. (1989) Surface roughness and bulk heat transfer on a glacier: comparison with eddy correlation, *Journal of Glaciology*, 35 (121), 343-348.
- Munro, D.S. and Young, G.J. (1982) An operational radiation model for glacier basins, *Water Resources Research*, 18, 220-230.

- Nash, J.E. and Sutcliffe, J.V. (1970) Riverflow forecasting through conceptual models, Part I A discussion of principals, *Journal of Hydrology*, 10, 282 - 290.
- Neale, S.M. and Fitzharris, B.B. (1997) Energy balance and synoptic climatology of a melting snowpack in the Southern Alps, New Zealand, *International Journal of Climatology*, 17, 1595-1609.
- NOAA, <http://www.noaa.org>, National Oceanic and Atmospheric Administration, Feb 2005.
- NSIDC , <http://www.nsidc.org>, National Snow and Ice Data Center, Feb 2005.
- Obled, C.H., Harder, H. (1979) *A review of snow melt in the mountain environment*, In Proceedings on Modeling of snow cover Runoff, S.C. Colbeck and M. Ray (eds.), US Army Cold Region Research Engineering Lab, Hanover.
- Oerlemans, J. (2000) Analysis of a three year meteorological record from the ablation zone of Moteratschgletscher, Switzerland: energy and mass balance, *Journal of Glaciology*, 46 (155), 571-579.
- Ohmura, A. (2001) Physical basis for the temperature/melt-index method, *Journal of Applied Meteorology*, 40, 753-761.
- Ohmura, A. (1981) *Climate and energy balance on arctic tundra. Axel Heiberg Island, Canadian Arctic Archipelago, spring and summer 1969, 1970, 1972*. Zurich, Department of Geography, ETH: 448.
- Oke (1990) *Boundary Layer Climates*, London, Routledge.
- Olyphant, G.A. (1986) Longwave radiation in mountainous areas and its influence on the energy balance of alpine snowfields, *Water Resources Research*, 22, 62-66.
- Parajka, J., Holko, L. and Kostka, Z. (2000) Distributed modeling of snow water equivalent –coupling a snow accumulation and melt model and GIS, *Institute of Hydrology, Slovak Academy of Sciences, Slovakia*.
- Peck, E.L. (1972) *Methods of Measuring Snow Cover, Snowmelt and Streamflow Under Winter Conditions*, Proc. Int. Symposia on the Role of Snow and Ice in Hydrology: Measurement and Forecasting, (Banff, Canada: UNESCO-WMO-IAHS) Vol 1, September 6-20.
- Pellicciotti, F., Strasser, U., Brock, B., Burlando, P., Funk, M. and Corripio, J. (2002) *An enhanced albedo accounting degree day melt model for distributed application*, American Geophysical Union, Fall Meeting.
- Plüss, C. and Ohmura, A. (1997) Longwave radiation on snow-covered mountainous surfaces, *Journal of Applied Meteorology*, 36 (6), 818-824.

- Pomeroy, J.W., Marsh P. and Gray D.M. (1997) Application of a distributed blowing snow model to the Arctic, *Hydrological Processes*, 11 (11), 1451- 1464.
- Press, W.H., Flannery, S.A., Teukolsky, S.A. and Vetterling, W.T. (1988) *Numerical recipes in C – The art of scientific computing*, Cambridge University Press, Cambridge, UK.
- Pulliainen, J. and Hallikainen, M. (2001) Retrieval of regional snow water equivalent from space-borne passive microwave observations, *Remote Sensing of Environment*, 75 (1), 76-85.
- Rango, A. (1994) Application of remote sensing methods to hydrology and water resources, *Hydrological Sciences*, 34 (4), 309-320.
- Rango, A. (1993) Snow hydrology processes an remote-sensing, *Hydrological Processes*, 7 (2), 121-138.
- Rango, A., Walker, A.E. and Goodison, B.E. (2000) *Snow and Ice*, In G.A. Schultz and E.T. Engman (eds.), *Remote Sensing in Hydrology and Water Management*, 239-262, Springer-Verlag.
- Rango, A. and van Katwijk, V. (1990) Development and testing of a snowmelt runoff forecasting technique, *Water Resources Bulletin*, 26(1), 135-144.
- Rango, A. and Martinec, J. (1982) Snow accumulation derived from modified depletion curves of snow coverage, *In Hydrological Aspects of Alpine and High Mountain areas, Proceedings of Exeter Symposium (eds. J.W. Glen)*, IAHS Publication 138, 83-90.
- Ranzi, R., Rosso, R. (1995) Distributed estimation of incoming direct solar radiation over a drainage basin, *Journal of Hydrology*, 166, 461-478.
- Rich, P.M. (1990) Characterizing plant canopies with hemispherical photography, In: N.S. Goel and J.M. Norman (eds), *Instrumentation for studying vegetation canopies for remote sensing in optical and thermal infrared regions, Remote Sensing Reviews*, 5, 13-29.
- Rich, P.M. (1989) *A manual for analysis of hemispherical canopy photography*, Los Alamos National Laboratory Report, LA-11733-M.
- Rich, P.M., Hetrick, W.A. and Saving, S.C. (1995) *Modeling Topographic Influences on Solar Radiation: a manual for the Solarflux model*, Los Alamos National Laboratory Report LA-12989-M.

- Riggs, G.A., Hall, D.K. and Salomonson, V.V. (2003) *MODIS Snow products User Guide for collection 4 Data Products*, Available online at (<http://www.modis-snow-ice.gsfc.nasa.gov/sugkc2.html>) (www.modis-snow-ce.gsfc.nasa.gov/sug.pdf)
- Risley, J., Marks, D. and Link, T.E. (1997) Application of a quasi-energy balance model to simulate snowmelt under variable canopies during a major rain-on-snow event, *EOS, Transactions of the American Geophysical Union* 78, F320.
- Sand, K. (1990) *Modeling snowmelt runoff processes in temperature and Arctic environments*, Ph.D. Dissertation, Department of Civil Engineering, the Norwegian Institute of Technology.
- Satterland, D.R. (1979) An improved equation for estimating longwave radiation from the atmosphere, *Water Resources Research*, 15, 1649-1650.
- Schmidt, R.A. (1972) *Sublimation of wind transported snow - a model*, Research paper RM 90, USDA Forestry Service, Rocky Mountain Forest and Range Experimental Station, Ford Collins, CO.
- Schultz, G.A. (1993) Hydrological modeling based on remote sensing information, *Advanced Space Research*, 3 (5), 149-166.
- Shi, J. and Dozier, J. (2000) Estimation of snow water equivalence using SIR-C/X-SAR. I. Inferring snow density and subsurface properties, *IEEE Transactions on Geoscience and Remote Sensing*, 38, 2465-2473.
- Shumann, A.H. and Garen, D.C. (1998) *Spatially distributed hydrologic modeling for streamflow simulation and forecasting*, Proceedings, First Federal Interagency Hydrologic Modeling Conference, Las Vegas, Nevada, 7130-7146.
- Shusun, Li., Zhou, X. and Morris, K. (1999) Measurement of Snow and Sea Ice Surface Temperature and Emissivity in the Ross Sea, *Proceedings of IEEE 1999 International Geoscience and Remote Sensing Symposium (IGARSS'99)*, Hamburg, Germany, 1034-1036.
- Slater, A.G. (2000) The representation of snow in land surface schemes; results from PILPS 2(d), *Journal of Hydrometeorology*, 2 (1), 7-25.
- SMHI (1996) *IHMS: integrated modeling system manual (Version 4)*, Swedish Meteorological and Hydrological Institute.
- Solar Analyst (2000) *The Solar-Analyst 1.0 User Manual*, Helios Environmental Modelin Institute, USA (<http://www.fs.fed.us/informs/solaranalyst>)
- Susong, D., Marks, D. and Garen, D.C. (1999) Methods for developing time-series climate surfaces to drive topographically distributed energy- and water balance models, *Hydrological Processes*, 13 (14-15), 2003-2021.

Swamy, N.A. and Brivio, P.A. (1997) Modeling runoff using optical satellite remote sensing data in a high mountainous alpine catchment of Italy, *Hydrological Processes*, 11, 1475-1491.

Şensoy, A. (2000) *Spatially distributed hydrologic modeling approach using geographic information systems*, MSc. Thesis, Department of Civil Engineering, Middle East Technical University

Şensoy, A., Tekeli, A.E., Şorman, A.A. and Şorman, A.Ü. (2003) Simulation of event based snowmelt runoff hydrographs based on snow depletion curves and the degree-day method, *Canadian Journal of Remote Sensing*, 29 (6), 693-700.

Şensoy, A. and Şorman, Ü. (2001) Coupling of GIS and RS in Hydrologic Model Application to Upper Karasu Basin, *Application of Remote Sensing in Hydrology*, 2-5 October 2001, Montpellier, FRANCE.

Şorman, A.A. (2005) *Use of satellite observed snow cover in hydrological modeling through automatic multi-objective calibration and snowmelt runoff prediction in Upper Euphrates Basin, Turkey*, PhD. Thesis, Department of Civil Engineering, Middle East Technical University (in progress)

Şorman, A.A., Tekeli, A.E., Şorman, A.Ü. (2002) Application of snowmelt runoff models by RS/GIS Techniques over the central Asia and Turkey, XXII. Nordic Hydrological Conference, Nordic Association for Hydrology-Nordic Hydrological Programme NHP Report no 47, Volume 1, 161-173.

Şorman, A.Ü., Uzunoğlu, E. and Kaya, I. (2001) *Applications of SRM and SLURP models in eastern Turkey using remote sensing and geographic information systems*, In Remote Sensing and Hydrology, M. Owe, K. Brubaker, J. Ritchie, A. Rango (eds.), Proceedings Santa Fe Symp. April 2000, (81-86) IAHS Publication No 267.

Tarboton, D.G. and Luce, C.H. (1996) *Utah Energy Balance Snow Accumulation and Melt Model (UEB) Computer model technical description and users guide*, Utah Water Research Laboratory and USDA Forest Service Intermountain Research Station: 64.

Tarboton, D.G., Jackson, T.H., Liu, J.Z., Neale, C.M.U., Cooley, K.R. and McDonnell, J.J. (1995) *A Grid Based Distributed Hydrologic Model: Testing Against Data from Reynolds Creek Experimental Watershed*, American Meteorological Society Conference on Hydrology, January 15±20, 1995: Dallas, Texas.

Tekeli, A.E. (2005) *Operational hydrological forecasting of snowmelt runoff by remote sensing and geographic information systems integration*, PhD. Thesis, Department of Civil Engineering, Middle East Technical University (in progress)

Tekeli, A.E. (2000) *Integration of remote sensing and geographic information systems on snow hydrology modeling*, MSc. Thesis, Department of Civil Engineering, Middle East Technical University

- Tekeli, A.E., Şorman, A.A., Şensoy, A., Şorman, A.Ü., Bonta, J. and Schaefer, G. (2005a) Snowmelt Lysimeters for Real-Time Snowmelt Studies in Turkey, *Turkish Journal of Engineering and Environmental Sciences*, 29 (1), 29-40.
- Tekeli, A.E., Akyürek, Z., Şorman, A.A., Şensoy, A., Şorman, A.Ü. (2005b) Using MODIS Snow Cover Maps in Modeling Snowmelt Runoff Process in the Eastern Part of Turkey, *Remote Sensing of Environment*, in press.
- Turpin, O., Ferguson, R. and Johansson, B. (1999) Use of remote sensing to test and update simulated snow cover in hydrological models, *Hydrological Processes*, 13 (14-15), 2067-2077.
- US Army, (1956) *Snow Hydrology: Summary report of the snow investigations*. Portland, Oregon, US Army Corps of Engineers.
- Uzunoglu, E. (1999) *Application of the SLURP model using remote sensing and geographic information systems*, MSc. Thesis, Department of Civil Engineering, Middle East Technical University.
- Varley, M.J., Beven, K.J. and Oliver, H.R. (1996) Modeling solar radiation in steeply sloping terrain, *International Journal of Climatology*, 16, 93-104.
- Verseghy, D. (1991) CLASS - A Canadian Land Surface Scheme for GCMs. I. Soil model, *International Journal of Climatology*, 11, 111-133.
- Wigmosta, M.S., Vail, L.W. and Lettenmaier, D.P. (1994) A distributed hydrology vegetation model for complex terrain, *Water Resources Research*, 30 (6), 1665- 1679.
- Williams, K. S. (1998) *The Development and Validation of a Model for the Spatial Distribution of Snowmelt Based on Topography and Point Melt Measurements*, MSc. Thesis, Utah State University, Logan, Utah.
- Williams, K.S. and Tarboton, D.G. (1999) The ABC's of snowmelt: a topographically factorized energy component snowmelt model, *Hydrological Processes*, 13, 1905-1920.
- Wiscombe, W.J. and Warren, S.G. (1980) A model for the spectral albedo of snow I. Pure snow, *Journal of the Atmospheric Sciences*, 37. 2712 - 2733.
- Wood, E.F., Sivapalan, M., Beven, K. and Band, L. (1998) Effects of spatial variability and scale with implications to hydrologic modeling, *Journal of Hydrology*, 102, 29-47.
- WMO (1999) *Areal modeling in hydrology using remote sensing data and geographical information system*, Publication No. 885, Operational Hydrology Report No. 44, World Meteorological Organization, Geneva.

WMO (1986) *Intercomparison of models of snowmelt runoff*, Publication No. 646, Operational Hydrology Report No. 23. World Meteorological Organization, Geneva.

Zhou, X., Xie, H., and Hendrickx, J.M.H. (2005) Statistical evaluation of remotely sensed snow-cover products with constraints from streamflow and SNOTEL measurements, *Remote Sensing of Environment*, 94, 214-231.

Zhou, X. (2002) *Optical remote sensing of snow and ice: Ground measurements, satellite data analysis, and radiative transfer modeling*, Ph.D. Dissertation, Department of Geology and Geophysics, University of Alaska Fairbanks.

APPENDIX A

THE METHODOLOGY OF THE MODEL AND MODEL INPUTS

The maximum liquid water holding capacity, $w_{c,max}$ of the snow cover is a volume ratio defined as follows (Davis et al., 1985, Marks et al., 1999):

$$w_{c,max} = \frac{\text{Volume of water}}{\text{Volume of snow} - \text{Volume of ice}} \quad (\text{A.1})$$

It is the capacity of the void fraction of the snow cover to hold liquid water and is used to determine the relative saturation of the snow cover in the calculation of runoff, $w_{c,max}$ is set as a constant (usually 0.01) at the beginning of the model run. The initial relative saturation of the snow cover is set as an initial condition. From these two parameters the liquid water content of the snow cover and the maximum liquid water content (kg/m^2) are derived and updated during each time step.

If a precipitation event occurs, the model adjusts mass, depth, liquid water content, temperature and density. A precipitation input includes total precipitation mass, percentage of the total mass that was snow, average density of the snow portion and the average precipitation temperature. If snowfall or mixed rain/snowfall event occurs, the temperature of the surface snow layer, the average temperature of the snow cover, the thickness of the snow cover, the average density of snow cover, the relative liquid water saturation and the liquid water content are adjusted. If the precipitation temperature is equal to, or greater than 0°C and the percentage snow is set to less than 1.0, then the model assumes that rain has occurred. If rain occurs, snow cover compaction is estimated from rainfall intensity over the time step and snow cover thickness, densities and relative liquid water saturation is adjusted. If a warm rain event occurs, only adjustments from compaction and addition of liquid water are made. If rain occurs in the absence of a snow cover, the volume of water added becomes runoff (Marks et al., 1999).

After the snow cover thermal conditions have been set, the model reads the input data to calculate the energy balance of the snow cover for that time step. Net radiation, R_{nr} (W/m^2), is calculated by:

$$R_{net} = S_{net} + L_i - (\epsilon_s \sigma T_{s,0}^4) \quad (\text{A.2})$$

Net solar radiation, S_{net} (W/m^2) and thermal radiance L_i (W/m^2), are inputs; σ is the Stefan-Boltzmann constant ($5.6697 \times 10^{-8} \text{ J}/\text{m}^2/\text{K}^4$); the temperature of the surface layer $T_{s,0}$ begins at the interval input value and is then calculated and updated at the end of each time step by the model. Surface emissivity, ε_s , is set at a constant value of 0.99 by the model.

Turbulent transfer terms, H (W/m^2) and L (W/m^2), are calculated using a method adapted by Marks and Dozier (1992) as a system of non-linear equations that simultaneously solve for the Obukhov stability length, L , the friction velocity, u^* , the sensible heat flux, H , and the mass flux by evaporation or condensation from the snow surface, E , ($\text{kg}/\text{m}^2/\text{s}$).

$$L = \frac{u^{*3} \rho}{kg \left(\frac{H}{T_a C_p} + 0.61E \right)} \quad (\text{A.3})$$

$$u^* = \frac{uk}{\ln \left(\frac{z_u - d_0}{z_0} \right) - \Psi_{sm} \left(\frac{z_u}{L} \right)} \quad (\text{A.4})$$

$$H = \frac{(T_a - T_{s,0}) a_H k u^* \rho C_p}{\ln \left(\frac{z_T - d_0}{z_0} \right) - \Psi_{sh} \left(\frac{z_T}{L} \right)} \quad (\text{A.5})$$

$$E = \frac{(q - q_{s,0}) a_E k u^* \rho}{\ln \left(\frac{z_q - d_0}{z_0} \right) - \Psi_{sv} \left(\frac{z_q}{L} \right)} \quad (\text{A.6})$$

ρ is the density of the air, k is the von Karmen constant (≈ 0.40), g is the acceleration due to gravity ($9.80616 \text{ m}/\text{s}^2$), C_p is the specific heat of the dry air at constant pressure ($1005 \text{ J}/\text{kg}/\text{K}$), E is the mass flux by the evaporation and condensation from the snow surface ($\text{kg}/\text{m}^2/\text{s}$), u is the wind speed (m/s), d_0 is the zero-plane displacement height (m , $\approx (2/3)7.35 z_0$), a_H and a_E are the ratio of eddy diffusivity and viscosity for heat and vapor (Brutsaert, 1982) suggests $a_H = a_E = 1.0$) and Ψ_{sm} , Ψ_{sh} and Ψ_{sv} are stability functions for mass, heat and water vapor (positive when stable, negative when unstable). The measurement heights for temperature, humidity and wind (m), z_T , z_q and z_u are set as initial conditions and then updated by the model as the depth of the snow cover changes. The roughness length, z_0 (m), is set as a constant at the beginning of the run, but can be updated as conditions require. Air temperature, T_a (K), wind speed, u (m/s) and vapor pressure, e_a (Pa) are model inputs and specific humidity, q (g/kg), is calculated from e_a and site air pressure. Snow surface layer temperature, $T_{s,0}$ (K), is adjusted by the model at the end of each time step; snow surface specific humidity is

calculated as a function of site air pressure and the saturation vapor pressure at $T_{s,0}$. The latent heat flux, L (W/m^2), is $L \times E$, where the latent heat of fusion (J/kg), which varies with the temperature and state of the water (liquid or solid) from $2.501 \times 10^6 J/kg$ for liquid water at $0^\circ C$ or $2.834 J/kg$ for ice $0^\circ C$.

The model treats the soil as a moist, single layer system with thickness equal to the depth of the temperature measurement, z_g (m) and a temperature profile defined by input T_g (K) at depth z_g and the temperature of the lower snow layer, $T_{s,l}$. Therefore a vapor gradient between the snow/soil interface and a depth z_g defined by saturation vapor pressures at T_g and $T_{s,l}$, a base thermal conductivity for soil in mountainous regions, K_g ($J/m/K/s$) is set as a constant based on soil characteristics. Base thermal conductivities for snow layers are set as functions of layer densities (Yen, 1965). A base diffusion coefficient D_0 (m^2/s) is estimated for water vapor in snow or a saturated inorganic soil layer with a temperature of $0^\circ C$ at sea level pressure. Anderson (1976) developed an empirical relationship but can be used to adjust this base diffusion coefficient, D_e ($kg/m/s/K$). D_e is then used with base thermal conductivity and layer specific humidity for the snow or soil to compute an effective thermal conductivity that accounts for both heat conduction and vapor diffusion between layers

$$K_{es,0} = K_{s,0} + (L_v D_{e,0} q_{s,0}) \quad (A.7)$$

$$K_{es,l} = K_{s,l} + (L_v D_{e,l} q_{s,l}) \quad (A.8)$$

$$K_{eg} = K_g + (L_v D_{e,g} q_g) \quad (A.9)$$

$K_{es,0}$, $K_{es,l}$ and K_{eg} ($J/m/K/s$) are effective thermal conductivities for the surface and lower snow layers and for the soil, $K_{s,0}$, $K_{s,l}$ and K_g ($J/m/K/s$) are base thermal conductivities for the surface, lower snow layers and for the soil.

Energy transfer by conduction and diffusion between the soil and the lower layer of the snow cover, G (W/m^2) is calculated by

$$G = \left(\frac{2K_{es,l} K_{eg} (T_g - T_{s,l})}{K_{eg} z_{s,l} + K_{es,l} z_g} \right) \quad (A.10)$$

The depth of the soil measurement z_g (m) is an initial condition and the soil temperature at z_g , T_g (K) is an input data parameter. The temperature of the lower snow layer, $T_{s,l}$ (K) and the thickness of the lower snow layer, $z_{s,l}$ (m) are calculated by the model at each time step.

Energy transfer by conduction and diffusion between the snow surface layer and the lower snow layer G_0 (W/m^2) is calculated in the same manner.

$$G_0 = \left(\frac{2K_{es,0}K_{es,l}(T_{s,l} - T_{s,0})}{K_{es,l}z_{s,0} + K_{es,0}z_{s,l}} \right) \quad (\text{A.11})$$

The temperature of the surface snow layer, $T_{s,0}$ (K) and the thickness of the surface snow layer, $z_{s,0}$ (m) are calculated by the model at each time step.

Advected energy transfer to the surface layer, M (W/m²) is calculated only during time steps when precipitation input has occurred.

$$M = \frac{C_{p-p}\rho_{pp}z_{pp}(T_{pp} - T_{s,0})}{t_{step}} \quad (\text{A.12})$$

Advection is converted from a total (J/m²) to an average flux (W/m²) for the time step by dividing by the length of the time step in seconds, t_{step} . The density, mass, percentage snow and temperature by precipitation during the event are model inputs. From these, the model sets precipitation density, ρ_{pp} (kg/m³), precipitation depth, z_{pp} (m), and precipitation temperature, T_{pp} (K), as described below. The specific heat of precipitation, C_{p-p} , is calculated as a function of precipitation temperature, T_{pp} , and the state (liquid or solid). If a mixed rain/snow event occurs, C_{p-p} is estimated proportionally.

The surface energy exchange terms are summed to determine the net energy transfer to the surface snow layer ΔQ_0 (W/m²)

$$\Delta Q_0 = R_n + H + L + G_0 + M \quad (\text{A.13})$$

And the total energy transfers to the snow cover

$$\Delta Q = \Delta Q_0 + G \quad (\text{A.14})$$

These are used to determine the energy available for melting or refreezing in each layer. The energy available for melt or refreezing in each of the snow layers is (J/m²)

$$Q_0 = \Delta Q_0 \times t_{step} + cc_{s,0} \quad (\text{A.15})$$

$$Q_1 = (G - G_0) \times t_{step} + cc_{s,l} \quad (\text{A.16})$$

Since the computation of cold content hinges on the estimation of the snowpack temperature, the common approach to modeling the snow condition in continuous simulation is to maintain an accounting of the relative temperature of the snowpack below freezing as a function of time (ASCE, 1996).

T_{step} is the time step in seconds and $cc_{s,0}$ and $cc_{s,1}$ (J/m^2) are the layer cold contents or the energy required to bring the layer to T_{melt} . If Q_0 or Q_1 are positive, layer temperatures are set to T_{melt} , melt is calculated, the liquid water content of the snow cover is adjusted and the layer cold contents are set to 0. If Q_0 or Q_1 are negative and liquid water is present, the energy required for refreezing is calculated, the liquid water content is adjusted or set to 0, a new cold content is determined and the temperatures are adjusted for each layer.

Evaporation or condensation between the snow surface layer and the atmosphere, E , was determined during the calculation of latent heat flux, L . Evaporation or condensation between the lower snow layer and the soil E_1 ($kg/m^2/s$) is calculated by

$$E_1 = \rho D_{e.g} \left(\frac{q_g - q_{s,l}}{z_g} \right) \quad (A.17)$$

And the mass of evaporative loss or gain, E_s (kg/m^2) is

$$E_s = (E + E_t) \times t_{step} \quad (A.18)$$

The specific mass of the snow cover is adjusted by the total mass of evaporative loss or gain. If liquid water is present, it is preferentially evaporated by the ratio of the latent heat of vaporization to sublimation at $0^\circ C$ (0.882). The snow cover liquid water content is then adjusted for evaporation. The remaining evaporative loss or all evaporation after liquid water has been depleted, is modeled as sublimated ice. Half of the ice lost is assumed to be decreased depth. The remaining sublimated ice and all evaporated liquid water decrease the density and mass of the snow cover, so again snow cover thicknesses, density and liquid water capacity are adjusted. If the total liquid water exceeds the adjusted liquid water capacity, the excess becomes runoff and specific mass are adjusted (Marks et al., 1999).

The travel rate of meltwater or rain will be influenced by the condition of the snow as indicated by its temperature, crystalline structure, density etc. as it moves through the snowpack. In fresh snow, an initial quantity of meltwater or rain that enters the snowpack will freeze as it warms the snowpack to $0^\circ C$. Therefore, the snow condition effects can be thought as an initial loss that is subtracted from input, much in the same way as initial losses in dry soil conditions. An additional quantity of water is also required to satisfy liquid water holding capacity before the snow will release any water by gravity. Thus, liquid water holding capacity is the second factor that can be considered as initial loss in snow hydrology. It varies depending upon the depth and density of the snow, the mass of the ice layers and the canalizations and honey-combing of the snowpack. It has been observed that as $0^\circ C$ this factor is approximately 1-5 % of the SWE (ASCE, 1996).

The model input variables are presented in Figures A1-A5 for GY (2002-2004), OVA and CAT (2003-2004).

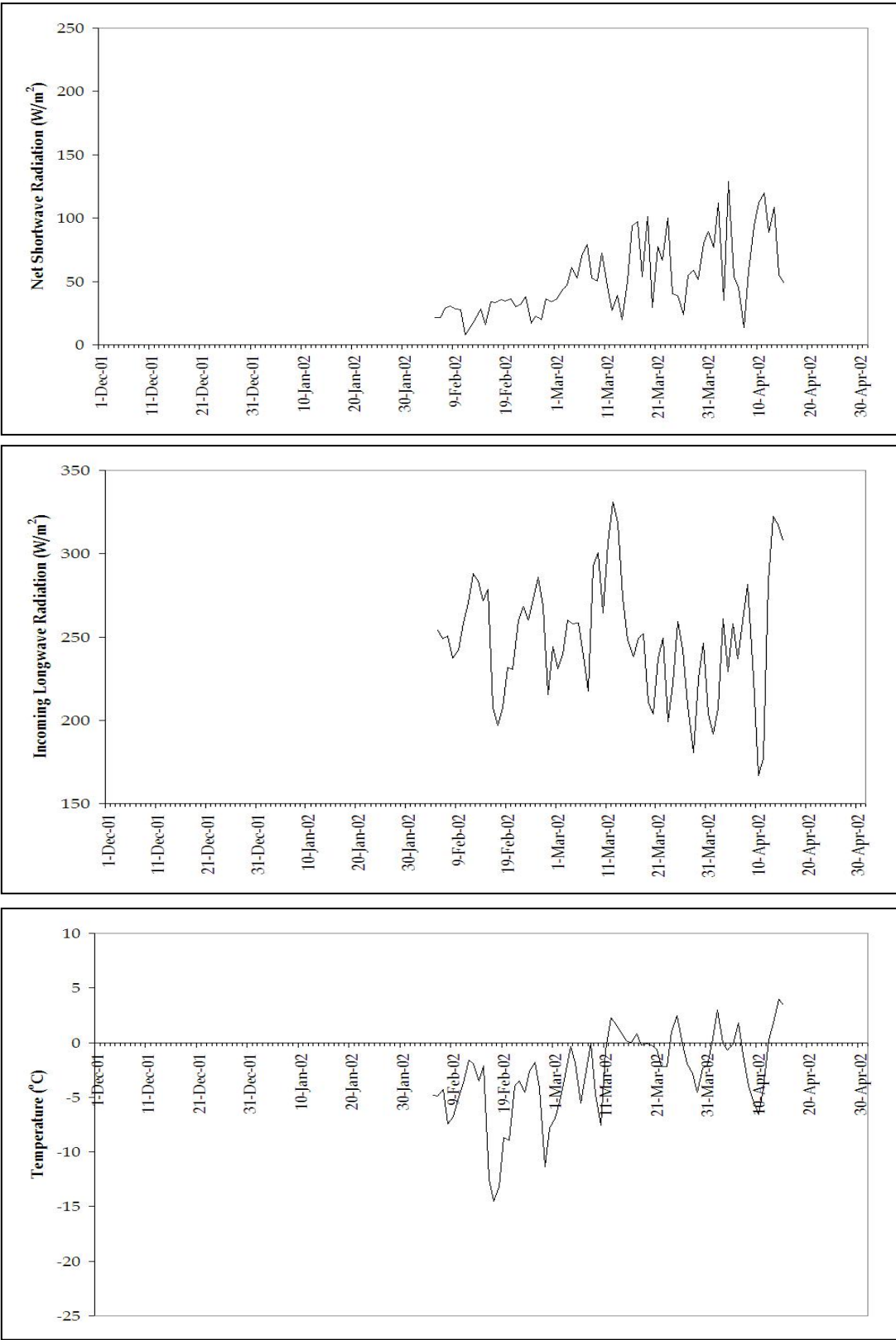


Figure A.1 Climate input parameters for 2001-2002 snow season, GY

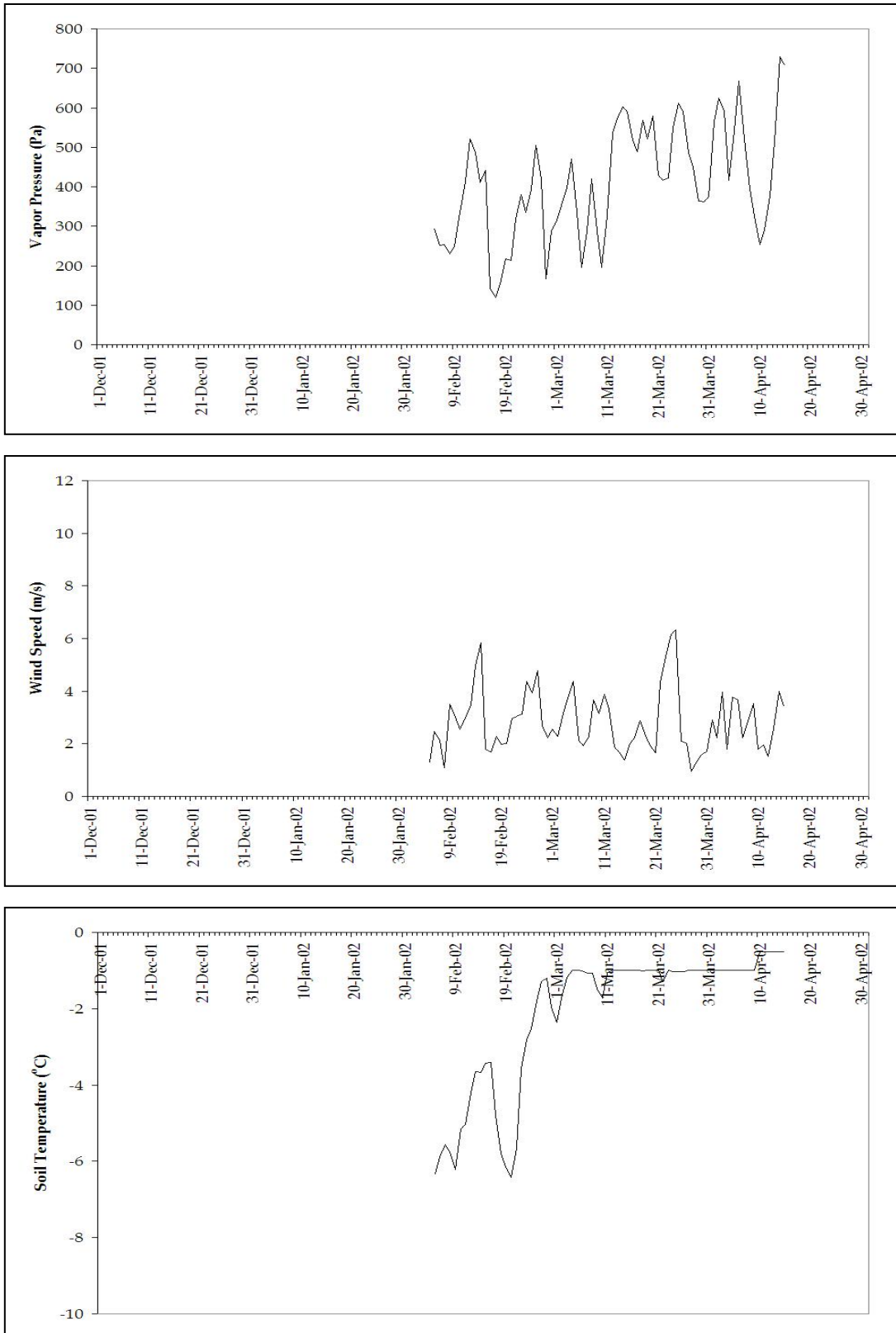


Figure A.1 (Cont'd) Climate input parameters for 2001-2002 snow season, GY

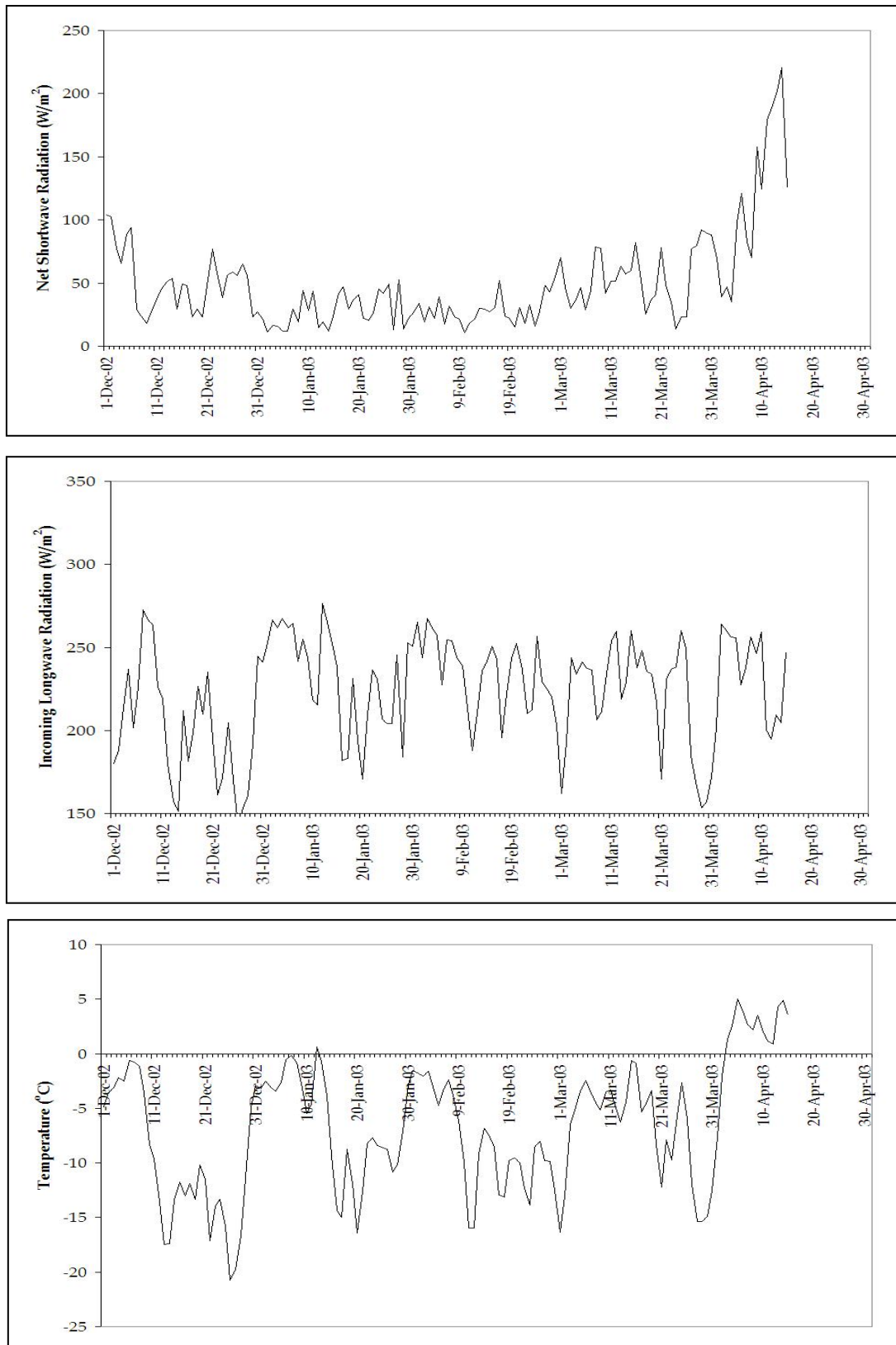


Figure A.2 Climate input parameters for 2002-2003 snow season, GY

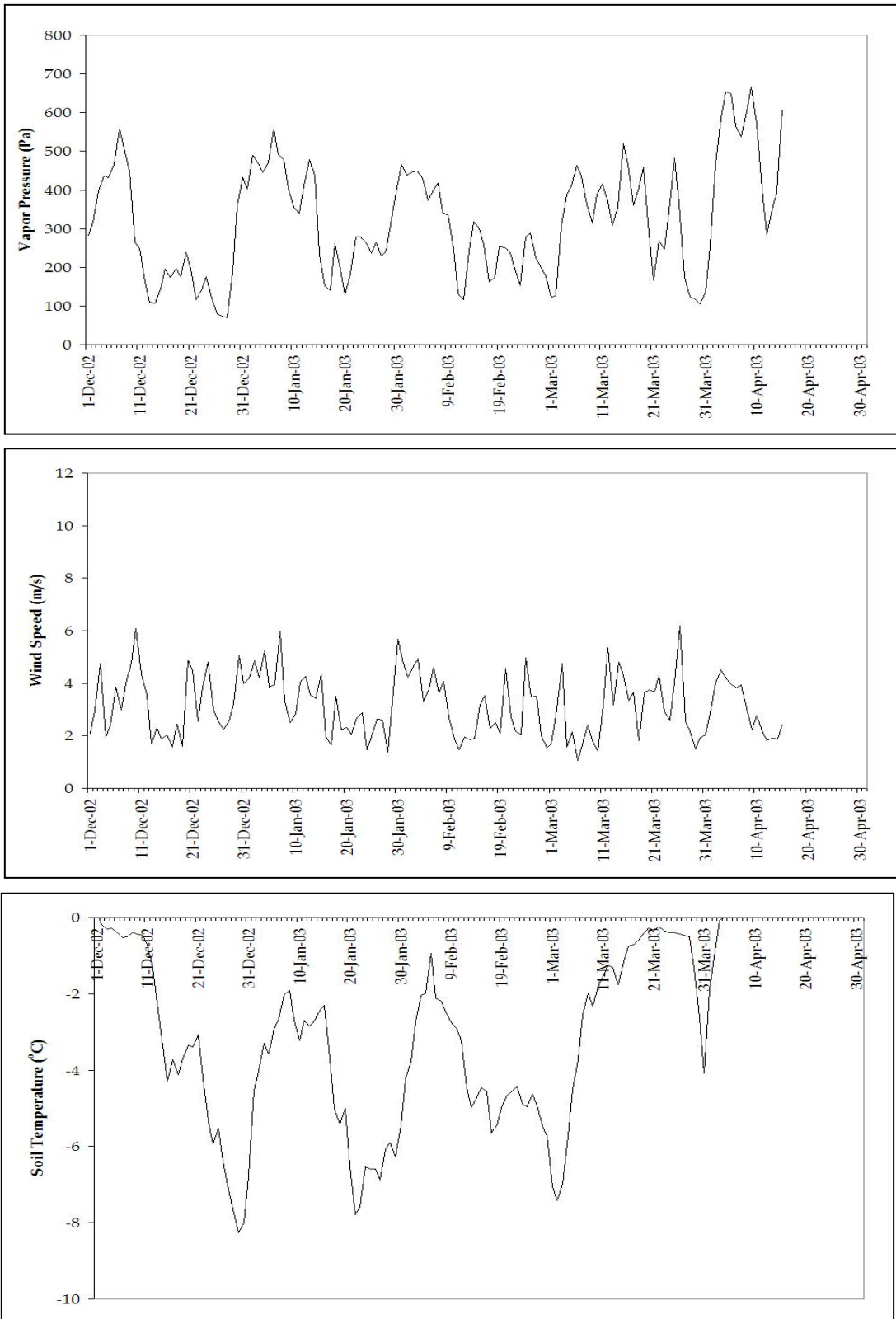


Figure A.2 (Cont'd) Climate input parameters for 2002-2003 snow season, GY

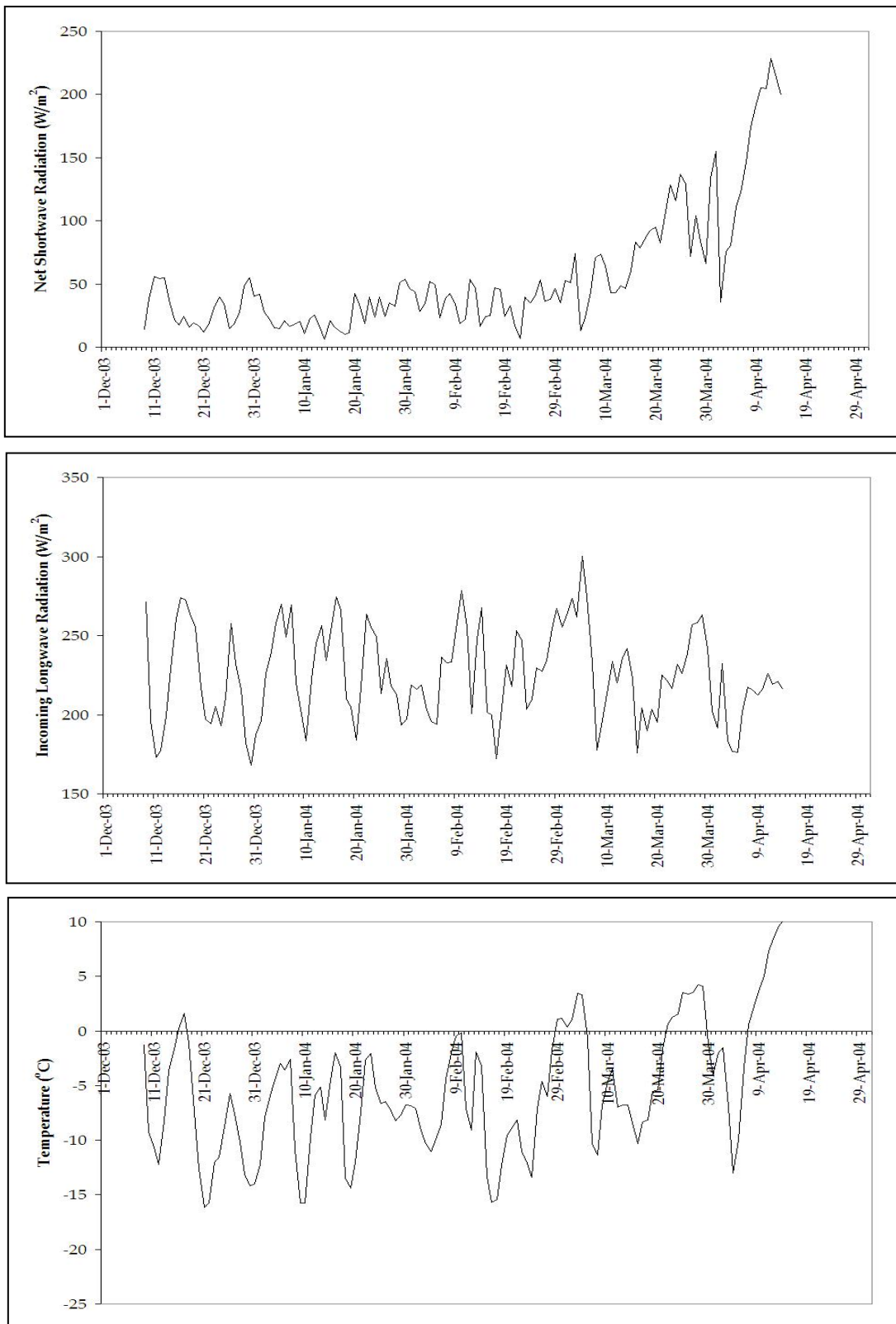


Figure A.3 Climate input parameters for 2003-2004 snow season, GY

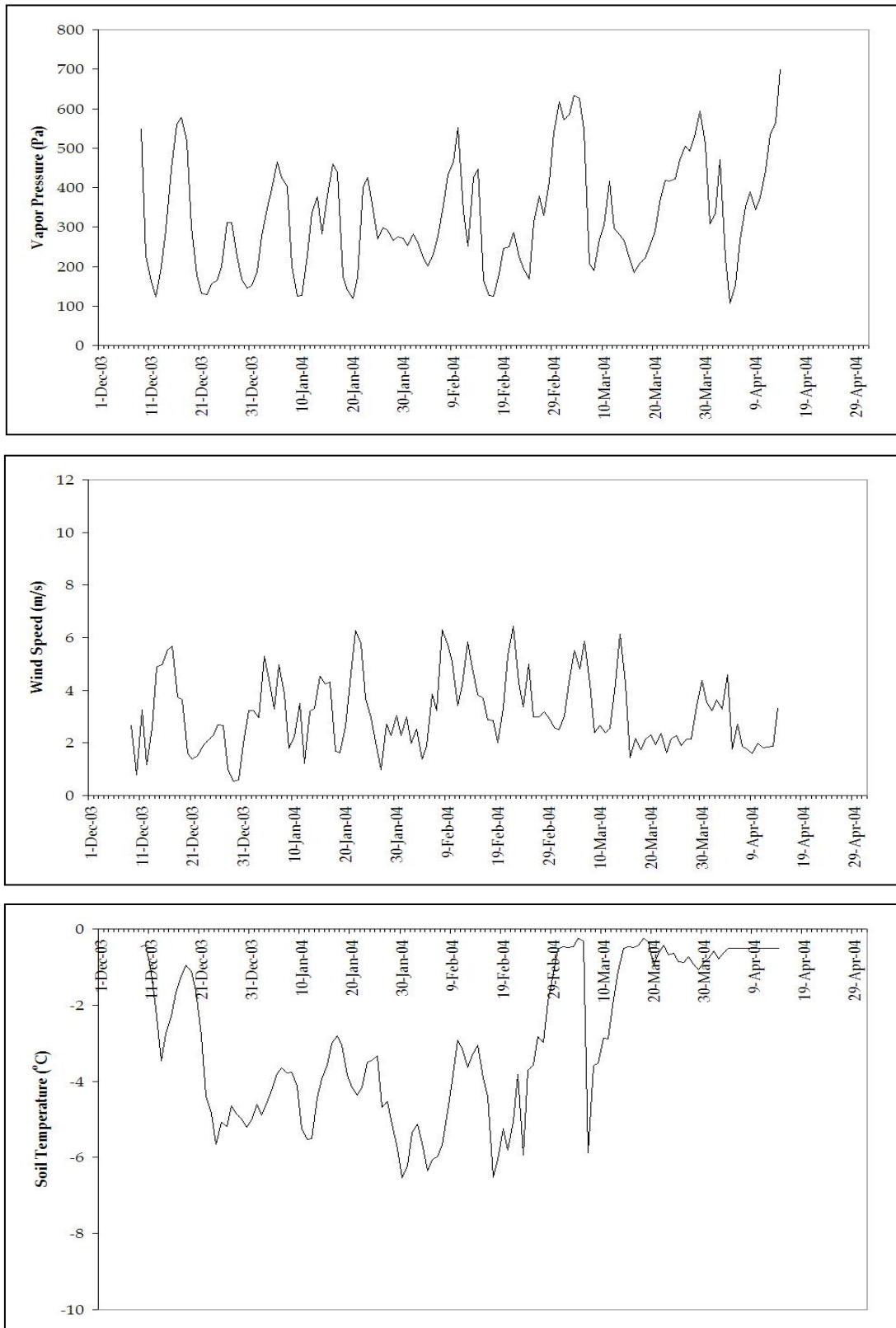


Figure A.3 (Cont'd) Climate input parameters for 2003-2004 snow season, GY

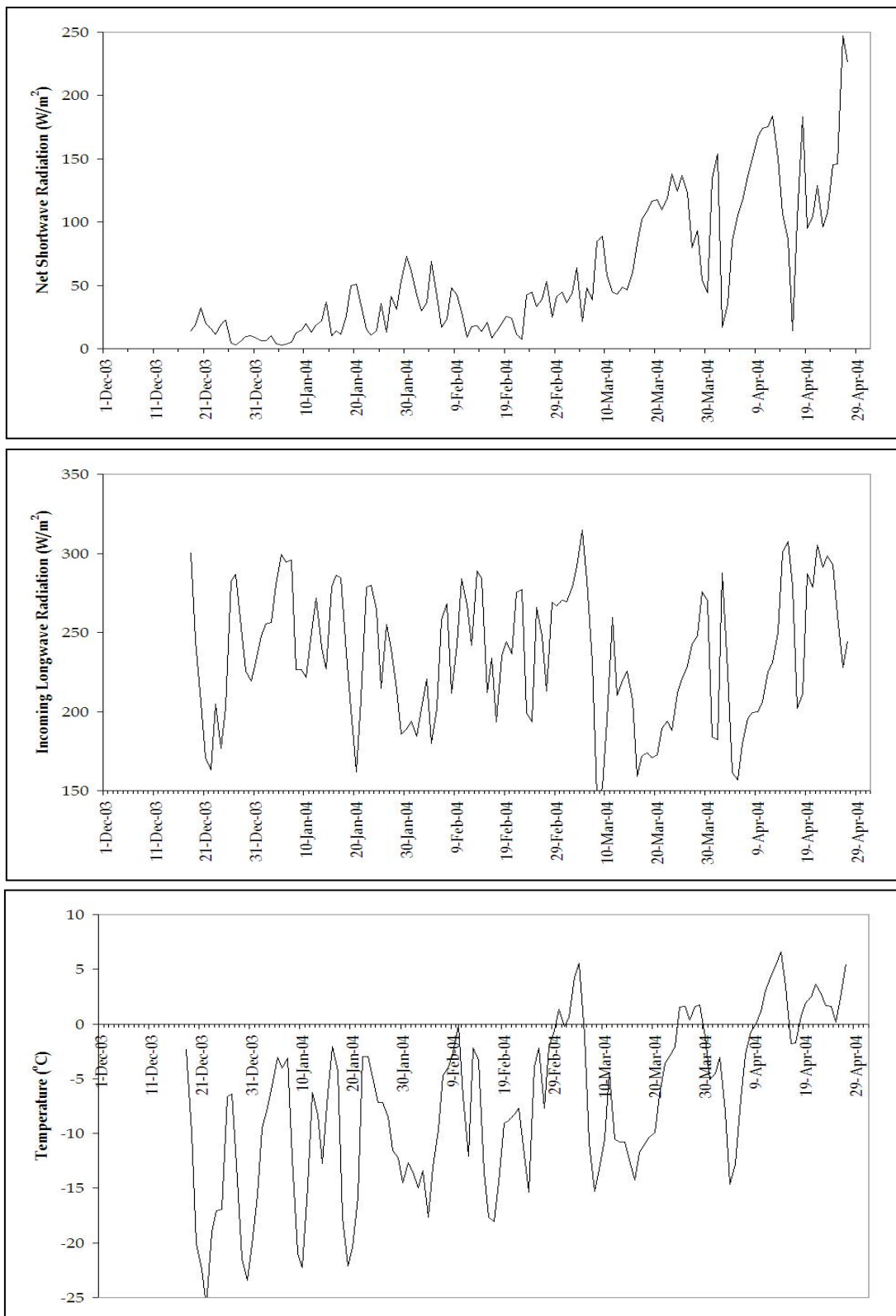


Figure A.4 Climate input parameters for 2003-2004 snow season, OVA

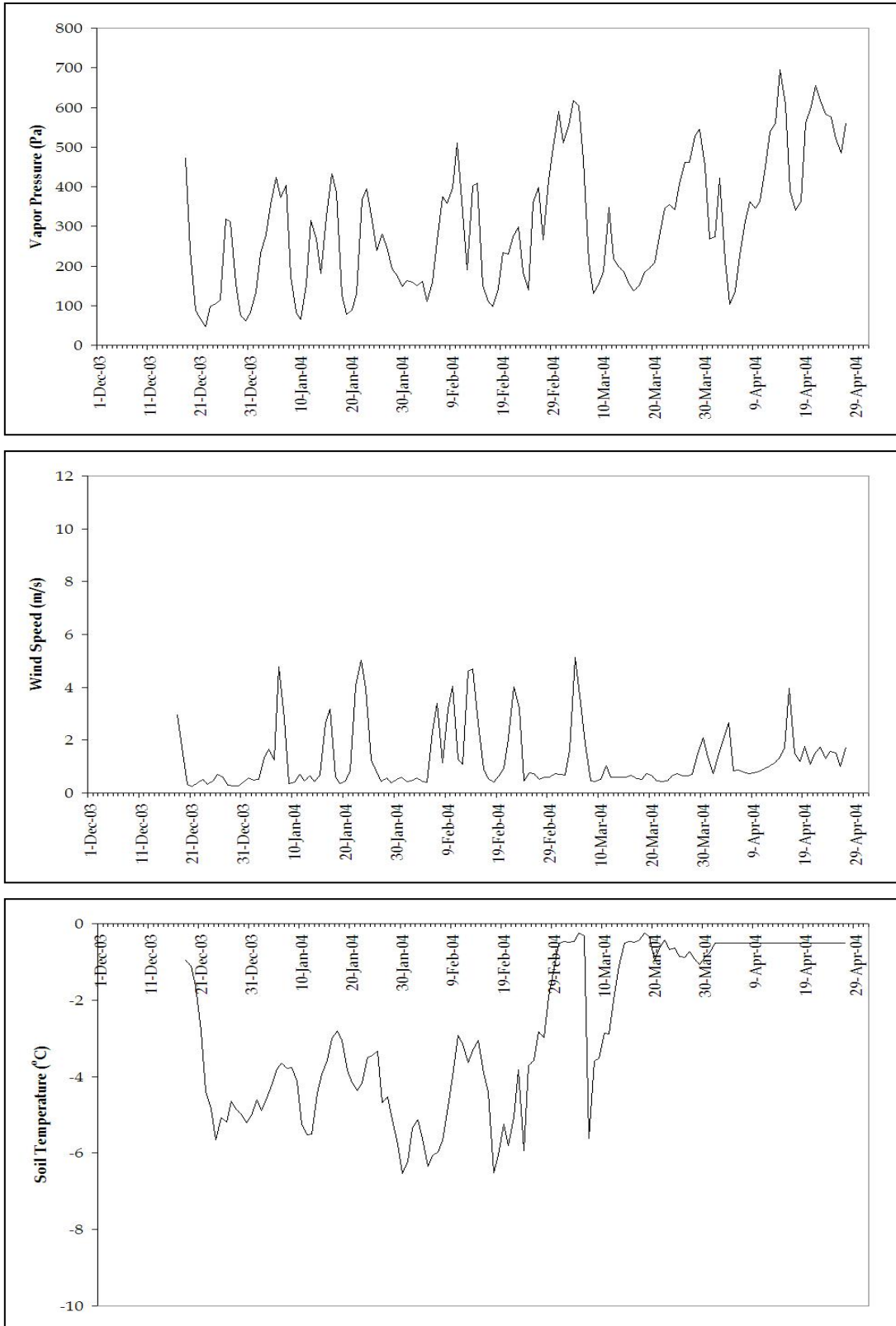


Figure A.4 (Cont'd) Climate input parameters for 2003-2004 snow season, OVA

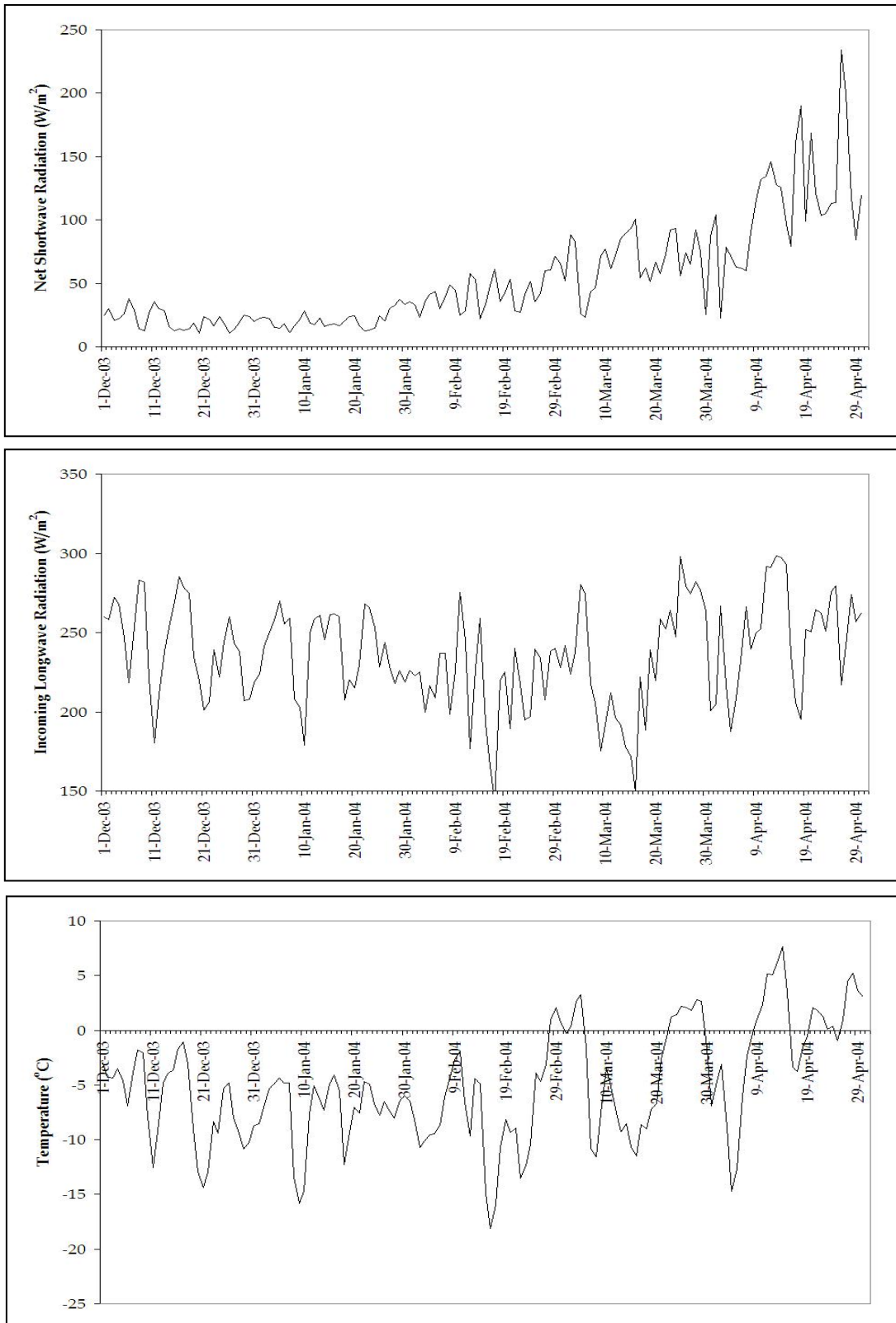


Figure A.5 Climate input parameters for 2003-2004 snow season, CAT

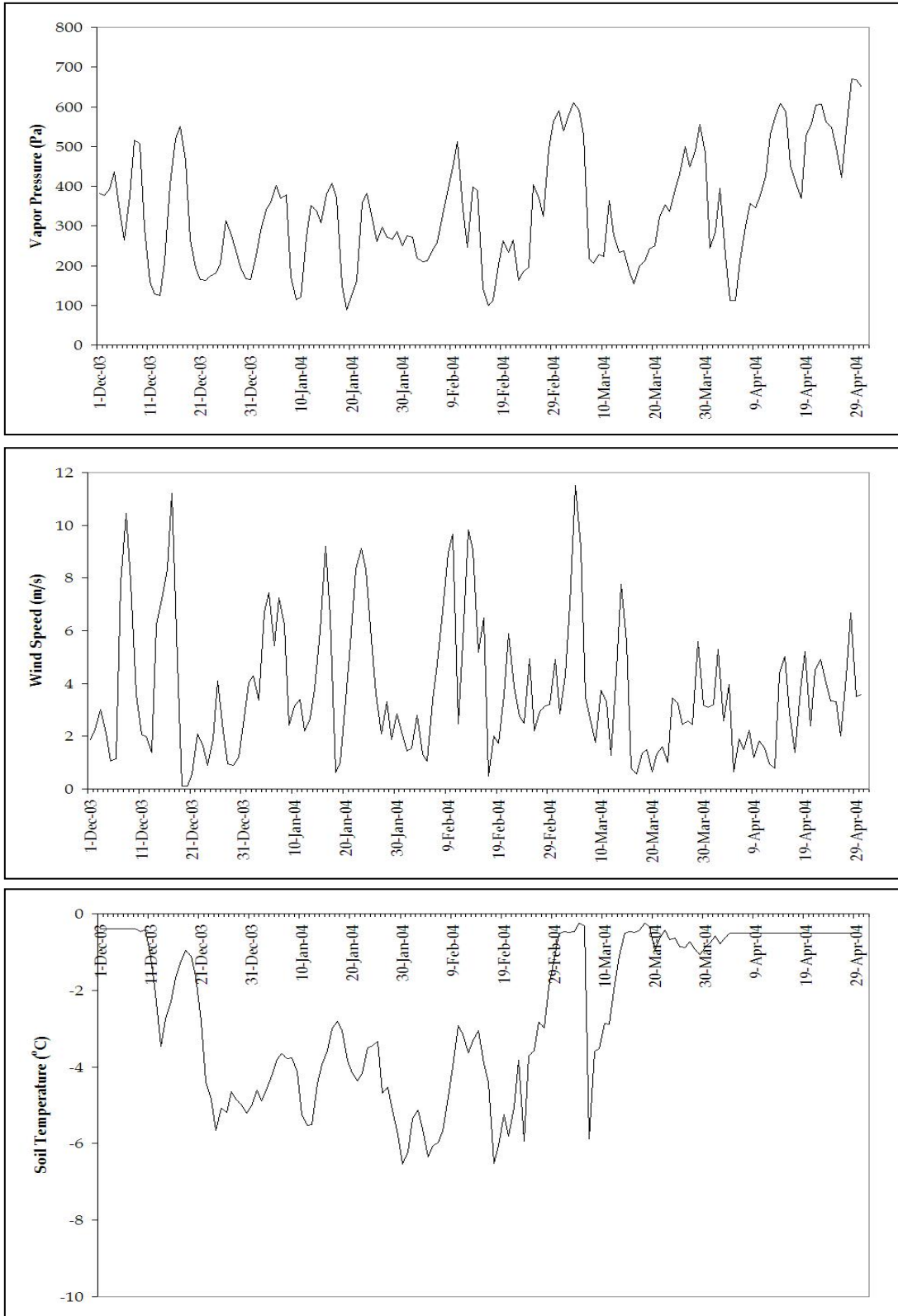


Figure A.5 (Cont'd) Climate input parameters for 2003-2004 snow season, CAT

CURRICULUM VITAE

PERSONAL INFORMATION

Surname, Name: Şensoy, Aynur

Nationality: Turkish (TC)

Date and Place of Birth: 5 September 1975, Ankara

Email: sensoy@metu.edu.tr

asensoy@anadolu.edu.tr

EDUCATION

Degree	Institution	Year of Graduation
PhD	METU Civil Engineering	2005
MS	METU Civil Engineering	2000
BS	METU Civil Engineering	1997
High School	Anittepe Lisesi, Ankara	1992

WORK EXPERIENCE

Year	Place	Enrollment
Nov 2004 - Present	AU Civil Engineering	Research Assistant
Dec 1997 - Nov 2004	METU Civil Engineering	Research Assistant
Jun - Oct 1997	Private	Civil Engineer

FOREIGN LANGUAGE

English

PUBLICATIONS

- Şensoy, A. (2000) *Spatially distributed hydrologic modeling approach using geographic information systems*, MSc. Thesis, Department of Civil Engineering, Middle East Technical University
- Şensoy, A., Tekeli, A.E., Şorman, A.A. and Şorman, A.Ü. (2003) Simulation of event based snowmelt runoff hydrographs based on snow depletion curves and the degree-day method, *Canadian Journal of Remote Sensing*, 29 (6), 693-700.
- Tekeli, A.E., Şorman, A.A., Şensoy, A., Şorman, A.Ü., Bonta, J. and Schaefer, G. (2005) Snowmelt Lysimeters for Real-Time Snowmelt Studies in Turkey, *Turkish Journal of Engineering and Environmental Sciences*, 29 (1), 29-40.
- Tekeli, A.E., Akyürek, Z., Şorman, A.A., Şensoy, A., Şorman, A.Ü. (2005) Using MODIS Snow Cover Maps in Modeling Snowmelt Runoff Process in the Eastern Part of Turkey, *Remote Sensing of Environment*, in press.